DISSERTATION

HIGH-RESOLUTION MULTI-HAZARD APPROACH TO QUANTIFY HURRICANE-INDUCED RISK FOR COASTAL AND INLAND COMMUNITIES

Submitted by

Omar M. Nofal

Department of Civil and Environmental Engineering

In partial fulfillment of the requirements

For Degree of Doctor of Philosophy

Colorado State University

Fort Collins, Colorado

Summer 2021

Doctoral Committee:

Advisor: John W. van de Lindt

Harvey Cutler
Hussam N. Mahmoud
Yanlin Guo

ABSTRACT

HIGH-RESOLUTION MULTI-HAZARD APPROACH TO QUANTIFY HURRICANE-INDUCED RISK FOR COASTAL AND INLAND COMMUNITIES

Hurricanes are devastating natural hazards that often cause damage to coastal and in-land communities as a result of their loadings which include storm surge, waves, wind, and rainfall and riverine flooding, often in combination. Modeling these hazards individually and their effects on buildings is a complex process in that each loading component within the hazard behaves differently affecting either the building envelope, the structural system, or the interior contents. For coastal communities, realistic modeling of hurricane effects requires a multi-hazard approach that considers the combined effects of wind, surge, and waves. Previous studies have focused primarily on modeling these hazards individually with less focus on the multi-hazard impact on the whole building system made up of the combination of structure and its interior contents. For inland communities, high-resolution hydrologic and hydrodynamic models are required to develop high-fidelity flood hazard maps that account for the different hazard characteristics (e.g., flood depth, velocity, duration, etc.). The current flood damage assessment standards are still using stage-damage functions to account for flood damage to buildings. These functions include inherent uncertainties in the damage assessment with significant limitations on their applications. Additionally, the analysis resolution used in these previous studies did not allow hurricane risk assessment through at the building component level (e.g., interior content, structural, and non-structural components).

To address these research gaps, a high-resolution flood risk model was developed for inland communities using robust probabilistic flood fragility functions developed for a portfolio of 15

building archetypes that can model the flood vulnerability at the community-level. For coastal communities, a regional-level multi-hazard hurricane risk analysis methodology is proposed to account for the combined impacts of wind-surge-wave loadings driven by hurricanes for both the building system and its interior contents. Fragility functions are used to describe building vulnerability to the multiple loadings driven by hurricanes, and a new convolutional vulnerability approach was developed to combine wind and wave/surge fragilities. The models developed in this dissertation were included in an open-source **I**nterdependent **N**etworked **Co**mmunity **R**esilience Modeling **E**nvironment (IN-CORE) to allow researchers/users to systematically use these models in different types of engineering, social, and economic analyses. The analysis resolution used in the hazard, exposure, and vulnerability models allowed investigation of different levels of mitigation measures including component-, building-, and community-level mitigation strategies.

The proposed hurricane risk models for coastal and in-land communities were then applied to a number of case studies to demonstrate the ability of the developed methods to predict damage at the building level across a large spatial domain of small and large communities. The main contribution of these efforts is the development of generalized fragility-based flood vulnerability functions that were applied to a suit of building archetypes and are extendable to be used for other buildings/facilities. These fragilities were then combined with another suite of existing wind fragilities and other storm surge-wave fragility functions to account for the impact of the hurricane-induced hazards on coastal communities. These models enable a better understanding of the damages caused by hurricanes for coastal and in-land communities, thereby setting initial post-impact conditions for community resilience assessment and investigation of recovery policy alternatives.

ACKNOWLEDGEMENTS

I would like to express my gratitude to my advisor, Prof. John van de Lindt for his guidance, support, and encouragement throughout my Ph.D. I appreciate his mentorship and giving me the opportunity to explore different research areas and engage with different research projects. He has been a great source of inspiration and allowed me to explore my research with freedom and enthusiasm along with his guidance and support. I will be always grateful to him. I would like to extend my appreciation to my doctoral committee members, Prof. Harvey Cutler, Dr. Hussam Hahmoud, and Dr. Yanlin Guo for providing their support, input, ideas, and comments.

The work done in this dissertation was funded by multiple federal agencies including the National Institute of Standards and Technology (NIST) under Cooperative Agreement 70NANB20H008 and 70NANB15H044, the National Science Foundation (NSF) under Grant 1940119, and the Coastal Resilience Center funded by the Department of Homeland Security (DHS). This support is greatly appreciated. Also, I would like to thank the Department of Civil and Environmental Engineering at Colorado State University for honoring me to be the recipient of several scholarships and fellowships during my doctoral degree including Walter Scott Jr. Fellowship in 2017, Kenneth G. Medearis Scholarship in 2018, Jack E. Cermak Wind Engineering Fellowship in 2019, the outstanding Graduate Student Award in 2020, Jack E. Cermak Wind Engineering Fellowship in 2020, and the teaching fellowship in the summer of 2021.

Last but not least, I would like to thank my parents, family, friends, and colleagues for their unconditional love, support, encouragement, and sacrifice. I would like to extend my deep gratitude to all my teachers, mentors, and advisors who always believed in me and support me to reach this milestone.

DEDICATION

To my beloved parents, and family

TABLE OF CONTENTS

ABSTRACT ii
ACKNOWLEDGEMENTS iv
DEDICATION v
LIST OF TABLES ix
LIST OF FIGURES x
CHAPTER 1: INTRODUCTION 1
1.1 Background 1
1.1.1 Hurricane Hazard 6
1.1.2 Hurricane Exposure 8
1.1.3 Hurricane Vulnerability 9
1.1.4 Hurricane Risk Analysis 16
1.1.5 Hurricane Risk Mitigation 19
1.1.6 Community Resilience 25
1.2 Motivation 28
1.3 Research Purpose and Objectives 31
1.4 Layout of the Dissertation 35
CHAPTER 2: FLOOD FRAGILITY AND LOSS ANALYSIS APPROACH 37
2.1 Introduction 37
2.2 Fragility Formulation and Loss Estimation Methodology 40
2.2.1 Fragility Analysis Approach 41
2.2.2 Loss Analysis Approach 51
2.2.3 Example Archetype to Illustrate the Proposed Approach 57
2.2.3.1 2-D Flood fragility function based on flood depth 61
2.2.3.2 2-D Flood loss function based on flood depth 63
2.2.3.3 3-D Flood fragility function based on flood depth and flood duration 67
2.2.3.4 3-D Flood loss function based on flood depth and flood duration 70
2.3 Minimal Building Flood Fragility and Loss Functions 71
CHAPTER 3: HURRICANE RISK ANALYSIS METHODOLOGY 85
3.1 Introduction 85

3.2 Inland Communities 86
3.2.1 Hazard Modeling 86
3.2.2 Exposure Modeling 89
3.2.3 Vulnerability Modeling 92
3.2.4 Risk Analysis 92
3.3 Coastal Communities 95
3.3.1 Hazard Modeling 96
3.3.2 Exposure Modeling 99
3.3.3 Vulnerability Modeling 100
3.3.4 Risk Analysis 107
CHAPTER 4: MITIGATION AND ADAPTATION ANALYSIS APPROACH........ 113
4.1 Introduction 113
4.2 Building-Level Mitigation and Adaptation Analysis 115
4.2.1 Temporary water barrier systems 116
4.2.2 Pumps 121
4.2.3 Resilient Construction 127
4.3 Community-Level Mitigation and Adaptation Analysis 130
CHAPTER 5: CASE STUDIES ANALYSIS RESULTS 137
5.1 Introduction 137
5.2 Example 1: Lumberton, North Carolina 137
5.2.1 Hazard Scenario 139
5.2.2 Hydrologic and Hydrodynamic Analysis 142
5.2.3 Exposure and Vulnerability Modeling 146
5.2.4 Flood Risk Analysis 148
5.2.5 Flood Mitigation Analysis Using Building-Level Mitigation Measures 151
5.2.6 Flood Mitigation Analysis Using Community-Level Mitigation Measures 160
5.2.6.1 Flood gates/ temporary berm 166
5.2.6.2 Permanent levees/floodwalls 167
5.2.6.3 Retention/Detention System 170
5.2.6.4 Buyout policy and elevating building first-floor elevation (FFE) 172
5.2.6.5 Discussion 172
5.2.7 Lumberton Testbed for IN-CORE Application 180

5.3 Example 2: The State of North Carolina 184
5.3.1 Hazard Scenario 185
5.3.2 Exposure and Vulnerability Modeling 188
5.3.3 Hurricane Risk Analysis 192
5.4 Example 3: Waveland, Mississippi 198
5.4.1 Hazard Scenario 199
5.4.2 Exposure and Vulnerability Modeling 201
5.4.3 Hurricane Risk Analysis 202
CHAPTER 6: SUMMARY AND CONCLUSIONS, CONTRIBUTIONS, AND RECOMMENDATIONS 205
6.1 Summary and Conclusions 205
6.2 Contributions 209
6.3 Recommendations 211
REFERENCES 213
APPENDIX A 239
APPENDIX B 249

LIST OF TABLES

Table 1-1. Damage function examples for different flood damage characteristics 14
Table 1-2. Classifications for the different types of hurricane-induced losses 17
Table 1-3. Classification of the actions that communities may choose to adopt to mitigate flood impacts and speed the recovery process 27
Table 2-1. Damage states description along with their damage scale and damage ratio as a percentage of the total building replacement cost... 44
Table 2-2. A list of the 65 damageable components used to represent the residential building archetype 59
Table 2-3. Damage states description along with their damage scale and damage ratio as a percentage of the total building replacement cost.. 60
Table 2-4. Flood loss statistics for each damage state along with the replacement cost for each DS 61
Table 2-5. The building archetypes description (more details provided in Appendix A) 73
Table 2-6. Lognormal parameters of the developed 2-D fragility functions for the 15 building archetypes (SI units) 79
Table 2-7. Damage states replacement cost data for each building archetype (μ_r: mean DS replacement cost USD \$, σ_r: standard deviation of DS replacement cost USD \$, μ_{rc}: mean cumulative DS replacement cost USD \$, Lr %: normalized DS loss ratio, and Lr_c %: normalized cumulative DS loss ratio).. 83
Table 3-1. Damage states description for the multiple hazards driven by hurricanes along with their damage scale.. 103
Table 3-2. Description of the wind building archetypes (Memari et al., 2018)......................... 105
Table 3-3. Loss percentage of content and structure damage for each damage state 111
Table 4-1. Data for select building components that could be elevated (Archetype 2 as an example).. 129
Table 5-1. Damage states exceedance probability for the flooded buildings 149
Table 5-2. Damage states exceedance probability for the flooded buildings corresponding to two select mitigation scenarios 155
Table 5-3. Policy-based flood mitigation scenarios details 165
Table 5-4. Analysis results for the 28 flood mitigation scenarios in this study......................... 174
Table 5-5. The number of buildings exposed to the hazards induced by Hurricane Florence (2018).. 190
Table 5-6. Damage states exceedance probability corresponding to each hurricane-induced hazard for the exposed buildings on the coastal line of the State of North Carolina................. 193
Table 5-7. Assigned damage states corresponding to each hurricane-induced hazard for the exposed buildings on the coastal line of North Carolina based on Hurricane Florence (2018) . 194
Table 5-8. Calculated losses for the impacted buildings in North Carolina in terms of structural, content, and total losses based on Hurricane Florence (2018).. 194

LIST OF FIGURES

Figure 1-1. Most expensive Hurricanes in the United States as of April 2020, by insured property losses 2
Figure 1-2. A schematic representation of the risk components 3
Figure 1-3. Hurricane disaster dimensions including physical damage, and socio-economic disruption 5
Figure 1-4. A flow chart showing the major steps to determine flood risk on community level . 19
Figure 1-5. An elevated building using solid walls foundation (picture taken from Princeville, NC for an elevated building on the banks of Tar River) Photo taken by Omar Nofal, 2020 25
Figure 1-6. The main components associated with the risk, resilience, and recovery analyses for the hurricane-induced hazards 33
Figure 2-1. A schematic representation of the methodology that has been applied in this research to account for fragility and loss curves/surfaces for a portfolio of minimal building archetype .. 43
Figure 2-2. Damaging water depth truncated normal distribution with respect to the normal and uniform distributions: (a) External AC unit; (b) Electrical outlet 46
Figure 2-3. Flow chart illustrating the methodology to develop single-variable and multi-variate flood fragility function for each component within the building where N_com = number of components, N_de = Number of depth steps, N_sim = number of simulations, N_dur = number of duration steps, D(x) = demand flood depth, and R = component resistant flood depth 47
Figure 2-4. Components and building fragility functions: (a) Component fragility curves for DS4 components along with their failure probability at flood depth = 3.0m; (b) Fitted (Solid lines) and non-fitted (dashed lines) building fragility curves 49
Figure 2-5. A flow chart illustrates a methodology to develop a single-variable and a multivariate flood fragility function for buildings 50
Figure 2-6. A truncated normal distribution with maximum, minimum, and average cost of painting a home (Home-Advisor, 2019) 53
Figure 2-7. A schematic illustration of the approaches used to develop flood fragility and loss functions 55
Figure 2-8. A flow chart illustrates a methodology to develop a single-variable and a multivariate flood loss function for buildings where N_com = number of components, N_de = Number of depth steps, N_sim = number of simulations, and N_dur = number of duration steps 56
Figure 2-9. Building archetype layout; (a) Plan view; (b) 3-D view; (c) Front view; (d) Side view 58
Figure 2-10. Visual representation of the building archetype interior design and some of its components 58
Figure 2-11. Truncated normal distribution for the wood flooring component with respect to the normal and uniform distributions: (a) Flood depth resistance; (b) Flood duration resistance 60
Figure 2-12. Components fragility curves for all the 65 components with six highlighted components for illustration 62

Figure 2-13. Building fragility curves function in the flood depth measured from the ground elevation 63
Figure 2-14. Components loss curves for the six-selected components for illustration 64
Figure 2-15. Building loss function for the multiple loss methods in the flood depth measured from the ground elevation 65
Figure 2-16. HAZUS total building loss percentage and their subassemblies loss percentages (FEMA, 2009a): (a) Relationship between subassembly loss and the total building loss; (b) RES1: a single family residential building 67
Figure 2-17. 3D flood fragility surfaces for six selected components in terms of flood depth and duration: (a) AC unit; (b) Wood framing 68
Figure 2-18. 3-D flood fragility surfaces for the whole building in terms of flood depth and duration: (a) All building fragility curves; (b) Fragility curve for DS0; (c) Fragility curve for DS1; (d) Fragility curve for DS2; (e) Fragility curve for DS3; (f) Fragility curve for DS4 69
Figure 2-19. Flood loss surface: (a) 3D flood loss surface for the whole building in terms of flood depth and duration; (b) The projection of the 2D flood loss curves on the 3D flood loss curves 71
Figure 2-20. Schematic representation of the 15 building archetypes portfolio to model a community 72
Figure 2-21. Building archetypes fragility curves: (a) DS0; (b) DS1; (c) DS2; (d) DS3; (e) DS481
Figure 2-22. Building archetypes normalized loss curves: (a) Loss curves using direct loss approach (M1); (b) Loss curves using fragility-based approach (M2) 82
Figure 3-1. An example of a flooded inland community with building overlaid with the developed hazard layer and the buildings are color-coded based on their archetype 88
Figure 3-2. A schematic representation of the community model based on a combined BIM and GIS Model: (a) A Google Earth image showing 3-D buildings for a select neighborhood ; (b and c) A general BIM models for a school and church, respectively; (d) A GIS model for the for the same neighborhood 91
Figure 3-3. A schematic representation of the flood risk (probability of occurrence of damage/loss) modeling framework developed in this dissertation to compute probabilistic damage/losses at the community level 93
Figure 3-4. Community-level flood fragility and loss analysis framework (Lj = replacement/repair cost of each DS, P_DS = the exceedance probability of a DS, P_in_DS = the probability of being in a DS) 94
Figure 3-5. A schematic representation of the proposed hurricane multi-hazard vulnerability model 96
Figure 3-6. Wind simulation based on the 2018 Hurricane Florence: (a) Maximum wind speed contours and vectors (m/s); (b) Close-up view on the maximum winds at North Carolina; (c) The National Weather Services tracking of the 2018 Hurricane Florence (NWS, 2018) 98
Figure 3-7. A schematic representation shows the different building components including structural and non-structural components along with interior contents 101
Figure 3-8. A schematic representation shows the different vulnerabilities of the building components to hurricane-induced hazards 102
Figure 3-9. A schematic representation shows how a portfolio of builing archetypes are mapped to buildings within a community based on detailed building data 106

Figure 3-10. A schematic representation of the hurricane risk components and their associated hazard, exposure, and vulnerability models with the example of North Carolina State, USA... 108
Figure 3-11. A detailed framework for the community-level multi-hazard hurricane risk assessment model that accounts for building damage and losses 112
Figure 4-1. A schematic representation of the different levels of data needed for loss/damage analysis, and mitigation analysis... 115
Figure 4-2. A comparison between the state flooding for a business in Lumberton, NC during the recent rainfall storms after Hurricane Matthew in 2016 and Hurricane Florence 2018: (a) State of flooding after Hurricane Matthew in 2016; (b) State of flooding after Hurricane Florence in 2018; (c) Drone image for the business after Hurricane Florence in 2018 showing the used flood barrier system.. 117
Figure 4-3. A flow chart illustrates a methodology to develop a single-variable and a multivariate flood loss and fragility functions for flood protected buildings where H_b = barrier height, N_com = number of components, N_de = Number of depth steps, N_sim = number of simulations, N_dur = number of duration steps, Fr_k = the component fragility, and Fr_{DSi} = The exceedance probability of a DS_i 119
Figure 4-4. Fragility and loss functions with and without flood barrier with a height of 1.0m for a one-story multi-family residential building: (a) Fragility curves without using a flood barrier; (b) Fragility curves with the 1.0m flood barrier; (c) Total building loss curve without a flood barrier; (d) Total building loss curve with the 1.0m flood barrier... 121
Figure 4-5. A comparison between the flooding at the levee in Lumberton, NC during the recent rainfall storms resulting from Hurricane Matthew in 2016 and Hurricane Florence in 2018 along with the pump locations: (a) The flooding after Hurricane Matthew in 2016; (b) The flooding after Hurricane Florence in 2018; (c) Drone image for the levee following Hurricane Florence in 2018 showing the location of the mega pumps... 123
Figure 4-6. Example flood loss curves for a number of flood duration scenarios for a one-story residential building: (a) 3-D flood loss surface; (b) Flood loss curves associated with each flood duration scenario.. 124
Figure 4-7. Example flood fragility curves for a number of flood duration scenarios for a one-story residential building: (a) 3-D flood fragility surfaces; (b,c,d,e, and f) Flood fragility curves associated with each flood duration scenario of 1 day, 2 days, 6 days, 8 days, and 10 days, respectively 125
Figure 4-8. The combined impact of using flood barriers and pumps simltinously on the flood vulnerability 126
Figure 4-9. A schematic representation of resilient building construction in terms of implementing a number of building-level flood mitigation and adaptation measures after Dhonau, and Rose (Dhonau and Rose, 2016) 128
Figure 4-10. Comparison between flood losses for building archetype F2 before and after elevating the select components: (a) State of flood losses at a number of flood duration scenarios before and after elevating the select components; (b) State of flood losses at 10 days flood duration before and after elevating the select components.. 130
Figure 4-11. A schematic flow chart showing the high-resolution community-level mitigation analysis framework and its different levels of analyses.. 131

Figure 4- 12. A flowchart showing a detailed framework to apply the buyout and increasing building elevation based on the flooded buildings damage state 136
Figure 5-1. The spatial location of Lumberton city with respect to the Robeson County and North Carolina State along with its physical boundary and building locations 138
Figure 5-2. Hurricane Matthew in 2016 path and the category evolving over the time 139
Figure 5-3. Hurricane Matthew flood inundation depth: (a) Flood inundation depth developed by Nofal and van de Lindt (2019); (b) Flood inundation depth developed by FEMA (2019) 140
Figure 5-4. NOAA maximum daily observed precipitation at Lumberton in inches: (a) Maximum rainfall from Hurricane Matthew; (b) Maximum rainfall from Hurricane Florence 141
Figure 5-5. Observed gage data at Lumber River near Maxton, NC due to Hurricane Matthew and Hurricane Florence: (a) Observed discharge; (b) Observed height 142
Figure 5-6. Observed gage data at Lumber River near Lumberton, NC due to Hurricane Matthew and Hurricane Florence: (a) Observed discharge; (b) Observed height 142
Figure 5-7. The location of the main streams, USGS stream gauges, and NOAA rainfall gages with respect to physical boundaries of Lumberton, NC 143
Figure 5-8. The observed discharge and water height at the USGS stream gauges: (a) Observed discharge and river height at Lumber River near Maxton; (b) Observed discharge and river height at Lumber River near Lumberton 144
Figure 5-9. Hydrologic study results at the major streams within the Lumberton area: (a) Observed vs calculated discharge for Lumber River near Maxton; (b) Observed vs calculated discharge for Lumber River near Lumberton; (c) Calculated discharge in the Red Springs stream; (d) Catchments location in and around Lumberton 145
Figure 5-11. Evolution of flooding after Hurricane Matthew in 2016 in Lumberton, NC: (a) Flood hazard map showing the state of flooding for all community; (b) Flood water flowing from the underpass; (c) The state of flooding at underpass and levee; (d) Flood water before approaching the residential area; (e) Maximum Flooding 146
Figure 5-10. Flood inundation depth (m) from Hurricane Matthew vs. FEMA flood insurance rate map (FIRM): (a) Flood inundation depth (m) from Hurricane Matthew; (b) FEMA flood rate map (FIRM) 146
Figure 5-12. The spatial location of the exposed buildings color-coded based on their archetype 147
Figure 5-13. Damage and losses to the exposed buildings: (a) Color-coded buildings based on fragility-based DS; (b) Color-coded buildings based on buildings loss percentage 151
Figure 5-14. A flow diagram showing the hierarchy of the 330 building-level mitigation scenarios including six mitigation techniques and five mitigation scenarios for each technique which are applied to 11 buildings groups based on randomly selected buildings percentages (E3 is the mitigation scenario that includes elevating select water-sensitive components listed in Table 4-1 for residential buildings only 153
Figure 5-15. Comparison between the state of community-level flood losses for different groups of buildings using a number of mitigation scenarios for different mitigation scenarios 157
Figure 5-16. The spatial distribution of flood losses across the community after using a number of mitigation measures: (a) Color-coded map for the baseline flood losses for buildings in the flood plain; (b) Color-coded buildings based on baseline flood losses for a select neighborhood;

(c) The state of flood losses for same neighborhood after using a 1.0m height flood barrier system; (d) The state of flood losses for same neighborhood after using Pumps with 1 day flood duration; (e) The state of flood losses for same neighborhood after using 1.0m flood barrier, pumps with 1.0 day flood duration, and elevating the select water-sensitive components 159
Figure 5-17. Lumberton topography with rivers and hydraulic structures: (a) Rivers/streams and hydraulic structures spatial location with respect to Lumberton; (b) Close-up view on the levee location; (c) Close up view at underpass location (at the intersection of I-95 with CSX railroad) 160
Figure 5-18. A comparison between the flooding at the underpass during recent rainfall storms after Hurricane Matthew 2016 and Hurricane Florence 2018: (a) Flooding at the underpass due to Hurricane Matthew 2016; (b) Flooding at the underpass due to Hurricane Florence 2018; (c) The city efforts to build a temporary berm before Hurricane Florence 2018; (d) The temporary berm in the wake of Hurricane Florence 2018; (e) A close-up view of the first line of the berm along with the pump; (f) A close-up view on the second line of the berm 162
Figure 5-19. A map shows the proposed locations of some of the hazard mitigation measures: (a) General view; (b) Retention pond; (c) Enhancing of the road embankments; (d) Flood gate 163
Figure 5-20. Flood hazard map after using the proposed levee enhancement along with the location of the protected buildings: (a) Flood hazard map with enhanced levee system (b) Embankment profile for segment (1) before and after enhancement; (c) Embankment profile for segment (2) before and after enhancement; (d) Embankment profile for segment (3) before and after enhancement 166
Figure 5-21. Evolution of Hurricane Matthew 2016 flooding in Lumberton, NC along with using flood gates at the underpass location: (a) Flood hazard map showing the state of flood depth (m) with flood gates; (b) and (c) Water accumulation behind levees; (c) Flood water before approaching the residential area; (d) Maximum Flooding 167
Figure 5-22. Flood hazard map with the flood extent for different scenarios of levee enhancement: (a) Scenario 0; (b) Scenario 2; (c) Scenario 3; (d) Scenario 4; (e) Scenario 5; (f) Scenario 6........ 169
Figure 5-23. Flood inundation map after applying different sizes and locations of retention ponds: (a) Scenario 7; (b) Scenario 8; (c) Scenario 10; (d) Scenario 11; (f) Scenario 12; (f) Scenario 13........ 171
Figure 5-24. Mitigation analysis results in terms of damage and losses corresponding to each one of the 28 mitigation scenarios: (a) Mitigation scenarios (0-6); (b) Mitigation scenarios (7-13); (c) Mitigation scenarios (14-20); (d) Mitigation scenarios (21-28) 178
Figure 5-25. The spatial distribution of buildings damage states corresponding to some select hazard mitigation scenarios: (a) Mitigation scenario (0); (b) Mitigation scenario (4); (c) Mitigation scenario (5); (d) Mitigation scenario (10); (e) Mitigation scenario (13)........ 179
Figure 5-26. IN-CORE components 180
Figure 5-27. IN-CORE website [https://incore.ncsa.illinois.edu/DFR3Viewer] 182
Figure 5-28. IN-CORE website [https://incore.ncsa.illinois.edu/DataViewer] 183
Figure 5-29. (a) A schematic representation of the geographical location of the State of North Carolina with respect to USA along with the spatial location of the buildings within NC; A close-

up view on a neighborhood on the bank of the Cape Fear River with color-coded buildings based on (b) The 15 flood archetypes; (c) The 19 wind archetypes 185
Figure 5-30. Hurricane Florence in 2018 path and the category evolving over the time 186
Figure 5-31. Hazard maps for the hazards induced by the 2018 Hurricane Florence: (a) Wind hazard map (m/s); (b) Surge hazard map (m); (c) Wave hazard map (m) 187
Figure 5-32. The different exposed zones to hurricane-induced hazards for the state of North Carolina corresponding to the 2018 Hurricane Florence 189
Figure 5-33. Example of the archetypes assignment to each building within the community based on each mapped building archetype: (a) A Google earth close-up view on Carolina Beach, NC; (b) Color-coded buildings based on the 15 flood archetypes; (c) Color-coded buildings based on the 19 wind archetypes 191
Figure 5-34. The surge map overlaid with the community model for Carolina Beach (Coastal Community in North Carolina) 191
Figure 5-35. The damage state for the exposed buildings on some selected locations on the coastal line of the State of North Carolina due to the 2018 Hurricane Florence: (a) The exposed buildings location; (b) A close-up view on the east bank of the Pamlico River; (c) A close-up view on the wind impacted locations; (d) Color-coded buildings based on content damage; (d) Color-coded buildings based on content damage; (d) Color-coded buildings based on structural damage; (d) Color-coded buildings based on total damage 196
Figure 5-36. The loss analysis results for the exposed buildings in Washington, NC due to the Hurricane Florence (2018): (a) Color-coded buildings based on content losses; (b) Color-coded buildings based on structural losses; (c) Color-coded buildings based on total losses; (d) Color-coded buildings based on building damage 197
Figure 5-37. The spatial location of Waveland city within Mississippi State 198
Figure 5-38. Hurricane Katrina in 2005 path and the category evolving over the time 199
Figure 5-39. Hazard maps for the multiple hazards driven by Hurricane Katrina 2005: (a) Maximum significant wave height (H_s_max (m)); (b) Maximum water level (surge) height (d_s_max (m)); (c) Maximum current speed (V_c_max (m/s)); (d) Maximum wind speed (V_w_max (m/s)) 200
Figure 5-40. Color-coded map based on the building flood archetypes 201
Figure 5- 41. A schematic representation of the community-level hurricane multi-hazard risk analysis framework 203
Figure 5-42. Color-coded map for the spatial distribution of damage/loss across the example community: (a) Building DS; (b) Building loss ratio 204

CHAPTER 1: INTRODUCTION

1.1 Background

Hurricanes drive multiple types of loading on coastal and inland communities including strong winds, storm surge, waves, and debris. Additionally, the torrential rains induced by decaying hurricanes drive fluvial (riverine) and pluvial (rainfall) flooding for inland communities. Therefore, both coastal and inland communities are usually subjected to a series of events during the lifecycle of hurricanes starting from evacuation (Dow and Cutter, 2002; Lindell, Lu, and Prater, 2005), infrastructure devastation (Leavitt and Kiefer, 2006), businesses disruption (Resurreccion and Santos, 2013; Sydnor, Niehm, Lee, Marshall, and Schrank, 2017), building damage (Q. Li, Wang, and Zhang, 2016; Van Verseveld, Van Dongeren, Plant, Jäger, and Den Heijer, 2015), business disruption (Sydnor et al., 2017), need for temporary shelters (Nigg, Barnshaw, and Torres, 2006), and temporary and sometimes permanent relocation (Baker et al., 2009; Hori and Schafer, 2010). Figure 1-1 shows the most costly hurricane disasters in the U.S. as of April 2020, by insured property losses (Statista, 2020). It shows that many of the costly hurricanes occurred over the last 10 years which underscores the likely role of climate change (Dinan, 2017) in terms of the severity and frequency of these hurricane events along with the accelerating urbanization (Hemmati, Ellingwood, and Mahmoud, 2020). Hurricanes are multi-hazard events and modeling each one of these hazards and its associated vulnerability is a complex process and requires multiple scientific backgrounds. Additionally, the spatio-temporal variation of the hurricane-induced hazards along with their diverse impacts on humans, buildings, and infrastructure made it very challenging to develop a multi-hazard risk and post-hazard functionality model.

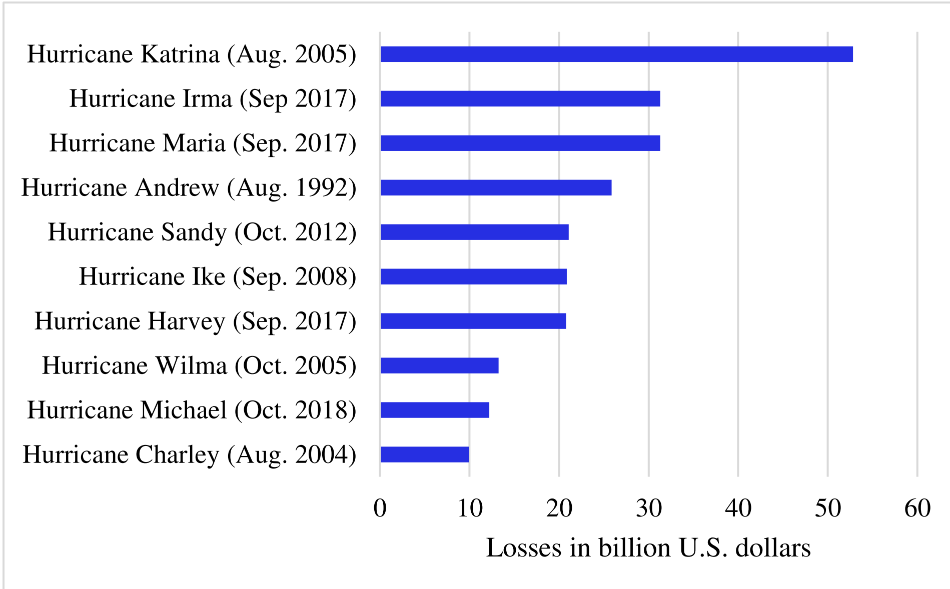

Figure 1-1. *Most expensive Hurricanes in the United States as of April 2020, by insured property losses*

Hurricane-induced winds can cause severe damage to buildings. However, storm surge is considered the most destructive and life-threatening loading and can collapse buildings, particularly when waves are present (Tomiczek, Kennedy, and Rogers, 2014). The impact of each hazard can vary significantly along the coastline. Although buildings at the coastline are vulnerable to wind, waves, and storm surge, the majority of the damage to these buildings is due to the hydrodynamic impacts of combined surge and waves. The hydrodynamic impacts dissipate rapidly as the water moves inland and the storm surge behaves more like inland flooding (coastal flooding) with buildings more vulnerable to the combined impacts of wind and flooding. A few kilometers from the shore, depending on the topography, flood impacts are minor with the wind hazard becoming the dominant loading. The uncertainties associated with hurricane damage assessment and the different hazards responsible for this damage along with the data scarcity pose many challenges to the development of multi-hazard hurricane risk and post-hazard functionality models for buildings and infrastructure. Previous studies have focused primarily on modeling the hurricane-induced hazards individually with less focus on the multi-hazard impact to the whole building system. Additionally, the analysis resolution used in these studies did not allow large-scale hurricane risk assessment through an individual assembly of building risk. In general, the risk is comprised of three major components, namely hazard, exposure, and vulnerability as shown in the schematic in Figure 1-2. Therefore, a high-resolution hurricane risk model requires high-resolution hazards, exposure, and vulnerability models.

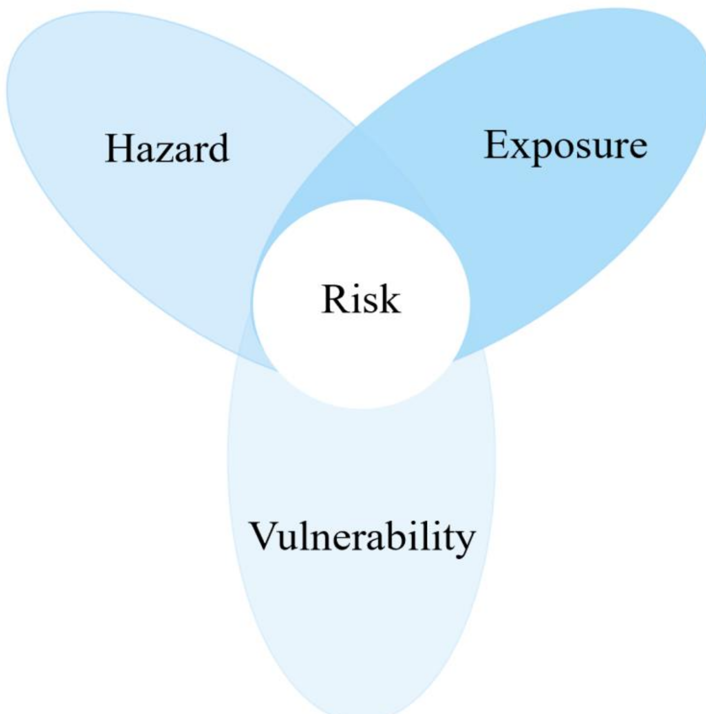

Figure 1-2. *A schematic representation of the risk components*

Additionally, component-based surge vulnerability analysis was conducted to develop fragility functions based on buildings and storm surge parameters (Hatzikyriakou et al., 2016). Combined wind, rainwater intrusion, and storm surge loss analysis was investigated by a number of researchers using assembly-based vulnerability methods (Y. Li, van de Lindt, Dao, Bjarnadottir, and Ahuja, 2012; Park, John W. van de Lindt, and Yue Li, 2014; Park, van de Lindt, and Li, 2013) and using other probabilistic methods (Baradaranshoraka, Pinelli, Gurley, Peng, and Zhao, 2017). The impact of combined waves and storm surge was also investigated in terms of hazard modeling (J C Dietrich et al., 2011) and loss estimation (Do, van de Lindt, and Cox, 2020; Tomiczek et al., 2017, 2014). There are also a number of multi-hazard models that account for the combined impacts of wind, wave, and surge on buildings with the goal of developing fragility functions for wood-frame structures (Masoomi, van de Lindt, Ameri, Do, and Webb, 2019) and introducing performance-based hurricane engineering (Barbato, Petrini, Unnikrishnan, and Ciampoli, 2013; McCullough, Kareem, Donahue, and Westerink, 2013).

The widespread torrential rains driven by hurricanes cause massive flooding, and sometimes flash flooding, in inland communities far away from the shoreline. The flooding part of hurricanes, on average, is the costliest component and can result in fatalities and often destroy a substantial portion of a communities' infrastructure. Flooding not only directly impacts the physical infrastructure but also affects the socio-economic systems supported by the physical infrastructure within the flooded community (Rufat et al., 2015). Figure 1-3 shows the hurricane disaster dimensions (physical, social, and economic dimensions) with real images from flooding events following major hurricanes. Each one of these dimensions has its own risk components (hazard, exposure, and vulnerability). Flooding is considered one of the most impactful hurricane-induced hazards with substantial consequences to the built environment. Therefore, flood hazards in terms of fluvial (Feyen, Dankers, Bódis, Salamon, and Barredo, 2012; Bruno Merz, Hall, Disse, and Schumann, 2010) and pluvial flooding (Blanc et al., 2012) have been investigated by researchers over the years to quantify flood hazard for the exposed communities. The past and current body of flood research provide a host of alternatives to account for flood risk and vulnerability (Harris, Dunn, and Deering, 2010; Lamb et al., 2010; Nasiri, Yusof, and Ali, 2016; Salman, Asce, Li, and

Asce, 2018; Ten Veldhuis and Clemens, 2010; Wobus, Lawson, Jones, Smith, and Martinich, 2014). Additionally, flood loss analyses research worldwide over the last decade (Dutta, Herath, and Musiake, 2003; Scawthorn et al., 2006; van Manen and Brinkhuis, 2005) has been pursued.

Figure 1-3. *Hurricane disaster dimensions including physical damage, and socio-economic disruption*

Current flood loss assessment methods rely primarily on deterministic approaches using damage functions (Aimilia Pistrika, Tsakiris, and Nalbantis, 2014) which makes it a challenge to propagate uncertainties in flood damage and loss models (Handmer, 2002). The flood risk analysis process is uncertain (Heiko Apel et al., 2010) with levels of complexity (H. Apel, Aronica, Kreibich, and Thieken, 2009). Further, the accuracy of the flood loss calculation process is a function of the availability of high-resolution flood data, specifically the level of detail in this data (H. Apel et al., 2009; Molinari and Scorzini, 2017). Flood risk is comprised of the three major components shown in Fig. (2), namely hazard, exposure, and vulnerability. Each one of these components is accompanied by a number of uncertainties from different sources that should be investigated and propagated to conduct risk-informed decision analyses and ultimately better prepare communities for future flood events(O.M. Nofal and van de Lindt, 2020).

1.1.1 Hurricane Hazard

The hazard is the probability that a hurricane-induced load with a certain intensity (e.g., wind speed, surge height, wave, height, etc.) occurs in a particular location with a certain frequency and magnitude. Coastal communities are exposed to different hurricane-induced hazards including surge, wave, and wind that cause different types of damage to the building structural and non-structural components along as well as the interior contents. A number of researchers have developed hurricane wind hazard models (Guo and van de Lindt, 2019; Vickery, Masters, Powell, and Wadhera, 2009). Several wind-borne debris trajectory models were also developed (M. Grayson, Pang, and Schiff, 2012; Huang, Wang, Fu, and Gu, 2016; Richards, Williams, Laing, McCarty, and Pond, 2008). Over the last several decades, researchers developed a number of wind-induced storm surge models including Sea, Lake, and the Overland Surges from Hurricanes (SLOSH) model (Jelesnianski, 1992) and the ADvanced CIRCulation model (ADCIRC), and the Simulating WAves Nearshore (SWAN) model (Westerink, Luettich Jr, Blain, and Scheffner, 1994) along with other physics-based storm surge models (Contento, Xu, and Gardoni, 2020; Irish, Resio, and Cialone, 2009; Irish, Resio, and Ratcliff, 2008; N. Lin, Emanuel, Smith, and Vanmarcke, 2010; Resio, Irish, and Cialone, 2009).

Flood hazard mapping for inland communities impacted by the rainfall from decaying hurricanes has received significant attention over the last several decades. This is because of climate change which has altered the flood intensity and frequency (e.g., Davies & Jones, 2009; Hirabayashi et al., 2013; Kleinen, Thomas, & Petschel-held, 2007; Milly et al., 2002). Flood hazard is usually distinguished by its characteristics, which are often termed as intensity parameters, that have an effect on physical infrastructure with the most prevalent being depth, velocity, duration, and debris. The importance of each flood hazard characteristic depends on the topography and the type of flooding that occurs in the study area. However, by and large, flood inundation depth is considered the best predictor of flood damage and thus the best predictor of flood loss estimation (HAZUS-MH, 2008; Scawthorn et al., 2006). Therefore, traditional flood loss models are based on flood depth which is usually expressed in terms of stage-damage functions (Bouwer et al., 2009; H De Moel & Aerts, 2015; Aimilia Pistrika, Tsakiris, & Nalbantis, 2014; Scawthorn et al., 2006; Scorzini & Frank, 2017; Smith, 1994; Thieken et al., 2008).

Flood velocity is also another intensity parameter that should be considered in the case of steep terrain or dikes and levees breaches. The water velocity results in significant additional pressure beyond the static water pressure resulting in additional damage (Kelman and Spence, 2004). Further, higher lateral loads and water going around the structure can result in scour causing additional damage (e.g., Kreibich et al. 2009). For accurate flood damage estimation in steeper terrain and coastal flooding driven by hurricanes and tsunamis, it is better to concurrently account for the combination of depth and velocity damage functions (Attary et al, 2019; R. D. Black, 1975; Dale et al., 2004). Additionally, flood duration is another important flood inundation characteristic in the case of polders in low-lying land areas with less permeable soil. Therefore, incorporating the flood duration data in stage-damage functions allows more accurate quantification of flood losses as detailed information about the affected components is used in the flood loss model. Furthermore, the amount of debris carried by the water is also considered an important flood hazard characteristic which typically increases as the floodwater velocity increases. Flood debris can be significant in the case of a floodwall breach, very steep terrain, and high-velocity coastal flooding such as a tsunami or surge combined with waves during a hurricane.

1.1.2 Hurricane Exposure

Exposure is defined as the people and physical assets within the community that are exposed to the hurricane-induced hazard and may be subjected to potential losses. Buildings in a coastal community are mainly exposed to surge, wave, and wind hazards but with different intensities based on building location and elevation. For inland communities, buildings are exposed mainly to flooding only due to the overflow of the rivers and main tributary streams or heavy rainfall. The exposure information is available in different forms such as population distribution maps, building information according to their location such as parcel data, and land use maps. There are many resolution levels for the exposure information ranging from single building exposure level to census block level. Often, researchers conduct exposure analysis using census block data (Scawthorn et al., 2006) and land use data (De Moel et al., 2011) because of flood-related data scarcity, but less information is available at the building (or tax lot) level. Individual building exposure information is the most accurate way to perform a flood damage assessment, but it requires significant effort to obtain or collect building data. Hurricane losses are a direct function of the value of the community assets including the number of people and the property exposed to flood hazard. As communities grow and there is increased development in hazard-prone areas, the potential for flood losses increases making hazard mitigation plans for flooding in these areas even more critical. Currently, in community resilience modeling, there is a critical demand for building-level data to enable capturing more accurate flood losses rather than higher aggregation levels such as census blocks.

1.1.3 Hurricane Vulnerability

The definition of vulnerability varies depending on discipline (e.g., social science, economics, engineering, etc.) and, to some degree, the audience such as policymakers, stakeholders, industry, response agencies, or engineers (Adger, 2006; Alexander, 2002; Borden, Schmidtlein, Emrich, Walter W. Piegorsch, and Cutter, 2007; Cannon, 1994; Ii et al., 2003; Liebow, 1996; Mileti, 1999; Næss, Norland, Lafferty, and Aall, 2006; Scira Menoni and Pergalani, 1996; Tsakiris, 2014). Characterizing hurricane vulnerability is a multi-hazard dynamic and complex process that changes over time (e.g., hazard frequency and intensity) and space (e.g., location and conditions of the physical infrastructure within a community). A comprehensive review of vulnerability definitions was developed by (Nasiri et al., 2016). Hurricane vulnerability is generally characterized as a function that describes the relationship between hurricane-induced hazard characteristics (e.g., wind speed, surge height, and wave height) with the potential to cause physical and non-physical damage to the building components, infrastructure system, or the entire community. The classification of the exposed infrastructure within a community at risk is needed to estimate the hurricane damage and each component could have its own vulnerability curve (Bruno Merz et al., 2010).

There are different ways to describe community vulnerability depending on the available vulnerability functions and community information. For example, in the case of land use data, the vulnerability curve for each land-use class could be used or developed to estimate the damage based on the land cover class (Budiyono, Aerts, Brinkman, Marfai, and Ward, 2015; Yi, Lee, and Shim, 2010). However, in the case of buildings, a vulnerability curve for each building type (e.g., occupancy) can be used to estimate the damage at the building level (Middelmann-Fernandes, 2010) and then aggregated from building level to a community level. Both qualitative and quantitative flood vulnerability assessment methods have been developed for social, economic, and physical infrastructure with the goal of determining which community components and institutions have greater vulnerability to a hurricane-induced hazard (Balica, Douben, and Wright, 2009; Barnett, Lambert, and Fry, 2008; Hinkel, 2011; Myers, Slack, and Singelmann, 2008; Tesliuc and Lindert, 2002; Török, 2018; Zoraster, 2010). Vulnerability functions are classified into deterministic and probabilistic approaches according to the inclusion of the uncertainty within each approach. Deterministic vulnerability functions represent a relationship between the intensity of a certain hazard characteristic (wind speed, flood depth, flood velocity, flood duration, and debris volume) and the corresponding expected damage as a percentage of the building market value.

Many studies investigated vulnerability models for hurricane-induced hazards which have been reviewed by Pita et al. (G. Pita, Pinelli, Gurley, and Mitrani-Reiser, 2015). These vulnerability models included developing probabilistic methods (i.e., fragility) (Do et al., 2020; Masoomi et al., 2019; Tomiczek et al., 2014) which enable uncertainty propagation through vulnerability models. A number of researchers have investigated the wind vulnerability driven by hurricanes (He, Pan, and Cai, 2017; G. L. Pita, Pinelli, Gurley, Weekes, and Mitrani-Reiser, 2011). Combined wind and wind-borne debris damage models were also developed by researchers over the last decade (Chung Yau, Lin, and Vanmarcke, 2011; J. M. Grayson, Pang, and Schiff, 2013; Wills, Lee, and Wyatt, 2002). Additionally, a component-based surge vulnerability analysis has been pursued to develop fragility functions based on buildings and storm surge parameters (Hatzikyriakou et al., 2016). The joint impact of wind and storm surge induced by hurricanes has been investigated using stochastic hurricane models (Bushra, Trepanier, and Rohli, 2019; Pei, Pang, Testik, and Ravichandran, 2013; Pei, Pang, Testik, Ravichandran, and Liu, 2014; Unnikrishnan and Barbato, 2017). Additionally, combined wind, rainwater intrusion, and storm surge loss analysis was investigated by several researchers using assembly-based vulnerability methods (Y. Li et al., 2012; Park et al., 2014, 2013) and other probabilistic methods (Baradaranshoraka et al., 2017). The impact of combined waves and storm surge was also investigated with a focus on vulnerability models (Do et al., 2020; Tomiczek et al., 2017, 2014). Several multi-hazard models were developed to account for the combined impacts of wind, wave, and storm surge on buildings to develop fragility functions for wood-frame structures (Masoomi et al., 2019; Massarra, Friedland, Marx, and Dietrich, 2019; Van Verseveld et al., 2015), and performance-based hurricane engineering models (Barbato et al., 2013; McCullough et al., 2013).

This significant body of literature showed that probabilistic vulnerability models for hurricane-induced hazards were the focus of the literature over the last two decades (Abdelhady, Spence, and McCormick, 2020; Do et al., 2020; Henderson and Ginger, 2007; Kakareko, Jung, Mishra, and Vanli, 2020; Khajwal and Noshadravan, 2020; Y. Li and Ellingwood, 2006; Mishra, Vanli, Alduse, and Jung, 2017; Omar M. Nofal, 2020; Paleo-Torres et al., 2020; Pinelli et al., 2004; Wang, Zhang, Feng, and Li, 2017; Zhang, Lin, Wang, Nicholson, and Xue, 2018). Fragility functions were shown to be the most reliable probabilistic vulnerability functions that can inform probabilistic safety margins for buildings and systems (Ellingwood, Rosowsky, Li, and Kim, 2004; Omar M. Nofal and van de Lindt, 2020b; Rosowsky and Ellingwood, 2002). Li and Ellingwood (2006) developed a probabilistic framework using fragility functions to evaluate residential buildings subjected to hurricane-induced wind. Probabilistic hurricane wind vulnerability models were developed using a Bayesian capacity model to propagate uncertainties in the damage analysis (Kakareko et al., 2020; Mishra et al., 2017). Multi-hazard fragility-based hurricane damage models were also developed for combined hurricane storm surge and wave (Do et al., 2020; Masoomi et al., 2019). For community-level analysis, Abdelhady et al. (2018, 2019) investigated hurricane vulnerability and community resilience in the context of hurricane-induced hazards using a distributed computational platform. Additionally, the concept of vulnerability function portfolios was recently introduced in the literature to assess community-level performance (P. Lin and Wang, 2016; Zhang et al., 2018). This allowed for multiple portfolios to be developed across multiple hazards including wind (Memari et al., 2018) and flooding (Omar M. Nofal and van de Lindt, 2020b).

On the other hand, most of the currently available flood vulnerability models are based on stage-damage functions (damage curves) that use empirical data to account for flood losses at the building- and community-level (Budiyono et al., 2015; Middelmann-Fernandes, 2010; Aim Pistrika, 2010; Scawthorn et al., 2006), including the HAZUS flood model (FEMA, 2009a). This includes coastal, fluvial, and pluvial flood vulnerability models. In general, these functions are developed based on survey data and field studies (Crawford et al., 2021; Nascimento, Baptista, Silva, Machado, and Lima, 2006; A. K. Pistrika and Jonkman, 2010) that relate a certain amount of damage to a flood inundation depth after a specific flooding event. This approach possesses inherent uncertainties since the amount of damage is qualitatively estimated from the outside of buildings based on visual observation and the variability from one estimator to another contributes uncertainty to the estimation process (Downton, Miller, and Pielke Jr, 2005). Additionally, the impact of flood duration on damage/loss has not yet been included, which highlights the need for multi-variable flood loss functions.

Damage functions are broadly used in a range of research such as damage quantification and assessment. Flood depth is considered the best intensity measure in the case of hydrostatic flooding (hurricane surge without waves) with very low velocity (less than 1 m/sec). Table 1-1 presents some examples of studies that have adopted different flood damage characteristics using deterministic approaches. Developing damage functions depends on post-disaster damage surveys in which collected/modeled hazard intensity data is used along with their corresponding assessed damage. The damage quantification process is based on human observations that relate a certain amount of observed damage to its corresponding modeled (e.g., wind speed) or observed (e.g., surge height) hazard intensity without propagating any uncertainties during the observation process. There are other approaches to develop stage-damage functions such as using empirical curves based on historical data from flooded areas to relate the existing damage to the flood inundation depth of a certain event (e.g., B. Merz et al., 2004; Nascimento et al., 2006). The data used in this method is usually from field surveys and this method is often used by insurance adjusters (e.g. Messner, 2007). In addition, field studies can provide the data needed to develop numerical fragility curves or damage curves that relate inundation characteristics to the probability of exceeding a certain predefined level of damage were also developed by van de Lindt and Taggart using an assembly-based vulnerability function that accounts for the variability in construction quality and flood depth and flood duration resistance for a specific residential building (van de Lindt and Taggart, 2009). In a later study, van de Lindt et. al. used collected field data in terms of observed damage states (DSs) and measured flood depth to develop empirical flood fragilities (van de Lindt et al., 2018). These fragilities were compared with the HAZUS stage-damage functions in a community-level case study by Nofal and van de Lindt (Omar M Nofal and van de Lindt, 2020) and showed good results. Nadal et. al. also developed a loss function that accounts for the dual impact of flood depth and flood duration using a Monte Carlo framework (Nadal, Zapata, Pagán, López, and Agudelo, 2009).

Table 1-1. *Damage function examples for different flood damage characteristics*

Damage Function	Reference
Flood Depth	(Dottori, Figueiredo, Martina, Molinari, and Scorzini, 2016; Aimilia Pistrika et al., 2014; Romali, Yusop, and Ismail, 2015; Smith, 1994)
Flood Depth and Velocity	(Middelmann-Fernandes, 2010)
Flood Depth and Duration	(van de Lindt and Taggart, 2009)
Flood Debris	(Haehnel and Daly, 2004; M Jakob, Stein, and Ulmi, 2012; Matthias Jakob, Holm, Weatherly, Liu, and Ripley, 2013a)

The other common method is using synthetic flood data which is broadly known as a synthetic stage-damage function. Synthetic means functions developed for a standardized building according to its size, usage, occupancy, and inventory components (Deniz et al., 2017; Middelmann-Fernandes, 2010; Naumann et al., 2009; van de Lindt & Taggart, 2009), which are more recently referred to as archetype buildings. However, the basic methodology to build a numerically developed stage-damage function is to track the damage to each component within a building and then use the component damage to convert to losses according to the component contribution to the percentage of the total building replacement value. Examples of the depth at which different components within a residential building are damaged and what percentage they contribute to the building's overall loss can be found in van de Lindt and Taggart (2009). In recent years, advances to stage-damage functions were made to include more parameters, factors, and indicators such as flood depth, flood duration, building type, construction material, contamination, and the preparedness measures taken before the disaster (Nicholas, Holt, & Proverbs, 2001; Thieken et al., 2008; Thieken et al., 2005). Later, this method was referred as a multi-variate flood risk assessment which has been shown to clearly outperform univariate functions (B Merz, Kreibich, and Lall, 2013; Spekkers, Kok, Clemens, and Ten Veldhuis, 2014; Van Ootegem, Verhofstadt, Van Herck, and Creten, 2015)

A probabilistic vulnerability function which, as mentioned earlier, is also known as a fragility function represents a relation between a certain flood characteristic intensity (depth, velocity, duration, and debris) and its corresponding exceedance probability of a certain predefined damage state (DS). This approach is more complex and requires more statistical information about the hazard and the resistance of the exposed assets. Most of the past flood damage assessment studies have relied on stage-damage functions because of the flood-related data scarcity. However, there is still considerable inherent uncertainty in the modeling chain including the flood hazard data, the characteristics of the exposed community assets, and the susceptibility of these assets. Therefore, in community resilience modeling where the objective is often risk-informed decision guidance, improved models are needed to propagate uncertainties through the decision model. Recently, researchers tried to propagate uncertainties through flood risk components with more focus on the flood hazard mapping process to predict rainfall and stream discharges using different techniques such as nonlinear parameter estimation (Liu et al., 2005), generalized likelihood uncertainty estimation (GLUE) (Jung and Merwade, 2011), Monto Carlo simulations (Apel et al., 2010; Egorova, Noortwijk, & Holterman, 2010; De Moel, Asselman, & Aerts, 2012; De Moel, Bouwer, & Aerts, 2014), Bayesian forecasting (Bates et al., 2004; Krzysztofowicz, 1999) and other uncertainty propagation methods (Blazkova & Beven 2009; Freni, Loggia, & Notaro 2010; Merz & Thieken 2005, 2009; De Moel & Aerts 2011; Saint-Geours et al., 2015; Xu, Yueping, & Martijn J. Booij 2007). Additionally, the concept of probabilistic vulnerability functions using fragility methods has only been base touched by several researchers (De Risi et al., 2013; van de Lindt & Taggart, 2009; Vorogushyn et al., 2010). However, a more comprehensive study is still needed to develop a standardized suite of fragility functions to represent a minimum portfolio of building archetypes to enable better flood risk assessment at the community level.

1.1.4 Hurricane Risk Analysis

Risk analysis necessitates accounting for both hazards and consequences. Therefore, the risk is defined as the expected damages corresponding to the hazard intensity and its occurrence probability, the value of the exposed assets, and their location within the exposed area, and the vulnerability of these assets. Predicting hurricane risk is the first step to study the resilience of a community. Quantifying the expected amount of losses associated with this risk for each of the different community sectors will help define the scope of the recovery process. Hurricane losses are often classified into direct and indirect losses. Direct loss is the physical damage induced by the hurricane event due to objects such as buildings and contents and their contact with the hurricane-induced hazards within the exposed area. Indirect loss is derived from the disruptions to businesses, public services, and can lead to business interruption inside and outside the impacted area. Hurricane losses are further classified into tangible and intangible losses, depending on whether or not these losses can reasonably be evaluated in monetary terms or not. Tangible losses can be monetized but intangible losses are the damages that cannot be directly assessed in monetary terms. Table 1-2 presents a summary of the different classifications of the different types of losses with examples for each one.

Table 1-2. *Classifications for the different types of hurricane-induced losses*

Loss Type	Direct	Indirect
Tangible	Physical damage to the community assets in the impacted area: • Damage and disruption to the physical infrastructure (buildings, bridges, water supply systems, water treatment plants, wastewater treatment plants, railroads, electric power network, transportation network buildings, and their contents). • Businesses disruption or closure in the impacted area. • Damage to crops in agriculture areas and loss of soil due to water saturation.	Socio-economic impacts to the services outside the impacted area: • Business disruption or closure outside the impacted area. • Public services disruption outside the impacted area (transportation network, water supply network, bridges, railroads, facilities, and public utilities). • Closure of companies outside the impacted area. • The inflation rate increase due to economic losses, business disruption, and business closure.
Intangible	Physical impacts of hurricane on humans, ecosystem, and culture: • Human life losses, injuries, and psychological stresses. • Loss of ecological system. • Loss of cultural heritage such as (museums, old cities, and libraries)	Societal impacts of hurricanes outside the impacted are: • Long-term health effects. • Resident out-migration • Losing trust in government and/or authorities.

Multiple studies have investigated the hurricane-induced risk at the building- and community-level (M. Amini and Memari, 2020; Bertinelli, Mohan, and Strobl, 2016; C.-Y. Lin and Cha, 2020; Rey et al., 2019). A number of researchers have also investigated wind loads driven by hurricanes in terms of risk assessment and loss estimation (M. Amini and Memari, 2021a; Kakareko et al., 2020; Khajwal and Noshadravan, 2020; Y. Li and Ellingwood, 2006; Mishra et al., 2017; Scheitlin, Elsner, Lewers, Malmstadt, and Jagger, 2011; Vickery et al., 2006). The risk assessment of coastal flood hazards driven by hurricanes (e.g., surge) was also investigated (Johnson, Fischbach, and Ortiz, 2013; N. Lin and Shullman, 2017). The flood risk in terms of fluvial and pluvial flooding induced by hurricanes in the inland communities was investigated (Omar M Nofal and van de Lindt, 2020; Rözer et al., 2019; van de Lindt et al., 2018, 2020). Flood risk assessment efforts related to debris are also available (Fuchs et al., 2007; Jakob et al., 2013). Currently, there has not been a comprehensive attempt to quantify the relationship between damage and the amount of debris because of the large uncertainty in the debris content, volume, location, orientation, and flow modeling. Meanwhile, modeling the potential hurricane risk for a specific community provides stakeholders with information to evaluate future investment strategies in exposed areas at a community scale. This provides planners the ability to allocate community resources to reduce risk and improve resilience as a result of protection measures (Büchele et al., 2006).

Figure 1-4 provides a schematic representation of the flood risk assessment process and the sequence of overlaying each component within an analysis process. The flood risk analysis started with a hydrologic analysis of the study area by conducting analyses on the digital elevation map to extract basins characteristics within the study area and extract the needed parameters to be used as an input for the hydrologic analysis method. Then, the precipitation data were used along with the soil, land use, and the digital elevation map to account for the surface water runoff. Then, the resulting discharges in each stream/river were used as the boundary conditions for a hydrodynamic analysis to determine the flood water depth and velocity spatially over the location of interest. The resulting flood hazard map is then overlaid on the community exposure information to predict the flood hazard characteristics at each building. Finally, vulnerability functions in terms of fragility/damage curves are used to predict the state of damage for each building. Therefore, generally, the flood risk assessment process depends on three major phases which include flood hazard mapping by applying the principles of hydrologic and hydraulic analysis, flood exposure information through data collection and numerical modeling, and flood vulnerability analysis to include the susceptibility of the community infrastructure.

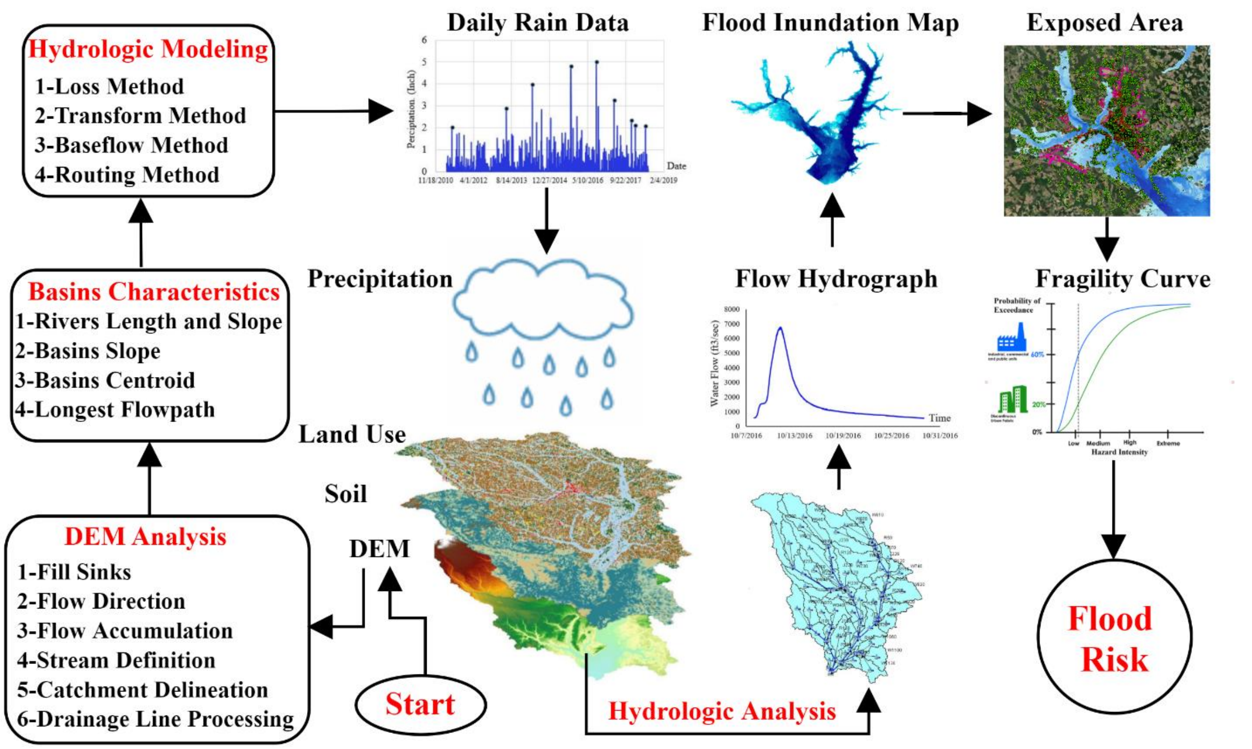

Figure 1-4. *A flow chart showing the major steps to determine flood risk on community level*

1.1.5 Hurricane Risk Mitigation

Hurricane mitigation measures are critical to enabling resilient communities, reduce future hurricane losses, and enable rapid recovery. In this context, it should be mentioned that hurricane risk mitigation differs from hurricane risk adaptation in terms of its objectives, techniques, strategies, and implementation. Hurricane risk mitigation strategies are defined, herein, as the measures, plans, and precautions that a community including stakeholders, public officials, and policymakers use to reduce the amount of hurricane risk (e.g. control the hazard intensity and frequency, decrease the community exposure including people and assets, decrease buildings vulnerability, etc.) which is consistent with the definition of the disaster risk mitigation by the IPCC-2012 (IPCC, 2012) in section 1.1.2.2 that include the reduction of the existing hazard, exposure, and vulnerability. Flood adaptation strategies are defined, herein, as the actions and implementations that a community uses including households, business owners, and social institutions to adapt to flood events (e.g. build barrier systems around properties, elevate appliances and furniture, allocation of pumps around critical assets/facilities, systematic evacuation, temporary shelter preparation, etc.) which is also consistent with the IPCC-2012 definition (IPCC, 2012) in section 1.1.2.2 that adaptation includes the adjustment of humans and the built environment to the increasing risk. There are different strategies to mitigate hurricane risk by controlling the risk components (hazard, exposure, and vulnerability) (Omar M. Nofal and van de Lindt, 2020a, 2021). The intensity of the flood hazard induced by hurricanes can be mitigated by building a seawall, a levee system, floodwalls, flood gates, flood retention/detention system, allocating mega-pump systems at critical locations, or any combination of these mitigation strategies. The amount of exposure to hurricane-induced hazards can be reduced by buying out a portion of the buildings in a floodplain (e.g., for severely flooding exposed areas). To reduce the vulnerability of buildings and infrastructure, some of the vulnerability reduction approaches can be part of the mitigation plans within a community (e.g. legalization of certain materials or techniques for construction), and others may be a part of the adaptation strategies for repetitive flood events (e.g., elevate the water-sensitive components or even elevate the whole building), underscoring that the mitigation strategies can, at times, overlap with the adaptation measures.

Communities differ in their ability to prepare and adapt over time, which is often related to their experience with past hurricanes. Risk mitigation studies and the development of standards over the last several decades investigated and recommended building-level (ABI, 2003; M. Amini and Memari, 2021b; Egli, 2002; FEMA, 2005; FEMA P-1037, 2015; Hayes, 2004; Holub and Fuchs, 2008; Heidi Kreibich, Christenberger, and Schwarze, 2011; Heidi Kreibich, Thieken, Petrow, Müller, and Merz, 2005; Lamond, Rose, Joseph, and Proverbs, 2016; Olfert and Schanze, 2009;

Proverbs and Lamond, 2017) and the community-level (Dierauer, Pinter, and Remo, 2012; Posner and Georgakakos, 2017; Remo, Carlson, and Pinter, 2012; Schanze, Zeman, and Marsalek, 2007; Wenger, 2015a, 2015b) flood mitigation measures. Additionally, building retrofitting to resist hurricane-induced wind (e.g., using hurricane clips, increase the number of nails, etc.) was investigated (Masoomi, Ameri, and van de Lindt, 2018). There are a number of building-level flood adaptation techniques which include water avoidance (Bowker, 2007b; Garrote, Bernal, Díez-Herrero, Martins, and Bodoque, 2019), water exclusion (Beddoes and Booth, 2015), and water entry (Fidler, Wood, Ridout, and Heritage, 2004) to name a few. However, the collective impact of some of these measures on the community is still unclear since accurate quantitative investigations that allow aggregation of building-level mitigation models to the community-level are few (Aerts et al., 2014; Aerts, Botzen, Moel, and Bowman, 2013; Hans De Moel, Vliet, and Aerts, 2014). A number of techniques such as expert judgment and practical studies (Bowker, 2007a; Egli, 2002; Glavovic, 2010; Thurston et al., 2008), and field/phone surveys (Bubeck, Botzen, Kreibich, and Aerts, 2013; Hudson, Botzen, Kreibich, Bubeck, and Aerts, 2014; Heidi Kreibich et al., 2005) have been pursued.

In terms of policy-based mitigation measures, there are a host of different processes related to the decision-making for risk and disaster management that occur at the federal, state, and local government levels. A large portion of funding for hazard mitigation and recovery comes from federal sources through different hazard mitigation programs (e.g., FEMA: the Hazard Mitigation Grant Program (FEMA, 2016a), BRIC: Building Resilient Infrastructure and Communities (FEMA, 2020), HUD: the CDGB-Disaster Recovery Program (HUD, 2020), the Small Business Association (SBA) (SBA, 2020), and the U.S. Department of Agriculture (USDA, 2020)). The local government plays a vital role in planning and protecting community infrastructure and assets located in the flood plain by establishing mitigation measures that can include reducing development in the flood plain to limit urbanization or to encourage certain construction practices in the flood plain. The state government intervenes when a disaster exceeds local government capacity (FEMA, 2009b) and can apply for federal grants for larger-scale events. There is some debate in the literature on how local, state, and federal governments are learning from past disasters and how policy is evolving and improving over time (Greer and Brokopp Binder, 2017; May, 1992, 1999). The decision of whether or not to implement a new policy, or which policy to implement, would benefit significantly from a quantitative tool that allows one to investigate pre- and post-disaster, short-term and long-term flood mitigation measures that measure the impact of implementing these different policies.

Investigating the impacts of policy changes that can be implemented within the floodplain requires a full realization of the hazard intensity and frequency, the exposures of buildings and human activity in the exposed areas, and reliable vulnerability functions that can capture the performance of the built environment. There are a large number of qualitative approaches (Brody, Zahran, Highfield, Bernhardt, and Vedlitz, 2009; Faisal, Kabir, and Nishat, 1999; Kourtis, Tsihrintzis, and Baltas, 2020; Montz and Gruntfest, 2002; Osberghaus, 2015; Paille, Reams, Argote, Lam, and Kirby, 2016) that assess community-level flood mitigation measures with less quantitative research. A quantitative analysis of the policy change impacts in the flood plain is a challenge since models that predict the probability of flood damage for buildings and other infrastructure, i.e. vulnerability models, are not widely available. Enabling policy decisions to mitigate flood risk using probabilistic vulnerability functions is the key to enabling resilient communities. There are a number of policy-based mitigation measures that could control flood hazards including building temporary berms, permanent levees/floodwalls, retention/detention ponds, and using water pumps.

Additionally, other policy-based mitigation measures can control community flood exposure such as property buyouts or zoning which effectively prohibits certain construction types in the floodplain. Further, policy-based mitigation measures can also be used to decrease building vulnerability by, for example, increasing building FFE's (i.e. elevating residential structures). Many of these mitigation measures have been all or partially implemented in the U.S. and around the world. The feasibility of these mitigation measures depends on many factors including flood plain characteristics, topography, accessibility, available funds, cost, and time of construction.

Temporary berms could be constructed for several reasons which include rerouting or blocking a water path which could serve as a pre- and post-disaster mitigation measure. This would be typical when the topology does not allow a permanent berm for one or more reasons. If permanent berms are allowed, levees, flood gates, and floodwalls could be a good option. Levees/floodwalls are considered one of the most effective flood detention measures that policymakers can use to protect flood plains near the banks of a river and are usually designed to resist a flood intensity associated with a certain flood return period. However, levees/floodwalls can be breached or overtopped during severe flooding events such as the Mississippi River after Hurricane Katrina 2005 (Duncan, Brandon, Wright, and Vroman, 2008; Sasanakul et al., 2008). Therefore, using a retention/detention system could be a good solution for severe flood events. A retention (wet) pond is a stormwater control structure that retains water for proper management and treatment. A detention (dry) pond is a stormwater control structure that detains water to be released with an appropriate discharge without causing any damage downstream. Wet and dry ponds are some of the most efficient pre-disaster flood mitigation measures to control stormwater upstream to reduce flooding downstream. According to the U.S. Environment Protection Agency (EPA), retention ponds cost US$17.5 to $35 per cubic meter and detention ponds cost US$5-$10 per cubic meter, as of 2020 market costs (NRC, 2020). Although costly, in some cases they can nearly guarantee safe floodplain management and protect human activity and community assets from severe flooding events. These mitigation measures work well when levees/floodwalls are not an option or if the flood demands exceed the capacity for other mitigation measures.

Property buyouts are also an effective mitigation strategy that can work for communities that have recurring flood issues. This mitigation approach controls the flood exposure of a community without implementing specific hazard mitigation (e.g., berms, levees, floodwalls, retention ponds, etc.). However, the home buyout program requires federal approval to proceed with such a policy, as well as the interest and approval of the homeowner. This approach is quite efficient when it is not possible to apply hazard mitigation measures or when buildings are in the flood plain but outside the flood-protected area. Implementing such an approach can protect both individuals and ultimately reduce the mitigation cost to the government. Elevating a building and thereby increasing its FFE is another way to decrease building vulnerability and protect structures located in the floodplain in lieu of exposure mitigation measures. There are a number of techniques to elevate buildings such as using a filled and open foundation or using a solid-walls foundation as shown in Figure 1-5. Increasing buildings FFE directly decreases flood losses and is an effective mitigation measure for buildings that are located outside of the zone protected by other mitigation alternatives described above. The price of elevating a building FFE depends on a number of factors including building size, location, number of stories, type of foundation, and the amount of required elevation. According to the Fixer database (Fixer, 2020), the average cost of increasing building elevation starts at US$10,000 for a one-story 140 m^2 (1500 ft^2) home and increases up to $30,000 for two-story homes. However, the cost of increasing elevation depends on the level of the provided service, e.g. “turn-key” or just the elevation, and therefore has a wide range from US$10-$90 per ft^2 (0.1 m2) of the building (Dawson Foundation Repair, 2020).

Figure 1-5. *An elevated building using solid walls foundation (picture taken from Princeville, NC for an elevated building on the banks of Tar River) Photo taken by Omar Nofal, 2020*

1.1.6 Community Resilience

Community resilience is generally defined by Presidential Policy Directive (PPD-21, 2013) as “*the ability to prepare for and adapt to changing conditions and withstand and recover rapidly from disruptions*”. A summary of the community resilience definitions across the literature over the last decade is listed herein (Bhamra, Dani, and Burnard, 2011; Koliou et al., 2018; Manyena, 2006; Martin-Breen and Anderies, 2011). Research in disaster-resilient communities has received substantial interest among researchers across different disciplines such as sociologists (Adger, 2000; Adger, Hughes, Folke, Carpenter, and Rockström, 2005; Berkes, Folke, and Colding, 2000; Levin et al., 1998; Maguire and Hagan, 2007; Walker, Holling, Carpenter, and Kinzig, 2004), economists (Briguglio, Cordina, Farrugia, and Vella, 2006; Hill, Wial, and Wolman, 2008; Rose, 2004, 2007; Rose and Liao, 2005), and engineers (Haimes, 2009; Leveson et al., 2006; Madni and

Jackson, 2009). Community resilience research in the context of natural hazards and engineering systems attempted to combine disciplines and became hazard-focused (Ayyub, 2014) to encompass different suites of hazards and their community-wide impacts such as seismic resilience of communities (Bruneau et al., 2003; Bruneau and Reinhorn, 2006; Franchin and Cavalieri, 2015; Renschler et al., 2010), hurricane resilience of communities (Burton, 2015; Colten, Kates, and Laska, 2008; Comes and Van de Walle, 2014; Ouyang and Duenas-Osorio, 2014), wind resilience of communities (Tokgoz and Gheorghe, 2013), and flood resilience of communities (Aerts et al., 2014; López-Marrero & Tschakert, 2011; Schelfaut et al., 2011; Thieken et al., 2014) along with integrating the socio-economic information of communities in the physical systems resilience of these communities to these hazards (e.g. National Academy of Engineering, 2019; Rosenheim et al., 2019).

Currently, there is significant progress in community resilience research and disaster-related science and technology (Cai et al., 2018; Cimellaro et al., 2010; Cutter et al., 2008; Henry & Ramirez-Marquez, 2012; Rus, Kilar, & Koren, 2018; Tran et al., 2017; Woolf et al., 2016). Furthermore, seismic hazard research with a focus on community resilience has received substantial interest among researchers over the last two decades with the development of new frameworks (Bruneau et al., 2003), implementation techniques (Chang and Shinozuka, 2004), and performance measures (Renschler et al., 2010) to measure resilience metrics. The main objective of these studies was to develop a set of policy actions and levers that could reduce the amount of future risk to enhance community resilience and develop tools to measure the efficiency of these actions. In terms of hurricane risk reduction, the resilience decisions and policies can be classified into short-term and long-term actions and can be further classified into pre-disaster (preparedness and mitigation) and post-disaster (response and recovery) actions as shown in Table 1-3 which describes the temporal and spatial dynamics of these measures. Some of the mitigation measures are the responsibility of the households and business owners including protecting their properties from surge water entry which may include elevating the building interiors including expensive components, appliances and important documents (Dhonau & Rose, 2016; Lamond et al., 2016) and using sandbags or homemade flood boards to slow the water ingress into their property (O'Neill et al., 2016).

Table 1-3. *Classification of the actions that communities may choose to adopt to mitigate flood impacts and speed the recovery process*

Resilient Measure	Short-term	Long-term
Pre-disaster	Immediate precautionary measures for the community to be implemented after the hurricane warnings: • Construct temporary berms/levees. • Install pumps at critical locations. • Use Sandbags around emergency and critical facilities. • Encourage volunteers to help with filling and moving the sandbags. • Elevate interior building expensive components such as furniture, appliances, and important documents on higher shelves.	Community plans for 100-year flood or any recurrence intervals to protect the buildings located in the floodplain: • Construct permanent berms/levees. • Construct dams, flood exits, flood barriers, floodwalls, and flood gates. • Increase first-floor elevation for the buildings on the floodplain. • Elevate heaters and air conditions. • Reroute ductwork from the crawlspace to the attic.
Post-disaster	Immediate actions for the community to be implemented just after the flooding event: • Evacuation Plans. • Temporary shelters. • Secure the food chain. • Provide funds for the impacted buildings. • Encourage voluntary institutions to help with community recovery. • Start Recovery.	New community plans after the lessons learned from past flooding events: • Redesign the flood drainage network based on the lessons learned. • Offer buyout program for the buildings on the floodplain. • Adopt resilient construction methods for new buildings. • Retrofit of the impacted infrastructure to resist future flooding according to the new plans.

1.2 Motivation

A high-resolution hurricane risk analysis in terms of developing hazard, exposure, and vulnerability models are needed to better address community-level aspects including community systems characterization, risk, and mitigation analysis, modeling community post-hazard functionality and recovery, and modeling the vulnerability of the interdependent networks. Although current studies provided a detailed insight into the multiple loadings driven by hurricanes and their impacts on buildings and infrastructure, the current literature still lacks a comprehensive approach that accounts for the combined impact of these multiple loadings at the building-level and community-level. Past studies have focused primarily on modeling these hazards individually with less focus on the multi-hazard impact on the whole building system made up of the combination of the structure and its interior contents. Additionally, the analysis resolution used in these studies did not allow large-scale hurricane risk assessment through an individual assembly of building risk. Further, the spatiotemporal variation of hurricane hazards in terms of hazard intensity and hazard type along with the hurricane-related data scarcity made it a challenge to develop a high-resolution multi-hazard building-level and community-level hurricane risk model. For buildings on the coast, each building can be subjected to one (e.g., surge) or multiple load types at a time (e.g., wind and coastal flooding) or one after another with different intensities. Further inland, buildings may have either wind or combined wind and flooding (pluvial or fluvial). The intensity of the hurricane-induced hazards varies with time as the hurricane approaches the coast and makes landfall. For example, buildings on the shoreline might survive wind loads but they could be severely impacted if the storm surge (dynamic flooding) height exceeds the building’s first-floor elevation (FFE).

Inland buildings far from the shoreline may not be subjected to any storm surge, but wind and fluvial and/or pluvial flooding induced by the rainfall from decaying hurricanes are still a threat that could cause both structural and content damage. Therefore, a building-level analysis will not enable to capture the diverse impacts of hurricanes on coastal and inland communities and a community-level multi-hazard hurricane risk model is needed. This model requires a full realization of the exposed building vulnerability along with a comprehensive understanding of the hurricane hazard mechanism and how it makes land landfall on coastal communities based on its spatial and physical characteristics. To develop such a model, an array of data types are needed such as hurricane characteristics (e.g., hurricane path, wind field, wind speed, surge height, wave height, etc.), building characteristics (e.g., location, no. of stories, first-floor elevation, roof shape, foundation type, construction material, etc.), building-level vulnerability functions (fragility or damage curves).

Risk-informed decisions require uncertainties to be propagated across the entire risk model. The current literature is populated with many studies that developed deterministic and probabilistic damage models for wind, surge, and wave that only focus on the structural damage with less focus on the damage to the whole building including structural and non-structural components along with the interior contents. Although a building's interior contents and non-structural components could exceed half of the building market value, their damage assessment has not received adequate research attention compared to the structural system. For example, the HAZUS-MH hurricane model uses an assembly-based approach to account for content damage resulting from flooding based on empirical assessment (FEMA, 2003). Then, the loss sub-assemblies from wind and flood hazards are combined in a single loss matrix. Although this approach is widely used across the U.S., it depends on empirical deterministic stage-damage functions with inherent uncertainties in the damage models. Therefore, a community-level multi-hazard probabilistic hurricane risk assessment model is needed to account for the collective impacts of the multi-hazards driven by hurricanes on both the building system and the interior contents.

Additionally, many of the current damage models are based on a qualitative and empirical assessment that does not allow uncertainty propagation across the damage model (Hall and Solomatine, 2008; Handmer, 2002). Additionally, a number of techniques such as expert judgment and practical studies (Bowker, 2007a; Egli, 2002; Glavovic, 2010; Thurston et al., 2008), and field/phone surveys (Bubeck et al., 2013; Hudson et al., 2014; Heidi Kreibich et al., 2005) have been pursued. Also, there have been several efforts aimed at developing probabilistic flood fragility functions (De Risi et al., 2013; Nadal et al., 2009; van de Lindt et al., 2018; van de Lindt and Taggart, 2009) and other probabilistic empirical (McGrath, El Ezz, and Nastev, 2019) and synthetic (Dottori et al., 2016) depth-damage curves. De Risi et. al. developed a convolution of flood hazard and flood fragility functions for a specific building class (masonry) at a specific limit state (life safety) using flood depth as a sole-damaging characteristic (De Risi et al., 2013). However, these models, while they are novel, did not enable developing a generalized vulnerability model that could be extended to develop flood vulnerability for a portfolio of building archetypes. The ability to propagate this uncertainty will enable a comprehensive risk-informed decision framework and allow better optimal allocation of community resources. Therefore, such scarcity in flood fragility development motivated part of this research to develop an approach that could be used to develop a multi-variate fragility function methodology.

These limitations in terms of the data scarcity and the level of aggregation used in the current risk models do not allow an analyst to quantitatively investigate the impact of building-level and community-level risk reduction mitigation measures on the community performance during extreme hazard events. Several mitigation studies and multiple standards over the last several decades investigated and recommended building-level (ABI, 2003; Egli, 2002; FEMA, 2005; FEMA P-1037, 2015; Hayes, 2004; Holub and Fuchs, 2008; Heidi Kreibich et al., 2011, 2005; Lamond et al., 2016; Olfert and Schanze, 2009; Proverbs and Lamond, 2017) and the community-level (Dierauer et al., 2012; Posner and Georgakakos, 2017; Remo et al., 2012; Schanze et al., 2007; Wenger, 2015a, 2015b) flood mitigation measures. There are a number of building-level flood adaptation techniques which include water avoidance (Bowker, 2007b; Garrote et al., 2019), water exclusion (Beddoes and Booth, 2015), and water entry (Fidler et al., 2004) to name a few. However, many of these mitigation studies still lack the generalization needed to quantitatively model building and community-level flood risk mitigation strategies because they are based on aggregated data and rely on qualitative models that possess significant uncertainty. The ability to propagate this uncertainty will enable a comprehensive risk-informed decision framework and allow better optimal allocation of community resources. Additionally, the collective impact of some of these measures on the community is still unclear since accurate quantitative investigations that allow aggregation of building-level mitigation models to the community-level are few (Aerts et al., 2014, 2013; Hans De Moel, Vliet, et al., 2014).

1.3 Research Purpose and Objectives

The dissertation focuses on several interrelated topics within the multi-hazard hurricane risk, resilience, and recovery analysis. Figure 1-6 shows a schematic representation of the major analyses needed to perform comprehensive multi-hazard hurricane risk, resilience, and recovery analyses. This figure shows the main stages that communities go through before, during, and after hurricane hazards including risk, resilience, and recovery analysis. The main components of each analysis stage are highlighted in this framework to emphasize the required data, models, and analyses to accomplish each analysis stage. Several parts of this framework have already been investigated and developed by other researchers and are included here for completeness. However, the focus of this dissertation is on the parts of the framework needed to make it whole. This will be accomplished by utilizing high-resolution models in terms of hazard, exposure, and vulnerability models for both inland and coastal communities. The dissertation focuses on the parts of the framework highlighted in cyan in Figure 1-6. This includes the development of models, data collection, development of analysis approaches, integration of existing developed components with new components and use illustrative examples to explain the developed approaches. Most of the dissertation hazard development is focused on static flooding driven by hurricane rainfall. However, the coastal hazards including surge, wave, and wind were directly implemented herein.

The main body of the framework starts with a risk analysis of the multi-hazards driven by hurricanes which requires models for hazard, exposure, and vulnerability. For the hazard, some models are from existing literature including wind, surge, and wave models. However, the flood hazard models are developed herein using hydrologic and hydrodynamic analysis tools. For the exposure, this dissertation will have less focus on networks and more focus on buildings. For vulnerability, the focus is the development of single-variable and multi-variate flood fragility and loss functions for a portfolio of building archetypes that can represent a community. Resilience-based decisions will be investigated in terms of pre- and post-disaster for short- and long-term mitigation at the building- and community level.

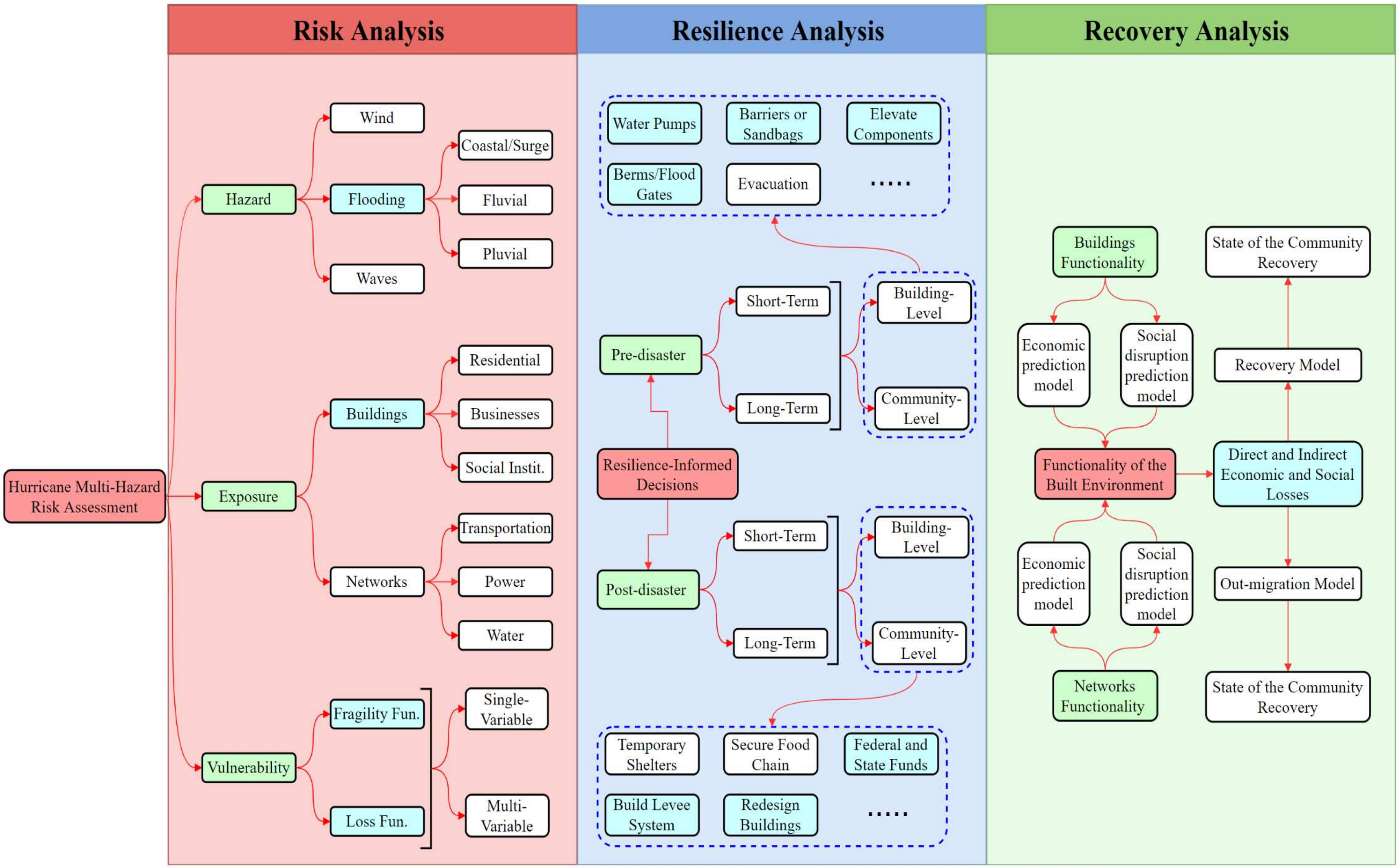

Figure 1-6. *The main components associated with the risk, resilience, and recovery analyses for the hurricane-induced hazards*

The main research objectives are to:

- **Introduce a probabilistic multivariate flood fragility and loss analysis approach:** The proposed flood fragility and loss approaches herein propagate uncertainties in flood depth, flood duration, and the component replacement costs. These functions do not require field study data to generate a flood fragility and probabilistic loss function for a building. The methodology also allows the analyst to, in theory, create a damage fragility and loss prediction model for any building of interest.
- **Develop flood fragility archetype portfolio:** Flood fragility and loss functions were developed for a portfolio of 15 building archetypes. Together, these archetypes are believed to be the minimum necessary to represent flood vulnerability for buildings within small to mid-size communities.
- **Develop a high-resolution community-level flood risk analysis framework:** This framework uses building-level information and a high-fidelity flood hazard model along with the building fragility portfolio to map the flood risk of each building across the community.
- **Demonstrate quantitative building-level and community-level flood mitigation analysis:** A high-resolution quantitative mitigation analysis framework is developed to account for multiple building-level and community-level mitigation measures. This framework allows the analysis to account for the impact of mitigation measures at component-, building-. And community-level.
- **Develop a hurricane multi-hazard risk model:** A multi-hazard high-resolution hurricane risk model is developed to account for the combined impacts of the storm surge, wave, and wind hazards on coastal communities in terms of the damage to the structural and non-

structural components along with the interior content. A framework for community-level analysis was also developed to enable risk-informed decisions at a regional scale.

1.4 Layout of the Dissertation

The dissertation is organized as follows:

- **Chapter 2:** This chapter provides a detailed description of a new multi-variate probabilistic method to develop component-based flood fragility and loss functions. These functions account for the impact of flood depth and flood duration on the amount of damage/losses. This method was applied to a portfolio of 15 building archetypes that represent the different building occupancies within a community. This would allow modeling flood vulnerability at the community-level.
- **Chapter 3:** A high-resolution multi-hazard hurricane risk analysis framework was developed for coastal and inland communities to account for the combined impact of the storm surge, wave, and wind on the building structural and non-structural components along with the interior contents. This was done using high-resolution hazard, exposure, and vulnerability models.
- **Chapter 4:** A component-level mitigation analysis methodology was developed to account for the impact of elevating water-sensitive components on the amount of damage/loss reduction. Additionally, a systematic methodology was developed to account for the impact of other building-level and community-level mitigation measures.
- **Chapter 5:** The developed models were applied to several case studies to illustrate the applicability of the developed approach. Detailed information about these case studies along with their analysis results are fully presented.

- **Chapter 6:** A summary of the developed models along with the different analyses conducted within the dissertation are presented. The main contribution to the literature and recommendations for future work are listed.

CHAPTER 2: FLOOD FRAGILITY AND LOSS ANALYSIS APPROACH

2.1 Introduction

Propagating uncertainties in flood damage models is a critical step towards a risk-informed decision methodology that is based on quantitative assessment. Flood-related data scarcity presents challenges when seeking to include uncertainties in flood damage modeling. Therefore, the current flood vulnerability analyses rely on deterministic methods (e.g. stage-damage functions) to quantify the flood damage and losses to the built environment. While such approaches have been used extensively by communities, they do not enable the propagation of uncertainty into a risk- or resilience-informed decision process. In general, the flood-related literature is well developed by hydrologists where the focus has been placed on propagating uncertainties in the hazard component of the flood risk analysis process (Candela and Aronica, 2017; Domeneghetti, Vorogushyn, Castellarin, Merz, and Brath, 2013; Merwade, Olivera, Arabi, and Edleman, 2008; Mukolwe, 2017; Teng et al., 2017). Propagating uncertainties in the flood exposure and vulnerability components have been slowed due to a lack of data (and particularly statistical distributions) for the flood resistance characteristics of buildings. Risk-informed decisions require uncertainty propagation across the whole risk model (hazard, exposure, and vulnerability) to define safety margins for buildings (Dubois and Guyonnet, 2011) and characterize the community functionality based on these margins (McAllister, 2015).

A review of the multiple flood hazard characteristics and their impacts on the built environment including flood depth, flood velocity, and flood duration was conducted by Nofal and van de Lindt (O.M. Nofal and van de Lindt, 2020) and previously by Soetanto and Proverbs (Soetanto and

Proverbs, 2004). Flood depth, flood velocity, and flood duration are considered the most important flood hazard characteristics causing the majority of buildings structural and content damage (Kelman and Spence, 2004; Middelmann-Fernandes, 2010). Although flood depth is considered the main damaging flood hazard characteristic that has been widely used to assess flood damage in the literature (Frongia, Ruiu, and Sechi, 2017; Martínez-Gomariz, Forero-Ortiz, Guerrero-Hidalga, Castán, and Gómez, 2020; Aim Pistrika, 2010; Aimilia Pistrika et al., 2014; Scawthorn et al., 2006; Scorzini and Frank, 2017), the inclusion of other flood damaging characteristics would increase the accuracy of the flood damage model (Marvi, 2020). Flood damage from coastal flooding resulting from hurricanes and tsunamis has been extensively investigated in the literature in terms of developing fragility functions to model the impact of flood depth and flood velocity on buildings' structural systems (Charvet, Macabuag, and Rossetto, 2017; Do et al., 2020; Masoomi et al., 2019; Massarra et al., 2019; Nadal et al., 2009; Reese et al., 2011; Rehman and Cho, 2016; Tomiczek et al., 2017).

Fragility functions for flood damage to the whole building including structural and non-structural components along with the interior content are scarce and there are no flood fragility portfolios that can be used to represent a community-level building stock. Fluvial and pluvial floods induced by hurricanes are usually static floods with very low velocity (except for steep channels, flash floods, dam\levees breach where flood velocity should be considered). the main damaging characteristics are flood depth and flood duration (which will be the focus of this chapter of this dissertation) such as shallow flooding which has been defined by FEMA in their guidance for flood risk analysis and mapping (FEMA, 2016b). Therefore, most of the building damage occurs to the interior contents and non-structural components with less damage to the structural system. Recently, there were some attempts to develop numerical flood fragilities for specific building classes including masonry buildings (De Risi et al., 2013), and wood frame buildings (van de Lindt and Taggart, 2009) along with other empirical flood fragilities based on collected field data from (Deniz et al., 2019; van de Lindt et al., 2018). Additionally, some researchers tried to enhance the current stage-damage functions (Molinari and Scorzini, 2017; Sairam et al., 2020) and propagate uncertainties in both the empirical (McGrath et al., 2019) and synthetic stage-damage functions (Dottori et al., 2016). However, those probabilistic methods were not general enough to develop a portfolio of flood fragility functions that could be used at the community-level. Additionally, the compound impact of flood depth and flood duration has not been well addressed in the literature.

In this dissertation, a single-variable and multi-variate component-based flood fragility method is proposed. The method uses expert-based data derived from online sources that are applied within a Monte Carlo framework to divide the building into independent components and then assigns these components to five predefined damage states that describe the building damage as a whole. Using a series of Monte Carlo simulations, uncertainties in flood depth and flood duration that result in each damage level for each component were propagated. Their damage is then characterized using component fragility functions to be used to develop total building fragility and loss functions. The resulting fragilities can be used as a probabilistic vulnerability function to be assigned to a real community based on building archetype and occupancy. The ability to develop flood fragility curves for buildings without the need for empirical field data is the primary contribution of this work. This allowed the development of fragility and loss functions for a portfolio of 15 building archetypes to represent the different building occupancies within a community which can be used to model the flood vulnerability for a typical community.

2.2 Fragility Formulation and Loss Estimation Methodology

Fragility is a conditional probability that describes the probability of a structural system or a building component exceeding a prescribed damage level at a certain level of hazard intensity (M. O. Amini and van de Lindt, 2013; Rosowsky and Ellingwood, 2002) which is expressed in Eq. (2-1). It also could be defined as a failure probability described by the probability of a certain demand exceeding resistance at a certain intensity measure (Masoomi and van de Lindt, 2016; Memari et al., 2018) such as calculating a component failure by using Eq. (2-2). For a good statistical fit, structural systems and component fragilities usually are expressed in terms of a lognormal cumulative distribution function (λ_r, ξ_r) as shown in Eq. (2-3) (Lee and Rosowsky, 2005).

$$P(DS) = \sum P(DS \mid D = x) \times P(D = x) \qquad \text{(2-1)}$$

$$F_r(x) = P\left[D(x) > R \mid IM(x) \right] \qquad \text{(2-2)}$$

$$F_r(x) = \Phi\left[\frac{Ln(x) - \lambda_R}{\xi_R} \right] \qquad \text{(2-3)}$$

where *P(DS)* = probability of being in a DS, *P(D = x)* = probability that demand have certain value x, *P(DS|D = x)* = conditional probability of being in DS condition on demand $D = x$, $Fr(x)$ = fragility function, *D(x)* = System or component demand, *R* = system or component resistance, and IM(x) is the intensity measure. $\Phi[\bullet]$ = standard normal cumulative distribution function, λ_R = logarithmic median of resistance R, ξ_R = logarithmic standard deviation of resistance R.

The flood susceptibility of the components of any building is uncertain in terms of flood depth and duration resistance for each component. Some of these components are considered a total loss and unrepairable if the most expensive element within the component is touched by water, e.g., motors (e.g., washer, dryer, fan, mixers, etc.), compressor (e.g., Air conditioning, fridge, freezer, etc.), and circuit boards (e.g., computer, laptop, phone, printer, etc.). For other components, immediate loss of a component does not occur when it is simply touched by water (e.g., drywall, painting, cabinets, desks, chairs, sheathing, etc.). Thus, water duration for some components is considered an important factor when determining damage to a component. Generally, flooded components are either replaced (e.g., insulation, carpet, appliances, etc.) or partially replaced (e.g., drywall, sheathing, painting, cladding, etc.) or even may not be significantly affected by water depth and duration (e.g., wood framing, foundation, decking, etc.), i.e. can be dried if the water is not contaminated. Additionally, the elevation of these components is different from building to building (e.g., TV, washer, dryer, electrical outlets, AC, heater, etc.) and the elevation of the damageable element within each component is different from model to model. Therefore, the variability in the response of different building components and the limited data related to their resistance increases the complexity of characterizing the probabilistic performance of buildings to flood hazards.

2.2.1 Fragility Analysis Approach

The proposed approach initially divides any building into independent components and then assigns a random variable to each component within the building as shown in the schematic in Figure 2-1. Afterwards, building damage was classified into five predefined damage states ranging from insignificant damage (DS0) up to complete damage (DS4). Each component damage was assigned to its corresponding DS based on the characterization of each DS. Table 2-1 shows the DSs developed in this research which provided a detailed description of each DS along with their damage scale and damage ratio as a percentage of the total building replacement cost. These DSs are general and can describe any building performance subjected to flood hazards. Each DS is characterized by the performance of the building components including structural, non-structural, and interior items. Then, a data approach that describes the damageable depth, and duration and the replacement cost of each component was developed using existing online sources that provide information on construction data, interior information, and component replacement costs (e.g., Home Advisor (Home-Advisor, 2019), Home Guides (Home-Guides, 2019), UpCodes (Up-Codes, 2019), and Fixer (Fixer, 2020), etc.). Some assumptions related to the flood depth and duration resistance are from van de Lindt and Taggart (van de Lindt and Taggart, 2009) along with the experimental investigation by Aglan (Aglan, 2005). Additionally, a number of logical assumptions related to flood depth and duration were made based on engineering judgment to be able to create a full probabilistic damage model. The flood depth and duration resistance for each component were assumed all to be statistically independent. However, one can envision when this may not be the case, e.g., the resistance of the building envelope and how sealed it is (e.g., exterior wall cladding, sheathing, doors, windows, etc.) controls the water depth and the water duration inside the building.

The final building data are in the form of a maximum and minimum value of the flood depth and flood duration resistance for each component along with a maximum and minimum value of the replacement cost for each component. These bounds were calculated using an array of types and models of components to account for the variability in the elevation of each component across model types. The damaging depth and duration were assumed to be normally distributed between these upper and lower bounds. Therefore, these maximum and minimum values were used to obtain the mean (μ) using Eq. (2-4) and standard deviation (σ) using Eq. (2-5) to create a normal distribution for both depth and duration. The mean is easily calculated by dividing the range of the values (max-min) by two but the standard deviation should, in theory, be derived statistically from observed or measured data which, in the present case, does not exist. Therefore, the Range Rule of Thumb (RRT) was used to compute the standard deviation that uses the characteristics of the normal distribution to give a reasonable estimate of standard deviation by assuming that the range is four times the standard deviation or as shown in Eq. (2-5). The RRT is a useful method of estimating the range from standard deviation and details can be found in the introductions to statistics textbooks (Triola, 2010). The standard deviation calculated using the RRT is felt to be reasonable, for now, until more data become available in the literature.

$$\mu = \frac{\max + \min}{2} \qquad (2\text{-}4)$$

$$\sigma = \frac{\max - \min}{4} \qquad (2\text{-}5)$$

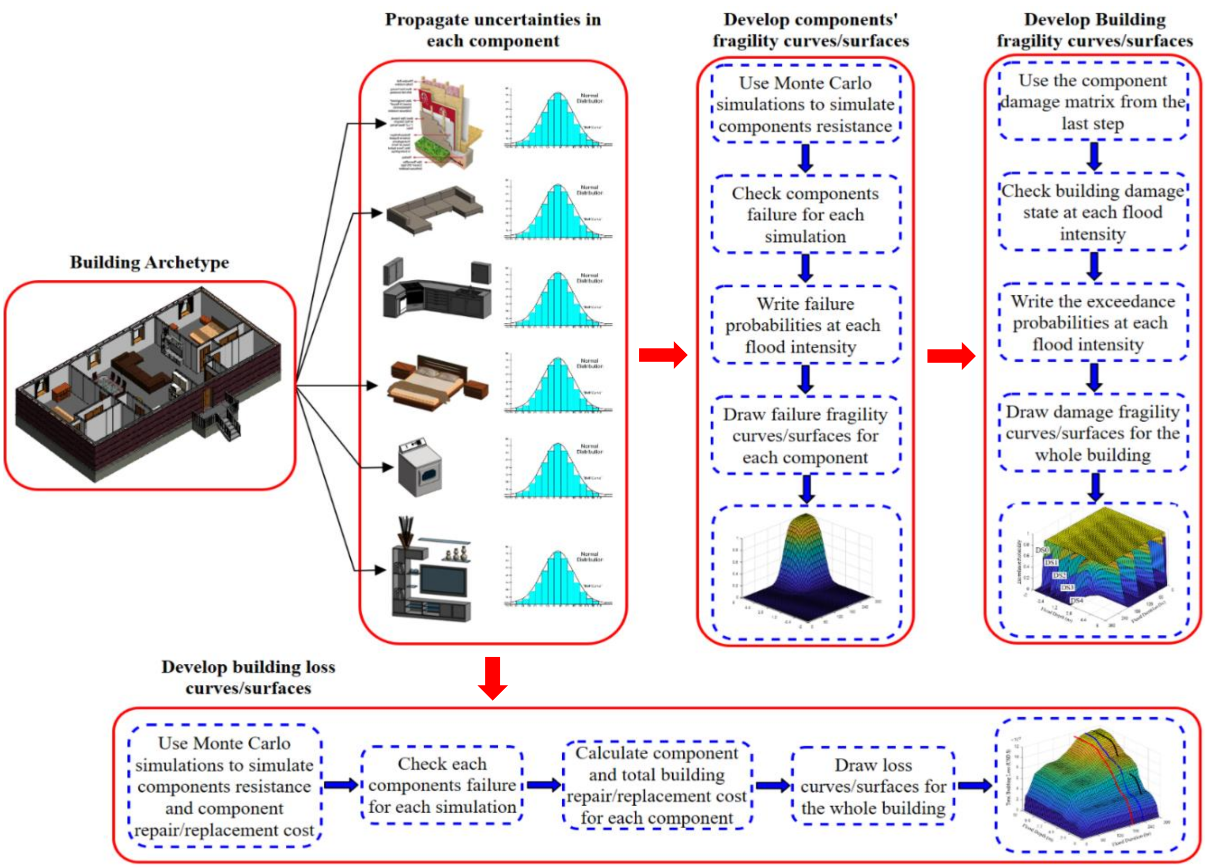

Figure 2-1. *A schematic representation of the methodology that has been applied in this research to account for fragility and loss curves/surfaces for a portfolio of minimal building archetype*

Table 2-1. *Damage states description along with their damage scale and damage ratio as a percentage of the total building replacement cost*

DS Level	Description	Damage Scale	Damage Ratio
0	Insignificant damage to components below first-floor elevation. Water enters crawlspace/basement and touches foundation (crawlspace or slab on grade). Damage to components within the crawlspace/basement including base insulation and stored inventory. Minor damage to garage interiors including drywall, cabinets, electrical outlets, wall insulation (Garage is below the FFE). No sewer backup into the living area.	Insignificant	0.0-0.03
1	Water touches floor joists up to minor water enters the building. Damage to carpets, pads, baseboards, flooring. Damage to the external AC unit (if the AC unit is not elevated) and the attached ductworks (if ductworks are in the crawlspace). Complete damage to the garage interior (if the garage is below FFE). No drywall damages with the potential of some mold on the subfloor above the crawlspace. Could have a minor sewer backup and/or minor mold issue.	Slight	0.03-0.15
2	Partial damage to drywalls along with damage to electrical components (base-outlets), water heater, and furnace. Complete damage to major equipment, appliances, and furniture on the first floor. Damage to the lower bathroom and kitchen cabinets. Doors and windows may need replacement. Could have a major sewer backup and major mold issues.	Moderate	0.15-0.5
3	Damage to the non-structural components and interiors within the whole building including (but not limited) drywall damage to upper stories for multi-story buildings (e.g., attic, the second story, etc.). Electrical switches and mid-outlets are destroyed. Damage to bathroom/kitchen upper cabinets, lighting fixtures on walls are destroyed with potential damage to ceiling lighting fixtures. Studs reusable; some may be damaged. Major sewer backup will happen along with major mold issues. Equipment, appliances, and furniture on the upper floors are also damaged (e.g., attic, second floor, etc.).	Extensive	0.5-0.7
4	Significant structural damage present (e.g., studs, trusses, joists, etc.). Non-structural components and interiors are destroyed including all drywall, appliances, cabinets, furniture, etc. Damage to rooftop units/components including roof insulation, sheathing, and electro-mechanical systems (rooftop AC units, electrical systems, cable railing, sound system, etc.). Foundation could be floated off. The building must be demolished or potentially replaced.	Complete	0.7-1.0

Truncated normal distributions between the lower and upper bounds for the building components were created for both flood depth resistance and flood duration resistance. Figures 2-2(a and b) show an example of the elevation of the external AC unit and a mid-electrical outlet, respectively along with their truncated normal distribution to provide some intuition related to the variability of component elevations. Once these distributions were assigned, two different fragility types were developed (single-variable and multi-variate fragility functions). The first analysis step is to consider the flood depth as a sole damaging characteristic without considering the impact of flood duration on the amount of damage (single-variable) then consider both flood depth and duration (multi-variate) concurrently to compute flood damage. MCSs are used to develop random samples for both flood depth and flood duration resistance for each component within the building using the proposed truncated normal distributions. Figure 2-3 shows a detailed flow chart that illustrates the proposed methodology to develop both single-variable and multi-variate flood fragility functions for each component. A four-dimensional damage matrix (Dm(i,j,u,k)) was then constructed that holds binary information for the state of each component, whether it is damaged or not (1: Damaged, 0: Not damaged) at each flood depth and/or flood duration for each simulation for each component.

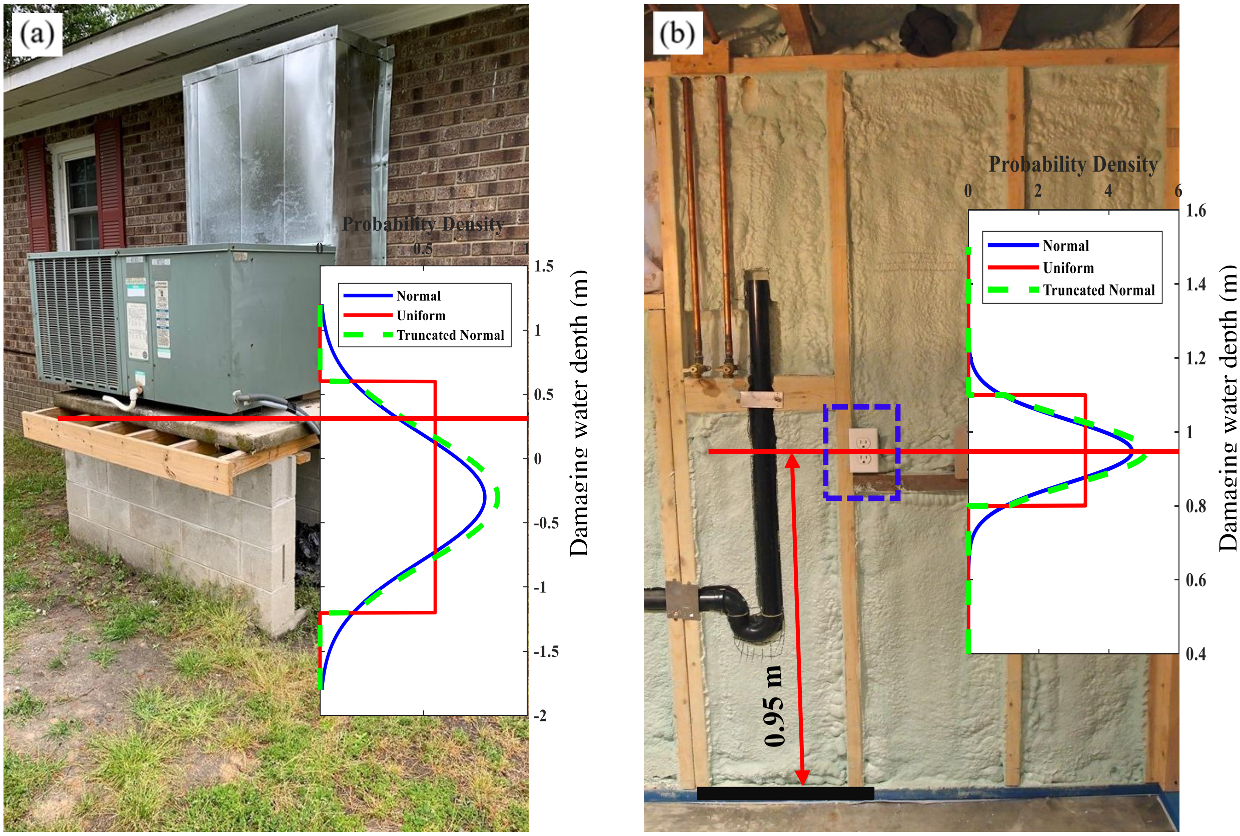

Figure 2-2. *Damaging water depth truncated normal distribution with respect to the normal and uniform distributions: (a) External AC unit; (b) Electrical outlet*

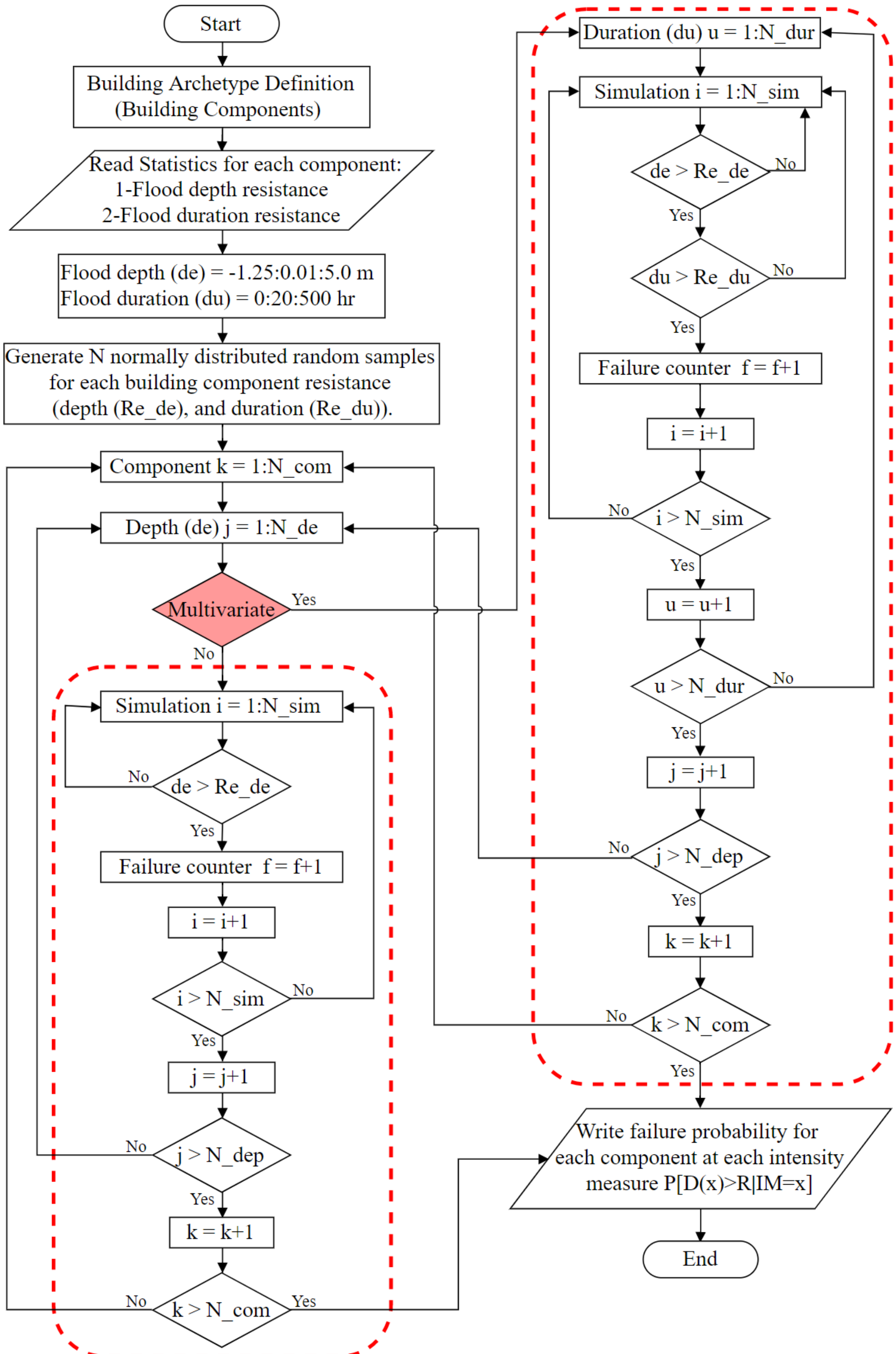

Figure 2-3. *Flow chart illustrating the methodology to develop single-variable and multi-variate flood fragility function for each component within the building where N_com = number of components, N_de = Number of depth steps, N_sim = number of simulations, N_dur = number of duration steps, D(x) = demand flood depth, and R = component resistant flood depth*

Moving from component fragility to building fragility, the 4-D damage matrix was then used to calculate the exceedance probability of each DS. For example, archetype F1 (a one-story residential building archetype on a crawl space foundation) which will be introduced later includes 65 components that were assigned to each five prescribed DSs based on the description of each DS. There are a number of assumptions that could define if a DS was exceeded or not. For example, a DS could be assumed to be exceeded only if all components within this DS are determined to have failed. It also could be assumed that a DS will be exceeded only if all components within the preceding DS were determined to have failed along with the failure of at least one component in the current DS. For example, DS3 will be exceeded only if all components within DS2 were determined to have failed along with at least one component listed in DS3. However, the most rational assumption of the exceedance probability of a certain DS at a certain flood intensity measure is to make it a function of the failure probability of the components comprises this DS. Therefore, the exceedance probability of each DS was calculated based on the failure probability of each component within each DS and then weighted by the ratio of the replacement cost of each component divided by the total replacement costs of all damageable components making up that DS using Eq. (2-6). Then, the calculated fragility was fitted using the lognormal cumulative distribution function (CDF) using Eq. (2-7).

$$P\left[DS_i \,|(IM = x)\right] = \sum_{k=1}^{n} Fr_k\,(IM = x) \times \frac{L_k}{L_{DS_i}} \tag{2-6}$$

$$Fr_{DS_i}(x) = \Phi\left[\frac{Ln(x) - \lambda_{DS_i}}{\xi_{DS_i}}\right] \tag{2-7}$$

where $P[DSi|IM=x)$ = the exceedance probability of DS_i at ($IM=x$), $Fr_k(IM=x)$ = fragility function (failure probability at $IM=x$) for component k, n = the number of components within DS_i, L_k = the replacement cost of component k, and L_{DSi} = the total replacement cost of DSi. Fr_{DSi} = the lognormal fitted fragility value at ($IM=x$), λ_{DSi} = logarithmic median of DS_i, ξ_{DSi} = logarithmic standard deviation of DS_i.

Figure 2-4 shows an example of how the exceedance probability of DS4 for a one-story residential building archetype on a slab on grade foundation (archetype F2) was derived from its component fragilities with lognormal fitted fragility curves as solid lines. Figure 2-5 shows a flow chart for the proposed building-level methodology to develop single-variable (depth) and multi-variate (depth and duration) building fragility functions using the 4-D damage matrix developed based on the procedure outlined in Figure 2-3.

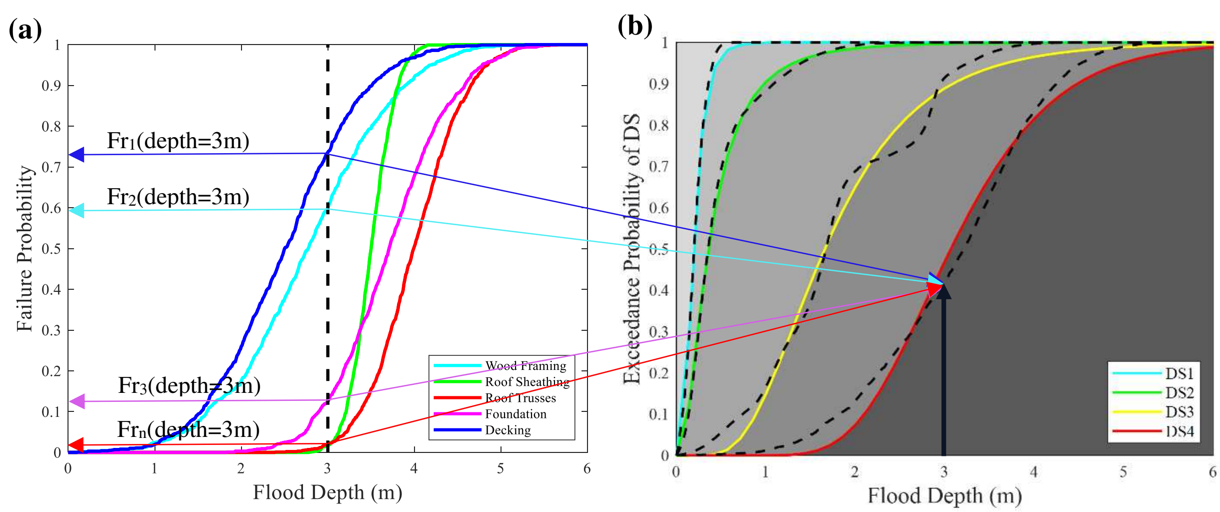

Figure 2-4. *Components and building fragility functions: (a) Component fragility curves for DS4 components along with their failure probability at flood depth = 3.0m; (b) Fitted (Solid lines) and non-fitted (dashed lines) building fragility curves*

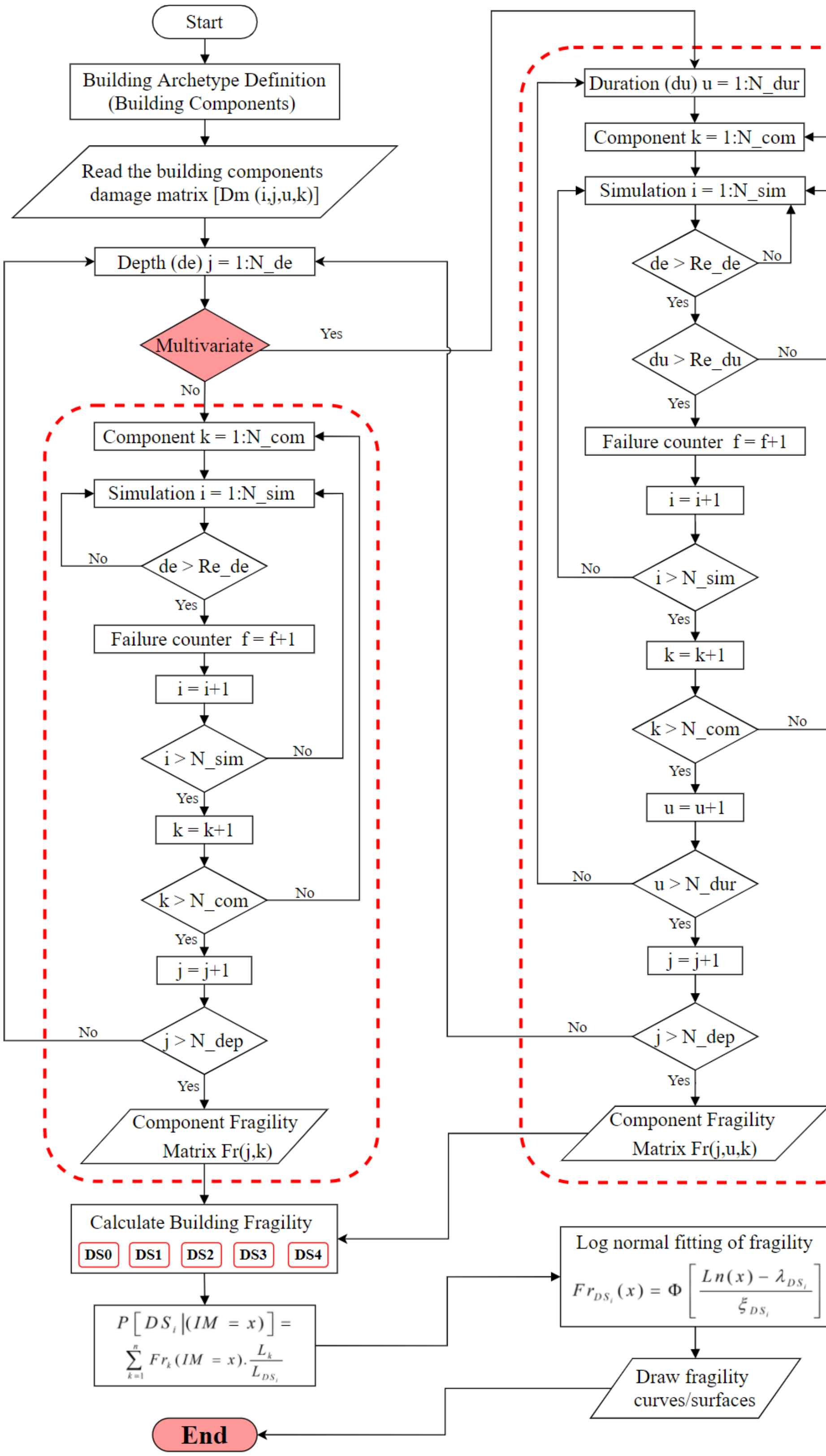

Figure 2-5. *A flow chart illustrates a methodology to develop a single-variable and a multivariate flood fragility function for buildings*

2.2.2 Loss Analysis Approach

Several alternative loss analyses were conducted in order to provide a comparison for loss estimation at the building-level and to enable the propagation of uncertainties for all building components. Three different methods were developed in this study to account for the total building flood losses. Method (1) accounts for flood losses using the resulted failure probability of building components (Components fragility functions). In this method, a vector of randomly generated component loss simulations was first calculated by multiplying the component failure probability by the simulated total replacement cost for each component as shown in Eq. (2-8). The truncated normal distribution of the component replacement cost was used to generate MC simulations for each component replacement cost between the provided upper and lower bounds using the calculated mean and the standard deviation. Afterwards, a vector of randomly generated total building replacement costs was calculated by summing the components replacement cost vectors as shown in Eq. (2-9). The mean total building replacement cost is then the summation of the mean replacement cost of its component using Eq. (2-10) and the standard deviation of the total building loss is calculated using Eq. (2-11) assuming the damage to any component to be statistically independent (uncorrelated) from the damage to other components. From a practical point of view, this assumption was necessary due to the lack of data that correlates component damage and the components with the structural system. The effect of such an assumption on the resulting fragility and loss curves is likely the introduction of epistemic uncertainty.

$$L_k(IM = x) = P\left[D(x) > R_k \middle| IM = x\right].\begin{pmatrix} Lr_k^1 \\ Lr_k^2 \\ \vdots \\ Lr_k^n \end{pmatrix} = \begin{pmatrix} L_k^1 \\ L_k^2 \\ \vdots \\ L_k^n \end{pmatrix} \qquad (2\text{-}8)$$

$$L_t(IM=x)=\begin{pmatrix}L_1^1\\L_1^2\\\vdots\\L_1^n\end{pmatrix}+\begin{pmatrix}L_2^1\\L_2^2\\\vdots\\L_2^n\end{pmatrix}+\begin{pmatrix}L_3^1\\L_3^2\\\vdots\\L_3^n\end{pmatrix}+\cdots+\begin{pmatrix}L_N^1\\L_N^2\\\vdots\\L_N^n\end{pmatrix}=\begin{pmatrix}L_t^1\\L_t^2\\\vdots\\L_t^n\end{pmatrix} \tag{2-9}$$

$$\mu_{L_t}(IM=x)=\sum_{k=1}^{N}\mu_{L_k}(IM=x)=\sum_{k=1}^{N}\frac{\sum_{i=1}^{n}L_k^i}{n} \tag{2-10}$$

$$\sigma_{L_t}(IM=x)=\sqrt{\sum_{k=1}^{N}\sigma_{L_k}^2(IM=x)} \tag{2-11}$$

where L_k = a randomly generated replacement cost vector for component k at a specified intensity measure ($IM=x$), Lr^i_k = an i th MC simulated total replacement cost of component k, and L^i_k = an i^{th} randomly MC simulated replacement cost for component k at a specified intensity measure ($IM=x$). L_t = a randomly generated total building replacement cost vector at a specified intensity measure ($IM=x$), L^i_t = an i^{th} randomly MC simulated total building replacement cost, and $P[D(x)>R_k|IM=x]$ = failure probability conditioned on the value of the intensity measure (depth, and duration) for component k. μ_{Lt} = mean total building replacement cost at a specified intensity measure ($IM=x$), *and* μ_{Lk} = mean replacement cost of component k at a specified intensity measure ($IM=x$). σ_{Lt} = the standard deviation of the total building replacement cost at a specified intensity measure ($IM=x$), and σ_{Lk} = the standard deviation of the replacement cost of component k at a specified intensity measure ($IM=x$). k = component number, N = the total number of building components, and n = the total number of MC simulations.

Due to the spatial (from city to another city and from state to another state) and temporal (from year to year as material costs increases) variation of the component replacement costs, they were extensively collected using the online published costing from Home Advisor (Home-Advisor, 2019) in which experts provide information about the combined material and labor cost for each building component. The price data are based on the zip code of the selected area that the building will be constructed in, but also provide maximum and minimum component replacement cost values along with the average cost of each component in a normal distribution form. Figure 2-6 shows an example of the data provided by the Home Advisor website for distribution of the variation of painting price for a single-family home. However, the unit price per ft^2 could also be obtained.

Figure 2-6. *A truncated normal distribution with maximum, minimum, and average cost of painting a home* (Home-Advisor, 2019)

The flood loss function using method (2) is the simplest flood loss method which derives flood losses directly from the total building fragilities developed herein without using the component fragilities. This was done using a concept similar to the approach used in HAZUS-Earthquake (FEMA, 2009c) to capture fragility-based losses by simply summing the products of the probability of being in each DS by the repair (or replacement) cost for its corresponding DS as shown in Eq. (2-12).

$$L_f(IM = x) = \sum_{i=0}^{4} \left[P\left(DS_i \middle| IM = x\right) - P\left(DS_{i+1} \middle| IM = x\right) \right] . Lr_{ci} . V_t \qquad (2\text{-}12)$$

where $L_f\,(IM{=}x)$ = total building fragility-based losses in monetary terms (replacement or repair cost) at a specified intensity measure ($IM{=}x$), $P(DS_i|IM{=}x)$ = exceedance probability of DS_i at a specified intensity measure ($IM{=}x$), $P(DS_{i+1}|IM{=}x)$ = exceedance probability of DS_{i+1} at a specified intensity measure ($IM{=}x$), Lr_{ci} = cumulative replacement cost ratio corresponding to DS_i, and V_t = total building cost (replacement cost).

Estimates for the replacement cost of each DS were provided earlier in Table 2-1 which gives a generalized estimate for a wide range of building archetypes. It should be again noted that the damage to any component within each DS was assumed to be statistically independent (uncorrelated) from the damage to other components. Based on this assumption, the mean and standard deviation of the replacement cost for each DS were calculated using Eq. (2-13) and (2-14), respectively.

$$\mu_{ti} = \sum_{k=1}^{N} \mu_k \qquad (2\text{-}13)$$

$$\sigma_{ti} = \sqrt{\sum_{k=1}^{N} \sigma_k^2} \qquad (2\text{-}14)$$

where μ_{ti} = mean replacement cost of DS_i, μ_k = mean replacement cost of component k, N = number of components in DS_i, σ_{ti} = standard deviation of DS_i replacement cost, σ_k = standard deviation of the replacement cost of component k.

For the flood loss function using method (3), a series of MC simulations were used to generate a matrix that contains a randomly generated replacement cost for each component at each flood intensity measure. This was done by transforming the randomly generated component damage matrix (*Dm(i,j,u,k)*) into a loss matrix. The binary information (1: Damaged, 0: Not damaged) contained in this matrix was then transformed into monetary component flood losses using the replacement cost information. This method is considered the most accurate and reliable approach to account for building-level flood losses because uncertainties were propagated in each parameter (flood depth resistance, flood duration resistance, and component replacement cost) systematically without deriving values from assumptions or averages. Therefore, this method was extended to include the impact of flood duration on the amount of flood losses. Figure 2-7 shows a schematic with the major steps to develop flood loss functions using Method (2) and Method (3). Figure 2-8 presents a flow chart that shows the framework used to develop flood loss function using Method (3) including a detailed procedure for the MCS analysis. Similar to the fragility analysis method, the loss analysis calculation was conducted in two steps (single-variable and multivariate).

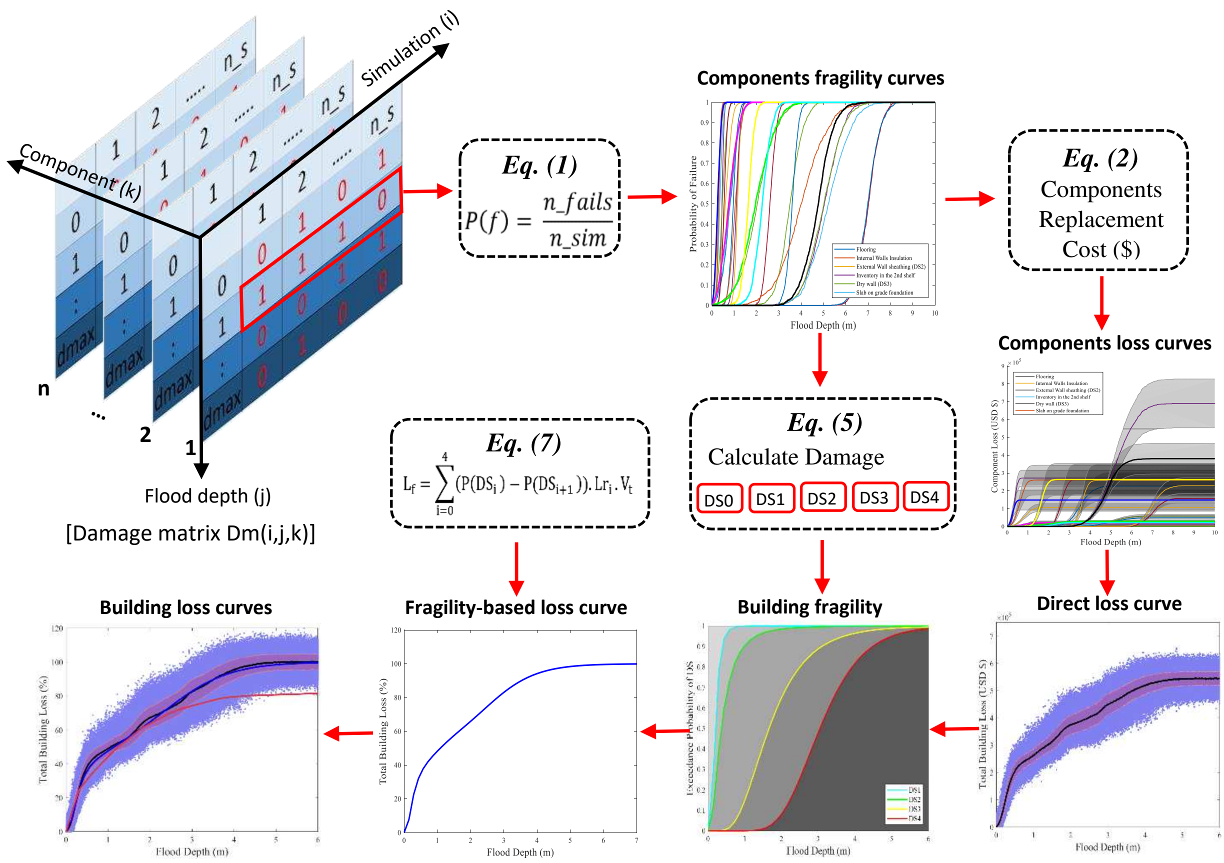

Figure 2-7. *A schematic illustration of the approaches used to develop flood fragility and loss functions*

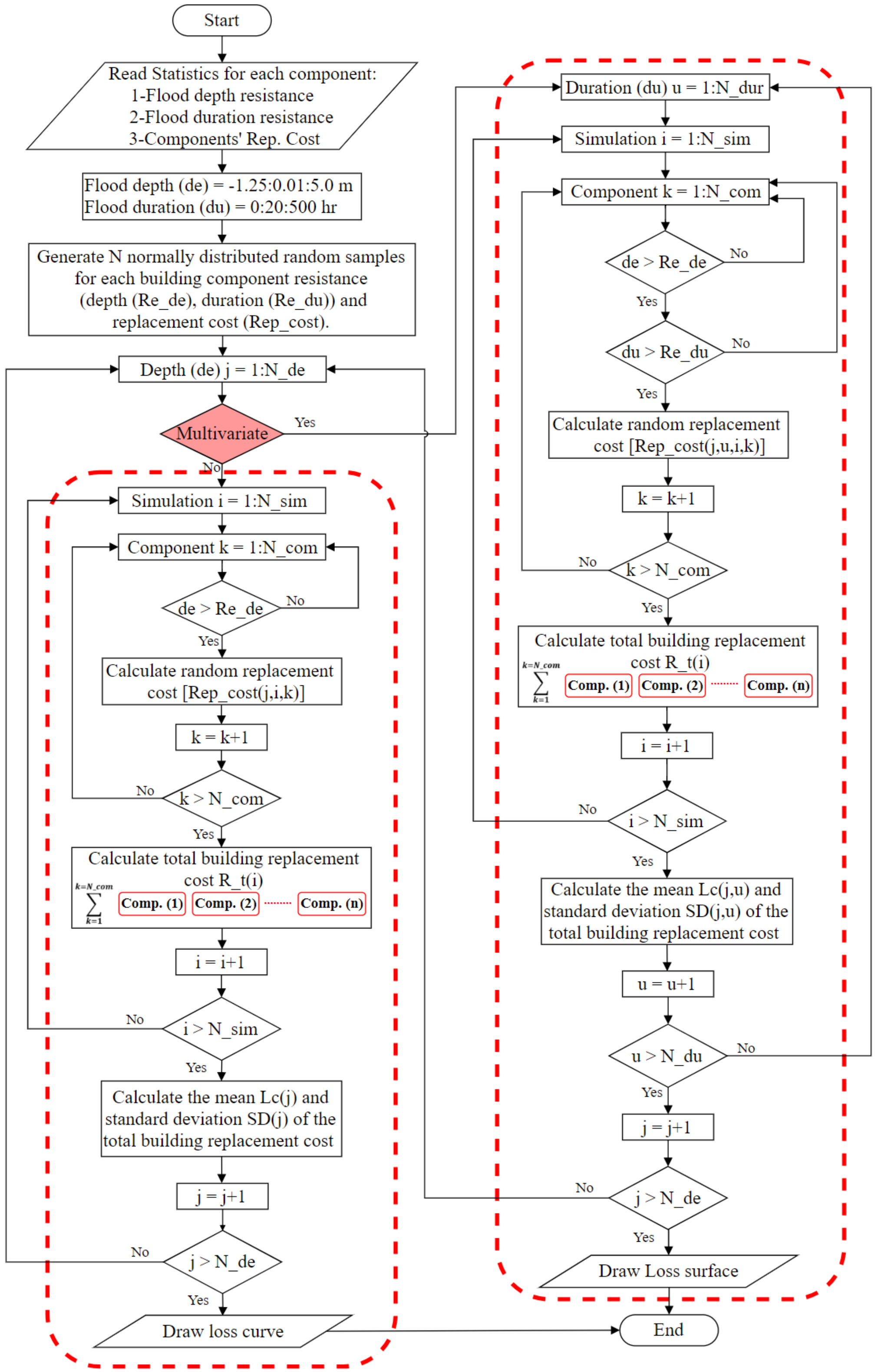

Figure 2-8. *A flow chart illustrates a methodology to develop a single-variable and a multivariate flood loss function for buildings where N_com = number of components, N_de = Number of depth steps, N_sim = number of simulations, and N_dur = number of duration steps*

2.2.3 *Example Archetype to Illustrate the Proposed Approach*

The proposed approach was applied to a one-story single-family residential wood building with a hip roof and crawl space foundation (archetype F1). This archetype has two bedrooms, two bathrooms, one large living room, and a kitchen. Figure 2-9 shows the details and dimensions of the illustrative archetype. The whole building is represented by 65 components that cover virtually all of the building structural, non-structural, and interior components. Figure 2-10 shows a visual representation for selected components along with a section plan view showing the interior design that shows the assumed location for each component within the building. Reasonable assumptions were made about the building interior design and the location of different components within the building. The HVAC ductwork was assumed to be located in the crawl space and some basic assumptions were made related to other components including the number and location of electrical outlets and switches. The total building replacement cost was calculated based on these assumptions. Table 2-2 provides a summary of these 65 components and Table 2-3 provides statistical details for 11 selected components which are in bold in Table 2-2. For complete data, readers are referred to the uploaded data provided with these publications (Omar M. Nofal and van de Lindt, 2020b; Omar M. Nofal, van de Lindt, and Do, 2020). Fig. 2-11(a and b) show an example of the used truncated normal distribution with respect to the regular normal and uniform distribution for the wood flooring component for both flood depth and flood duration, respectively. Table 2-4 presents the mean and standard deviation for the replacement cost corresponding to each DS for this specific example archetype. A detailed unit price analysis of each component was conducted to provide a final DS replacement cost percentage (Lr) and a cumulative DS replacement cost percentage (Lr_c).

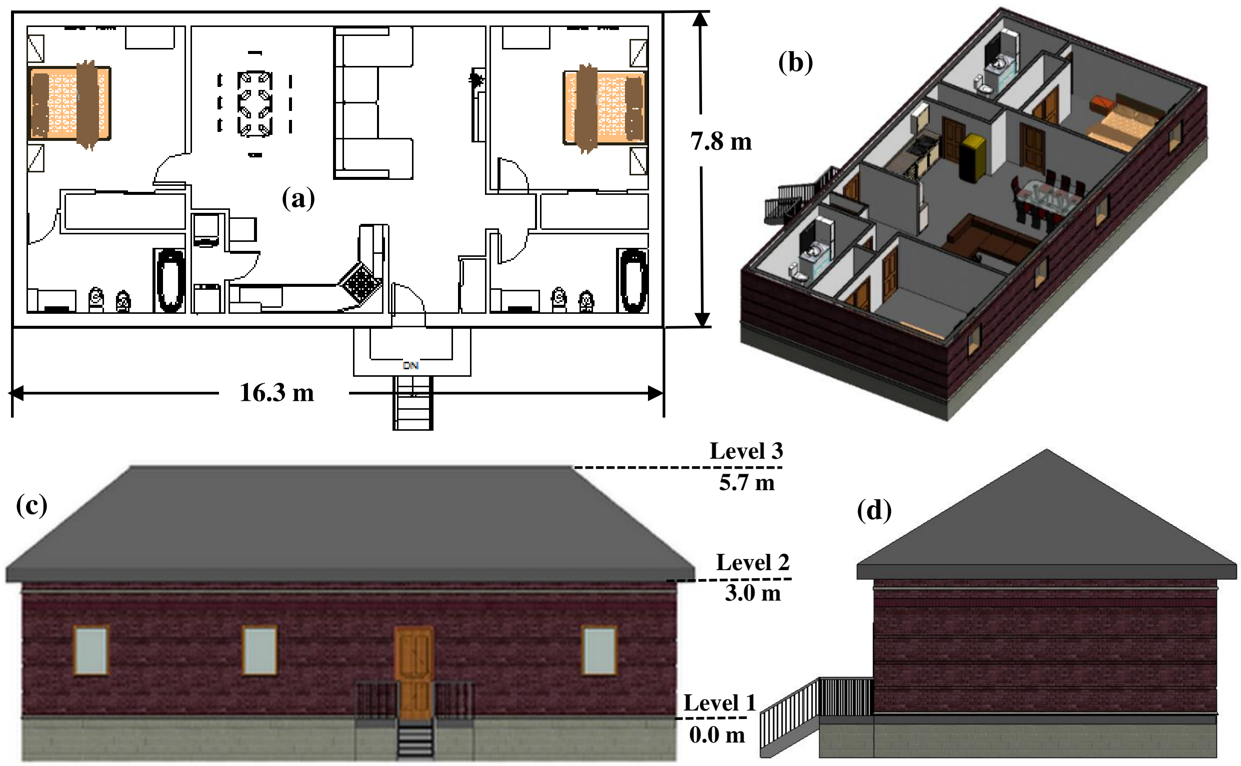

Figure 2-9. *Building archetype layout; (a) Plan view; (b) 3-D view; (c) Front view; (d) Side view*

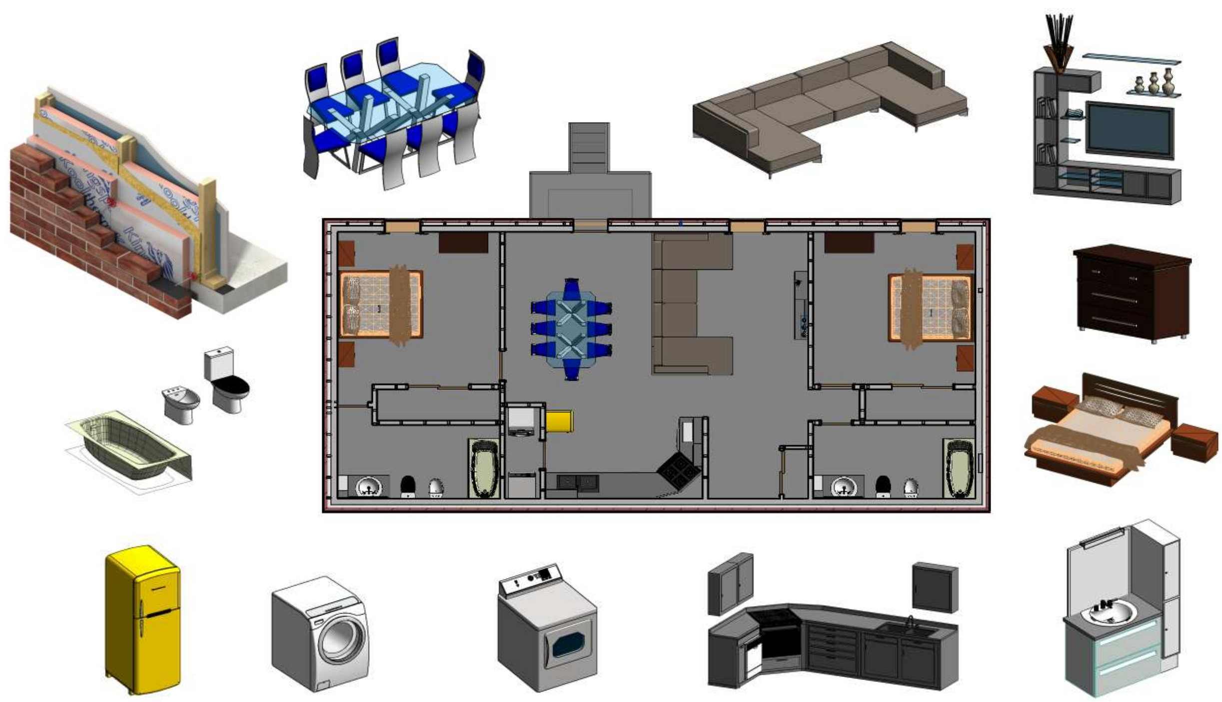

Figure 2-10. *Visual representation of the building archetype interior design and some of its components*

Table 2-2. *A list of the 65 damageable components used to represent the residential building archetype*

Building Components				
Chairs	**Wood Framing**	Windows	**Flooring Insulation**	Crawl Space Foundation
Desks	Heating Unit	Painting	**Drywall (DS3)**	**Wood Flooring/Tile flooring**
TV	Dishwasher	Bath Tube	Kitchen Countertop	Bathroom Upper Cabinets
AC Unit	Wood Trim	Entrance Stair	Baseboard Heaters	External Wall sheathing (DS2)
Speakers	Sofa and couches	Attic Insulation	Bathroom lower Cabinets	Exterior Cladding (DS2)
Ceiling	Bath Countertop	Lights fixtures	Internal walls Insulation	**Kitchen Upper Cabinets**
Baseboard	Drywall(DS2)	Exterior Doors	**Crawlspace Insulation**	External Wall sheathing (DS3)
Carpet	TV mount/Stand	Bath Sink	Roof (Trusses, Rafters)	Exterior Cladding (DS3)
Refrigerator	**Lower Cabinets**	Mixers	Mid Electrical outlets	Bed Room (Beds, mattress, etc.)
Stove	Bath Toilet	Microwave	Electrical Switches	Parking Pads and pavement
Washer	Interior Doors	Computer	Base Electrical outlets	**Decking (Floor Beams +Plywood)**
Dryer	Closet Doors	Laptop	Window AC Units	Roof (Membrane, Sheathing)
Water Heater	Control Box	Printer	Vented/Range Hood	HVAC Pipes/Ducts

Table 2-3. *Damage states description along with their damage scale and damage ratio as a percentage of the total building replacement cost.*

Component	DS0		DS1		DS2		DS3		DS4	
	Crawlspace Insulation	Flooring Insulation	AC Unit/ Heater	Wood Flooring	Washer/ Dryer	Lower Cabinets	Drywall (DS3)	Upper Cabinets	Wood Framing	Decking Flooring
Min depth (m)	0.0	0.6	0.0	1.0	1.05	1.0	2.5	2.3	2.0	2
Max depth (m)	0.4	1.0	1.5	1.5	1.25	1.9	4	3	5.5	5
Mean depth (m)	0.2	0.8	0.75	1.25	1.15	1.45	3.15	1.65	3.75	3.5
Stan. Dev. of depth(m)	0.1	0.1	0.375	0.125	0.05	0.225	0.375	0.175	0.875	0.75
Min duration (hr)	0.0	0.0	0	6	0.0	12	0	12	96	72
Max duration (hr)	1.0	1.0	1	48	0.5	36	1	36	240	240
Mean duration (hr)	0.5	0.5	0.5	27	0.25	24	0.5	24	168	156
Stan. Dev. of duration (hr)	0.25	0.25	0.25	10.5	0.125	6	0.25	6	36	42
Min Rep. Cost (USD $)	1420	710	3700	3720	350	9000	1167	6000	7100	14200
Max Rep. Cost (USD $)	4260	2130	7200	6820	1500	18000	3501	12000	18460	35500
Mean Rep. Cost (USD $)	2840	1420	5450	5270	925	13500	2334	9000	12780	24850
Stan. Dev. of Rep. Cost ($)	710	355	875	775	287	2250	583	1500	2840	5325

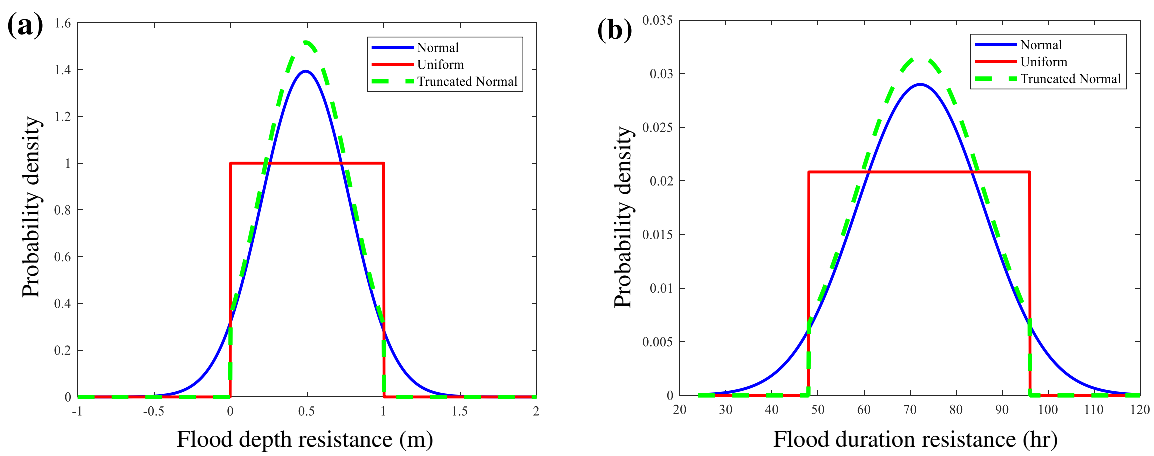

Figure 2-11. *Truncated normal distribution for the wood flooring component with respect to the normal and uniform distributions: (a) Flood depth resistance; (b) Flood duration resistance*

Table 2-4. *Flood loss statistics for each damage state along with the replacement cost for each DS*

DS	Mean DS Loss (USD $)	Standard Deviation of a DS Loss (USD $)	Mean DS Loss Cum.(USD $)	Lr %	Lr_c%
DS0	4260	794	4260	0.02	0.02
DS1	23654	2121	27914	0.11	0.13
DS2	65160	4978	93074	0.29	0.42
DS3	51832	3543	144906	0.23	0.65
DS4	78952	7924	223858	0.35	1.00

2.2.3.1 2-D Flood fragility function based on flood depth

The MCS procedure illustrated in the earlier flow chart in Figure 2-3 for developing single-variable component fragilities was used to develop fragility curves for building components. Each component failure was assumed to be statistically independent of the other components. Figure 2-12 presents the resulting fragility curves for all 65 building components with a legend for only six components as an example. The reader is referred to the full data set provided in this publication (Omar M. Nofal et al., 2020)for all components (and other data). Figure 2-12 helps explain the variability of the building components in terms of their susceptibility of being damaged as a function of flood depth. A number of components failure due to flood depth is almost deterministic because of the low uncertainty in their elevation from the FFE and their sensitivity to floodwater, i.e. they cannot resist water for more than a moment (e.g., electronics, appliances, machinery, etc.). These components are considered a total loss when their circuit board is touched by water which describes many of the fragility curves in Figure 2-12 whose entire fragility is contained between 0 and 0.5m depths. On the other hand, several fragility curves are damageable in a much longer depth range because of either the high uncertainty in their elevation or the uncertainty in their damage behavior.

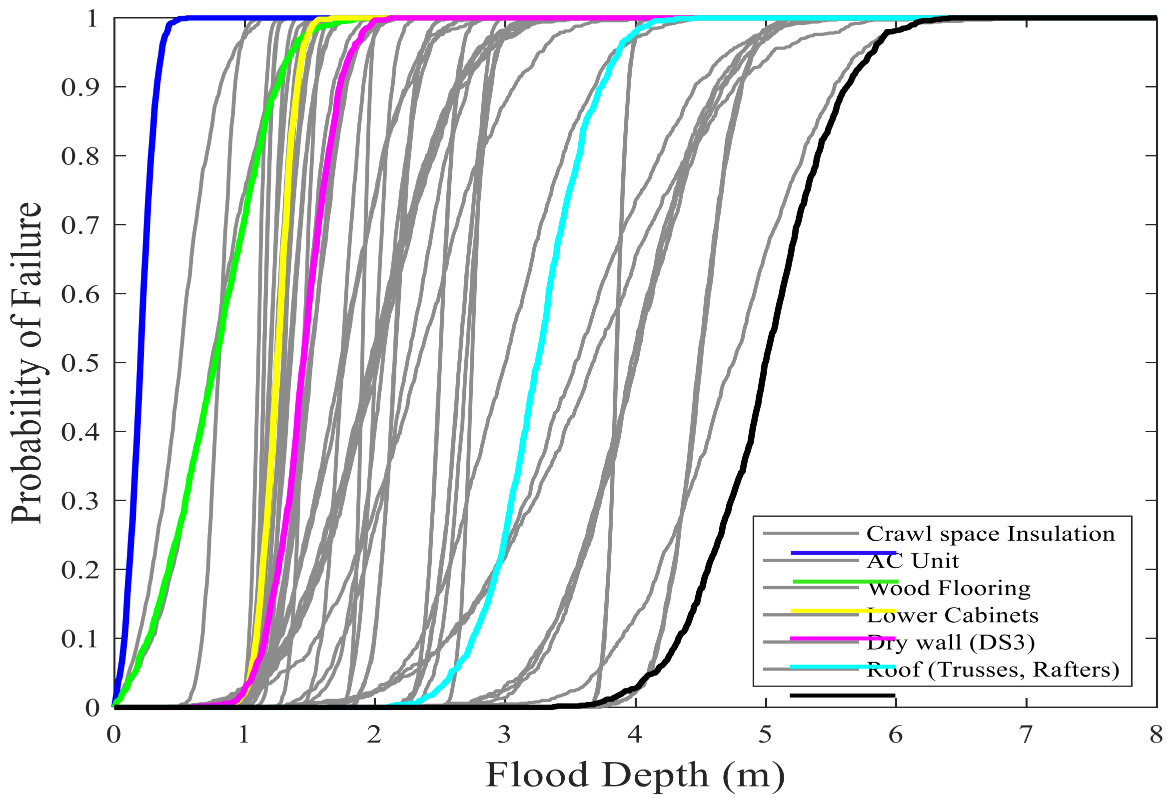

Figure 2-12. *Components fragility curves for all the 65 components with six highlighted components for illustration*

The total building fragility function uses component failure to characterize the whole building damage along with the DSs described in Table 2-1 using the framework described in the flow chart in Figure 2-5. A single-variable building fragility function was developed using the 3D component damage matrix (*Dm(i,j,k)*) to capture the exceedance probability for each DS at each flood depth without considering flood duration. Final building fragility curves are shown in Figure 2-13. Fragility curves for the DSs dominated by water-sensitive components (e.g., appliances, electronics, machinery, etc.) such as DS0, DS1, and DS2 are steeper than DS3 and DS4 because of their high susceptibility to being damaged from flood water which underscoring their low variance. On the other hand, most of the non-structural structural components are included in DS3 and DS4. Figure 2-13 also shows that the building will be completely damaged at approximately

7.0m flood depth with 100% exceedance probability of DS4. This is the stage of the flood depth that makes the building fully submerged with water and replacement of the whole structure is required.

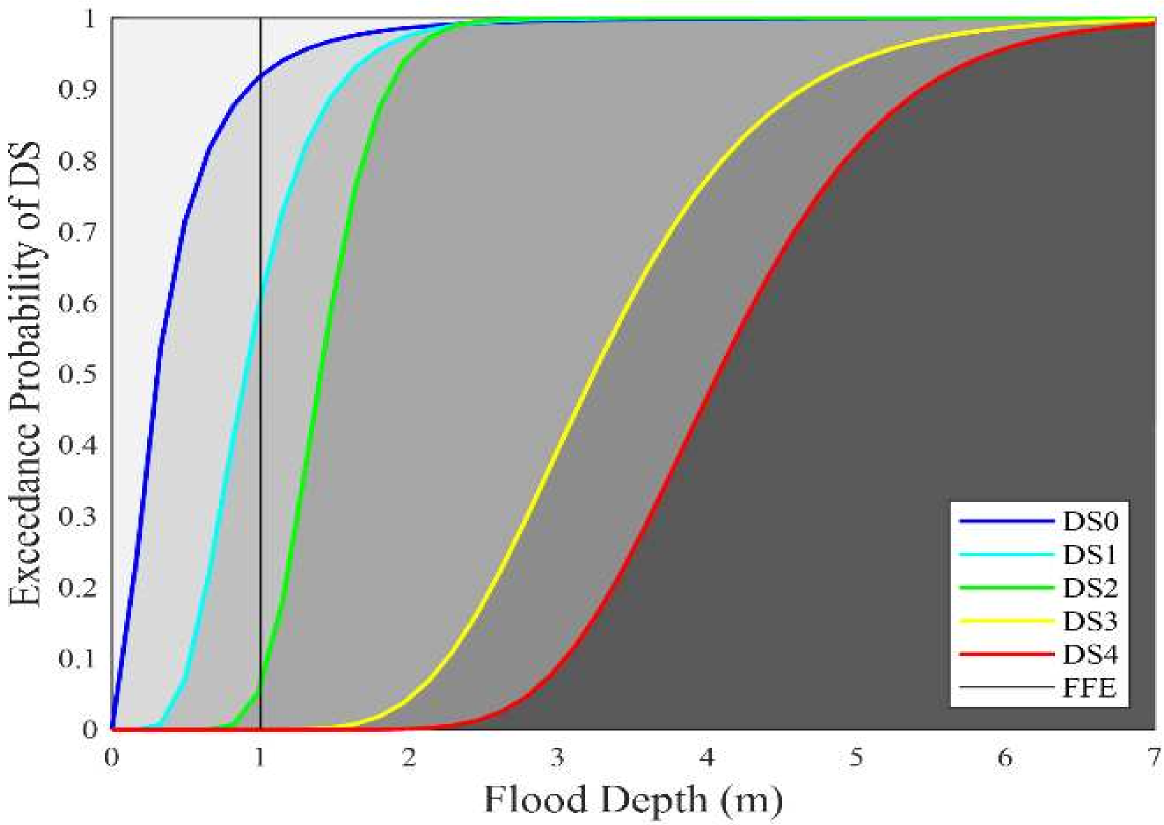

Figure 2-13. *Building fragility curves function in the flood depth measured from the ground elevation*

2.2.3.2 2-D Flood loss function based on flood depth

Three different flood loss approaches were developed and applied as described in the previous section. The analysis results are compared with the HAZUS flood loss function to provide some level of benchmarking. To account for component losses, the first part of method (1) was used to develop flood loss curves for each component by multiplying failure probabilities for each component by its replacement cost at each flood depth. Figure 2-14 only shows component loss curves for the six selected components that have been contrasted in the component's fragility. Each loss curve is shown with a one-standard-deviation (±σ) range to provide some measure of the uncertainty level within each component. The flood loss analysis shows that some components are quite costly and the loss of such components could be more than USD $25000 (e.g., Decking, cabinets, etc.) while other components may be less than USD $200 (e.g., TV mount, printer, etc.). This, in turn, explains the high variability in the component loss curves presented in Figure 2-14.

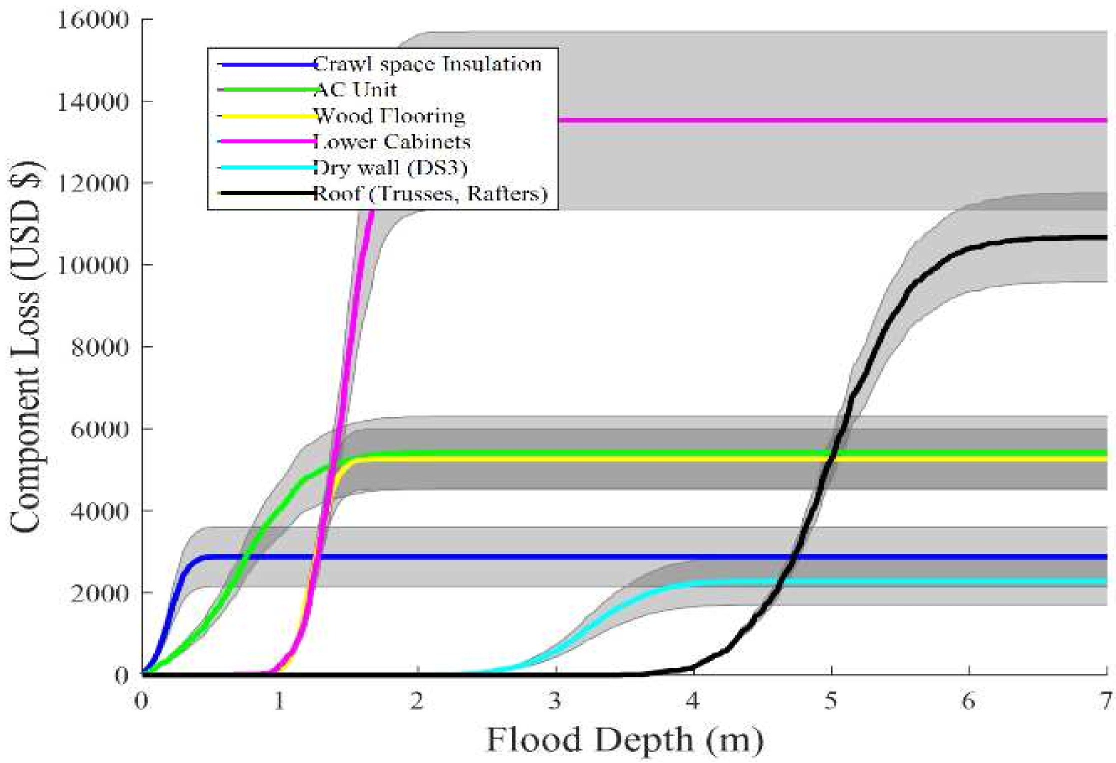

Figure 2-14. *Components loss curves for the six-selected components for illustration*

Figure 2-15 presents the resulting flood loss curves of the proposed three flood loss methods and the corresponding HAZUS stage-damage function for the example one-story residential building. The analysis shows that the flood loss curve using method (1) coincides with the flood loss curve using method (3). In the same figure, the flood loss curve using method (3) is shown with respect to the scatter of the randomly simulated total building flood losses, method (2), and HAZUS stage-damage function. The resulted flood loss functions using the proposed methods showed a good match with the HAZUS stage-damage function. The flood loss curve using method (2) is felt to be quite a practical estimate of flood losses given that it can be calculated directly from fragility curves.

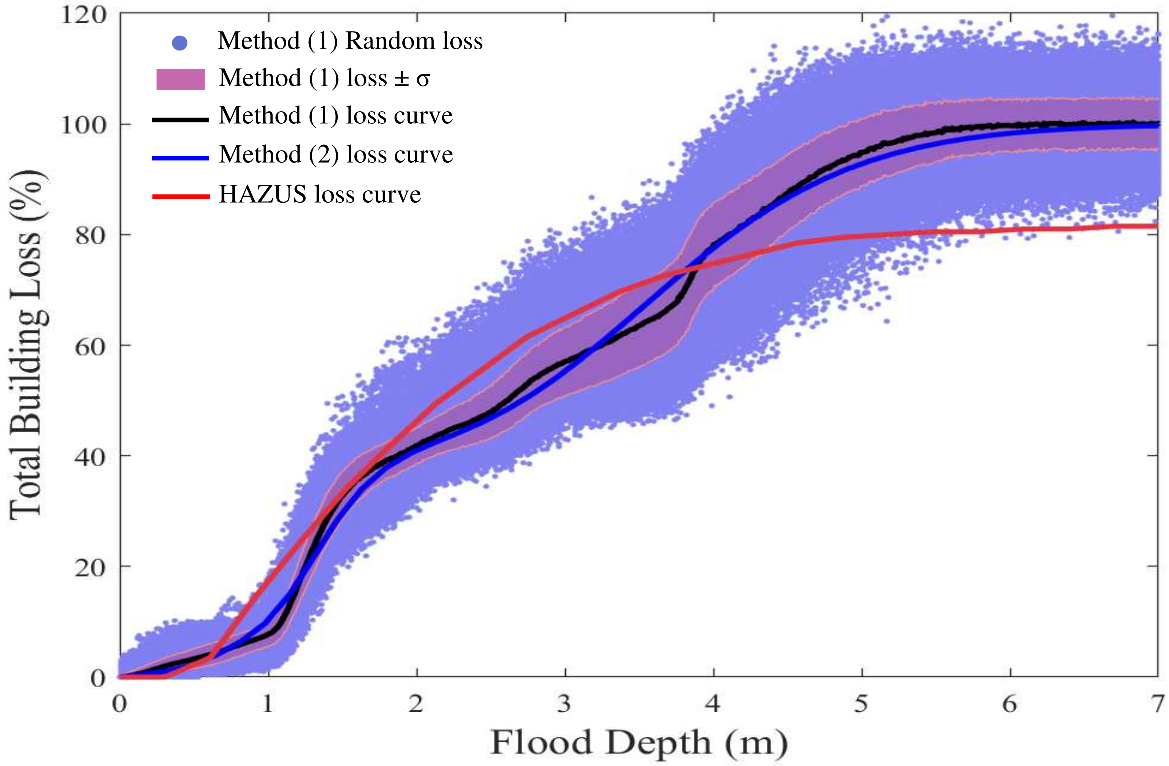

Figure 2-15. *Building loss function for the multiple loss methods in the flood depth measured from the ground elevation*

It should be noted that method (1) and method (3) are using the same randomly generated component damage matrix (Dm(i,j,u,k)) but different versions. Method (1) is using the Dm matrix that has binary values (1: Damaged, 0: Not damaged) in its fields and then these binary values are translated into component failure probabilities (component fragility functions), then these failure probabilities are multiplied by the replacement cost of each corresponding component to account for component losses and then summing up these component losses to account for the total building losses. Method (3) is using another version of the Dm matrix that has corresponding random loss values directly in its fields without the need to develop components fragilities, and then summing these component losses to account for the total building losses which is easier and more direct.

Therefore, method (1) and method (3) result in the same flood loss curves which would happen to any application because of this feature.

The proposed flood loss functions developed in this study show a good match with the HAZUS loss curve, which has been empirically validated, up to a flood depth of four meters. The small difference between the proposed flood loss method and HAZUS stage-damage functions in this range is likely related to the generalization in the HAZUS damage curve intended to cover a wide range of one-story buildings. The proposed loss functions in this study provide a good quantification of flood losses based on the selected building archetype and the assumed interior design. For flood depths of more than 4.5m, the loss functions developed in this study predict losses 18% higher than the losses predicted by the HAZUS damage curve. HAZUS damage curves are based on subassembly losses (FEMA, 2009a) and each subassembly represents a percentage of the total building replacement cost as shown in Figure 2-16(a). In HAZUS, structure and foundation subassemblies never reach 100% damage even when the building is considered a total loss. HAZUS assumes that buildings are considered a total loss at 20% foundation damage and 42% structural damage as shown in Figure 2-16(a). Additionally, the HAZUS damage curve separates structure damage from content damage and both show that the maximum damage that a building could have is 82% as shown in Figure 2-16(b). This assumption still exists even with a building submerged in seven meters of floodwater. However, the numerical loss functions developed herein assume that if a building reaches DS4, the building could be either replaced or demolished as described in Table 2-1. Therefore, based on the loss formulation in this study, buildings can reach 100% loss if the building is submerged even when the foundation and some structural elements may be salvageable.

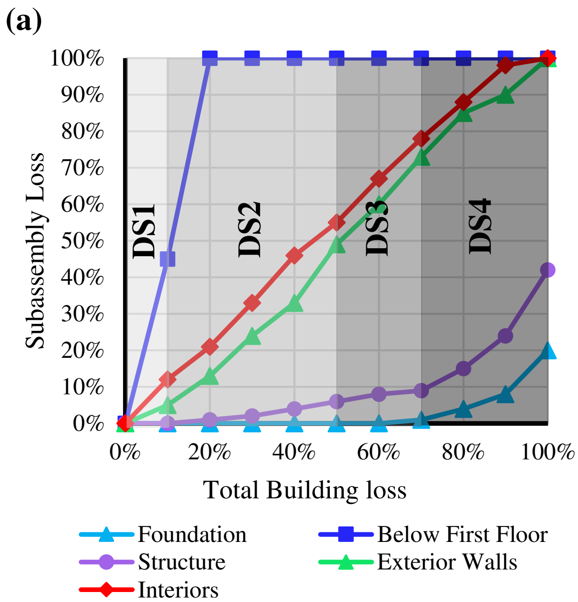

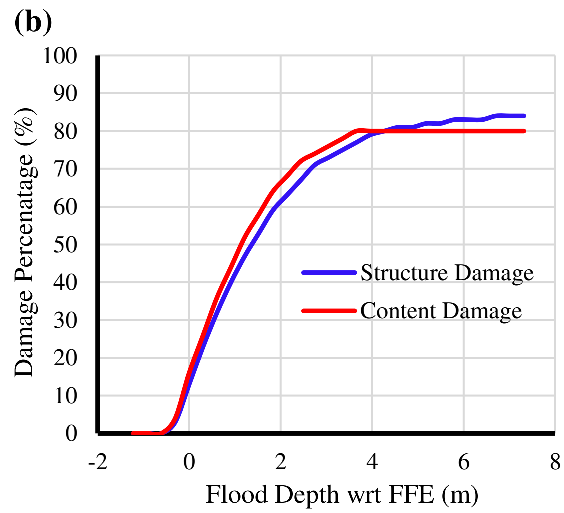

Figure 2-16. *HAZUS total building loss percentage and their subassemblies loss percentages* (FEMA, 2009a)*: (a) Relationship between subassembly loss and the total building loss; (b) RES1: a single family residential building*

2.2.3.3 3-D Flood fragility function based on flood depth and flood duration

As formulated earlier, a multi-variate fragility function is presented in terms of flood depth and flood duration resistance of each component. The approach summarized in the flow chart for the multi-variate components flood fragility function in Figure 2-3 was used to develop the 65 component fragilities. MCSs were used to generate random samples for each component's flood depth and flood duration resistance. A comparison of the fragility and loss curves and surfaces using 100 versus 1000 simulations was conducted as a sensitivity study. It was determined that 100 simulations were not quite sufficient for the level of accuracy needed in this study, but 1000 simulations were found to be accurate and applied at each flood depth and duration. Figure 2-17(a) shows a 3-D fragility surface for the AC unit component as an example. This figure shows that the fragility function variation is only a function of flood depth with little or no effect from the flood duration which is rational as the source of the uncertainty to the AC unit is its elevation and once it gets touched by water, it will be ruined. Other components can be observed to deteriorate over time (e.g., wood furniture, wood structural system components, sheathing, doors, etc.). Figure 2-17(b) shows a 3-D fragility surface for the wood framing component, as an example of components that are made of wood that take more time to deteriorate than, for example, electronics. Therefore, it can be seen that failure probability for such a component depends on both flood depth and duration. Once the component fragility surfaces were developed, they are assembled to form the 3D flood fragility surfaces for the entire building. The multi-variate fragility approach described in the flow chart in Figure 2-5 was applied. Figure 2-18 shows fragility surfaces for each DS along with a figure that has all the DS in one graph.

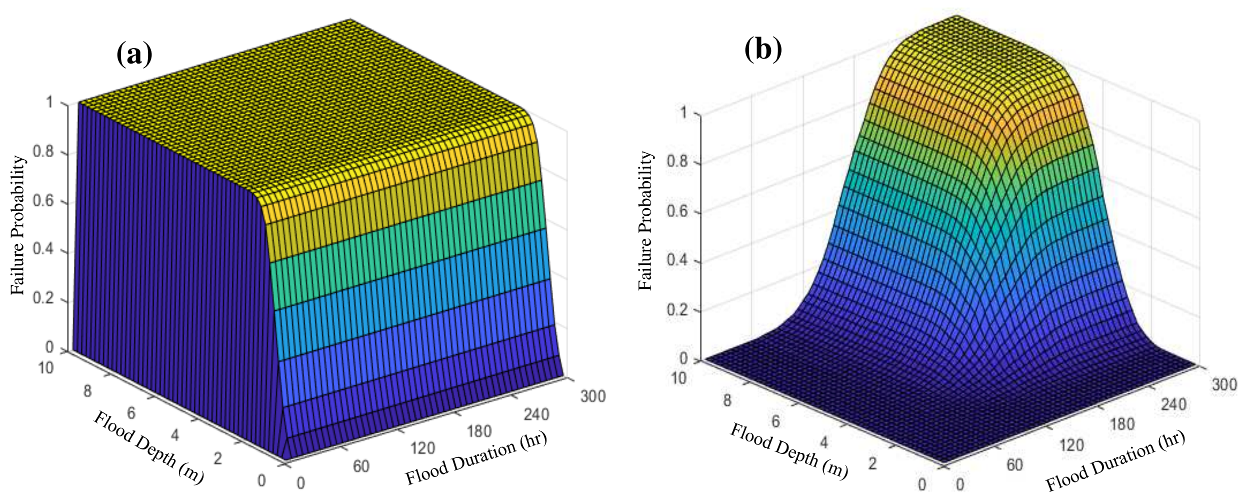

Figure 2-17. *3D flood fragility surfaces for six selected components in terms of flood depth and duration: (a) AC unit; (b) Wood framing*

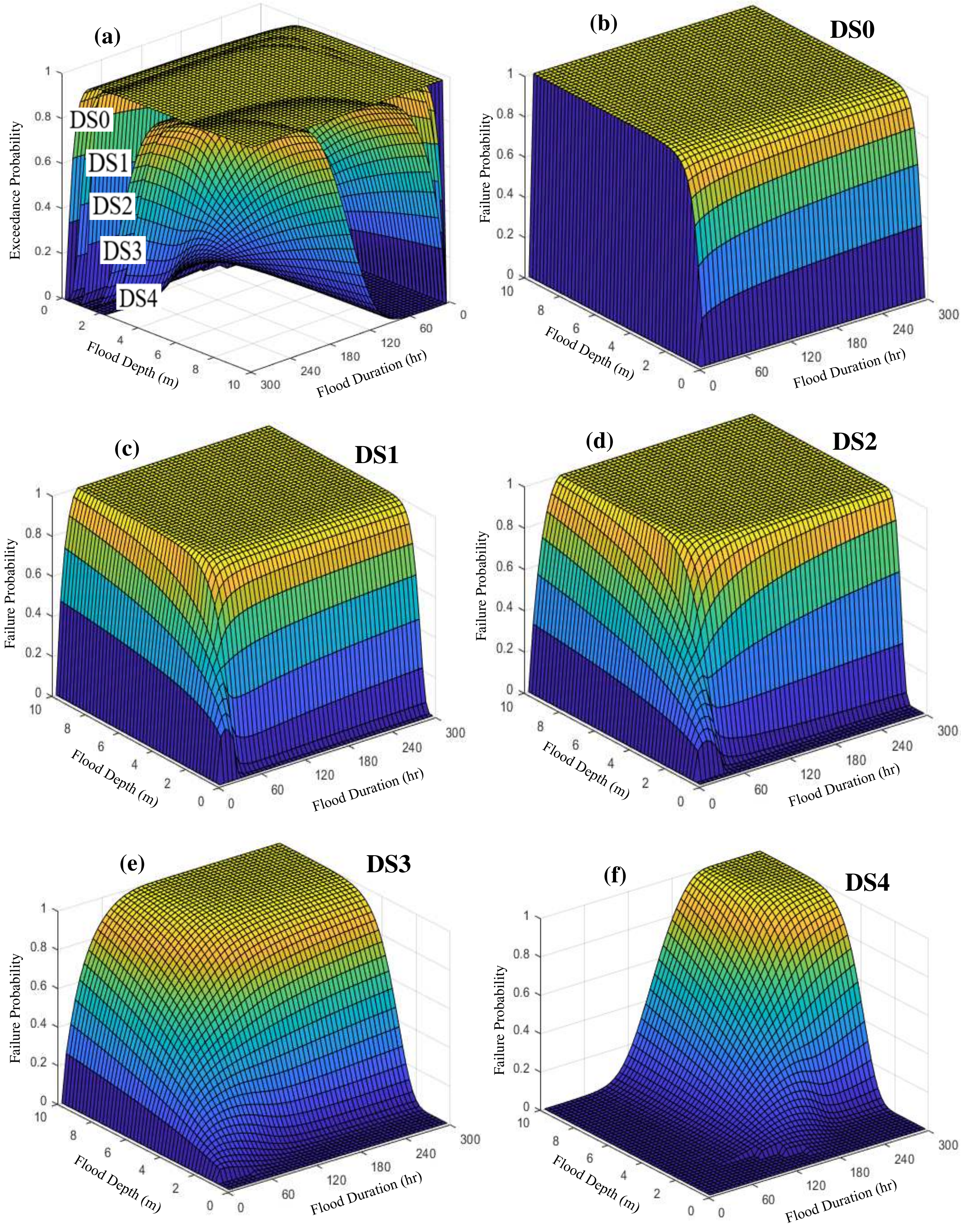

Figure 2-18. *3-D flood fragility surfaces for the whole building in terms of flood depth and duration: (a) All building fragility curves; (b) Fragility curve for DS0; (c) Fragility curve for DS1; (d) Fragility curve for DS2; (e) Fragility curve for DS3; (f) Fragility curve for DS4*

2.2.3.4 3-D Flood loss function based on flood depth and flood duration

In order to compute a 3-D loss surface using method (3), the analysis begins with the loss calculation for each component by propagating uncertainties in flood depth and flood duration resistance for each component as well as propagating uncertainty in each component replacement cost. For the entire analysis process including each flood depth, each flood duration, and each component, 1000 simulations were again generated to investigate the damage for the entire building component using the damage matrix. For each simulation, a replacement cost was generated from the associated distribution for each damaged component. For each component, the mean and standard deviation of the 1000 simulated replacement costs were calculated at each flood depth and flood duration. Then, the loss surface for each component can be developed which is similar to the component fragility curves but includes the replacement cost of the component as the probabilistic component replacement cost equal to the failure probability of the component multiplied by the replacement cost of this component.

Finally, in order to generate the total building loss surface, the replacement costs for all damaged components within each simulation are summed to calculate a stochastic total building replacement cost at each flood depth and duration. The mean of the 1000 simulated total building replacement costs was calculated and plotted as shown in Figure 2-19(a). Figure 2-19 shows that flood duration has a significant impact on flood losses implying that the application of loss functions that only depends solely on flood depth may result in less accuracy when estimating flood losses. The 2D flood loss curves that were developed previously are projected on the 3D flood loss surface in Figure 2-19(b) to better illustrate the impact of flood duration on the amount of total flood losses. It shows that the 2D flood loss curve developed using method (2) and method (3) represent the state of flood damage at flood duration of more than 200 hours, i.e. when flood duration is not accounted for, building components will be considered to be a total loss instantly when touched by water at the damaging flood depth. On the other hand, the HAZUS 2-D flood loss curve (stage-damage function) projection on the 3-D flood loss surface shows that the HAZUS 2D flood loss curve better express the state of flood damage at flood duration in the range between 120 to 180 hrs which could explain their lower estimate of flood losses than the proposed method.

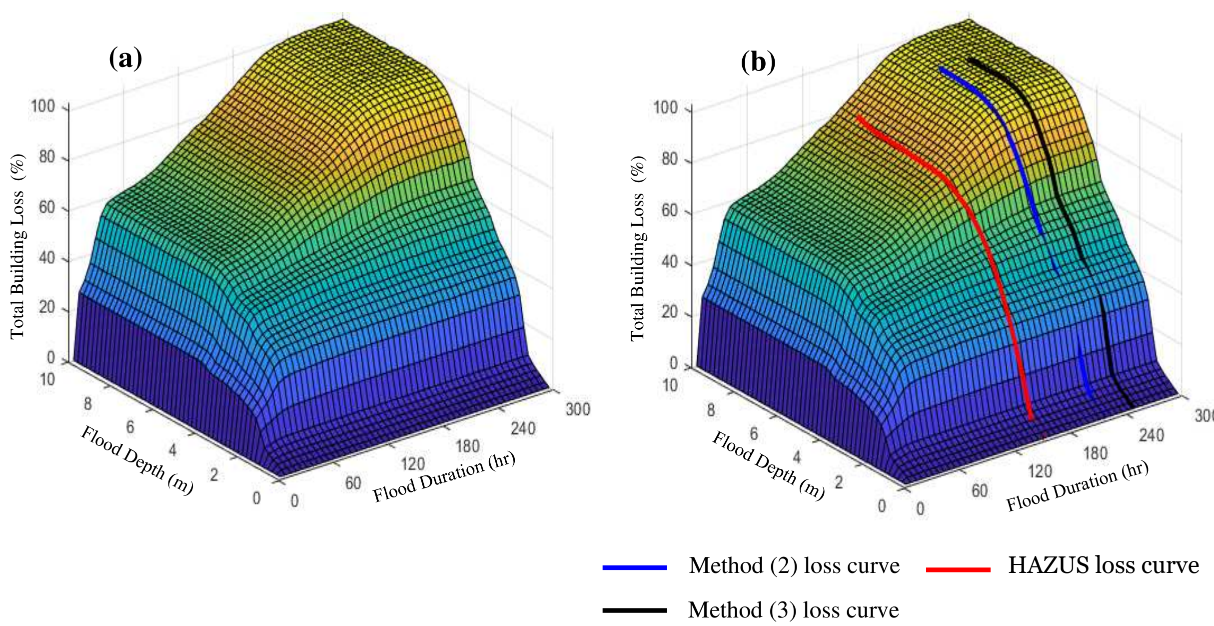

Figure 2-19. *Flood loss surface: (a) 3D flood loss surface for the whole building in terms of flood depth and duration; (b) The projection of the 2D flood loss curves on the 3D flood loss curves*

2.3 Minimal Building Flood Fragility and Loss Functions

Building sectors within a community including the residential sector, commercial/business sector, and social institutions (e.g. schools, hospitals) were divided into 15 building archetypes as shown in Figure 2-20. Table 2-5 shows a list of these archetypes along with a brief description for each one. Full details for each building archetype including dimensions, interior design, plans, 2-D, and 3-D views are all provided in Appendix A at the end of this dissertation. These archetypes are intended to provide a reasonable representation of the buildings within a small to middle size community, however, it is recognized that some buildings and community-specific buildings may not be represented (e.g. water treatment plants, electric power plants, or substations, water tanks, etc.). It is planned to eventually include such buildings and facilities in future work, but it is beyond the scope of the current dissertation. The exterior and interior design of these building archetypes are based on real buildings existing in the United States.

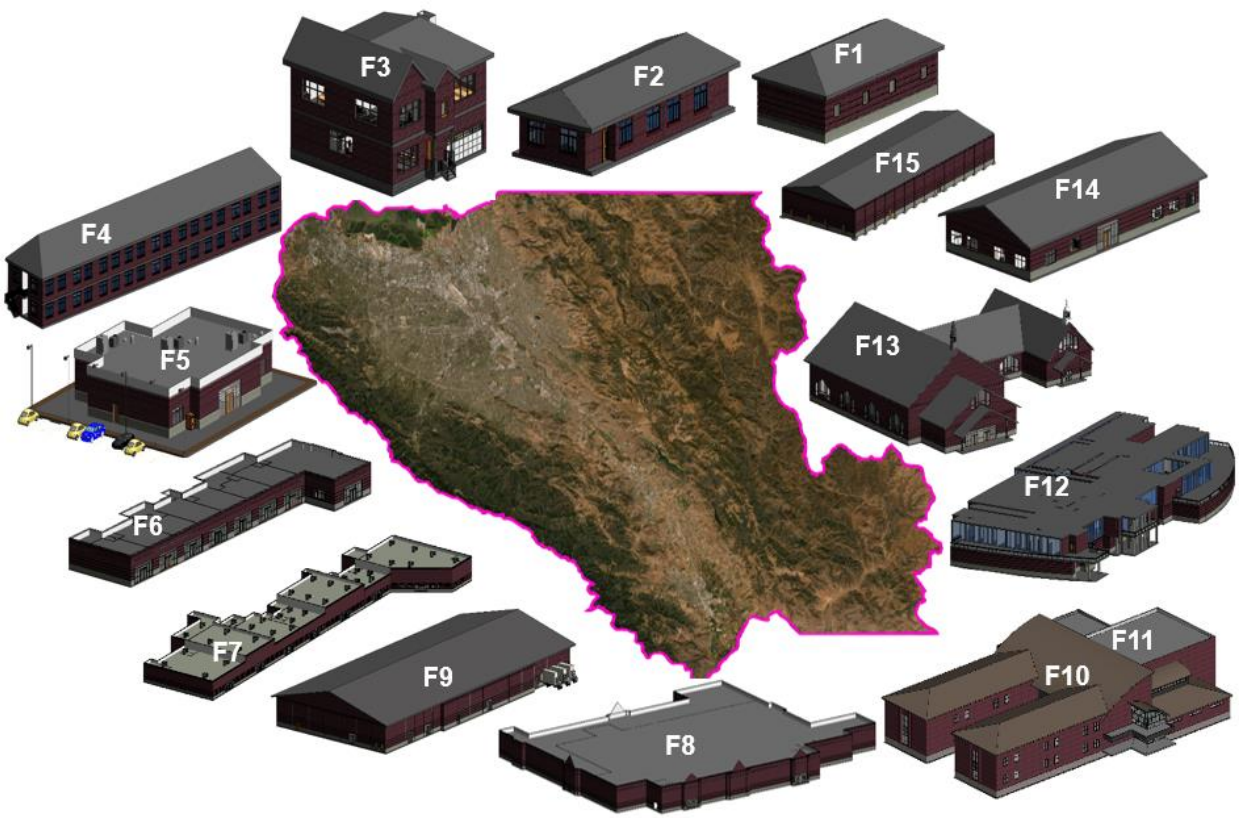

Figure 2-20. *Schematic representation of the 15 building archetypes portfolio to model a community*

These archetypes were selected by navigating more than 20,000 buildings within a typical eastern U.S. community using Google Street Map view (Omar M Nofal and van de Lindt, 2020) and field-surveying a number of these buildings during a longitudinal Field study (van de Lindt et al., 2018). The assumed building size and shape can be modified to match other sizes and shapes of buildings as needed to ensure loss calculations are proportional to building size, so simple multipliers can provide a relatively straight forward expansion of the archetype portfolio for more accuracy. A building information model (BIM) for each building archetype was created using Autodesk Revit Architecture (Autodesk, 2020). BIM models help to visualize building components and enable fast surveying/counting of construction quantities. Building price variability in terms of economy and luxury components is also considered by assuming upper and lower bounds for each component replacement/repair cost. Once this process was completed, MCS was used to include these uncertainties to account for a probabilistic building replacement/repair cost.

Table 2-5. *The building archetypes description (more details provided in Appendix A)*

Building archetype	Building description
F1	One-story single-family residential building on a crawlspace foundation
F2	One-story multi-family residential building on a slab-on-grade foundation
F3	Two-story single-family residential building on a crawlspace foundation
F4	Two-story multi-family residential building on a slab-on-grade foundation
F5	Small grocery store/Gas station with a convenience store
F6	Multi-unit retail building (strip mall)
F7	Small multi-unit commercial building
F8	Super retail center
F9	Industrial building
F10	One-story school
F11	Two-story school
F12	Hospital/Clinic
F13	Community center (place of worship)
F14	Office building
F15	Warehouse (small/large box)

Here are more details related to each building archetype including descriptions, dimensions, and interior design is presented. Appendix A provides detailed archetypes dimensions and 3-D views. It should be noted that mid- and high-rise buildings are not explicitly included in the suite of archetypes since these are generally very unique and would be handled on a case-by-case assignment basis while setting up a community-level model:

F1: One-Story Single-Family Residential Building: F1 archetype is considered a typical one-story single-family residential housing unit in the US with a small rectangular plan (16.3 x 7.8) with a total area of 127 m2 (1370 ft2). This housing unit could be in the form of a modular home. It consists of two bedrooms and a medium-size living room with a wood frame structural system and exterior brick walls on a crawlspace foundation. Uncertainties in the structure system type and the component's flood resistance (flood depth and flood duration resistance) along with its replacement/repair cost were considered. This housing unit can be assigned to a regular one-story single-family residential building. More details on this archetype could be found in a manuscript that details the methodology to develop a flood fragility surface and loss surface as a function of both flood depth and duration (Omar M. Nofal et al., 2020).

F2: One-Story Multi-Family Residential Building: The F2 archetype is a typical one-story multi-family residential archetype that has a medium size rectangular building (27m x 11m) with a total area of 297 m2 (3200 ft2). Such a building consists of four apartments with an area of 74 m2 (795 ft2) each. The structure system was assumed to be a wood frame with exterior brick walls on a slab-on-grade foundation. The interior design of the building was assumed to account for the components that could be accommodated in this area.

F3: Two-Story Single-Family Residential Building: The F3 archetype is a regular two-story single-family residential building in the US with a small size square plan (12.3m x 11.8m) with a total area of 145 m2 (1562 ft2). The building structure system is assumed to be a wood frame with exterior brick walls on a crawl space foundation with an interior garage on a slab-on-grade foundation.

F4: Two-Story Multi-Family Residential Building: This archetype, F4, is a two-story multi-family residential building with a large rectangular plan (81.6m x 14.0m) with a total area of 1142 m2 (12290 ft2). It consists of 24 apartments with an area of 74 m2 (795 ft2) each. Multi-family residential buildings could be found in other forms such as a stacked duplex or multi-story buildings. However, the selected building archetype could represent a number of different two-story buildings within a community. The building structure system was assumed to be a wood frame building with exterior brick walls on a slab-on-grade foundation.

F5: Small Grocery Store/Gas Station with a Convenience Store: The F 5archetype is a typical small to a medium gas station (as opposed to a truck stop size gas/diesel station) attached with a convenience store that has a medium size rectangular plan (27m x 15m) with a total area of 405 m2 (4360 ft2). The same archetype could be assigned to a small size grocery store since the building is under consideration in the damage and loss analyses herein. The structural system is a bolted steel frame with light gauge steel or wood studs along with exterior brick walls resting on a slab-on-grade foundation. Full interior design was assumed based on field visits to a number of gas stations.

F6: Multi-unit retail building (strip mall): The F6 archetype is a large strip mall that includes a number of large size businesses such as restaurants/café, bars, grocery stores, clothes stores, toy stores, auto parts stores, etc. This archetype has a large size rectangular plan (230m x 55m) with a total area of 9370 m2 (100860 ft2). The F6 archetype could be assigned to large-size multi-unit retail/business buildings (strip malls) within a community using proper scaling and factorization based on building size. The structural system is a steel frame with steel/wood studs along with exterior brick walls rested on a slab-on-grade foundation. Full interior design was assumed based on several visits and surveying many strip malls.

F7: Small multi-unit commercial building: The F7 archetype is a small-size multi-unit commercial building that includes a number of small businesses such as a restaurant/café, grocery store, office, pharmacy, electronics store, etc. This archetype has a small size rectangular plan (68m x 13m) with a total area of 1037 m2 (11160 ft2). The F7 archetype could be assigned to small size buildings with multiple businesses represented within a community again with proper scaling and factorization based on building size. The structural system is a steel frame building along with exterior brick walls rested on a slab-on-grade foundation. Full interior design was assumed based on several visits and surveying small businesses.

F8: Super retail center: The F8 archetype is a regular mega-market/shopping/retail center (e.g., Walmart or Target in the U.S.) with a large size rectangular plan (200m x145m) with a total area of 29000 m2 (312153 ft2). This archetype could be assigned to stores/shopping centers from medium size to big sizes with proper scaling of the buildings' market value. The structural system is a steel frame with steel/wood studs along with exterior brick walls rested on a slab-on-grade foundation. Full interior design was assumed based on several visits and surveying many supermarkets.

F9: Industrial building: The F9 archetype is a medium industrial building (e.g., light bulbs, clothes, pets' food, etc.) with a large rectangular floor plan (140m x 65m) with a total area of 9100 m2 (9800 ft2). This archetype could be assigned to any industrial building ranging from light to heavy industry with proper scaling of the building market value. The structure system is a steel frame along with exterior brick walls resting on a slab-on-grade foundation.

F10: One-story School: A one-story school building with a large size rectangular floor plan (92m x68m) with a total area of 6256 m2 (67340 ft2) is assigned as archetype F10. The structural system is assumed to be unreinforced masonry on a slab-on-grade foundation. It could be assigned for any school building (e.g. elementary, middle, high school, etc.) that matches the same size and the archetype properties. The layout of this school will be the same as archetype F11 but one-story other than two stories.

F11: Two-story School: The F11 archetype is a two-story school building that has the same characteristics as archetype F10, but it is a two-story school building.

F12: Hospital/Clinic: The F12 archetype is a medium-size two-story hospital with a rectangular plan (160m x75m) with a total area of 12000 m2 (129160 ft2). The structural system could be a concrete/steel frame on a raft foundation. Prices for hospital units (e.g., X-RAY, ICU, NICU, ER, Mortuary, Dental, etc.), equipment furniture, essential facilities, and materials were retrieved from the published data by the World Health Organization (World Health Organization, 2020) and Cost Finder (Cost Finder, 2020). Essential units' prices were scaled down based on hospital size with proper assumed standard deviations. It should be mentioned that the hospital's essential units are very expensive representing more than half of the hospital total value.

F13: Community center (place of worship): The F13 archetype is considered a typical community center or place of worship with a U-shape (66m x50m) and having a total area of 2350 m2 (25300 ft2). This archetype could be assigned to any community center ranging from a small to a large floor plan with proper scaling based on building footprint. The structural system is a steel frame with steel studs along with exterior brick walls rested on a slab-on-grade foundation. The full interior design was developed based on on-site visits to community centers and churches.

F14: Office building: A small office building with a rectangle shape (45.0m x 22.0 m) having a total area of 990 m2 (10656 ft2) is archetype F14. This archetype could be assigned to office buildings ranging from small to large floor plans with proper scaling based on building size. The structural system is a wood frame/masonry with wood studs along with exterior brick walls resting on a slab-on-grade foundation.

F15: Warehouse (small/large box): The F15 archetype represents a medium-size warehouse (medium box building) with a rectangle shape (90.0m x 35.0 m) having a total area of 3242m2 (34895 ft2). This archetype could be assigned to warehouses ranging from small to large size buildings with proper scaling based on building size. The structural system is a steel frame with steel studs along with exterior brick walls or corrugated steel sheets rested on a slab-on-grade foundation.

The same procedures described in subsection 2.2 were applied to the 15 building archetypes to account for the components damage/loss and thereby developing the 2-D and 3-D flood fragility and loss functions. Table 2-6 shows the lognormal parameters for the developed 2-D fragility functions for each building archetype. Figure 2-21 shows the lognormal fitted fragility curves for the 15 building archetypes for each DS. It should be mentioned that DS0 only exists for archetypes with a crawlspace foundation which are archetypes F1 and F3. For all building archetypes, flood depth is measured from FFE. However, for the archetypes with crawl space foundation, flood depth is measured from ground elevation and the FFE is assumed to be at 1.0m from the ground elevation which explains why DS1 and DS2 for archetypes F1 and F3 are shifted from the suit of fragilities as shown in Figure 2-21. Detailed results in terms of six figures for each building archetype (component fragility curves, total building fragility curves, selected components loss curves, total building loss curves, total building fragility surfaces, and total building loss surface) are provided in Appendix B with this dissertation. The resulting fragility and loss functions including the 2-D and 3-D functions are organized into user-friendly matrices such that they can be easily used by researchers or be read by any algorithm to account for flood damage/loss at any intensity measure for any building archetype. This output data for these fragilities and loss functions are provided in an article published by Nofal and van de Lindt (Omar M. Nofal and van de Lindt, 2020b) to enable reproduction based on our findings.

Table 2-6. *Lognormal parameters of the developed 2-D fragility functions for the 15 building archetypes (SI units)*

Archetype	DS0		DS1		DS2		DS3		DS4	
	λ	ξ	λ	ξ	λ	ξ	λ	ξ	λ	ξ
F1	-1.187	0.849	-0.106	0.397	0.333	0.220	1.173	0.278	1.405	0.227
F2	-	-	-1.664	0.533	-1.064	0.745	0.589	0.439	1.122	0.294
F3	-1.001	0.639	-0.109	0.414	0.393	0.233	1.512	0.240	1.693	0.322
F4	-	-	-1.666	0.553	-0.984	0.798	1.214	0.288	1.477	0.389
F5	-	-	-1.595	0.486	-0.827	0.616	0.533	0.681	1.435	0.242
F6	-	-	-1.461	0.493	-0.798	0.740	0.450	0.860	2.029	0.191
F7	-	-	-1.419	0.462	-0.736	0.745	0.456	0.724	1.585	0.198
F8	-	-	-1.420	0.467	-0.908	0.681	0.412	0.913	2.025	0.195
F9	-	-	-1.470	0.475	-0.540	0.667	0.865	0.928	2.023	0.153
F10	-	-	-1.570	0.502	-0.681	0.738	0.824	0.531	1.573	0.186
F11	-	-	-1.546	0.488	-0.678	0.740	1.388	0.435	2.006	0.254
F12	-	-	-1.434	0.471	-0.594	0.586	1.034	0.742	2.051	0.146
F13	-	-	-1.622	0.492	-0.911	0.660	1.418	0.506	1.968	0.187
F14	-	-	-1.757	0.658	-0.581	0.687	0.229	0.928	1.482	0.269
F15	-	-	-1.450	0.463	-0.228	0.532	1.038	0.350	1.618	0.262

The results revealed that residential buildings damage (fragility curves) do not depend on the occupancy whether it is single-family or multi-family. This is because damage criteria only depend on the component type (e.g., furniture, appliances, structural and non-structural components, etc.) which are the same for both occupancies but with different component numbers. However, multi-family buildings exhibit more losses than single-family as flood losses are on the order of the number of components included within each building. Another factor that affects damage and losses is the foundation type (e.g., crawlspace, slab-on-grade, etc.). The analysis shows that buildings with a crawlspace foundation are more vulnerable than the building with a slab-on-grade foundation. This looks rational due to the additional damage to the components below the FFE within the crawlspace area, such as ductwork. The number of stories is also another factor the affects the amount of flood damage/losses. For example, a one-story buildings are susceptible to have more losses than a two-story building at the same flood depth because more building components including interior contents, structural, and non-structural components are located in the second story that might not get touched with water.

DS1 for all building archetypes is very close in their values to one another due to the similarities in terms of the components within this DS which is the same case for DS0, and DS2 as shown in Figures 2-21(a-c). However, archetypes F1 and F3 are shifted because flood depth is measured from the ground elevation. For DS3 and DS4, there is much higher variability in the fragility curves between building archetypes as shown in Figures 2-21(d, e) which is highly controlled by the building type and the elevation of the components for each building archetype. Generally, building fragility curves for DS0, DS1, and DS2 are steeper than fragility curves for DS3, and DS4. This can be explained such that most components within DS0, DS1, and DS2 are water-sensitive components (e.g., carpet, insulation, appliances, machinery, electronics, furniture, etc.). This is also evident from the component fragility curves presented in Appendix B which show that many component fragility curves are encompassed in the first 1.0m damage range (0.0-1.0m) which is the depth range for water-sensitive components to be damaged. For two-story archetypes, this damage range will be repeated for the second story with damage range occurring in depths from 3.2m up to 4.2m. For DS3 and DS4, fragility curves are less steep with a larger damage range as shown in Figures 2-21(d, c). This can be explained by the fact that the structural and some non-structural components are non-water sensitive and may be salvageable after being submerged in water which imposes a large uncertainty in their damaging range. This appears clear upon inspection of the component fragility curves which have a larger depth range to be fully damaged including framing and the foundation.

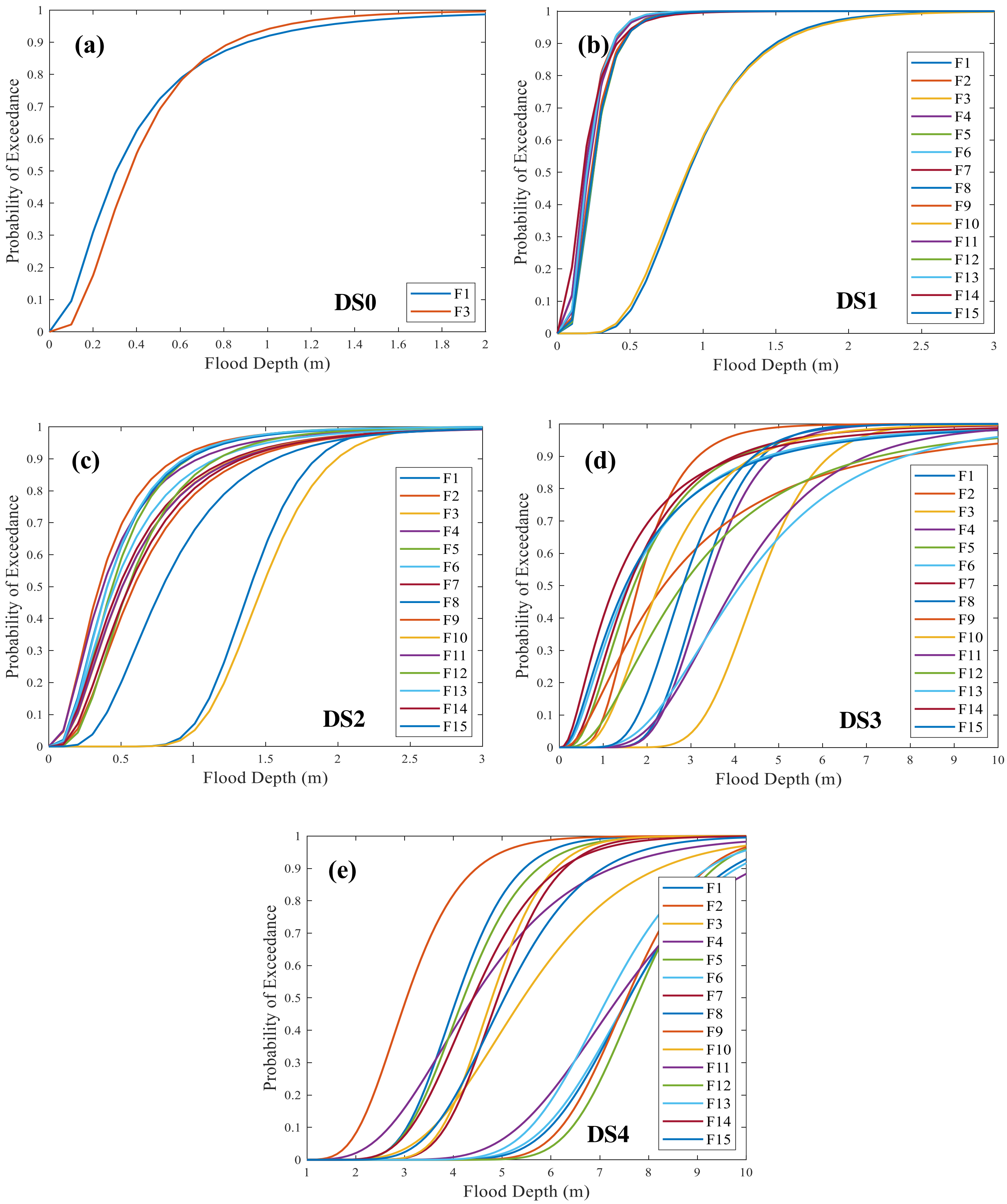

Figure 2-21. *Building archetypes fragility curves: (a) DS0; (b) DS1; (c) DS2; (d) DS3; (e) DS4*

For flood losses, the replacement/repair cost in terms of the mean and standard deviation of the replacement/repair cost for each DS was calculated in an absolute and normalized form as shown in Table 2-7. This enabled developing loss functions for the suite of 15 building archetypes using the direct approach and the fragility-based loss approach. The observed difference between the direct and the fragility-based loss approach results from using the lognormal fitted fragilities in deriving the fragility-based flood losses as discussed in Section 2.2.2. However, this difference is minor as shown in the loss figures in Appendix B and the fragility approach can be used to assess both damage and loss with acceptable accuracy. Figure 2-22 shows the flood loss curves for each building archetype using both the direct loss approach as shown in Figure 2-22(a) and the fragility-based loss approach as shown in Figure 2-22(b). Both fragility-based and direct flood loss methods were compared with the HAZUS stage-damage function and showed a good match for almost all building archetypes. However, almost all of the HAZUS stage-damage functions stop short of 100% losses for complete damage whereas those in the current study do reach 100% as shown in loss figures in Appendix B. This is because HAZUS stage-damage functions (FEMA, 2009d) for the foundation and structure subassembly only reach 20% and 42% damage ratio, respectively.

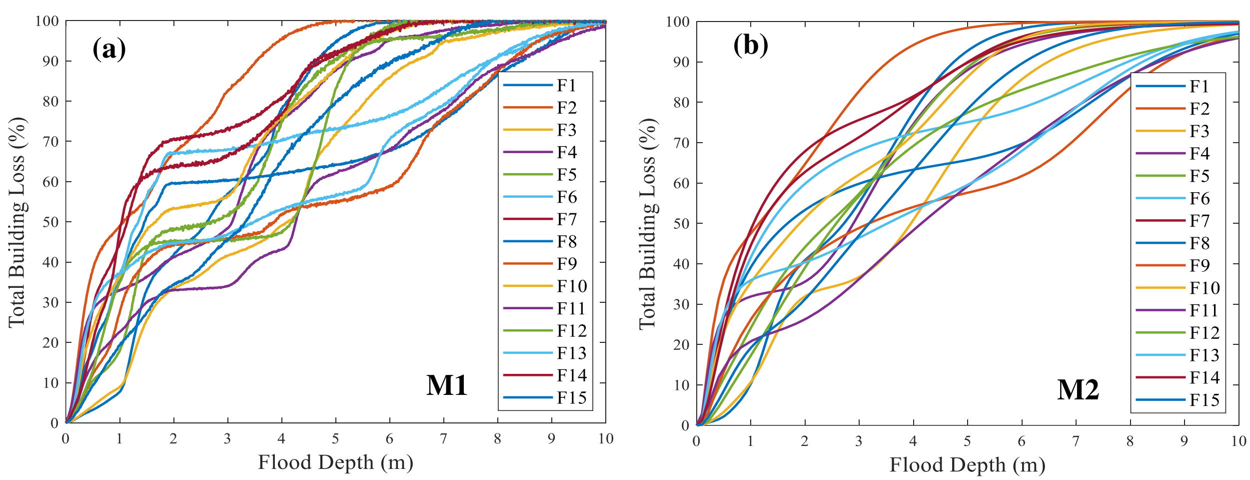

Figure 2-22. *Building archetypes normalized loss curves: (a) Loss curves using direct loss approach (M1); (b) Loss curves using fragility-based approach (M2)*

Most of the building archetypes showed a high dependency on flood duration and neglecting such a parameter would affect flood loss calculations as shown in the fragility and loss surfaces in Appendix B. It should be noted that water contamination was not accounted for in any of the analyses and could alter the ability to dry building (and other) components. The 2-D flood loss functions developed herein consider a component to be damaged if the water level reaches its damaging depth regardless of water duration, which is not accurate for the water non-sensitive components. Therefore, 3-D loss functions consider a component to be damaged if the water level reaches its damaging depth along with the component damaging duration. Considering flood duration enhances the accuracy of the fragilities, albeit complicating the analysis. For the hospital archetype (F12), the building's total value is dominated by the essential hospital facilities representing more than 80% of the total building replacement cost. The hospital essential facilities are water-sensitive components with an average duration resistance of 1 hour which makes the fragility and loss surface less dependent on flood duration and highly dependent on flood depth.

Table 2-7. *Damage states replacement cost data for each building archetype (μ_r: mean DS replacement cost USD \$, σ_r: standard deviation of DS replacement cost USD \$, μ_{rc}: mean cumulative DS replacement cost USD \$, Lr %: normalized DS loss ratio, and Lr_c %: normalized cumulative DS loss ratio)*

Archetype	DS	μ_r (USD \$)	σ_r (USD \$)	μ_{rc} (USD \$)	Lr %	Lr_c %
F1	DS0	4260	794	4260	0.02	0.02
	DS1	23654	2121	27914	0.11	0.13
	DS2	61560	4277	89474	0.29	0.41
	DS3	60724	5032	150199	0.28	0.7
	DS4	65675	7031	215874	0.3	1
F2	DS1	48849	4135	48849	0.09	0.09
	DS2	213251	16444	262100	0.39	0.48
	DS3	133569	9561	395669	0.25	0.73
	DS4	147861	15829	543530	0.27	1
F3	DS0	16227	1736	16227	0.03	0.04
	DS1	48789	4053	65016	0.11	0.14
	DS2	92980	6475	157996	0.2	0.34
	DS3	190569	13622	348565	0.41	0.75
	DS4	114019	11166	462584	0.25	1
F4	DS1	598903	49851	598903	0.16	0.16
	DS2	692169	51262	1291072	0.18	0.34
	DS3	1681135	76270	2972207	0.44	0.78

	DS4	839248	82159	3811456	0.22	1
F5	DS1	70250	12515	70250	0.04	0.04
	DS2	153849	14617	224099	0.10	0.14
	DS3	829515	121483	1053613	0.51	0.65
	DS4	569865	85480	1623478	0.35	1
F6	DS1	449721	164013	449721	0.02	0.03
	DS2	5168222	339949	5617944	0.29	0.31
	DS3	8543276	770670	14161219	0.48	0.79
	DS4	3782973	492271	17944192	0.21	1
F7	DS1	53036	18209	53036	0.03	0.02
	DS2	1072040	70627	1125076	0.44	0.46
	DS3	878243	129259	2003319	0.36	0.83
	DS4	418985	54522	2422304	0.17	1
F8	DS1	1058663	397138	1058663	0.04	0.04
	DS2	7248632	553895	8307295	0.24	0.28
	DS3	12315180	791378	20622475	0.41	0.69
	DS4	9163981	1192491.8	29786456	0.31	1
F9	DS1	486936	165808	486936	0.04	0.04
	DS2	2083967	162066	2570903	0.18	0.22
	DS3	5176670	610200	7747573	0.45	0.67
	DS4	3818494	496893	11566066	0.33	1
F10	DS1	569036	93693	569036	0.08	0.08
	DS2	2125013	170009	2694050	0.31	0.39
	DS3	2317758	172624	5011808	0.33	0.72
	DS4	1929440	200005	6941248	0.28	1
F11	DS1	569036	93693	569036	0.05	0.05
	DS2	2125013	170009	2694050	0.19	0.24
	DS3	5362654	270722	8056704	0.48	0.72
	DS4	3080165	323559	11136869	0.28	1
F12	DS1	1292430	133099	1292430	0.01	0.01
	DS2	17919792	1142953	19212222	0.11	0.12
	DS3	132148680	9220348	151360903	0.84	0.96
	DS4	6788170	830969	158149072	0.04	1
F13	DS1	413457	69333	413457	0.1	0.1
	DS2	1109923	124113	1523380	0.29	0.38
	DS3	1252727	80179	2776107	0.31	0.7
	DS4	1211644	104102	3987751	0.3	1
F14	DS1	101767	21334	101767	0.04	0.04
	DS2	609794	63305	711561	0.26	0.31
	DS3	1105491	182337	1817052	0.48	0.78
	DS4	505344	53193	2322396	0.22	1
F15	DS1	151644	56713	151644	0.04	0.04
	DS2	741449	100999	893093	0.22	0.26
	DS3	1190923	170109	2084016	0.35	0.61
	DS4	1308621	170288	3392637	0.39	1

CHAPTER 3: HURRICANE RISK ANALYSIS METHODOLOGY

3.1 Introduction

Hurricanes drive multiple hazards to coastal and inland communities. The intensities of these hazards vary in time and space. Quantifying the spatiotemporal variation of risk due to hurricane-induced hazards requires a full realization of the different hazard mechanisms and the way they impact communities. Therefore, a high-resolution community-level multi-hazard hurricane risk analysis methodology is proposed in this dissertation which accounts for damage and loss at the individual building-level but can be applied for large-scale damage and loss assessment at the regional-level. This method accounts for the combined impact of the main hazards driven by hurricanes on coastal communities (wind, wave, and storm surge) on buildings. It also accounts for the impact of the fluvial and pluvial flooding driven by decaying hurricanes on inland communities. The methodology uses high-resolution models for hazard, exposure, and vulnerability analysis. The novel contributions of the work done in this chapter are (1) the proposed probabilistic hurricane risk model accounts for both content and structural damage resulting from the multiple hazards induced by hurricanes; and (2) the approach of combining fragilities based on an array of intensity parameters. This methodology requires a full realization of the vulnerability of the exposed buildings corresponding to each hazard type along with a comprehensive understanding of the hurricane hazard mechanism and how it makes landfall such as hurricane path, wind field, wind speed, surge height, wave height, etc.) as well as building characteristics (e.g., location, number of stories, first-floor elevation, roof shape, foundation type, construction material (including the type of building envelope), etc.), and building vulnerability functions (fragility or loss functions). This building-level methodology will allow for better damage quantification by including the damage contribution from each hazard induced by hurricanes, thereby enabling decision-support at the community and regional levels. In this method, communities are divided, herein, into inland and coastal communities based on their vulnerability to hurricane-induced hazards and a separate framework was developed for each one.

3.2 Inland Communities

Inland communities are vulnerable to torrential rains associated with hurricane landfall which can drive significant fluvial and pluvial flooding. There is also a possibility of having low to moderate winds based on the hurricane category, path, and wind field size. For hurricanes-induced hazards, much of the focus is on the shoreline and its associated hazards including storm surge, waves, and wind because of the risk to human life. However, the largest percentage of damage can occur many miles inland due to rainfall and/or riverine flooding. Although inland flooding causes devastation to the physical infrastructure and disruption to the socio-economic systems, there is less literature that specifically investigates the subsequent risk from hurricane-induced inland flooding. Therefore, a portion of this dissertation is devoted to inland flooding risk modeling in terms of developing flood hazard, exposure, and vulnerability models.

3.2.1 Hazard Modeling

Flood hazard modeling for inland communities due to fluvial and pluvial flooding driven by decaying hurricanes or other drivers requires hydrodynamic analysis. This analysis requires to account for the streamflow data that feeds the main streams within the study area. However, sometimes, the water flow data is not complete such as hydrographs for some of the main streams in the study area are not available because of the lack of gauges. Therefore, a detailed hydrologic analysis is needed to predict the water discharge in the ungagged streams within the study area. This would allow more accurate flood inundation modeling that accounts for the contribution of the major streams within the study area. For hydrologic analysis, a Digital Elevation Map (DEM) was used for the hydrologic analysis. The DEM data, used in this dissertation, was obtained from The National Map (TNM) provided by USGS with 10-m accuracy. Additionally, other high-resolution DEMs retrieved from NOAA (NOAA, 2020) with 1.5m accuracy were also used.

The DEM is then used to delineate the catchments within the study area after a number of analyses including (fill sinks, flow direction, flow accumulation, stream definition, etc.). After conducting the needed DEM calculations, the characteristics of the basin will be calculated along with determining the methods that will be used in the hydrologic modeling which was schematically shown in Figure 1-4. These calculations are usually done in a GIS environment using Arc Hydro (Strassberg, Jones, and Maidment, 2011), HEC-GeoHMS (Doan, 2000), and other toolboxes in the ArcGIS platform (ESRI, 2018). Then, the geomorphological data in terms of DEM, land use, and soil data were used to determine the Soil Conservation Service (SCS) Curve Number (CN) in the form of a raster map to be used to account for the surface water runoff. Then, HEC-HMS (US Hydrologic Engineering Center, 2001) can be used to perform hydrologic analysis using SCS Type 2 storm with the observed rainfall intensity. Finally, the model parameters (CN and lag time) were properly adjusted to validate the calculated hydrograph with the observed one.

The hydrodynamic analysis process was performed after obtaining hydrographs at the location of the boundary conditions in the ungauged streams. Then, the principles of hydraulics and water flow analysis in streams (steady or unsteady flow) were applied to determine the flood characteristics (depth, extent, velocity, duration, etc.). In this study, HEC-RAS (Brunner, 2010) was used to develop the hydrodynamic model and uses the finite difference approach to solve the unsteady full momentum 2D Saint-Venant flow equations or solves the 2D diffusion-wave equations (Brunner, 2002). This HEC-HMS analysis environment uses finite volume and 2D Saint-

Venant flow equations to calculate water depth and velocity for a predefined computational domain. In this analysis environment, a detailed flood hazard map in terms of the effect of levees and other existing hydraulic structures on the flood hazard characteristics could be modeled. The last step in the hydrodynamic analysis stage was to validate the calculated hydrographs from the hydrodynamic analysis with any of the observed measurements from the stream gauges to confirm the resulting flow depth and velocity. Additionally, any available satellite images can be used to validate the flood inundation extent. Then, the flood hazard map will be overlaid with the community model to identify the hazard intensity at each exposed building as shown in the example community in Figure 3-1. An application of the hazard modeling for an inland community will be fully covered in the case study section in Chapter 7 of this dissertation.

Figure 3-1. *An example of a flooded inland community with building overlaid with the developed hazard layer and the buildings are color-coded based on their archetype*

3.2.2 Exposure Modeling

The exposed building information is relatively important data that significantly controls the accuracy of the risk assessment process. Therefore, the more detailed the exposure information, the more accurate and reliable the resulting flood risk prediction. Most of the building inventory data needed for the probabilistic flood damage assessment was extracted from the parcel data which usually available online. This data includes buildings location, area, market value, basic building occupancy, flood zone, and the year built. However, this data is not enough to begin the flood risk assessment process and more details about the building characteristics including construction material, the number of stories, foundation type, and first-floor elevation (FFE) are needed to capture the flood damage at a community-level. After identifying this information about the buildings, the 15 building archetypes outlined in Chapter 2 were used to model the building stock within a community.

The collected buildings data and the building portfolio were used to develop a detailed exposure model for the community based on a combined BIM and GIS model. The BIM model for a portfolio of 15 building archetypes developed by Nofal and van de Lindt (Omar M. Nofal and van de Lindt, 2020b) was used. The BIM model holds the essential information about the exposed components within the buildings (e.g., component type, upper and lower bound of the damaging elevation and the damaging flood duration, upper and lower bound of the replacement cost, etc.) which was used to develop the flood fragility and loss functions. The GIS model holds the essential information about the buildings within the community (e.g., location, FFE, market value, occupancy, foundation type, number of stories, etc.). In order to assign each building archetype within the developed building portfolio to each building within the real community, a mapping algorithm was developed to link the building archetypes portfolio with the community based on each building characteristic. Figure 3-2 shows a schematic representation of a portion of the community with a school and community center (church) as an example for mapping the 15 building archetypes to a real community. The modeled community is then overlaid with the hazard layer in a GIS environment to identify the hazard intensity at each building location. Figure 3-1 shows a part of an example community with the exposed buildings color-coded based on their archetypes overlaid with the hazard map.

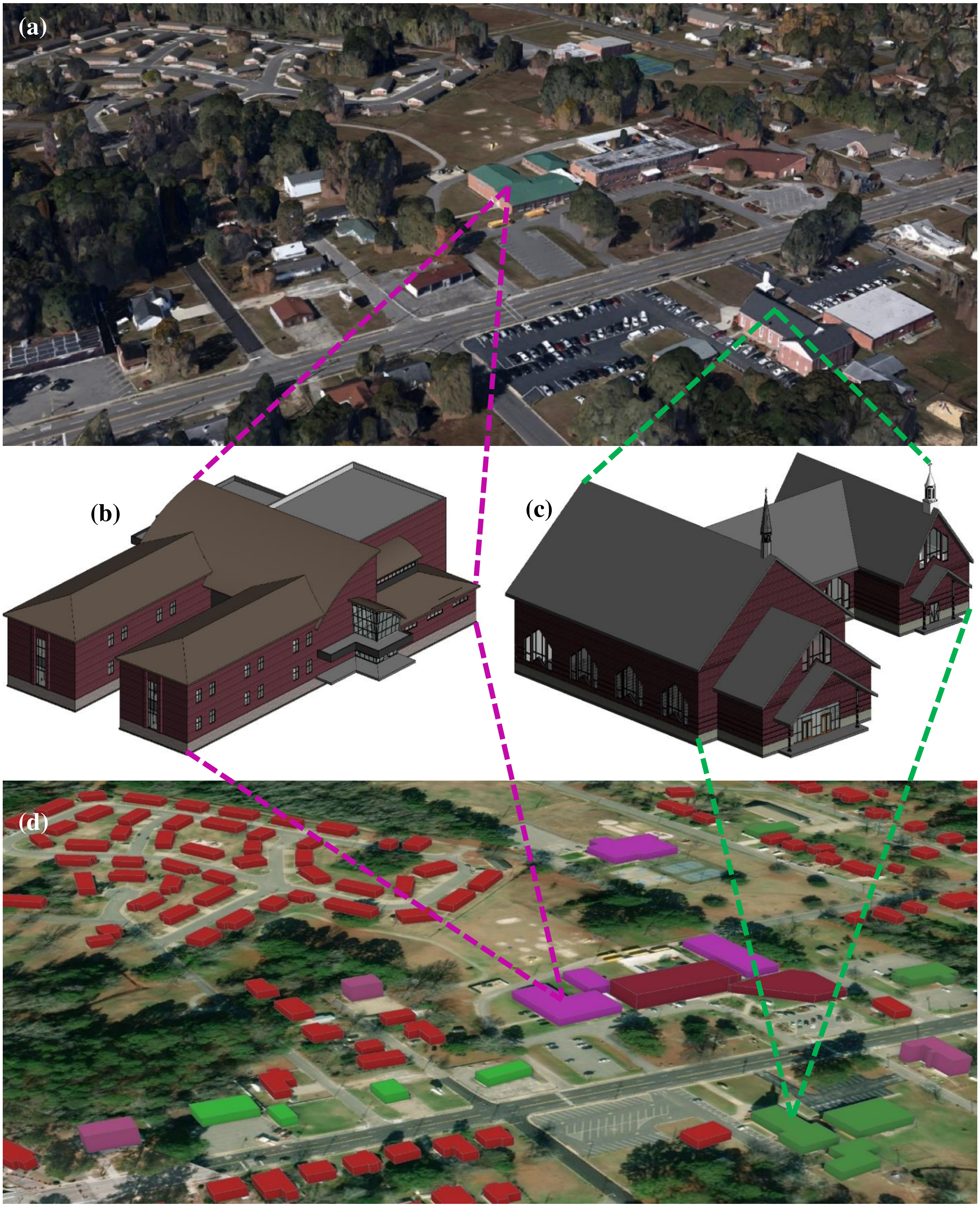

Figure 3-2. *A schematic representation of the community model based on a combined BIM and GIS Model: (a) A Google Earth image showing 3-D buildings for a select neighborhood ; (b and c) A general BIM models for a school and church, respectively; (d) A GIS model for the for the same neighborhood*

3.2.3 Vulnerability Modeling

As mentioned earlier in subsection 2.2 and the first chapter of this dissertation, the current literature is still lacking a complete flood fragility portfolio for an array of building archetypes that could model the flood vulnerability at the community-level. Therefore, the 2-D and 3-D flood fragility and loss functions, developed herein as a part of this dissertation, were used to model the flood vulnerability. These functions account for fragility-based flood damage for buildings in terms of the exceedance probability of certain predefined DSs. Additionally, component-based flood loss functions were also used to account for the direct monetary flood losses. The advantage of using these functions is the uncertainties propagation throughout the whole damage model (e.g., flood depth resistance, flood duration resistance, and the replacement/repair cost). The flood duration was included in the vulnerability function to account for the compound impact of flood depth and flood duration. Afterwards, the flood vulnerability curve/surfaces (fragility or loss function) associated with each building archetype was assigned to each corresponding building using the same mapping algorithm developed from the last step. The extracted hazard intensity at each building location was then used as an input for the flood vulnerability curves/surfaces.

3.2.4 Risk Analysis

The flood hazard map, community exposure, and building vulnerability models were overlaid in a community-level loss/damage analysis framework in Figure 3-3. Then, flood loss/damage for each building within the community was calculated using an algorithm based on the framework illustrated in the flow chart in Figure 3-4. This framework identifies the hazard intensity at each building location and the assigned archetypes for this building and its associated vulnerability function. The flood risk is calculated in terms of the exceedance probability of each damage state to be used in community resilience analysis and a DS was assigned to each building to be used in damage/loss analysis. Afterwards, fragility-based flood loss for each building is calculated as a percentage of the total building market value.

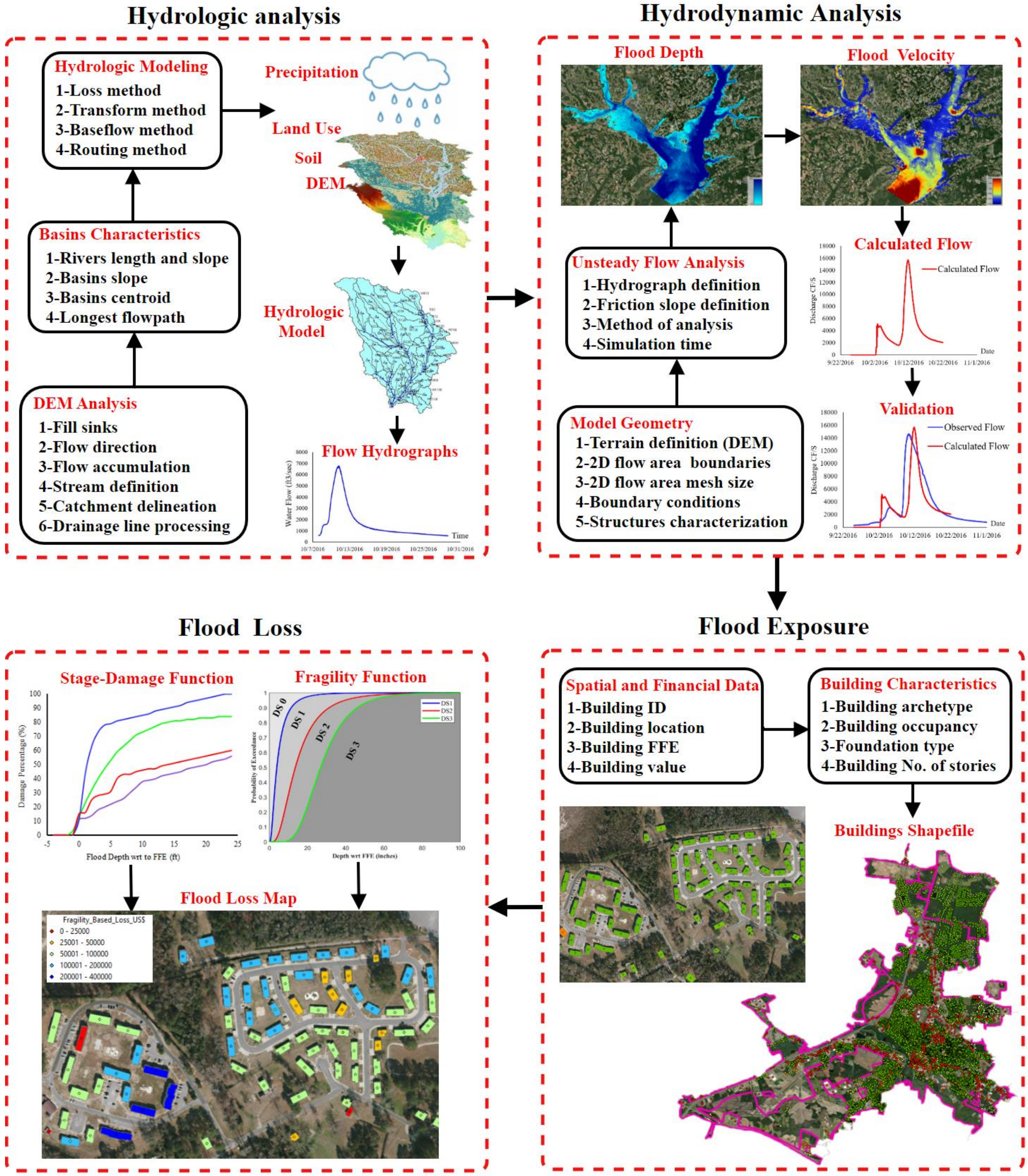

Figure 3-3. *A schematic representation of the flood risk (probability of occurrence of damage/loss) modeling framework developed in this dissertation to compute probabilistic damage/losses at the community level*

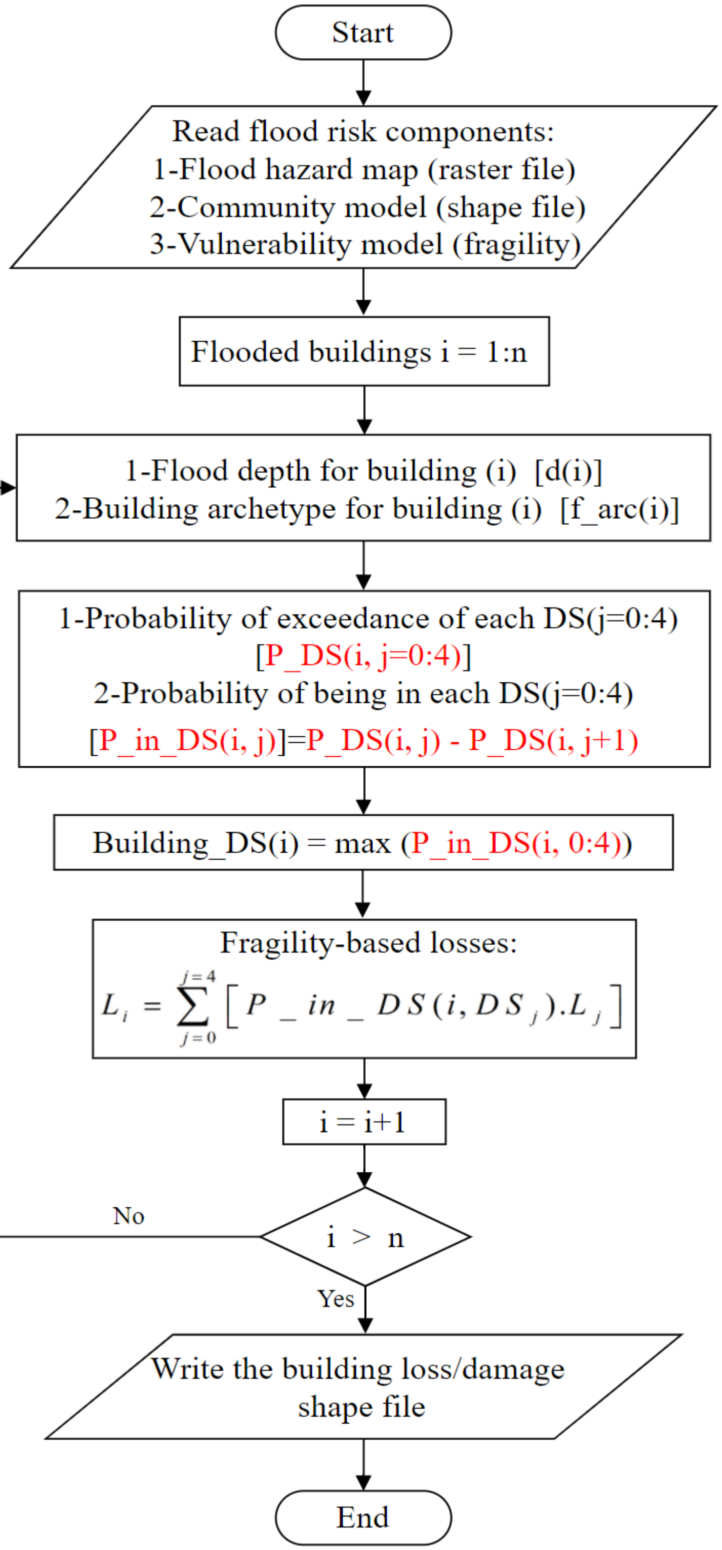

Figure 3-4. *Community-level flood fragility and loss analysis framework (Lj = replacement/repair cost of each DS, P_DS = the exceedance probability of a DS, P_in_DS = the probability of being in a DS)*

3.3 Coastal Communities

Coastal communities are highly vulnerable to wind, storm surge, and waves resulting from hurricanes. Hurricane-induced winds can cause severe structural damage to the building system or even destroy it. However, the storm surge part is considered the most destructive loading from hurricanes resulting in damage or even collapse to the impacted building, particularly when waves are present. Even with strong windstorms associated with hurricanes, higher fatalities are usually associated with hurricanes storm surge due to drowning. Although buildings on the shoreline are vulnerable to both wind and storm surge hazards, almost all of the damage to these buildings is due to the hydrodynamic impacts of the combined storm surge and waves. These impacts get reduced significantly as the water moves inland where inland flooding (coastal flooding) is common. A few miles from the shoreline, flood impacts become minor with more domination from wind hazards. A community-level hurricane risk assessment model is developed to account for building damage resulting from the multiple hazards driven by hurricanes (Omar M. Nofal, Lindt, Do, et al., 2021; Omar M. Nofal, Lindt, Yan, Hamideh, and Dietrich, 2021). Figure 3-5 shows a schematic representation of the proposed framework that lays out the main component of the multi-hazards driven by hurricanes and their associated community-level exposure and vulnerability.

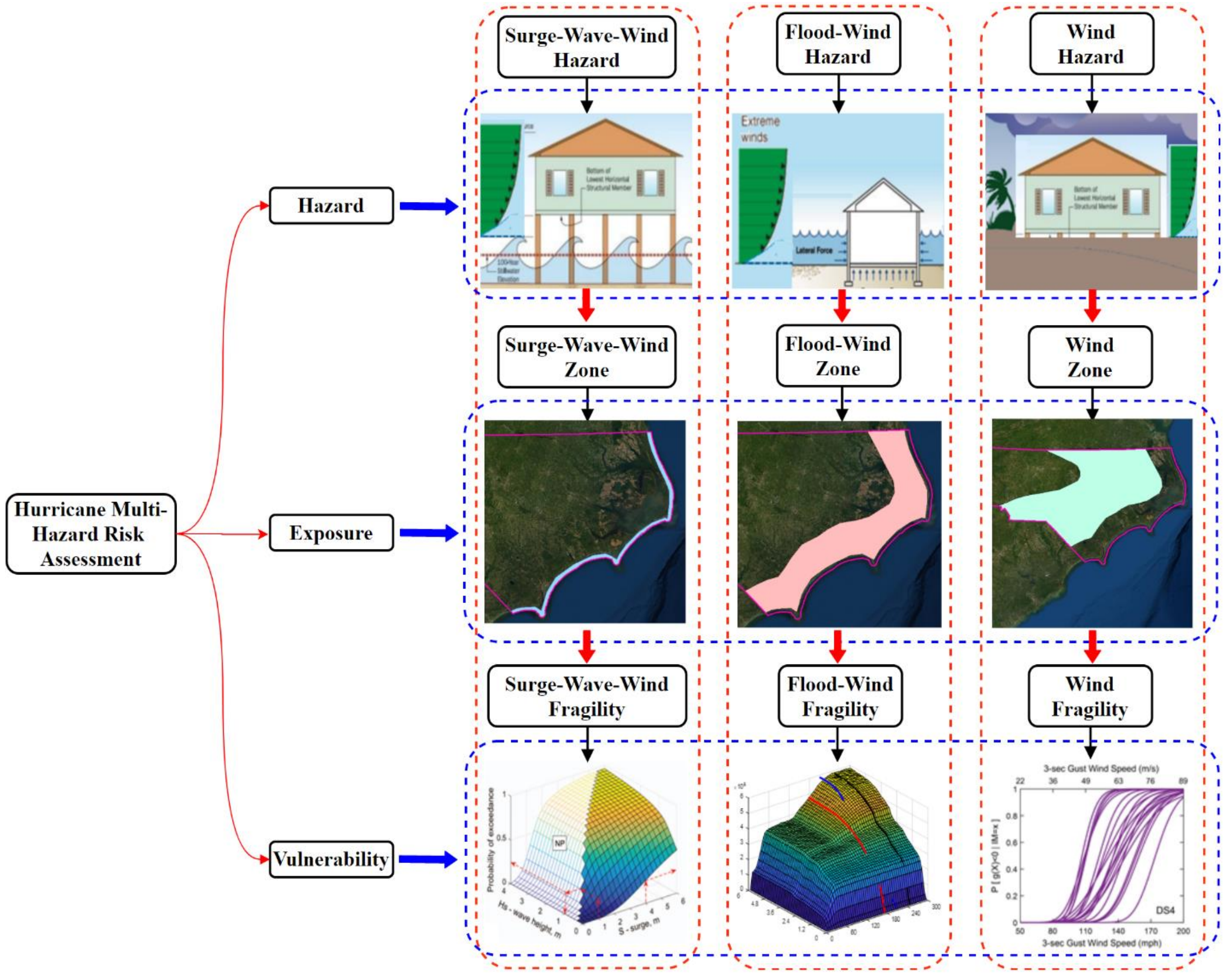

Figure 3-5. *A schematic representation of the proposed hurricane multi-hazard vulnerability model*

3.3.1 Hazard Modeling

The intensities of hurricane-induced hazards vary in time and space. Quantifying the spatiotemporal variation of these hazards requires detailed modeling of these hazards and the interaction between them. Developing the hazard models induced by hurricanes including wind, surge, and wave on coastal communities was beyond the scope of this dissertation. Therefore, only hazard data processing was conducted herein to be used in the developed hurricane risk assessment framework. The wind field hazard map was taken from a data-assimilated hindcast product, which blends an inner-core wind field to a peripheral large-scale wind field using the Interactive

Objective Kinematic Analysis (IOKA) system (Powell et al., 2010), and allowed for the assimilation of in-situ, satellite, and aircraft observations, and which enabled the prediction of the spatial variation of wind speed across the coast with the example of the east coast of the U.S. after the 2018 Hurricane Florence, as shown in Figure 3-6 which will be used in one of the case studies in Chapter 7. The wind speed provided in Figure 3-6 is based on the average wind speed in 10.0 minutes at 10.0 m elevation and was used as input to the surge and wave model described below. This wind speed is based on the full marine-strength wind (open water exposure) but the fragility functions used here are based on the 3-second gust wind speed at 33 ft (10 m) (consistent with ASCE 7) above ground in Exposure C (open terrain). Therefore, the wind hazard map was adjusted from open water exposure to open terrain exposure. Then, the wind reference period was adjusted from an average wind speed of 10.0 minutes to a 3-second gust wind speed. The transformation criteria for wind speed provided by the ASCE 7-16 (2016) was used to calculate a gust factor of 1.24.

The surge and wave hazard maps were developed using a high-resolution simulation with the tightly coupled ADCIRC+SWAN model (J Casey Dietrich et al., 2012). The maximum values were used for all hazards, not their time-varying information. These maximum values are not necessarily co-located in time and the maximum wind can occur at a different time than the maximum surge. The wind hazard was provided on a regular grid with a spacing of 0.25 degrees. The wave and surge hazards were taken from the ADCIRC+SWAN model resolution, which has typical values of 100 to 200 m in coastal regions, but which can vary down to 10 m in small-scale channels. The wind, wave, and surge hazards were then mapped onto a raster with a resolution of 10.0 m. Then values were interpolated at the coordinates of each building including wind speed (m/s), the surge height measured from the ground (m), and the significant wave height (m). Hazard modeling can be either based on a return period (e.g., a 100-year return period) or based on a scenario event. In the example provided later in the case studies in Chapter 7 with this dissertation, a scenario-based hurricane hazard was utilized for the 2018 Hurricane Florence. Florence was a large storm that caused widespread flooding in multiple cities and counties across the state of North Carolina, resulting in 40 confirmed fatalities and left more than a million people without power with an estimated $17 billion in damage across the state ($5.6 billion of housing damage, 5.7 billion of business damage, and $2.4 billion of agriculture industry losses) (NC State, 2018).

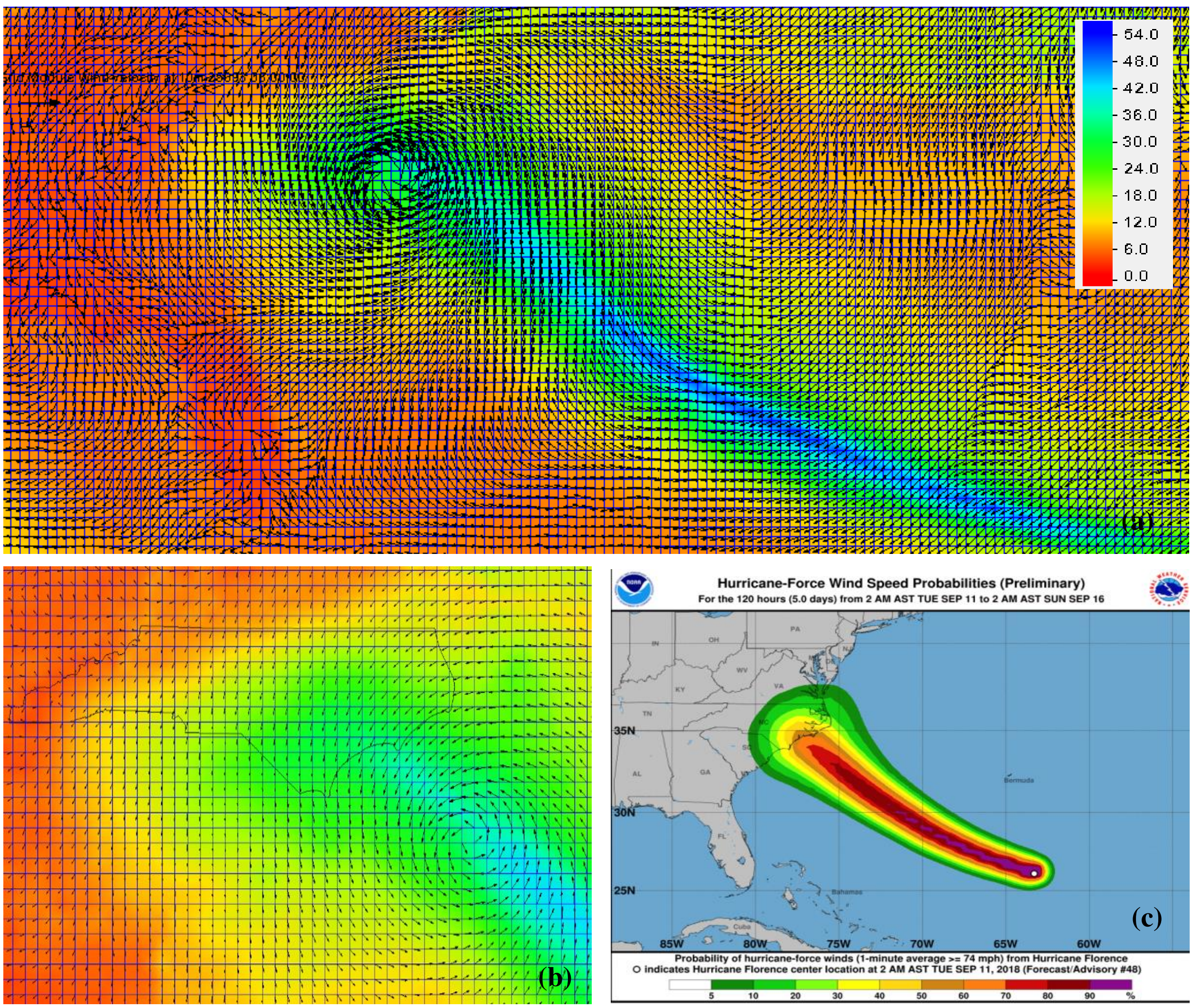

Figure 3-6. *Wind simulation based on the 2018 Hurricane Florence: (a) Maximum wind speed contours and vectors (m/s); (b) Close-up view on the maximum winds at North Carolina; (c) The National Weather Services tracking of the 2018 Hurricane Florence* (NWS, 2018)

3.3.2 Exposure Modeling

Buildings in a coastal community are mainly exposed to surge, wave, and wind hazards but with different intensities based on building location and elevation. Therefore, the hazard exposure in coastal communities is divided herein, into three zones based on their exposure to the hurricane-induced hazard, namely: surge-wave-wind zone, surge-wind zone, and wind zone. Each zone size is proportional to the hazard parameters including hurricane intensity (e.g., category), wind field size, the angle of attack, the elevation of the coast, which was obtained from the hazard map. The first zone is the surge-wave-wind zone, which is approximately the first kilometer of the coast for this particular topography, with a maximum significant wave height close to the coast, which then decreases as the water makes its way inland. These waves are on the top of the surge, which is a big volume of water pushed inland from the ocean by strong hurricane winds. The surge and wave action drive multiple hydrodynamic impacts on coastal buildings thereby jeopardizing their integrity. Additionally, the impact of surge accompanied by hurricanes results in immediate loss of building interior contents and some of the non-structural components, which jeopardizes the serviceability of the impacted buildings. Most of the buildings on the coast are elevated from the ground by 2.0m to 5.0m as a precautionary measure in many coastal communities to decrease the impact of storm surge and waves but this would make them more vulnerable to wind hazards. Therefore, the vulnerability model for buildings on the coast should include the combined impact of surge, wave, and wind. The second zone is the surge-wind zone, which can extend from 3.0 km to 30.0 km from the coast, depending on the hurricane category and coast configuration. Afterwards, the storm surge starts to weaken and becomes less prevalent in the third zone which would only include wind hazards.

3.3.3 Vulnerability Modeling

Initially, a building-level vulnerability analysis was conducted using fragility functions corresponding to each hurricane-induced hazard within each exposed zone. Each component within the building may be vulnerable to one or multiple hazards at a time, depending on the component type and the hazard characteristics. Figure 3-7 shows a schematic representation of the different building components including structural, non-structural, and interior content components for an example of a building archetype. The impact of some of the hurricane-induced hazards on buildings is combined such as surge-wave action. However, other hazards are independent and can be calculated from different vulnerability functions, such as the surge-wind action. In zone (1), the impact of the surge-wave action on buildings was assumed to be independent of the wind impacts. The surge-wave action was modeled using the surge-wave fragility surfaces developed by Do. et al. (2020), while the wind action was modeled using the wind fragility functions developed by Memari et al. (2018). None of the surge-wave and wind fragility used herein accounts for content damage. Therefore, the flood fragility functions developed in this dissertation and published by Nofal and van de Lindt (Omar M. Nofal and van de Lindt, 2020b) were used to account for content damage in this zone, i.e. due to surge. Figure 3-8 shows a detailed schematic describing the steps to obtain the hurricane-induced vulnerability of building components using fragility functions for an example building archetype. The vulnerability of structural components (e.g., roof, walls, foundation, slabs, etc.) was derived from the surge-wave fragility surface developed by Do. et al. (2020) and the wind fragility curves developed by Memari et al. (2018) after extracting the intensities of surge, wave, and wind hazards from the hazard maps. The vulnerability of the interior contents and other non-structural components were calculated from flood fragility functions (e.g., depth fragility function, depth-duration fragility function) based on the extracted surge height.

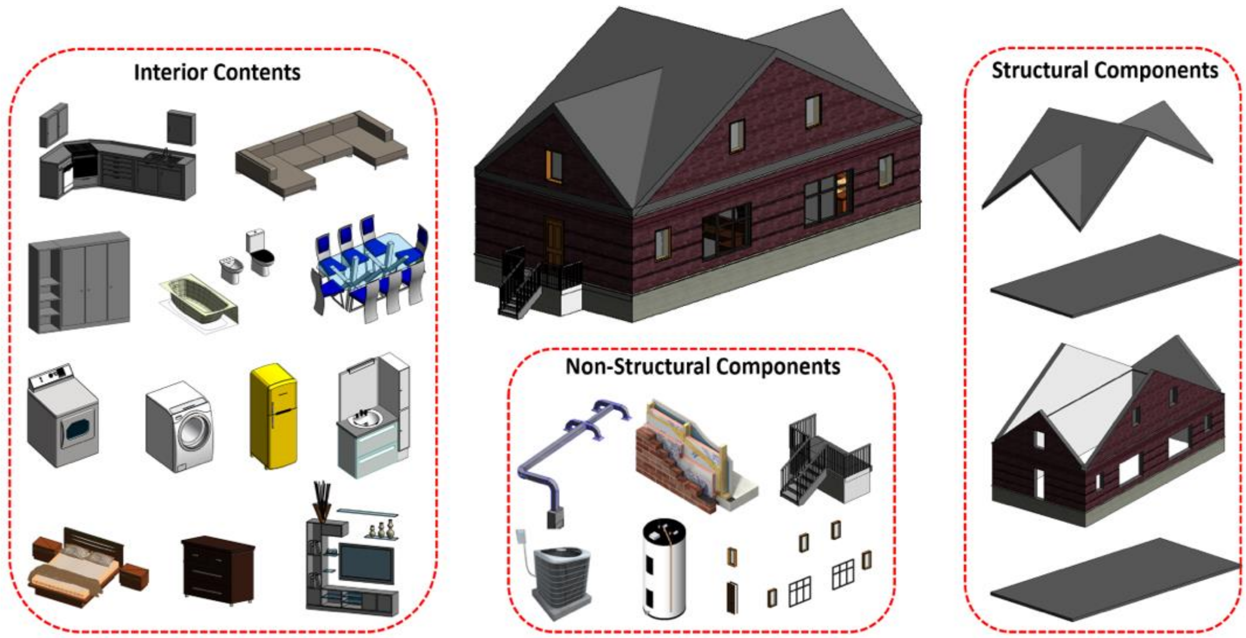

Figure 3-7. *A schematic representation shows the different building components including structural and non-structural components along with interior contents*

In zone (2), the impact of surge on buildings can be assumed to be independent from the impact of wind hazard, because each of these hazards has different mechanisms for causing damage to buildings. This allowed for the implementation of separate vulnerability functions for each of these hazards. Therefore, the wind fragility portfolio developed by Memari et al. (2018) was used to account for wind damage to buildings. Additionally, the structural damage resulting from the surge-only in this zone (this zone does not include wave action) was calculated using the surge fragility curves derived from the surge-wave fragility surfaces (at significant wave height = zero) developed by Do. et al. (2020). The content damage was calculated using the fragility portfolio developed by Nofal and van de Lindt (Omar M. Nofal and van de Lindt, 2020b) similar to the way described for zone (1). For zone (3), buildings were assumed to be vulnerable only to wind hazard with no vulnerability from surge and/or waves. Therefore, the wind fragilities developed by Memari et al. (2018) were applied to model building vulnerability in zone (3).

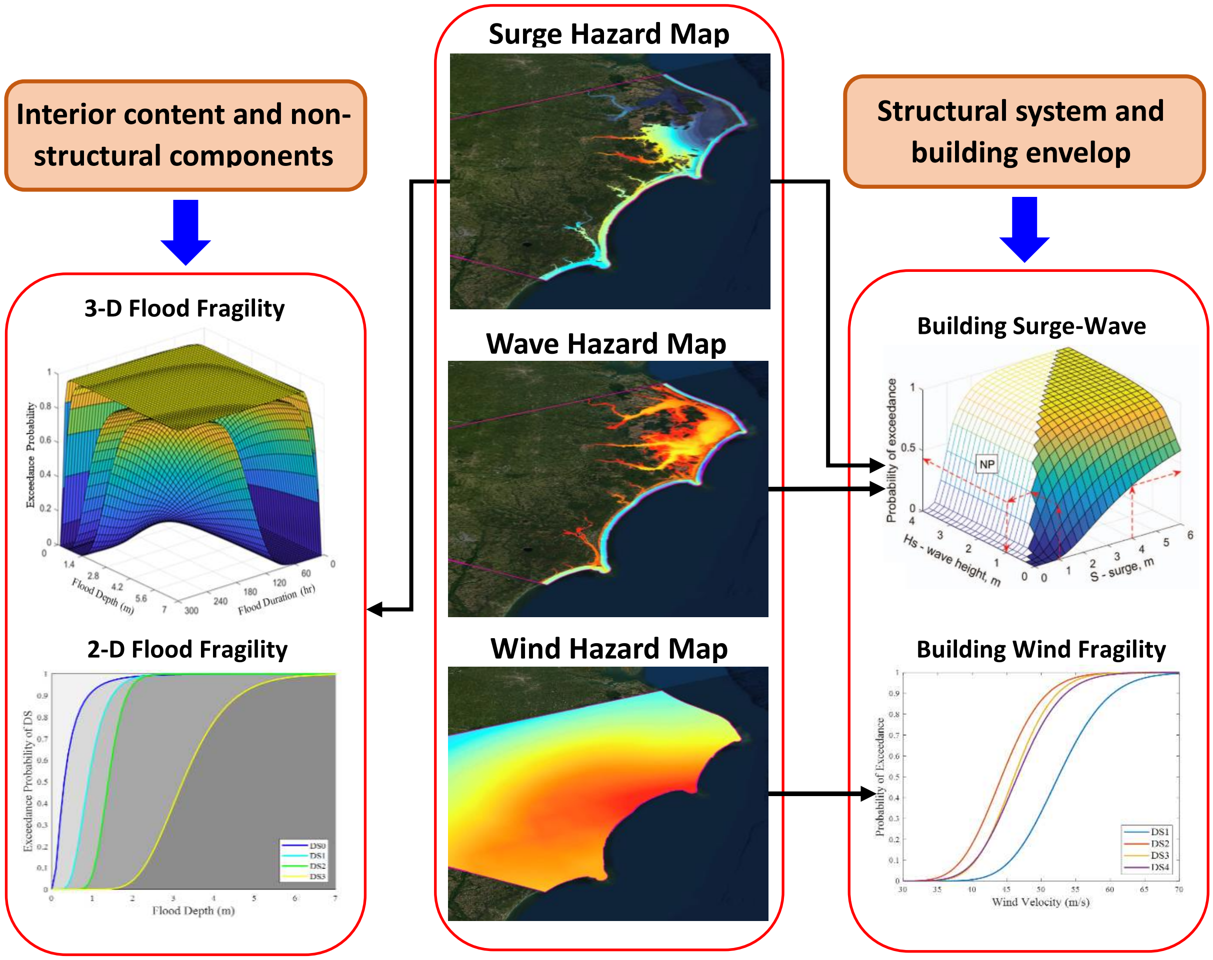

Figure 3-8. *A schematic representation shows the different vulnerabilities of the building components to hurricane-induced hazards*

It should be noted that some of these fragility functions are based on a single variable, such as wind fragility (wind velocity is the only intensity measure) which is in-line with state-of-the-art for those hazards. However, most other fragility functions used here are multi-variate including the surge-wave (wave height and surge depth are the intensity measures) and the surge fragility (flood depth and flood duration are the intensity measures). In this context, both wind fragility functions and surge-wave fragility functions were used to account for structural damage, without including the damage to the building interior content. The content damage resulting from static flooding was calculated from the multi-variate fragility function portfolio developed by Nofal and van de Lindt (2020). These static flood fragility functions are mainly based on content damage starting from DS0 up to DS3 and the structural damage is included separately in DS4 when the structure system deteriorates due to the long duration of flooding, which is the case with urban flooding. Therefore, in this study, DS4 associated with static flooding was excluded because the structural damage resulting from urban flooding has a completely different mechanism from the one caused by coastal flooding. Coastal flooding causes gradual structural damage starting from DS1 up to DS4 because of the hydrodynamic impact of the combined surge and waves. The description of each DS for each hazard is summarized in Table 3-1 along with their corresponding damage scale. Detailed DSs description associated with each hazard can be found in each corresponding publication related to each fragility function (Do et al., 2020; Memari et al., 2018; Omar M. Nofal and van de Lindt, 2020b).

Table 3-1. *Damage states description for the multiple hazards driven by hurricanes along with their damage scale*

Damage State	Damage Scale	Structure Damage		Content Damage
		Surge-Wave	Wind	Static Flooding
DS0	Insignificant	No structural damage		Insignificant damage to the components below FFE such as crawlspace items (e.g., insulation, storage, etc.). Minor damage to the garage interiors.
DS1	Slight	Minor damage to the building envelope with damage to: =< 15% of the roof covering =< 2 doors\windows, =< 25% of the exterior wall, with no roof structure damage.		Damage to the flooring items including carpets, pads, and baseboards. The AC and other HVAC items will be lost if they are not elevated.
DS2	Moderate	Moderate damage to the building envelope with damage to: =< 50% of the roof covering =< 25% of doors\windows, =< 50% of the exterior wall, with no roof structure damage.		Partial damage to the drywall, electrical components, and cabinets. Complete damage to equipment, appliances, and furniture on the first floor.
DS3	Extensive	Extensive damage to the building envelope with damage to: > 50% of the roof covering > 25% of doors\windows, =< 75% of the exterior wall, with no roof structure damage.		Complete damage to the building interiors including major damage to the non-structural components, drywalls, upper cabinets, and lighting fixtures.
DS4	Complete	Complete damage to the building envelope along with extensive structure damage: > 50% of the roof covering, > 25% of doors\windows, > 75% of the exterior wall, with roof structure damage.		Complete damage to the interior content and the non-structural components.

The community-level hurricane vulnerability analysis was then conducted using the building portfolio concept (P. Lin and Wang, 2016), where a certain number of archetypes make up a portfolio could be used to model the different building types within a community. Each hazard has its own portfolio of building archetypes based on the hazard characteristics and the mechanism through which each hazard causes damage to each building archetype. The assignment process of building archetypes within each portfolio on a community was done using a robust mapping algorithm along with GIS tools for spatial analysis similar to the one used for inland communities but more advanced to include the archetypes associated with the other hazards. The building data (e.g., HAZUS-based building occupancy, number of stories, building area, roof shape, foundation type, and construction material) were used as an input for this algorithm to specify the archetype corresponding to each building within a community. Figure 3-9 shows a detailed schematic representation of the mapping process with the visualization of a real community and the mapped archetypes to this community.

The building archetypes within each portfolio are assigned such that they represent the number of different occupancy types needed to accurately represent a community. Full descriptions of these wind archetypes are listed in Table 3-2. For the surge inundation, a portfolio of 15 building archetypes developed by Nofal and van de Lindt (Omar M. Nofal and van de Lindt, 2020b) was used to account for the impacts of flood depth and flood duration on building damage. Full descriptions of these flood archetypes are listed in Table 2-5 from Chapter 2. For surge and wave hazards, there is not any available portfolio that could be used to model the surge-wave vulnerability. Therefore, a one-story residential building archetype developed by Do et al. (2020), which allows different first floor-elevations to be accounted for, was used to account for surge and wave actions on residential buildings. However, a portfolio of surge-wave archetypes is still needed for accurate modeling of the community-level vulnerability analysis. Finally, these portfolios were assigned to an example coastal region to illustrate the applicability of the proposed multi-hazard framework and its scalability to be used at the regional-level which will be fully illustrated in the case studies in Chapter 7 in this dissertation.

Table 3-2. *Description of the wind building archetypes* (Memari et al., 2018)

Archetype	Building description
T1	Residential wood building, small rectangular plan, gable roof, 1 story
T2	Residential wood building, small square plan, gable roof, 2 stories
T3	Residential wood building, medium rectangular plan, gable roof, 1 story
T4	Residential wood building, medium rectangular plan, hip roof, 2 stories
T5	Residential wood building, large rectangular plan, gable, roof, 2 stories
T6	Business and retail building (strip mall)
T7	Light industrial building
T8	Heavy industrial building
T9	Elementary/middle school (unreinforced masonry)
T10	High school (reinforced masonry)
T11	Fire/police station
T12	Hospital
T13	Community center/church
T14	Government building
T15	Large big-box
T16	Small big-box
T17	Mobile home
T18	Shopping center
T19	Office building

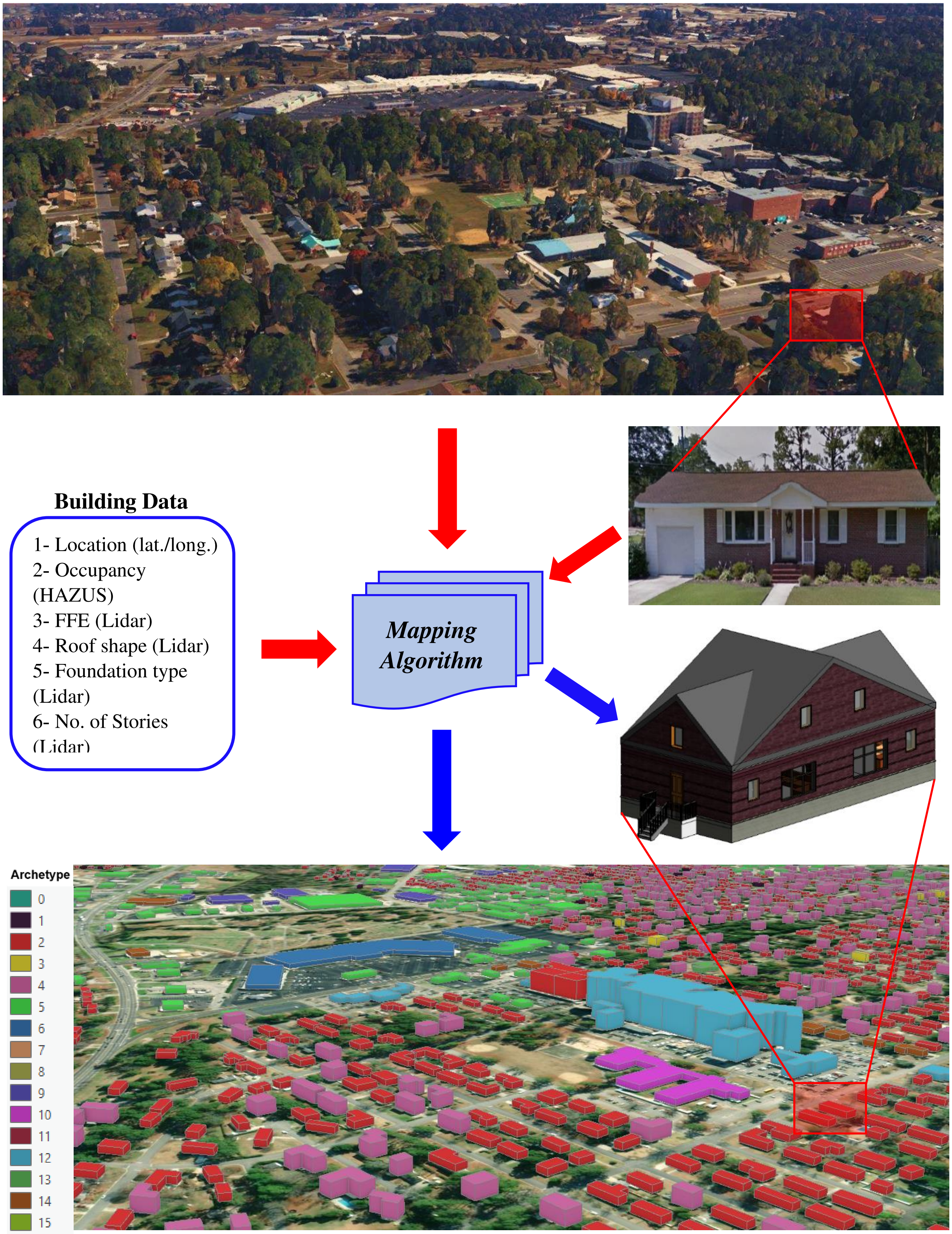

Figure 3-9. *A schematic representation shows how a portfolio of building archetypes are mapped to buildings within a community based on detailed building data*

3.3.4 Risk Analysis

Risk analysis necessitates accounting for both hazard and consequences. Building-level and regional-level risk analyses were conducted herein to illustrate the scalability of the proposed methodology. The high-resolution multi-hazard hurricane risk analysis methodology presented begins with the mapping of each risk component which includes hazard, exposure, and vulnerability, as shown in the flowchart in Figure 3-10. This was done by overlaying the hazard map layers (surge, wave, and wind) with information about the exposed buildings in a GIS environment to relate the spatial location of each building to the spatial variation of the different hazard types across the community. This could also be done using either scenario-based hazard maps or recurrence interval hazard maps (e.g., 100-year, 500-year, etc.). Then, the value of each hazard intensity (surge, wave, and wind) corresponding to each building location was calculated. The mapping algorithm was applied to map the building archetypes to each building within the community. This also included mapping the associated vulnerability functions for each portfolio corresponding to each hazard type. This enabled the calculation of the exceedance probability of each DS for each building corresponding to each hazard.

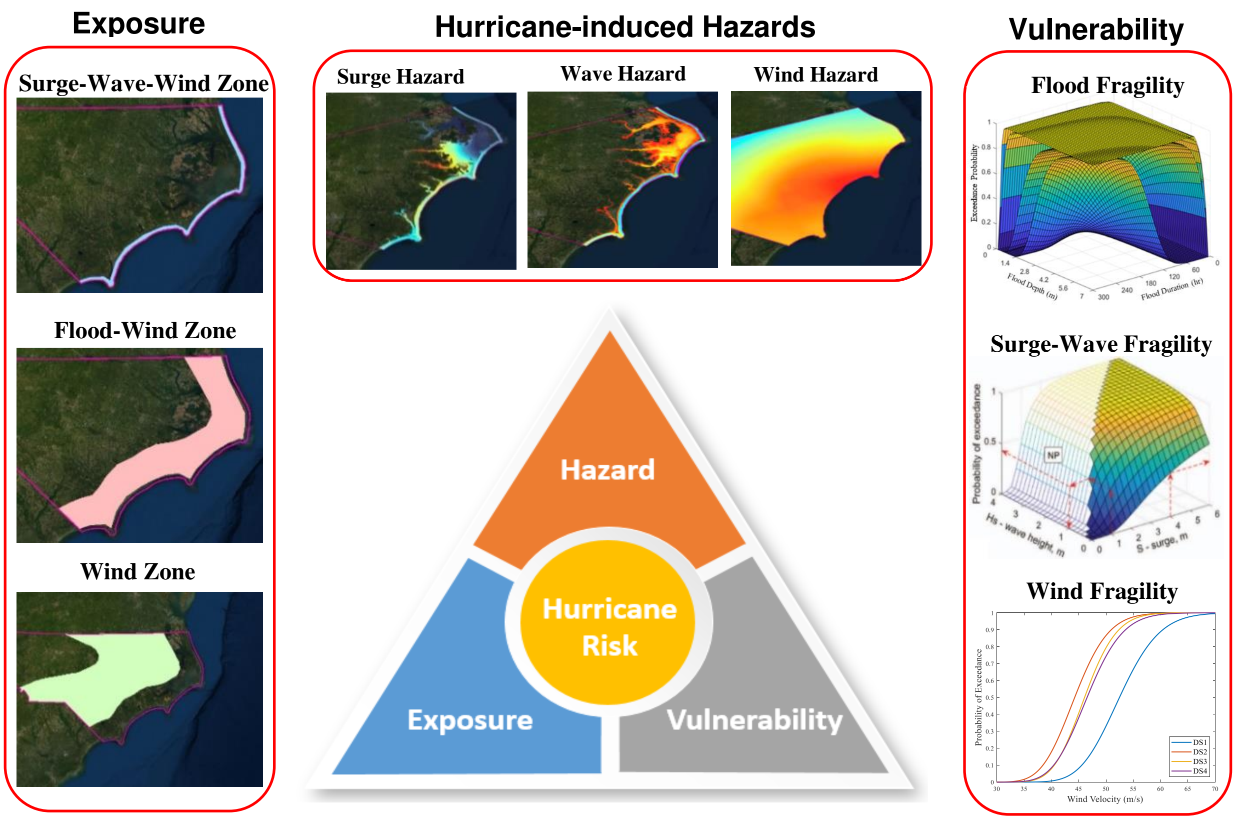

Figure 3-10. *A schematic representation of the hurricane risk components and their associated hazard, exposure, and vulnerability models with the example of North Carolina State, USA*

For building-level analysis, the proposed framework uses five input variables (x_1, x_2, x_3, x_4, x_5) for each building to account for hurricane risk and its associated damage and loss. These variables are the significant wave height, the surge depth, building elevation from the ground, maximum wind speed, and flood duration, respectively. For zone (1), all these variables were used as inputs for three stages of fragility analysis to account for structure and content damage and losses for each building within the community. For stage one, the significant wave height, the surge still water depth, and the building elevation from the ground were used to account for the structural system exceedance probability of each DS using the multi-variate 3-D surge-wave fragility function developed by Do et al. (2020). For loss analysis, the maximum probability of being in each DS corresponding to stage one was calculated and designated as DS_SW. For stage two, the maximum wind speed for each building was used to account for another list of exceedance probabilities of each DS using the fragility portfolio developed by Memari et al. (2018) and then the maximum probability of being in each DS corresponding to stage two was calculated and designated as DS_W. For stage three, flood depth, flood duration, and the building elevation from the ground for each building were used in a 3-D multi-variate static flood fragility function developed by Nofal and van de Lindt (Omar M. Nofal and van de Lindt, 2020b) to account for content damage. Then, the maximum probability of being in each DS corresponding to stage three was calculated and designated as DS_F. For loss and damage analysis, a single DS was assigned to each building based on the maximum DS calculated at each stage (DS_SW, DS_W, and DS_F) using Eq. (3-1). The total building loss was then calculated by multiplying the probability of being in each DS by the replacement cost of each DS corresponding to each analysis stage using Eq. (3-2). For zone (2), the same procedures were used but with replacing the 3-D surge-wave fragility function with its 2-D version at a significant wave height equal to zero because of the domination of static flooding on this zone. For zone (3), stage two was only conducted which only includes wind damage to the building envelope and structural system assuming no rainfall intrusion.

Eq. (3-1):

$$Bldg\_DS(IMs = x_1 : x_5) = Max\begin{pmatrix} DS\_SW_{\max} \\ DS\_W_{\max} \\ DS\_F_{\max} \end{pmatrix} \rightarrow \begin{pmatrix} \underset{i=1}{\overset{i=4}{Max}}\left[P\left(DS\_SW_i \middle| IMs\right) - P\left(DS\_SW_{i+1} \middle| IMs\right)\right] \\ \underset{i=1}{\overset{i=4}{Max}}\left[P\left(DS\_W_i \middle| IMs\right) - P\left(DS\_W_{i+1} \middle| IMs\right)\right] \\ \underset{i=0}{\overset{i=3}{Max}}\left[P\left(DS\_F_i \middle| IMs\right) - P\left(DS\_F_{i+1} \middle| IMs\right)\right] \end{pmatrix}$$

Eq. (3-2):

$$\begin{aligned} L_f(IMs = x_1 : x_5) = &\sum_{i=1}^{4}\left[P\left(DS\_SW_i \middle| IMs = x_1 : x_3\right) - P\left(DS\_SW_{i+1} \middle| IM = x_1 : x_3\right)\right] \times Lr_{s1,i} \times V_{s1} \\ &+ \sum_{i=1}^{4}\left[P\left(DS\_W_i \middle| IMs = x_4\right) - P\left(DS\_W_{i+1} \middle| IM = x_4\right)\right] \times Lr_{s2,i} \times V_{s2} \\ &+ \sum_{i=0}^{3}\left[P\left(DS\_F_i \middle| IMs = x_1, x_3, x_5\right) - P\left(DS\_F_{i+1} \middle| IM = x_1, x_3, x_5\right)\right] \times Lr_{c,i} \times V_c \end{aligned}$$

where $Bldg\_DS(IMs = x_1{:}\ x_5)$ is the building DS corresponding to the five intensity m*easures*. $P[DS\_SW_i|(IM = x_1{:}x_3)]$ = the exceedance probability of DS_SW_i at ($IMs = x_1{:}x_3$) calculated from the surge-wave fragility, and $P[DS\_SW_{i+1}|(IM = x_1{:}x_3)]$ = the exceedance probability of DS_SW_{i+1} at ($IMs = x_1{:}\ x_3$) calculated from the surge-wave fragility. $P[DS\_W_i|(IM = x_4)]$ = the exceedance probability of DS_W_i at ($IMs = x_4$) calculated from the wind fragility, and $P[DS\_W_{i+1}|(IM = x_4)]$ = the exceedance probability of DS_W_{i+1} at ($IMs = x_1, x_2, x_3$) calculated from the wind fragility. $P[DS\_F_i|(IM = x_1, x_3, x_5)]$ = the exceedance probability of DS_F_i at ($IMs = x_1, x_3, x_5$) calculated from the flood fragility, and $P[DS\_F_{i+1}|(IM = x_1, x_3, x_5)]$ = the exceedance probability of DS_F_{i+1} at ($IMs = x_1, x_2, x_3$) calculated from the flood fragility. $Lr_{s1,i}$ = cumulative replacement cost ratio of the structure damage associated with surge and wave loads corresponding to DS_SW_i, and V_{s1}= structure replacement cost associated with surge and wave loads. $Lr_{s2,i}$ = cumulative replacement cost ratio of the structure damage associated with wind load corresponding to DS_W_i, and V_{s2}= structure replacement cost associated with wind loads. $Lr_{c,i}$ = cumulative replacement cost ratio of the building content corresponding to DS_F_i, and V_c= content replacement cost.

In terms of losses, the total building replacement cost was divided into structure and content losses. The structure losses were further divided into three parts, which are walls and framing, roof sheathing and roof framing, and decking and foundation. Table 3-3 shows the loss percentage ranges associated with each one of these divisions corresponding to each DS. These percentages were derived from the DSs description listed in these references (Do et al., 2020; Memari et al., 2018; Omar M. Nofal and van de Lindt, 2020b). However, specific loss percentages for each building archetype corresponding to each DS were used herein based on the detailed cost analysis conducted as a part of this dissertation and published herein (Omar M. Nofal and van de Lindt, 2020b). Roof losses were calculated using the wind DSs since roof damage is assumed to result from wind loads while floor system and foundation losses were calculated using surge-wave DSs because most of their damage results from surge and waves. Walls and framing are typically impacted by both wind and surge-wave loads. Therefore, the higher DS from both wind and surge-wave was used to account for walls and framing losses. Finally, content damage was calculated using the static flood fragility.

Table 3-3. *Loss percentage of content and structure damage for each damage state*

Damage state	Damage scale	Structure Damage			Content damage
		Walls sheathing and framing	Roof sheathing and framing	Decking and foundation	
DS0	Insignificant	0.00	0.00	0.00	0.00-0.04
DS1	Slight	0.02-0.25	0.02-0.15	0.02-0.10	0.04-0.20
DS2	Moderate	0.25-0.50	0.15-0.50	0.10-0.50	0.20-0.70
DS3	Extensive	0.50-0.75	0.50-0.75	0.50-0.75	0.70-1.00
DS4	Complete	0.75-1.00	0.75-1.00	0.75-1.00	1.00

For a regional-level analysis, an algorithm was developed to extract the hazard value at each building and then distinguish each exposure zone associated with each building based on the calculated hazard intensity and, consequently perform the corresponding needed vulnerability analyses, as shown in the flowchart in Figure 3-11. The exceedance probabilities of each DS for each building associated with each hazard intensities were calculated. A detailed damage and loss analysis are then conducted to identify the final DS for each building and the total amount of losses based on its vulnerability to the combinations of hazards induced by the hurricane scenario. Finally, these losses are mapped back to the community to identify the spatial extent and severity of damage induced by hurricanes across the community.

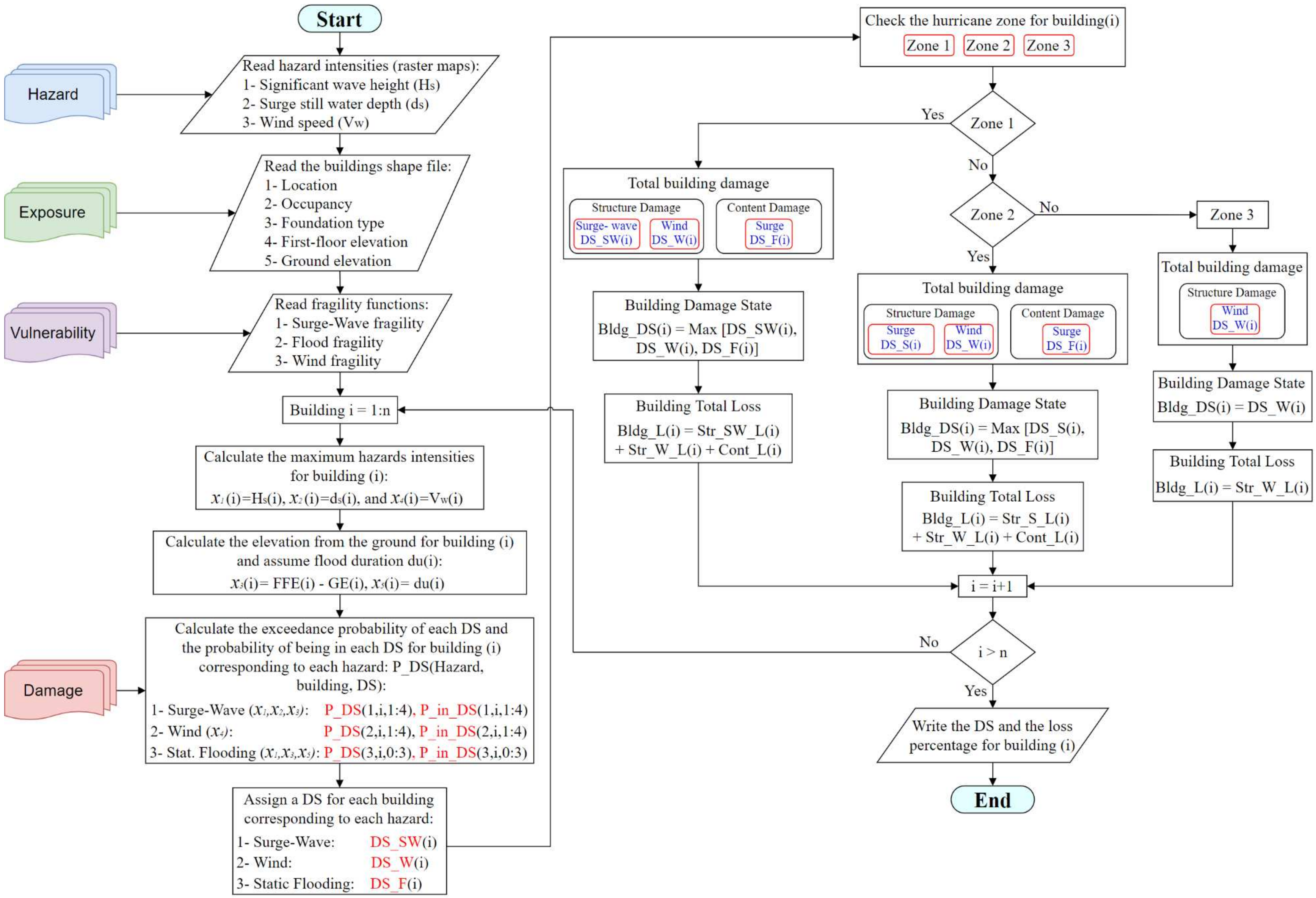

Figure 3-11. *A detailed framework for the community-level multi-hazard hurricane risk assessment model that accounts for building*

CHAPTER 4: MITIGATION AND ADAPTATION ANALYSIS APPROACH

4.1 Introduction

Risk mitigation for hurricane-induced hazards is crucial for vulnerable communities to decrease their exposure to severe events and enable these communities to better adapt for future events. Over the last few decades, researchers have investigated the impact of using a number of flood mitigation measures for buildings and mitigation strategies for the entire community. However, most of these studies investigated hazard control measures and their impact on hazard intensity reduction with less focus on loss reduction for the exposed buildings and the impact of using building-level mitigation measures. Additionally, most of the available models use aggregated data in qualitative vulnerability models which possess significant inherent uncertainties. In this dissertation, the impact of using a number of building- and community-level flood mitigation measures will be investigated in terms of using a levee system, retention/detention ponds, flood gates, flood barrier systems, water pumps, and increasing the elevation of some selected-water sensitive components. A general framework is proposed herein to include the impact of using some building-level mitigation measures on building vulnerability by applying fragility and loss functions (Omar M. Nofal and van de Lindt, 2020a). Then, a methodology that includes the impact of using a number of flood hazard mitigation strategies was developed to account for their impact on building-level flood loss reduction. The developed approaches are based on a probabilistic vulnerability method that includes uncertainties propagation across the damage/loss models. A suite of mitigation scenarios that use a combination of building-level mitigation measures and community-level mitigation strategies was investigated (Omar M. Nofal and van de Lindt, 2021). The building archetype portfolio introduced in Chapter 2 was used herein to model the flood vulnerability reduction associated with each mitigation scenario. Afterwards, a detailed analysis of the impact of these mitigation scenarios on an example community was conducted and presented in the case studies in Chapter 6.

Modeling the impact of either community-level or building-level flood mitigation measures on the total flood losses reduction requires several levels of data analysis. Figure 4-1 shows a schematic representation of these levels along with the different levels of damage and loss analysis needed to investigate the impact of using different mitigation measures. Figure 4-1 focuses only on the level of detail used within this dissertation, and methodological details appear in later flow charts in this chapter. Beginning at the top of Figure 4-1, community-level data from the flood hazard maps are used to simulate the flood hazard scenario and then account for the flood depth at each building location (coordinates). The building-level data such as value, location, and the other physical characteristics are then used to assign the building archetype from the building portfolio and link the vulnerability model associated with this archetype. Each assigned archetype is represented by damage fragilities, and each set of damage fragilities were developed by modeling the damageable components within a building type as explained earlier in Chapter 2. However, in the mitigation analysis, it is possible to change the fragilities based on a change in the components within the building, which will be explained in this chapter. Returning to Figure 4-1, then a community-level spatial analysis enables the relationship between the community-level data with the building-level data to be formulated including any modifications to the building level fragilities as a function of changes in their damageable components.

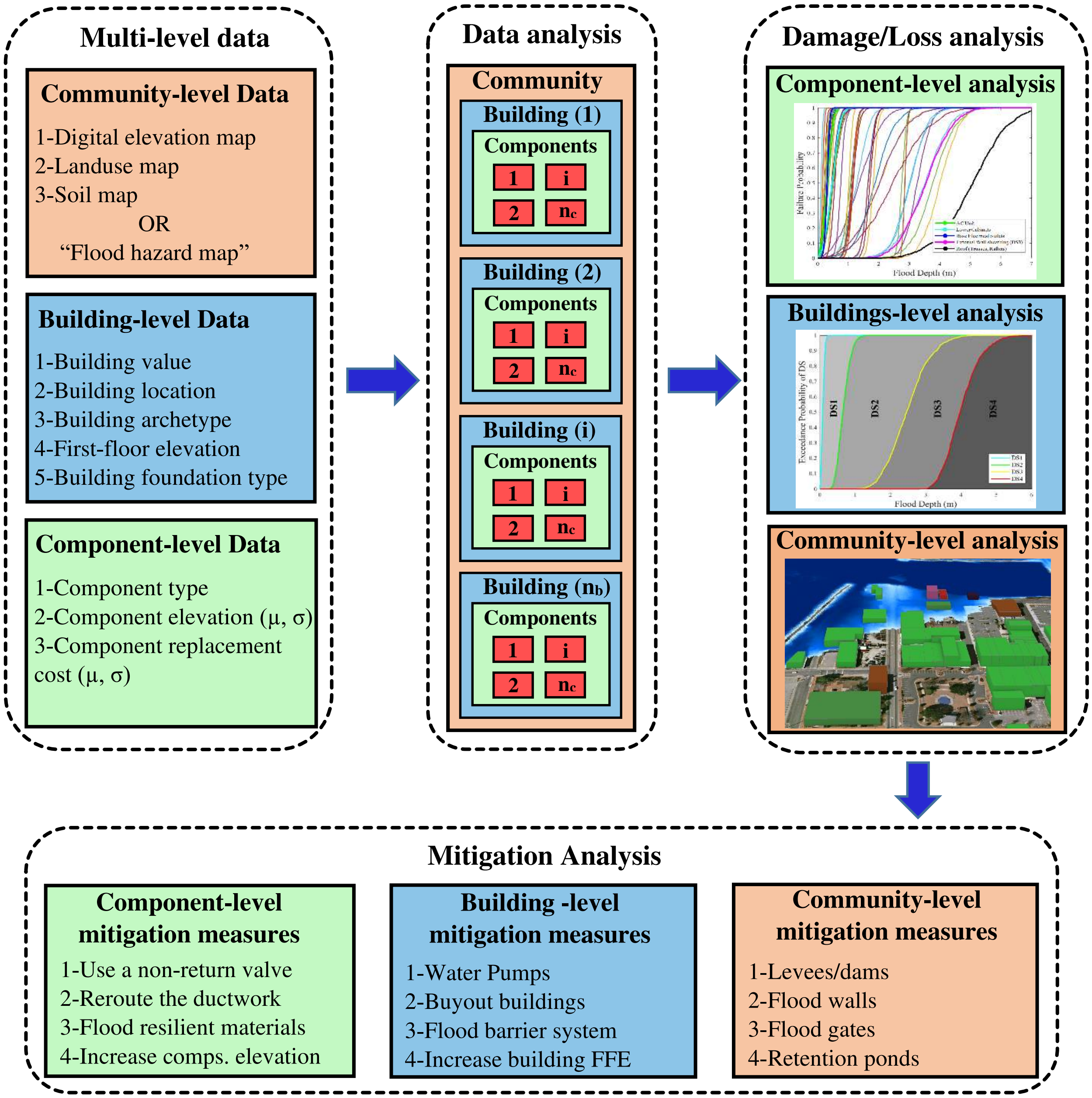

Figure 4-1. *A schematic representation of the different levels of data needed for loss/damage analysis, and mitigation analysis*

4.2 Building-Level Mitigation and Adaptation Analysis

In this dissertation, several building-level mitigation strategies were modeled which essentially modify the damage (and loss) fragilities. Specifically, three different building-level flood mitigation techniques were investigated in terms of modeling their associated flood damage/loss reduction at the building-level and then propagated up to the community-level. The mitigation measures analysis and their corresponding scenarios were applied to the 15 building archetype that comprises the community. For brevity, the methodology used to modify the flood fragility and loss function for each building archetype based on each flood protection technique is illustrated only for Archetype 2 (one-story multi-family residential building). However, the mitigation analysis methodology was applied for all 15 building archetypes developed in Chapter 2.

4.2.1 Temporary water barrier systems

Installing a temporary flood barrier system requires enough lead time prior to an event for the installation of the system. The installation time depends on the type of this system (e.g., sandbags, bladder dam, water wall, aquafence, water-gate, etc.) and the size of the protected area. This underscores the importance of weather prediction to provide early flood warnings to enable enough time to either prepare and/or evacuate. Figure 4-2(a) shows an aerial image from google earth for a business that was severely flooded as a result of rainfall from Hurricane Matthew, 2016. However, when Hurricane Florence struck two years later in 2018, this business had approximately three days warning before the flood which allowed enough time to set up a large bladder dam as shown in Figures 4-2(b and c). Modeling a building-level flood barrier system requires an understanding of a number of different ways that water can breach a building (e.g., doors, walls, a sewer backup, etc.) and how the temporary barrier system operates (partial or complete). Some flood barriers are installed locally at critical locations around the building including at/near doors and other openings using sandbags and flood shields. Other flood barriers provide complete protection by surrounding the whole building using a bladder dam as shown in Figure 4-2. In addition, backflow valves for sewer pipes/drains are not standard and therefore contaminated water will breach the inside of the building. Therefore, a non-return valve is needed to ensure that any of the flood mitigation measures are not in vain.

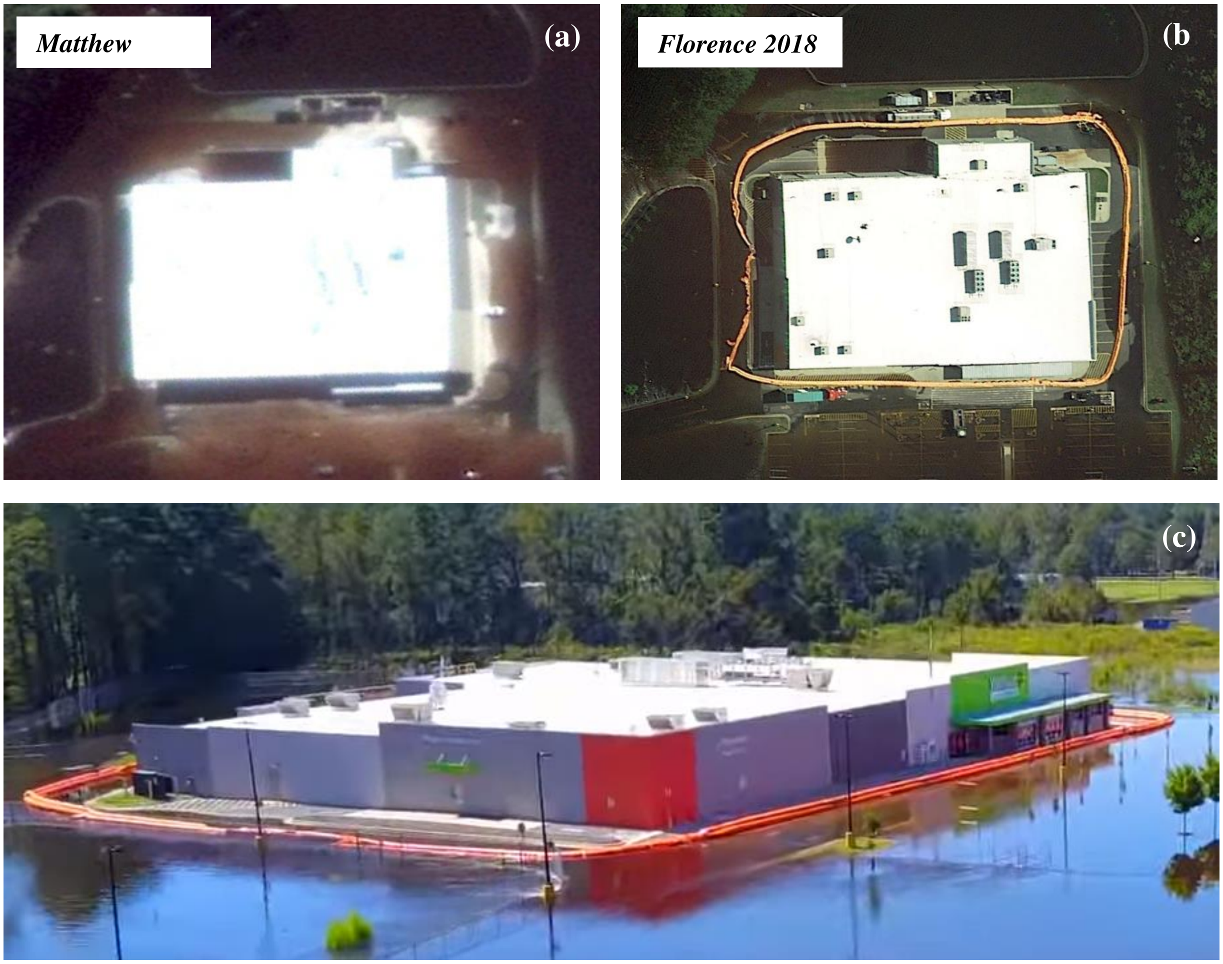

Figure 4-2. *A comparison between the state flooding for a business in Lumberton, NC during the recent rainfall storms after Hurricane Matthew in 2016 and Hurricane Florence 2018: (a) State of flooding after Hurricane Matthew in 2016; (b) State of flooding after Hurricane Florence in 2018; (c) Drone image for the business after Hurricane Florence in 2018 showing the used flood barrier system*

The approach used herein to model a temporary flood barrier system and modify a building-level flood fragility is presented in the flow chart in Figure 4-2. The updated framework accounts for zero flood losses if a number of conditions are satisfied including the existence of a sewer backflow valve, flood-resistant walls, flood barrier, and the barrier height (H_b) is higher than the flood depth. These conditions are necessary to make sure that the temporary flood barrier works efficiently without any leakage from other locations (e.g., sewers backup) or flood water overtopping. If these conditions are not satisfied, a Monte Carlo simulation (MCS) is applied to develop the fragility by investigating the damage to each component within the building using the framework shown in Figure 4-2. This framework begins with several inputs for the building components including flood depth resistance, flood duration resistance, and the replacement cost of each component along with the characteristics of the flood barrier. Then, it checks the feasibility of the flood barrier conditioned on the barrier height with respect to the flood depth as well as the existence of a sewer backflow valve. Next, two separate analyses start based on these initial conditions, namely fragility analysis and loss analysis with both analyses being probabilistic, i.e. using MCSs to propagate uncertainties. Each one of these analyses is then divided into another sub-analysis to conduct single-variable and multi-variate flood fragility and loss analysis. For the fragility analysis, a component fragility matrix was developed (Fr(j,k) for single-variable and Fr(j,u,k) for the muli-variate) using 1000 simulations within the MCS for each component to calculate the failure probability for each component k at each intensity measure flood depth (j) and flood duration (u). Then, building fragility curves/surfaces were derived from component fragilities weighted by their replacement costs based on the approach developed in Chapter 2. For the loss analysis, another series of MCSs was used to calculate the total building replacement cost (Rep_cost(j,i,k) for single-variable function or Rep_cost(j,u,i,k) for the multi-variate function). This was done by summing the losses for all damaged components (k) at each simulation (i) at each intensity measure (flood depth (j) and flood duration (u)).

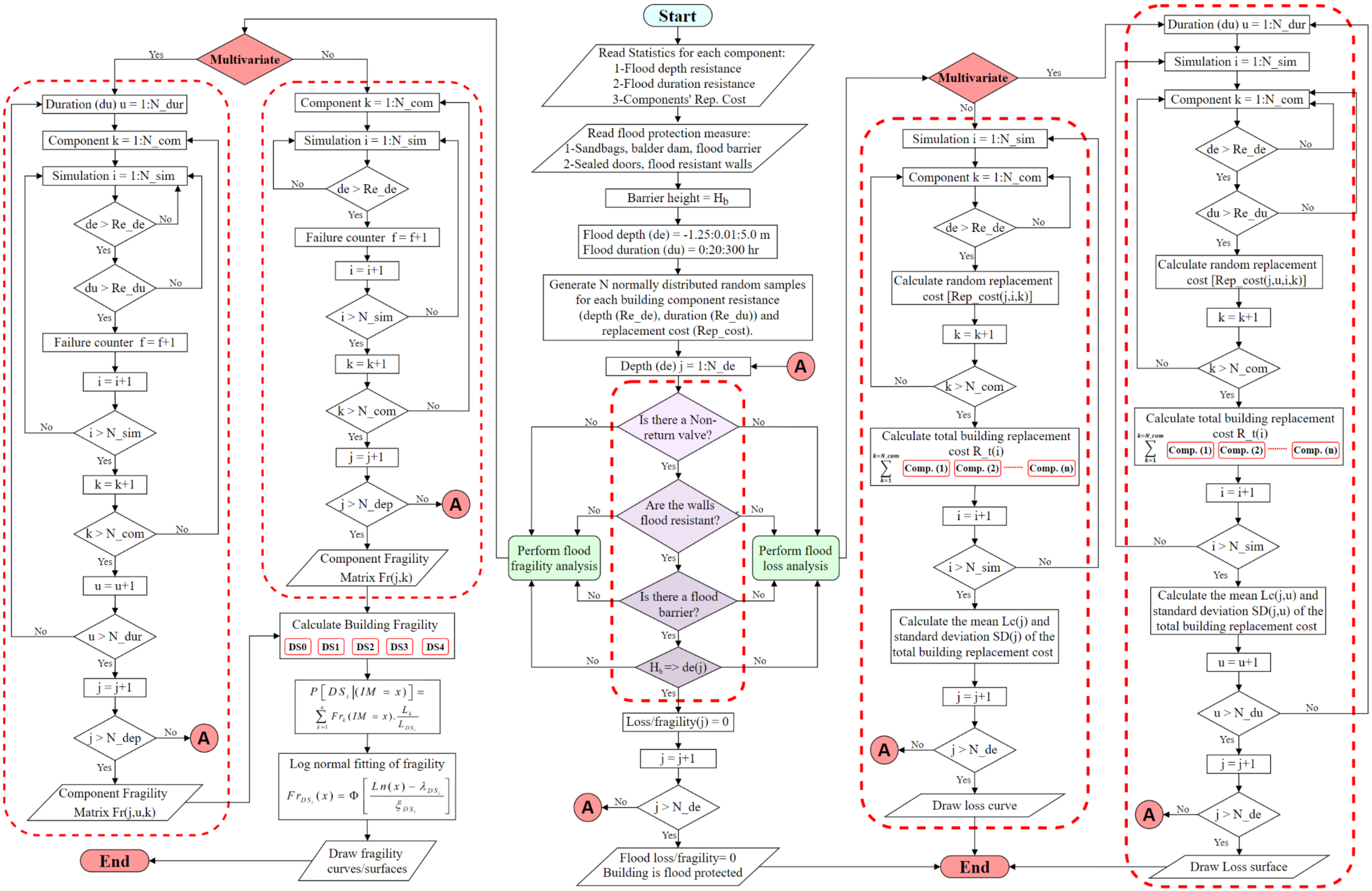

Figure 4-3. *A flow chart illustrates a methodology to develop a single-variable and a multivariate flood loss and fragility functions for flood protected buildings where H_b = barrier height, N_com = number of components, N_de = Number of depth steps, N_sim = number of simulations, N_dur = number of duration steps, Fr_k = the component fragility, and Fr_{DS_i} = The exceedance probability of a DS_i*

Modified flood fragility and loss functions were developed based on the barrier height for the building portfolio described in Chapter 2. The updated fragility and loss functions truncate any damage/loss values at flood depths less than the barrier height and set it to zero, assuming no damage if the water depth is below the barrier height. Figure 4-3. shows an example of fragility and loss functions for the one-story multi-family residential building on a slab-on-grade foundation (archetype F2 from Table 2-5) with and without a 1.0m height flood barrier. Using this barrier height would reduce flood losses by almost 50% as shown in Figure 4-3(d) with complete protection up to DS2 and a very low probability of exceeding DS3 as shown in Figure 4-3(b). However, if the flood depth was higher than the barrier height (e.g., 1.0m), this building archetype will immediately lose 50% of its value with a 95% exceedance probability of DS2, meaning that building interior content will be immediately lost if they are touched with water neglecting the impact of flood duration (or assuming that flood duration is more than 10 days).

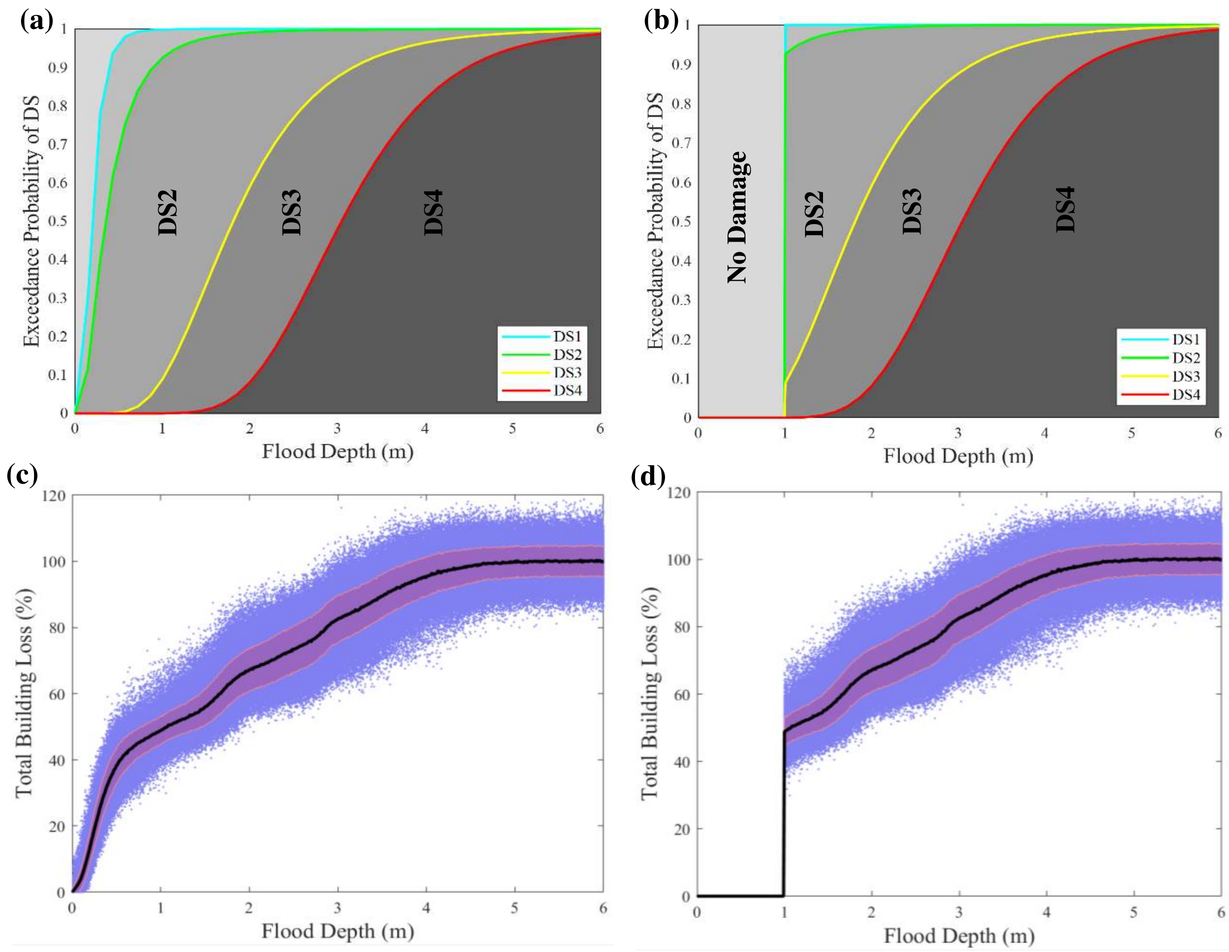

Figure 4-4. *Fragility and loss functions with and without flood barrier with a height of 1.0m for a one-story multi-family residential building: (a) Fragility curves without using a flood barrier; (b) Fragility curves with the 1.0m flood barrier; (c) Total building loss curve without a flood barrier; (d) Total building loss curve with the 1.0m flood barrier*

4.2.2 Pumps

The use of pumps usually comes as a post-disaster mitigation measure when emergency personnel discovers water breaches inside a community from any flood protection structure (e.g., levees, floodwalls, etc.). They can also be used by households or businesses to protect their property. Pumping water from a property may require the simultaneous use of temporary berms or flood barriers to prohibit the water from returning to the property depending on the topography. The size, number, and location of pumps are determined based on the availability of pumps and the severity of flooding. For example, during Hurricane Matthew in 2016, the city of Lumberton, NC was not prepared for flooding and did not have enough time to locate pumps as depicted in the photo in Figure 4-5(a). On the other hand, two years later with the arrival of Hurricane Florence in 2018, Lumberton had enough lead time to order and position several very large pumps at critical locations such as those shown in Figure 4-5(b). The city was able to position more than 25 pumps of varying size at critical locations on their levee to move the water from the city side to the riverside as shown in Figure 4-5(c). Modeling pumps within a building-level flood vulnerability model affects both the flood depth and the flood duration. However, in this dissertation, using pumps is assumed to affect flood duration only, a simplification that can be improved upon later. This assumption appears rational if this mitigation option is treated as a post-event mitigation measure when water is potentially already breaching buildings or neighborhoods and sometimes it takes a day or two to order, position, and set up the pump system. Therefore, in this model, pumps only reduce the flood duration of the still water depth. A number of flood durations were assumed based on a number of pumping scenarios associated with the pumping system characteristics (number of pumps, location, pumping discharge, pump size/capacity, etc.). Therefore, the multi-variate flood fragility and loss functions, which include duration and depth, developed in Chapter 2 were used to account for the impact of decreasing flood duration.

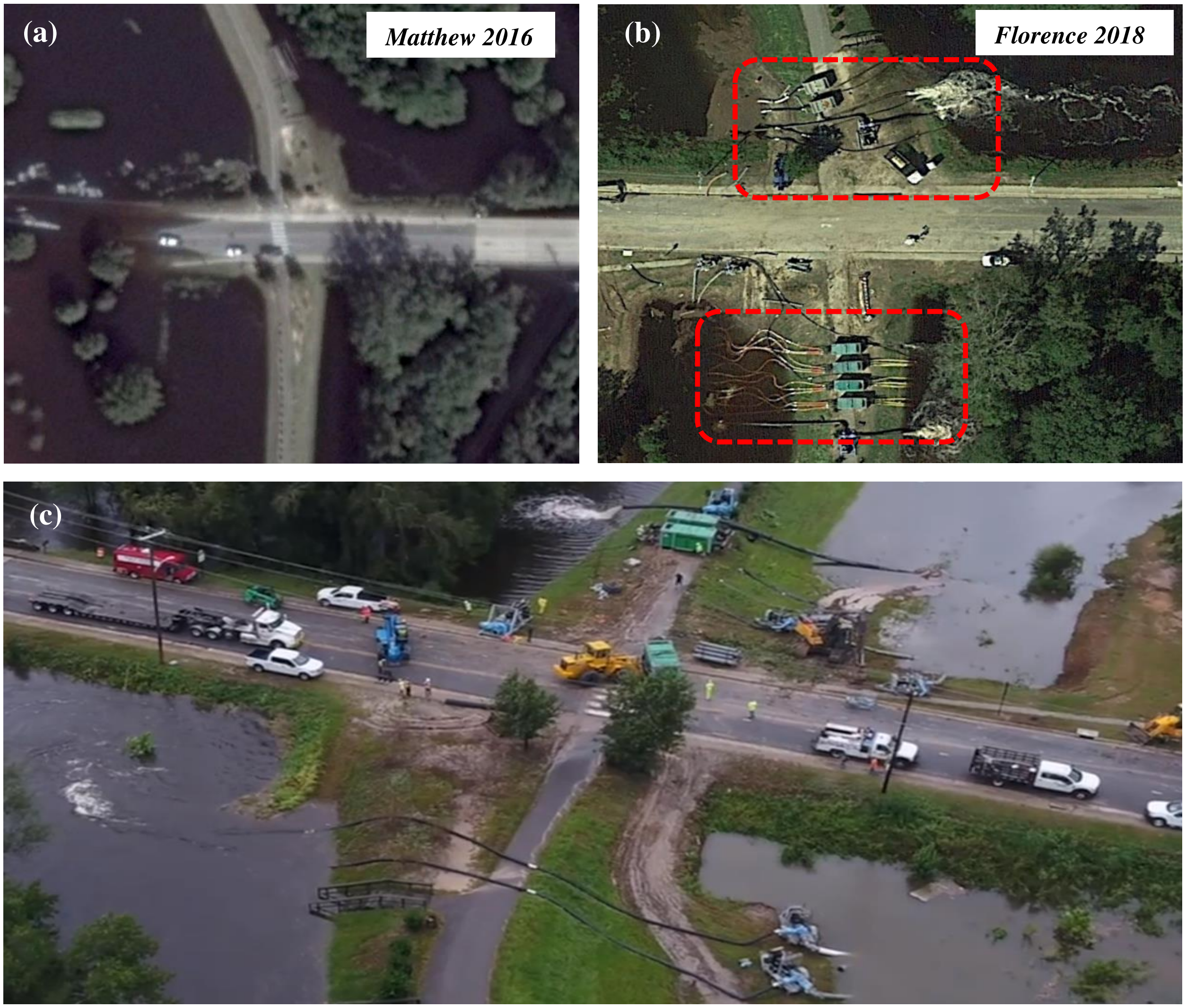

Figure 4-5. *A comparison between the flooding at the levee in Lumberton, NC during the recent rainfall storms resulting from Hurricane Matthew in 2016 and Hurricane Florence in 2018 along with the pump locations: (a) The flooding after Hurricane Matthew in 2016; (b) The flooding after Hurricane Florence in 2018; (c) Drone image for the levee following Hurricane Florence in 2018 showing the location of the mega pumps*

A number of flood duration scenarios were used to model (and quantify) the effect of using pumps in this study. Figure 4-6 (a) shows the flood loss surface for archetype F2 and its corresponding loss curves for five select flood durations based on hypothetical pumping scenarios (1 day, 2 days, 6 days, 8 days, and 10 days) are shown in Figure 4-6 (a). Figure 4-7 shows 3-D flood fragility surfaces for the same building archetype along with the state of flood fragility at each flood duration. The analysis results highlight the impact of flood duration on the amount of flood losses.

For example, if this building archetype (F2) was completely flooded and then drained in one day, this could guarantee that DS4 will not be exceeded with a 50% exceedance probability of DS3 which would save most of the structural components along with some non-structural components as shown in Figure 4-7. This also would reduce the amount of losses by 45% from the state of losses at 10 days as shown in Figure 4-6(b). Decreasing flood duration would slow or even prevent foundation scouring and floating. However, most of the building content will be lost along with significant damage to the non-structural components, and it should be further noted here that contaminated water could result in additional damage at short flood durations. Usually, portable water pumps are used with flood barriers due to the possible leaks or water over topping. Therefore, the combined impact of using flood barriers along with decreasing flood duration using pumps was also investigated as shown in Figure 4-8.

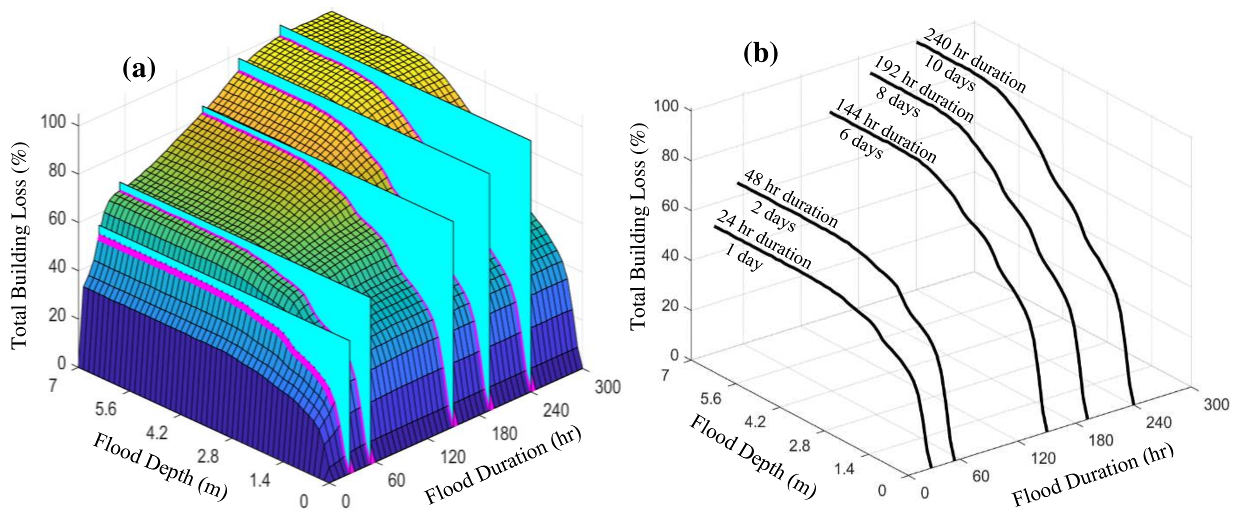

Figure 4-6. *Example flood loss curves for a number of flood duration scenarios for a one-story residential building: (a) 3-D flood loss surface; (b) Flood loss curves associated with each flood duration scenario*

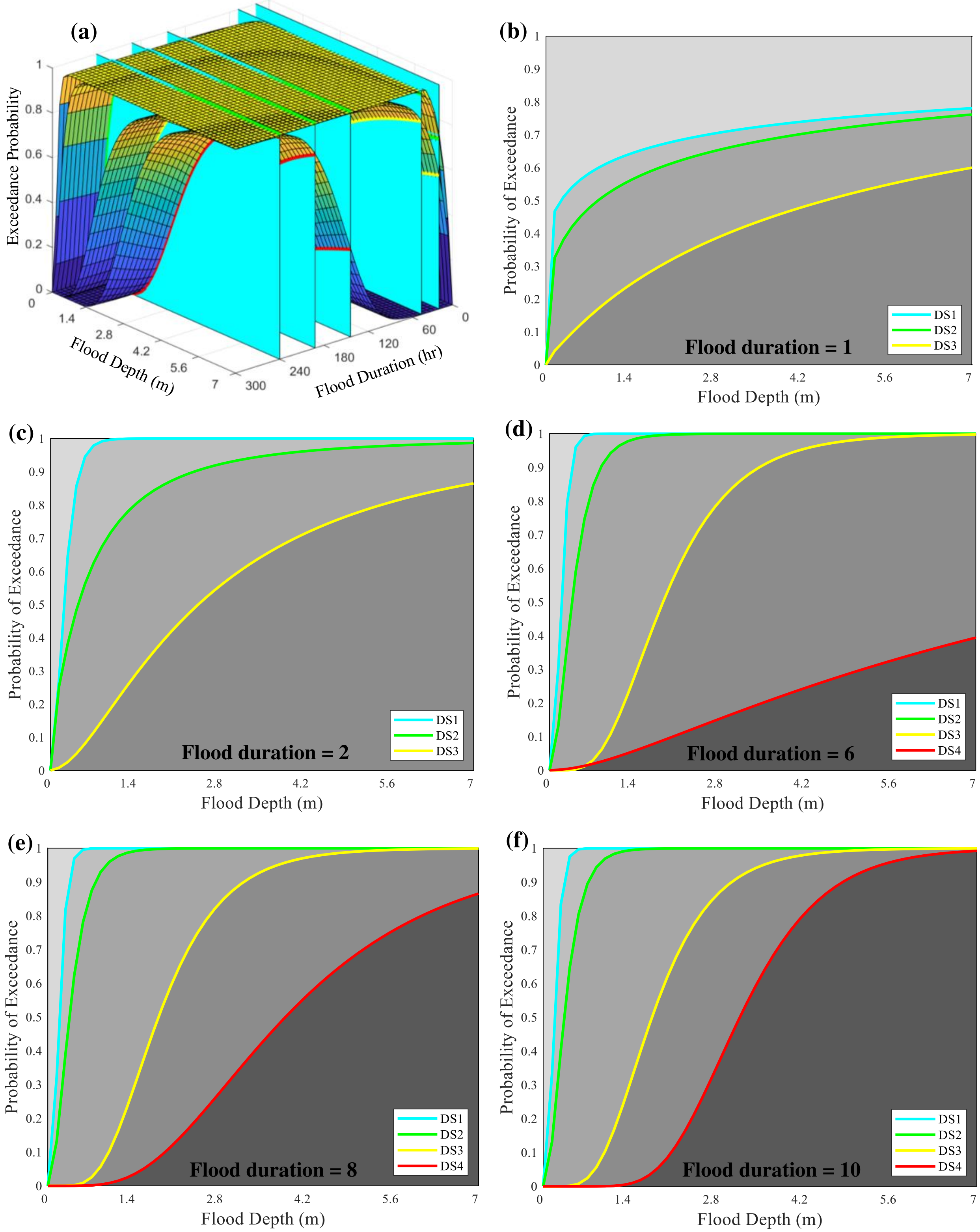

Figure 4-7. *Example flood fragility curves for a number of flood duration scenarios for a one-story residential building: (a) 3-D flood fragility surfaces; (b,c,d,e, and f) Flood fragility curves associated with each flood duration scenario of 1 day, 2 days, 6 days, 8 days, and 10 days, respectively*

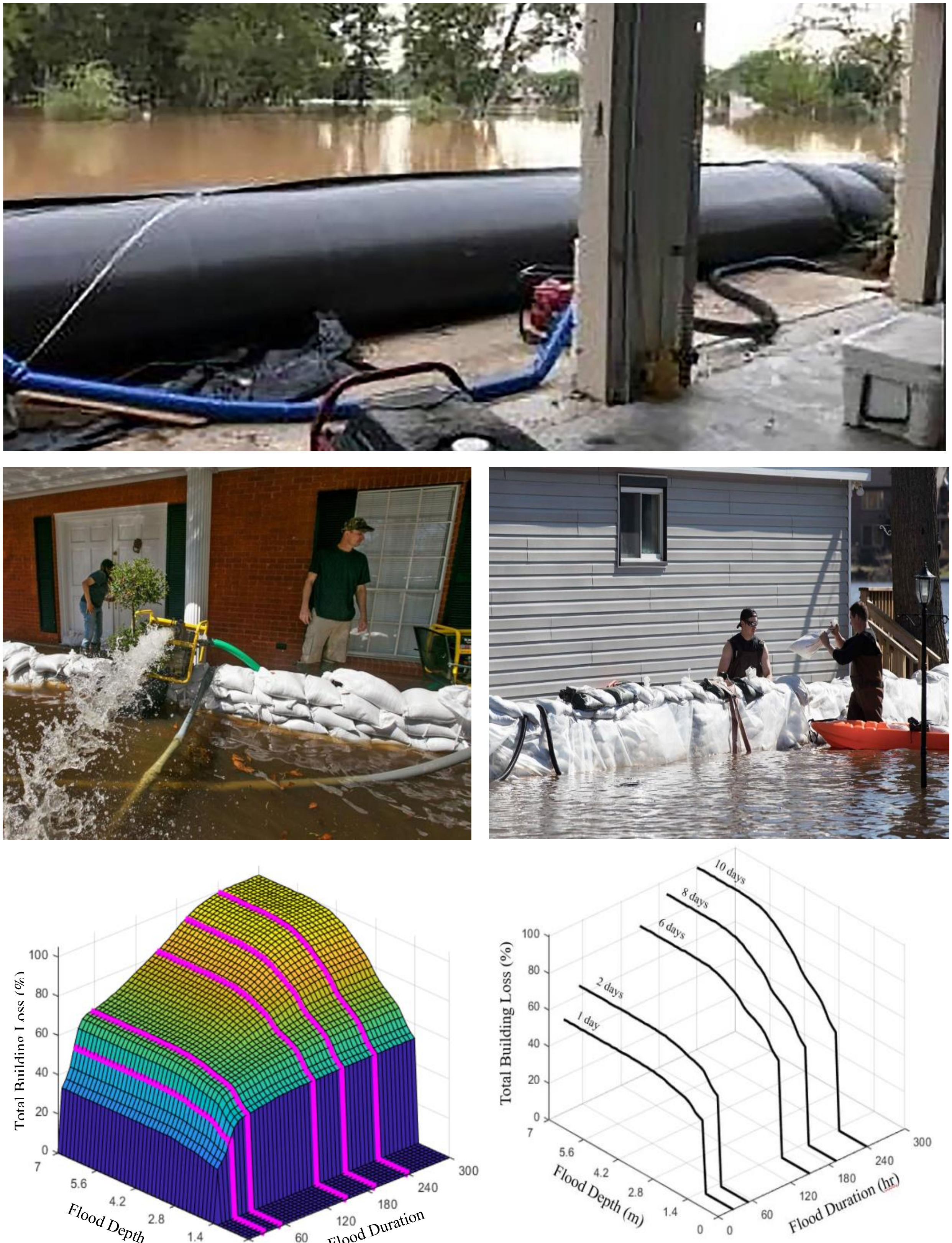

Figure 4-8. *The combined impact of using flood barriers and pumps simultaneously on the flood*

4.2.3 Resilient Construction

There are other building-level flood mitigation and adaptation measures that can increase building resilience to flood hazards such as shown in Figure 4-9. These measures include using a backflow valve in the sewer pipe as mentioned earlier, flood-resistant front door, walls with a moisture barrier, appliances on raised plinth/mechanism (e.g., washer, dryer, coolers, etc), and flood resilient plasterboards. Although the price of the electrical system is not expensive with respect to other building systems, it is critical for the continued occupancy of the building by the households. Therefore, separating the electrical circuit of the upper floors from the lower floor and raising the elevation of the base electrical socket/outlets can help mitigate flood impacts on the occupants due to the electrical system (Omar M. Nofal and van de Lindt, 2020b). Similarly, ventilation, air conditioning, and heaters are necessary and sometimes critical to occupy a building. Therefore, elevating the AC and heating units along with rerouting the ductwork from the crawlspace to the attic (of the second-floor diaphragm) will significantly contribute to flood adaptation. These mitigation approaches not only decrease flood losses but contribute significantly to increase the probability of building functionality during or following a flood.

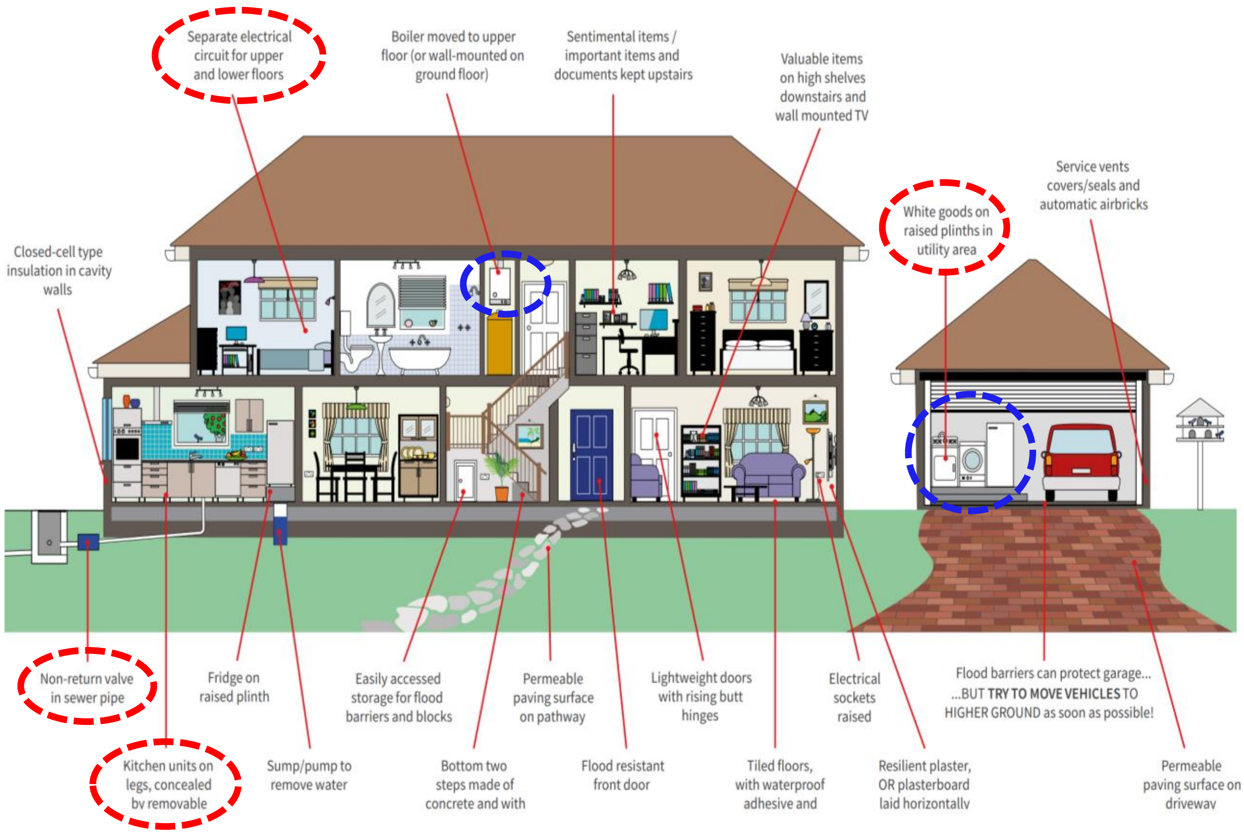

Figure 4-9. *A schematic representation of resilient building construction in terms of implementing a number of building-level flood mitigation and adaptation measures after Dhonau, and Rose* (Dhonau and Rose, 2016)

The component-based fragility and loss functions developed by Nofal and van de Lindt (Omar M. Nofal and van de Lindt, 2020b) were modified to include the impact of any changes in the elevation to each component and the full modified analysis was reproduced using MCS. For example, select components that could be elevated within a residential building (e.g., archetype F2) were adjusted by increasing their elevation (e.g., rerouting ductwork, elevating the AC unit, etc. as described earlier) or elevating them just before flooding using elevation blocks (e.g., washer, dryer, TV, etc.). Table 4-1 shows the statistical data (mean (μ) and standard deviation (σ)) for the original and elevated components and their replacement/repair costs (the market value of the component). The mean value of the replacement cost of these components is more than $74,000 (for four units of a multi-family building F2) which is more than 13% of the mean total building replacement cost.

Table 4-1. *Data for select building components that could be elevated (Archetype 2 as an example)*

Component	DS	Old-Elevation (m)		New-Elevation (m)		Component Cost (USD $)*	
		μ	σ	μ	σ	μ	σ
HVAC Pipes/Ducts	DS1	0.15	0.08	3.50	0.25	6711	2237
AC Unit		0.20	0.10	3.20	0.10	10900	1750
Heating Unit		0.20	0.10	3.20	0.10	10900	1750
Refrigerator	DS2	0.20	0.08	0.50	0.10	6900	2550
Stove		0.25	0.10	0.50	0.10	5300	1350
Washer		0.15	0.05	0.50	0.10	3700	1150
Dryer		0.15	0.05	0.50	0.10	3700	1150
Water Heater		1.30	0.60	3.20	0.10	4420	690
TV		1.05	0.23	1.70	0.15	2400	800
Dishwasher		0.25	0.13	1.70	0.15	2200	300
Base Electrical outlets		0.30	0.08	0.50	0.10	688	296
Mixers	DS3	1.15	0.13	1.7	0.15	660	270
Microwave		1.15	0.13	1.7	0.15	1100	250
Computer		0.5	0.23	1.7	0.15	6600	2700
Laptop		0.5	0.23	1.7	0.15	6600	2700
Printer		0.5	0.20	1.7	0.15	500	150
Window AC Units		0.75	0.13	1.7	0.15	1100	250

*The replacement cost of these components is based on the 2020 prices for a multi-family one-story residential building consisting of four units (archetype F2) and the listed components cost are for all the appliances within the whole building (four units).

The input data for the flood damage/loss framework was changed for the select water-sensitive components in Table 4-1 using their new elevation. Figure 4-10(a) shows a comparison between flood losses before and after elevating the select components (at 10 days flood duration) which reveals that this mitigation technique could be effective for flood depth between 0.0m up to 3.0m with flood loss reduction in the range from 5.0% to 13.0%. This is considered a very low flood loss reduction in comparison with the effort needed to elevate these components. However, elevating these components along with decreasing flood duration using pumping scenarios would be more effective as shown in Figure 4-10(b). Additionally, using other mitigation measures (e.g., temporary flood barriers) along with elevating the select water-sensitive components could more significantly reduce flood losses which will be explored later.

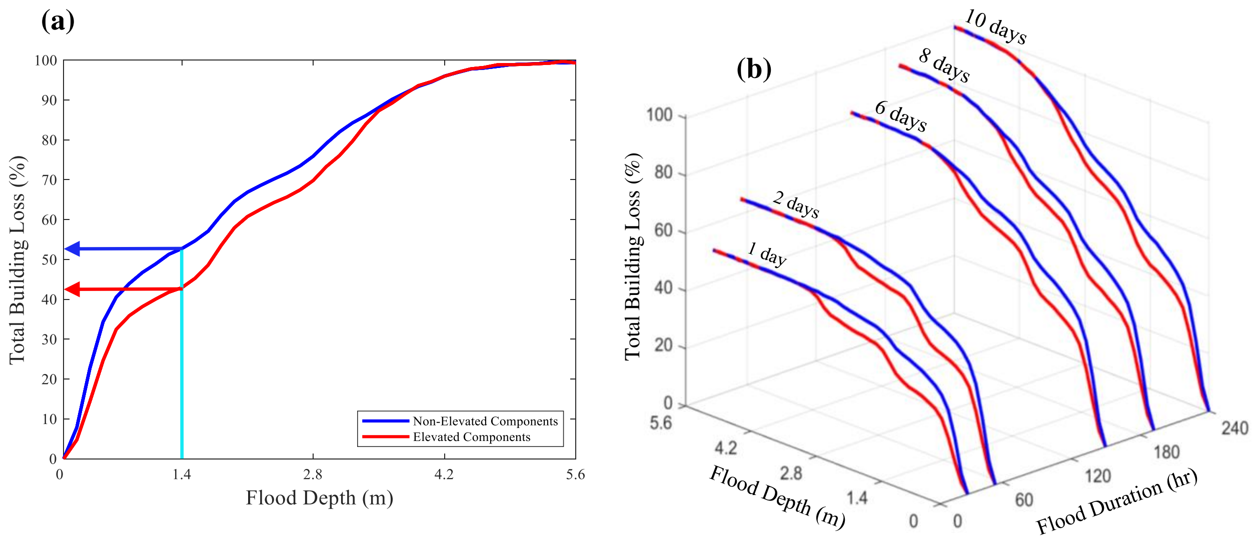

Figure 4-10. *Comparison between flood losses for building archetype F2 before and after elevating the select components: (a) State of flood losses at a number of flood duration scenarios before and after elevating the select components; (b) State of flood losses at 10 days flood duration before and after elevating the select components*

4.3 Community-Level Mitigation and Adaptation Analysis

A high-resolution mitigation analysis methodology is developed in this dissertation to investigate the impact of a number of different community-level mitigation policies on the flood loss reduction at the building- and community-level. The main components of this framework include community-level analysis, building-level analysis, and mitigation analysis as illustrated in Figure 4-11. The approach begins with a number of community-level analyses to develop a flood hazard map and model the community exposure by identifying each flooded building within the community and then determine the characteristics of these buildings (e.g., occupancy, no. of stories, foundation type, first-floor elevation, etc.) to model its corresponding flood vulnerability as illustrated before in Chapter 3. Then, a building-level analysis is conducted to account for flood hazard intensity at each building based on the building location and FFE with respect to the flood location to compute building-level vulnerability. Finally, a damage state (DS) for each building is calculated along with its associated flood losses as a percentage of the building market value. In terms of mitigation analysis and modeling flood risk reduction associated with any flood mitigation policy, a baseline flood risk analysis is conducted without implementing any mitigation and then the process is repeated when each mitigation policy is implemented. This includes all the policy-based mitigation measures that focus on hazard, exposure, and vulnerability mitigation measures.

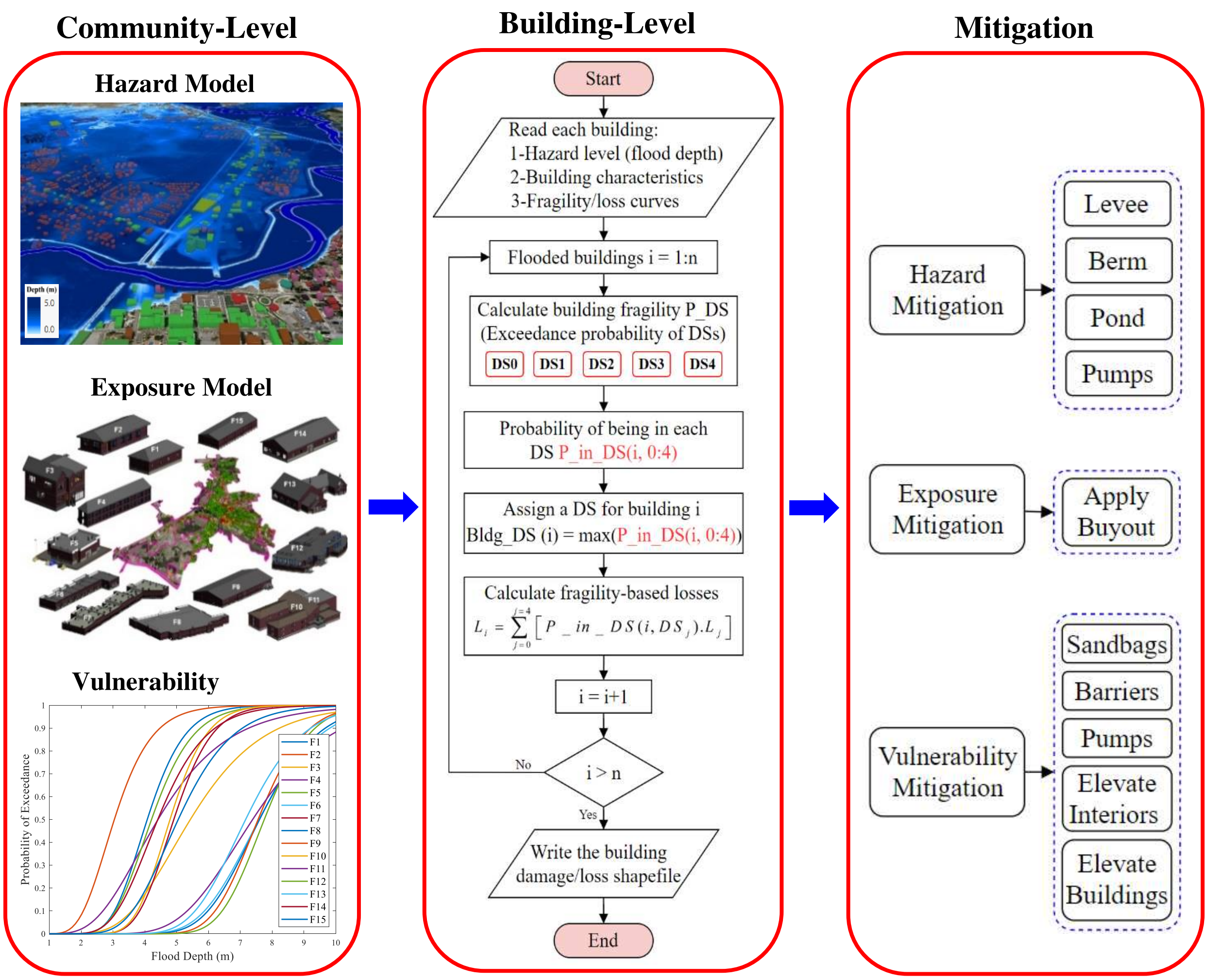

Figure 4-11. *A schematic flow chart showing the high-resolution community-level mitigation analysis framework and its different levels of analyses*

The main components needed to model flood risk at the community-level (hazard, exposure, and vulnerability) have been quantified using high-resolution models by applying the framework developed in this dissertation and published by Nofal and van de Lindt (Omar M Nofal and van de Lindt, 2020). Flood hazard is modeled using high fidelity models for hydrologic analysis using HEC-HMS (US Hydrologic Engineering Center, 2001) and hydrodynamic analysis using HEC-RAS (Brunner, 1995). The hazard analysis is conducted based on a select simulation or a prescribed return period to serve as a baseline analysis for comparison with results from the analysis conducted for the mitigation policy scenarios. High-resolution input data, namely a 1.5m resolution digital elevation map (DEM), along with a small mesh size of 15m x 15m is used to develop the flood hazard map. Then, a suite of mitigation scenarios is investigated to identify the feasibility of a number of flood, exposure, and vulnerability mitigation approaches, each representing a policy that could be implemented in the flood plain. Each mitigation scenario, or policy, includes one or a combination of several mitigation measures. Therefore, each flood hazard mitigation measure (e.g., flood gates, levees, retention pond) is first implemented by itself to investigate its impact on the depth and the extent of the flood inundation. Multiple scenarios for each mitigation policy are investigated herein including different levee and retention pond characteristics (e.g., size, location, top/bottom elevation, etc.). Several initial trials were conducted to determine the initial location and size of the retention system and levee enhancements that can provide optimal flood protection for the study area with minimum excavation/embankment work. The output of each one of the hazard mitigation scenarios is a raster hazard map with different values of flood depths across the community. These hazard maps are then overlaid with the community model (buildings as feature points) in a GIS environment to calculate the value of flood depth at each building corresponding to each mitigation scenario associated with each policy. This is done using a detailed exposure model for the community based on a combined BIM and GIS model developed in Chapter 3.

After quantifying the flood depth for each building, a two-stage vulnerability analysis is conducted; first at the building-level; then assembled into the community-level. The building-level flood vulnerability analysis is conducted using a probabilistic formulation that propagates uncertainties in the resistance of all building components for damage estimation, and the uncertainties in component replacement costs for loss estimation that has been fully described in Chapter 3. Flood fragility functions are used to probabilistically characterize building damage in terms of the exceedance probability of five prescribed damage states (DSs). Then, a community-level flood vulnerability analysis is conducted by assigning each building an archetype that has fragility curves representing the boundary between each DS. The flood intensity (hazard) model and the community exposure model are then geographically overlaid with the vulnerability model to perform a high-resolution (building-scale) mitigation analysis for the entire community. Once each building is assigned a DS based on the maximum probability of being in each DS which is based on Monte Carol simulation, fragility-based flood losses are then calculated for each building in the community and summed to account for the community-level flood losses associated with each analysis. Each analysis represents a different mitigation scenario under consideration for the community.

To illustrate the proposed methodology, some of the community-level mitigation measures discussed earlier were applied to an example community. Policy-based hazard, exposure, and vulnerability mitigation measures are only investigated in this subsection. Initially, the floodplain is analyzed first without any mitigation measures applied to develop a baseline, then different mitigation scenarios are applied, which are combinations of other scenarios, to examine their effect on losses at the community-level. A total of 28 mitigation scenarios are investigated herein which was felt to be enough to enable conclusions of the feasibility of these measures and their impact on flood losses at the community-level. These scenarios will be discussed in detail in the case studies in Chapter 6. It should be noted that each mitigation scenario requires separate vulnerability analysis due to the change in the intensity of the flood hazard. Additionally, a different exposure model is required due to the change in the flood extent corresponding to each mitigation scenario which alters the number of the impacted buildings, thus each of the 28 scenarios requires a full application of the methodology from start to finish.

Although applying hazard control measures (such as a flood gate) can significantly reduce the flood hazard intensity for a number of buildings in the flood plain, this can make other buildings more vulnerable. Therefore, either acquisition of these buildings or increasing their first-floor elevation (FFE) should be applied. In some cases, the acquisition of the buildings in the flood plain is critical such as for buildings located in a planned retention pond area or buildings that are still susceptible to more flooding even after substantial increases in their FFE. There is usually a specific amount of funds approved for the buyout (acquisition) of buildings (M1) and other funds to increase FFE (M2). Therefore, applying buyout policies or increasing building FFE's requires guidelines to prioritize buildings that are eligible for either buyout or increasing their elevation based on flood susceptibility, essentially as a function of available funds. However, a homeowner in the U.S. can refuse buyout of their property and apply other mitigation measures (e.g., increase FFE, flood barrier, pumps, etc.). In this dissertation, the buyout policy and increase in building FFE's are initially investigated without applying hazard control measures. Then, these approaches are investigated as a combination with other hazard control measures. The eligibility of a property to receive federal funds for hazard mitigation (buyout or elevation) depends on several factors including flood risk, market value, the price of the buyout or elevation increase, and most importantly the willingness of the household to relocate (FEMA, 2016a).

A methodology that prioritizes buildings for buyout and increases their elevation was developed and is shown in the flowchart in Figure 4-12. It provides a logical approach to sort flood-damaged buildings from the highest to lowest damage level and then priorities the buyout for buildings with DS4 and DS3. Buildings with DSs less than DS3 can increase their FFE if the cost is less than 50% of the building market value or apply for the buyout. This is applied for buildings until the mitigation budget is exceeded. However, the final mitigation decision is conditional on the household decision. Optimal buyout and increasing elevation solutions are investigated herein without considering the decision of the household which requires further social and cultural considerations (beyond the scope of this dissertation). The cost of increasing building FFE's is assumed to be \$215/m^2 (\$20/ft^2) for one-story buildings and \$375/m^2 (\$35/ft^2) for two-story buildings per 2020 market prices. However, these costs can vary based on a number of other parameters related to the characteristics and the location of buildings.

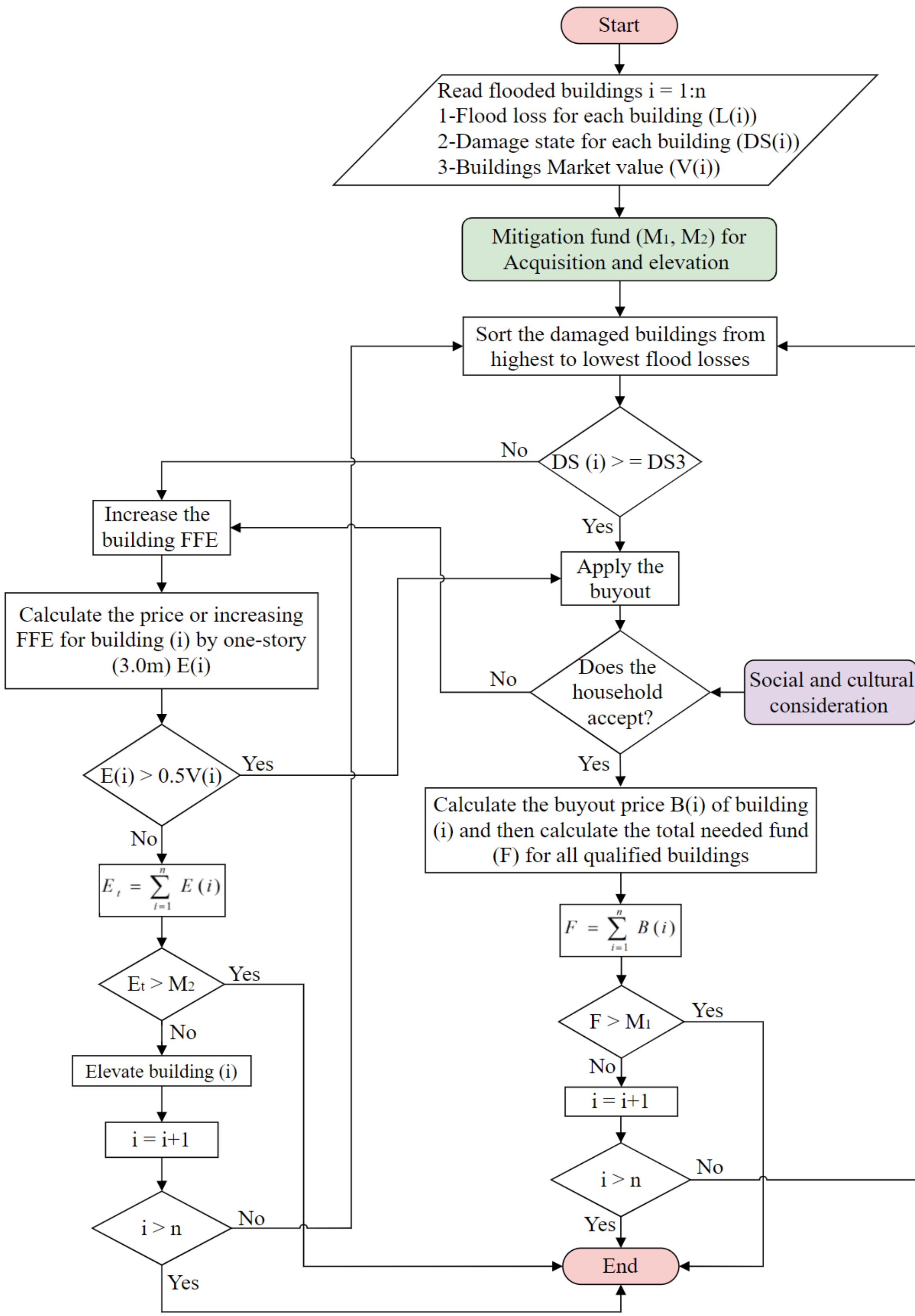

Figure 4- 12. *A flowchart showing a detailed framework to apply the buyout and increasing building elevation based on damage state to each the flooded building*

CHAPTER 5: CASE STUDIES ANALYSIS RESULTS

5.1 Introduction

There are several case studies that have been investigated as a part of this dissertation. Some of these case studies are for coastal communities and others for inland communities. The selected case studies are mostly impacted by severe events such as Hurricane Katrina 2005, Hurricane Matthew 2016, and Hurricane Florence 2018. Some of the case studies are a part of large on-going research projects and the outcomes from the research done in this dissertation will contribute to other collaborative and future research. Some of the data used in these case studies were available online and others were collected using Google Street Map View. In the next subsections, each case study will be presented along with brief illustrations of the model used in each one along with detailed discussions on the analysis results.

5.2 Example 1: Lumberton, North Carolina

Lumberton is a medium-size inland community within Robeson County, North Carolina. Lumberton was selected to be one of the case studies in this dissertation to leverage the on-going longitudinal field study in progress as part of the Center of Risk-Based Community Resilience Planning at Colorado State University. Figure 5-1 shows the spatial location of Lumberton with respect to the State of North Carolina along with a close-up view of the Lumberton city with buildings color-coded based on their archetype. The racial makeup and ethnic composition and the repeated flood events after major hurricanes made it a good location for investigating the impact of flooding after major hurricanes and documenting the recovery process. Lumberton is a culturally diverse city with a population of 21,040 according to the most recent United States census estimates. This population mainly settled on the banks of the Lumber River and most of the households are low-medium income with an average $31,899 gross annual income with 39.0% White, 36.7% African American, 12.7% Native American (the Lumbee Tribe), and 6.7% Hispanic/Latino. More details about Lumberton and its socio-economic information can found here (van de Lindt et al., 2018, 2020). In this study, buildings within and around Lumberton that share the city facilities were included in the analysis with a total number of building equal to 20,000 buildings.

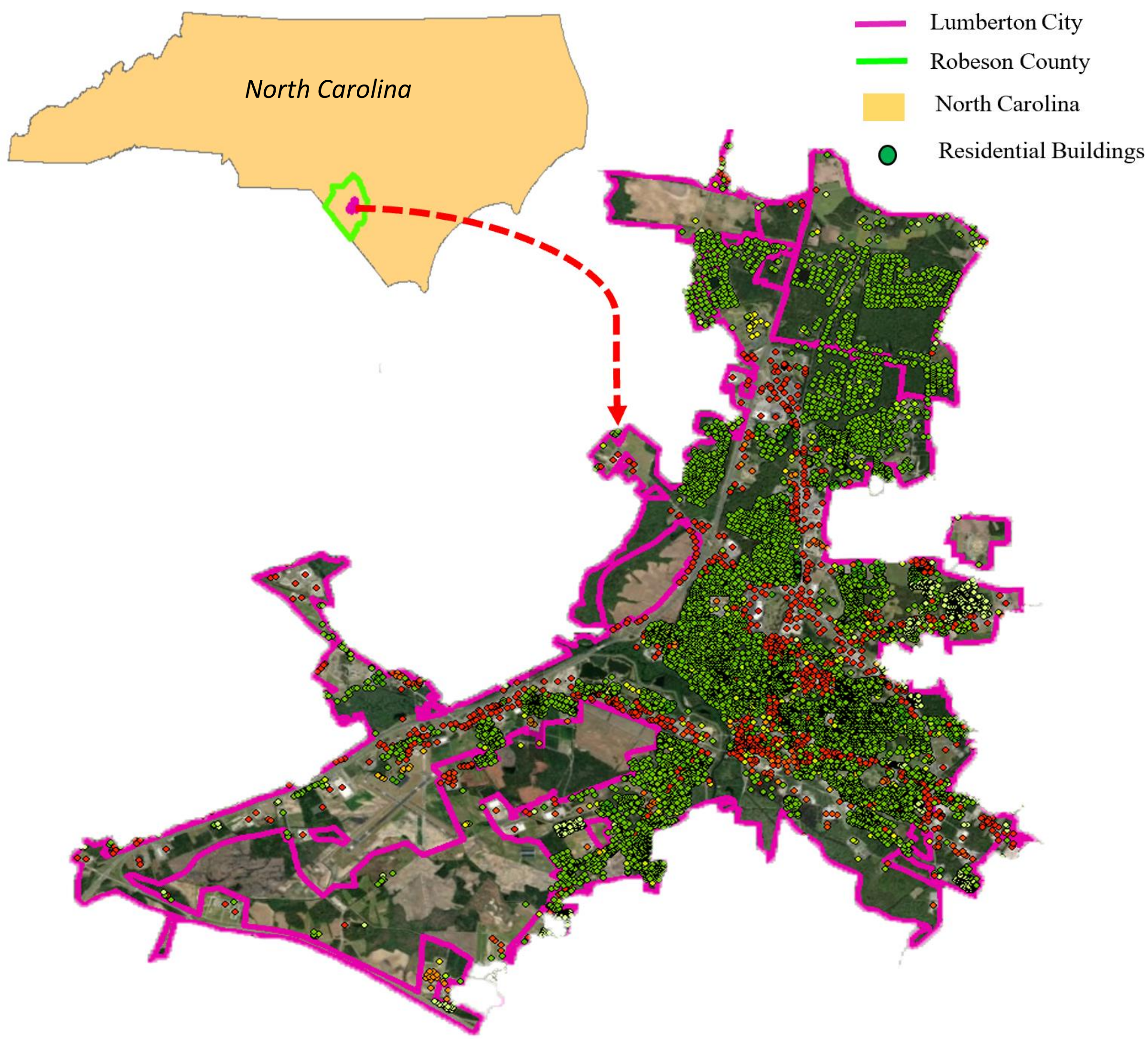

Figure 5-1. *The spatial location of Lumberton city with respect to the Robeson County and North Carolina State along with its physical boundary and building locations*

5.2.1 Hazard Scenario

Both Hurricane Matthew in 2016 and Hurricane Florence in 2018 were devastating events with catastrophic impacts on Lumberton city as well as many other cities in North Carolina. Significant effort had been exerted by federal and other emergency response agencies such as Federal Emergency Management Agency (FEMA) to predict the expected flooding from both hurricanes. However, in this case study, the flooding event after Hurricane Matthew will be used to illustrate the proposed approach. Hurricane Matthew started as a category 1 storm in the Caribbean Sea on September 29, 2016 and intensified to be a category 5 storm on September 30. Matthew weakened to a category 4 storm on October 1 and made landfall on Florida as a category 2 storm and North Carolina as a category 1 storm. Figure 5-2 shows the evolution of Hurricane Matthew in the Caribbean until it made landfall on the east coast of the U.S.

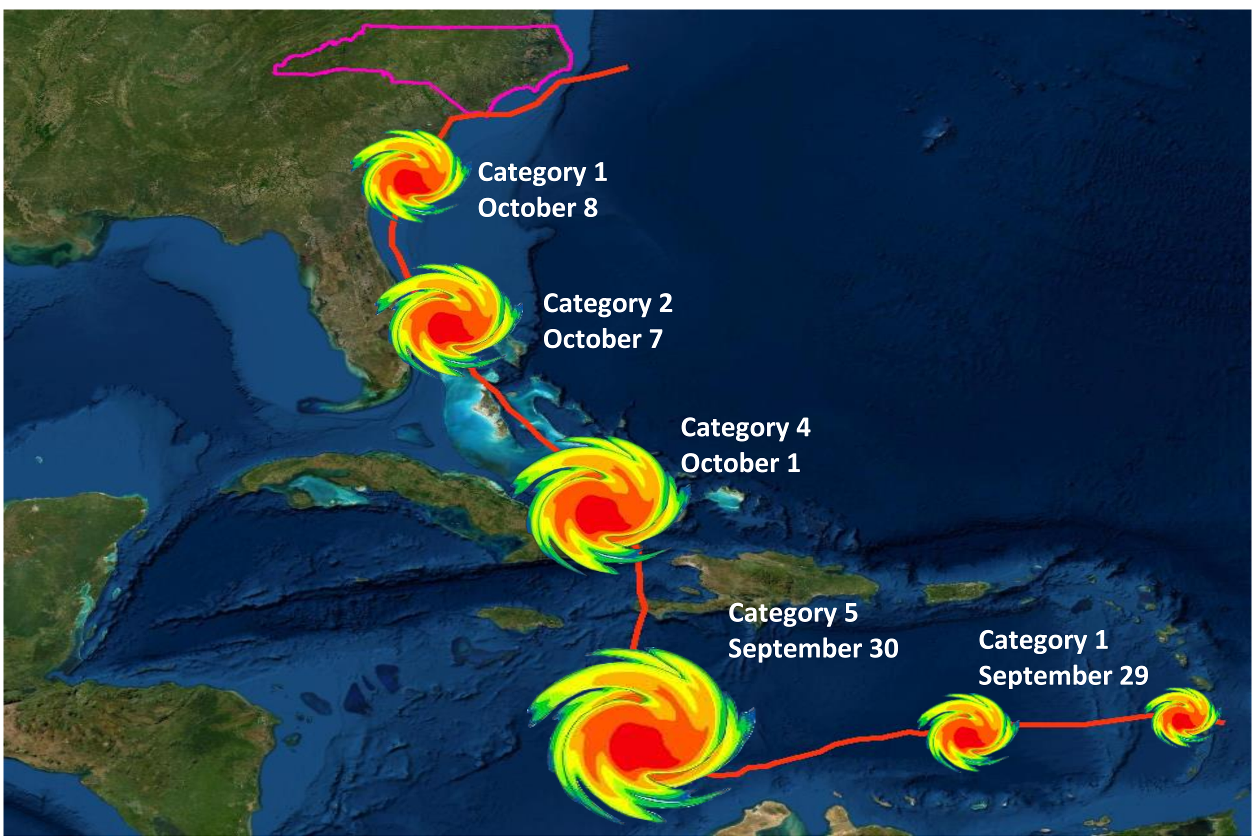

Figure 5-2. *Hurricane Matthew in 2016 path and the category evolving over the time*

Figure 5-3 (a, and b) show the modeled flood inundation depth by Nofal and van de Lindt (2019) and the predicted flood depth by (FEMA, 2019) for Hurricane Matthew. These models are based on the observed precipitation which initialized a hydrologic and hydrodynamic analysis for the Lumber River basin. According to the NOAA daily precipitation, Hurricane Matthew in 2016 derived a rainstorm that lasted for two days which started with two inches of rain and ended the next day with eight inches of rain. On the other hand, Hurricane Florence in 2018 derived three days of a rainstorm started by 6.5 inches of rain on the first day, followed by 15 inches of rain on the second day, and ended by 14 inches of rain on the last day of the storm. This explains the higher discharges from Hurricane Florence within Lumber River upstream and downstream. Figure 5-4 (a and b) shows NOAA maximum daily precipitation distribution all over North Carolina for both Hurricane Matthew and Hurricane Florence. Also, USGS is providing hourly discharge and height date for Lumber River (USGS, 2018) at two major stations (Maxton in the upstream and Lumberton in the downstream of Lumber River) as shown in Figure 5-5 and 5-6. Additionally, NOAA provides daily observed precipitation at Lumberton station (NOAA, 2018) as shown in the designated location in Figure 5-6.

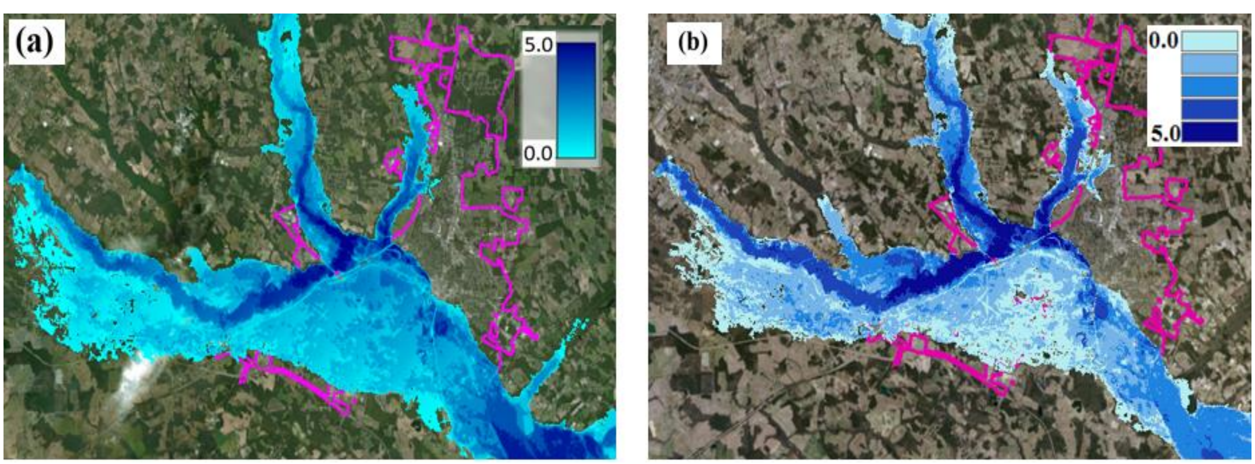

Figure 5-3. *Hurricane Matthew flood inundation depth: (a) Flood inundation depth developed by Nofal and van de Lindt (2019); (b) Flood inundation depth developed by FEMA (2019)*

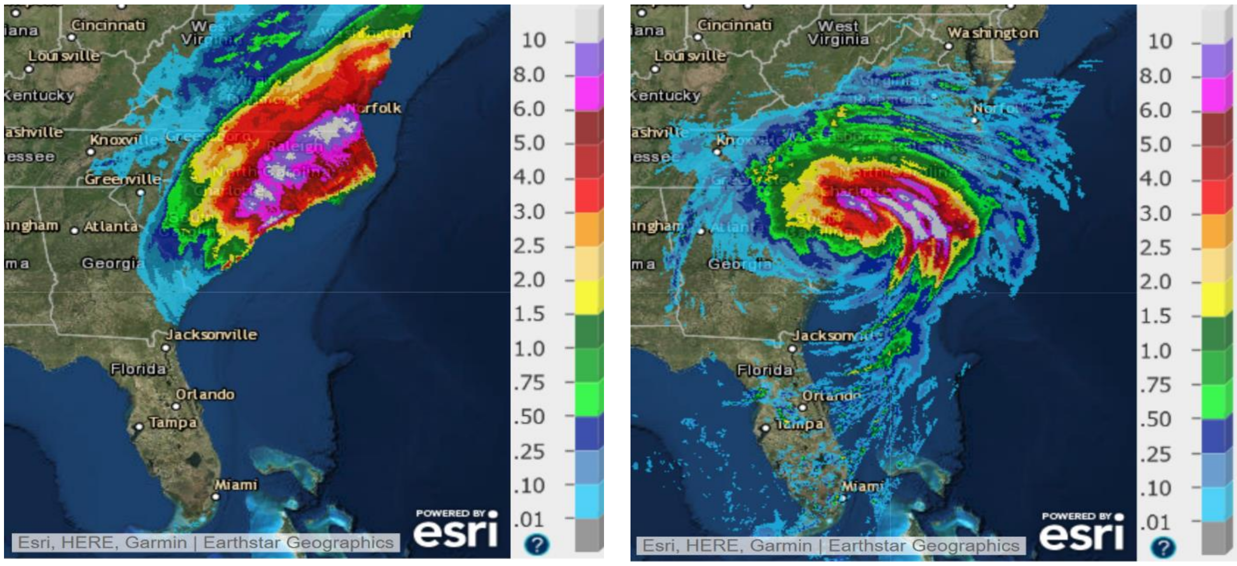

Figure 5-4. *NOAA maximum daily observed precipitation at Lumberton in inches: (a) Maximum rainfall from Hurricane Matthew; (b) Maximum rainfall from Hurricane Florence*

Figure 5-5 (a and b) is capturing the Lumber River discharge and water level from Hurricane Matthew and Florence upstream at Maxton city. It shows that Hurricane Florence at Maxton derive almost double the discharge from Hurricane Matthew with nearly 6000 cubic feet per second difference which caused the water level to get increased by 2.5 ft within the river stream. This amount of the increased discharge upstream of Lumber River at Maxton was reflected on the amount of discharge downstream at Lumberton as shown in Figure 5-6. It is not the same amount of increase due to the water losses through the 25 miles between Maxton and Lumberton including water evaporation, and the deep and surface water infiltration. From this brief hazard description, the flooding event from Hurricane Matthew in 2016 is almost similar to the one derived by Hurricane Florence in 2018 in terms of the discharge intensity and the gauge height. Although the little higher water discharge from Hurricane Florence, the flood impacts from Hurricane Florence was lower than the impacts from Hurricane Matthew on the buildings and infrastructure within Lumberton city. This could be explained by the small peak in the discharge from Hurricane Matthew just a couple of days before the high peak making the soil saturated with less deep infiltration and more surface runoff at the time of the high peak. Additionally, the immediate response of the city of Lumberton by building temporary berms and using pumping tamed the severity of the event with less water swelling from the riversides.

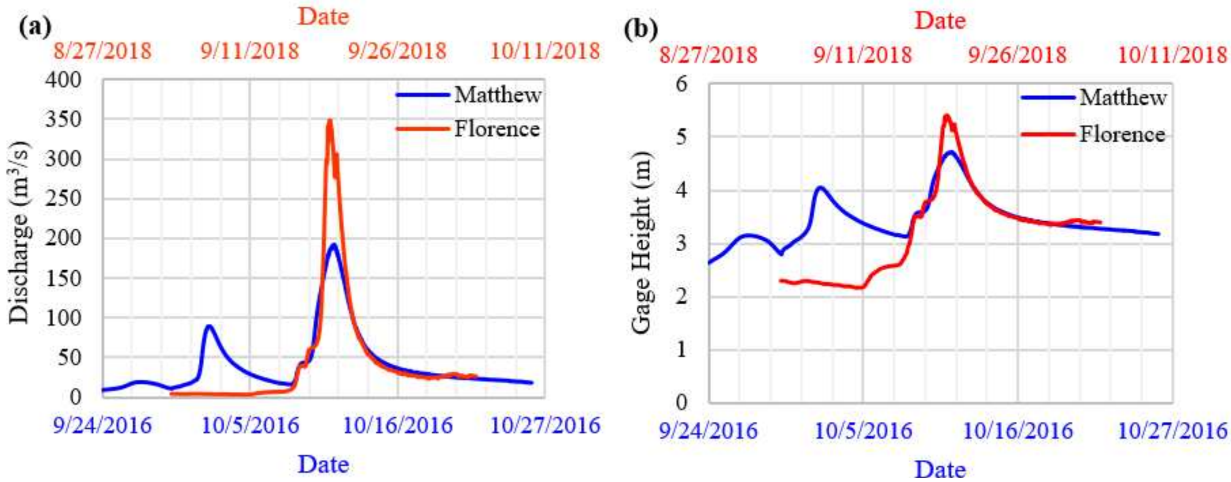

Figure 5-5. *Observed gage data at Lumber River near Maxton, NC due to Hurricane Matthew and Hurricane Florence: (a) Observed discharge; (b) Observed height*

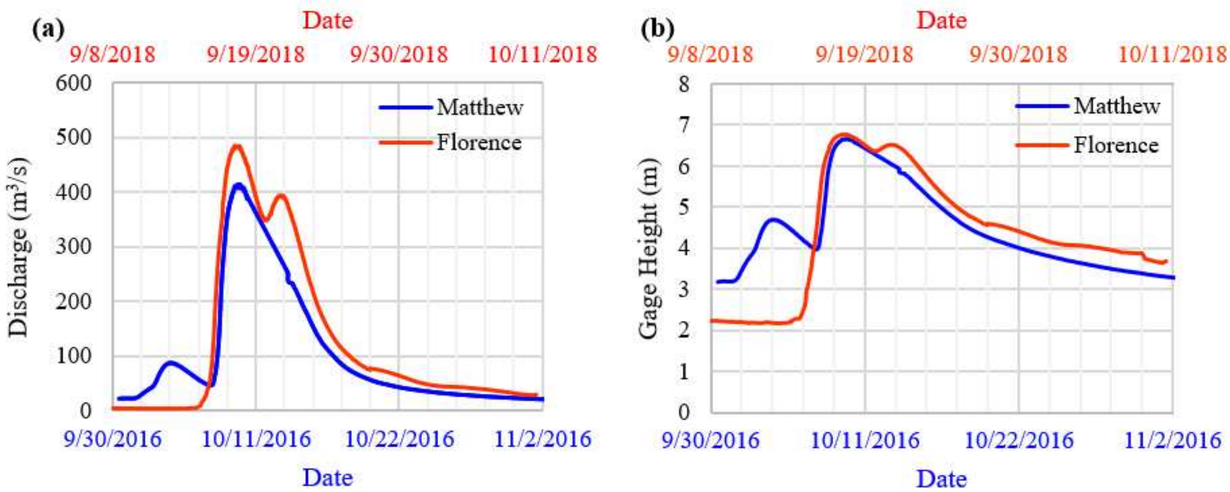

Figure 5-6. *Observed gage data at Lumber River near Lumberton, NC due to Hurricane Matthew and Hurricane Florence: (a) Observed discharge; (b) Observed height*

5.2.2 Hydrologic and Hydrodynamic Analysis

A scenario-based flood hazard map will be used herein to illustrate the high-resolution flood risk method developed in this dissertation in Chapter 3. The flooding event after Hurricane Matthew in 2016 was used a hazard scenario in this study. As discussed in the methodology, a hydrodynamic analysis is required to account for the spatial distribution of the flood inundation across the community. However, in order to perform a detailed hydrodynamic analysis of Lumberton, streamflow data that feeds the flooded area is needed. For Lumberton, there were only two available stream hydrographs located on the Lumber River, one upstream near the city of Maxton and the other in the lower stream in Lumberton. Figure 5-7 shows the location of the two available USGS stream gauges along with the location of one NOAA rainfall gauge near Lumberton. The observed water discharge and height for the two available stream gages are plotted in the same chart in Figure 5-8, however, this data is still not enough to develop a hydrodynamic model for the study area. There are other ungauged streams that deliver water to the study area and their flood contribution cannot be neglected as shown in Figure 5-7. Therefore, a detailed hydrologic study of the Lumberton area was conducted in order to predict water discharge in the ungagged streams in the study area with the goal of having a more accurate flood inundation map that represents the actual flooding from Hurricane Matthew.

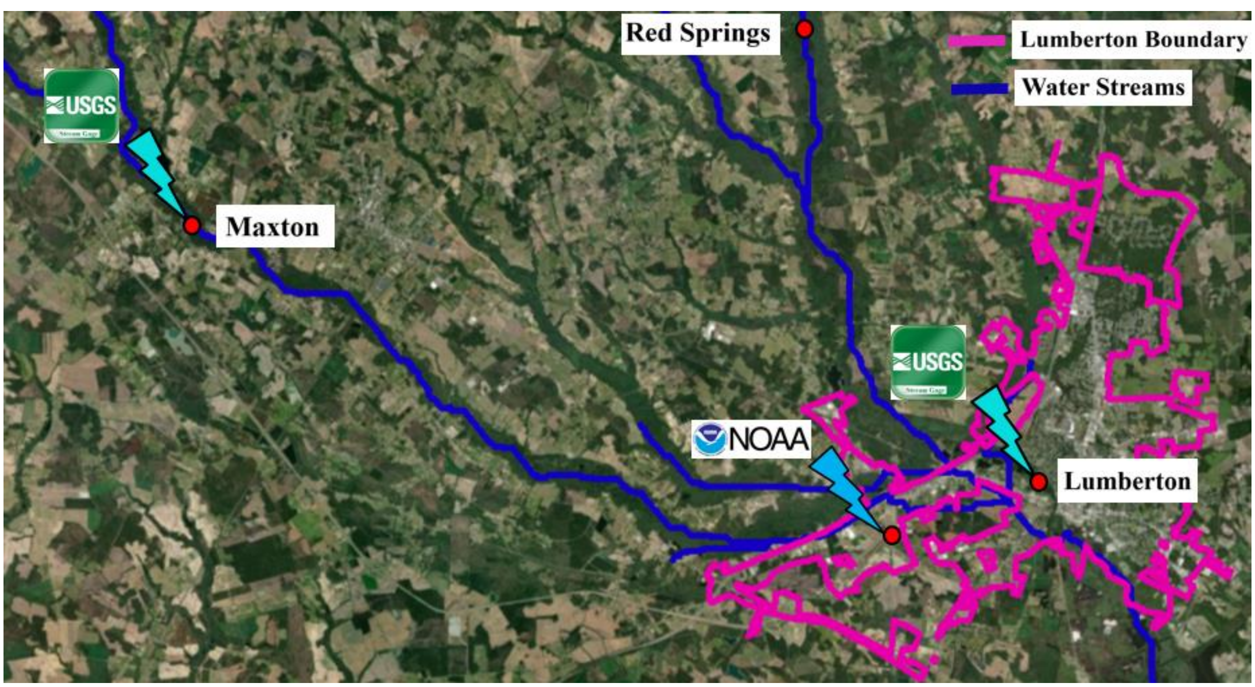

Figure 5-7. *The location of the main streams, USGS stream gauges, and NOAA rainfall gages with respect to physical boundaries of Lumberton, NC*

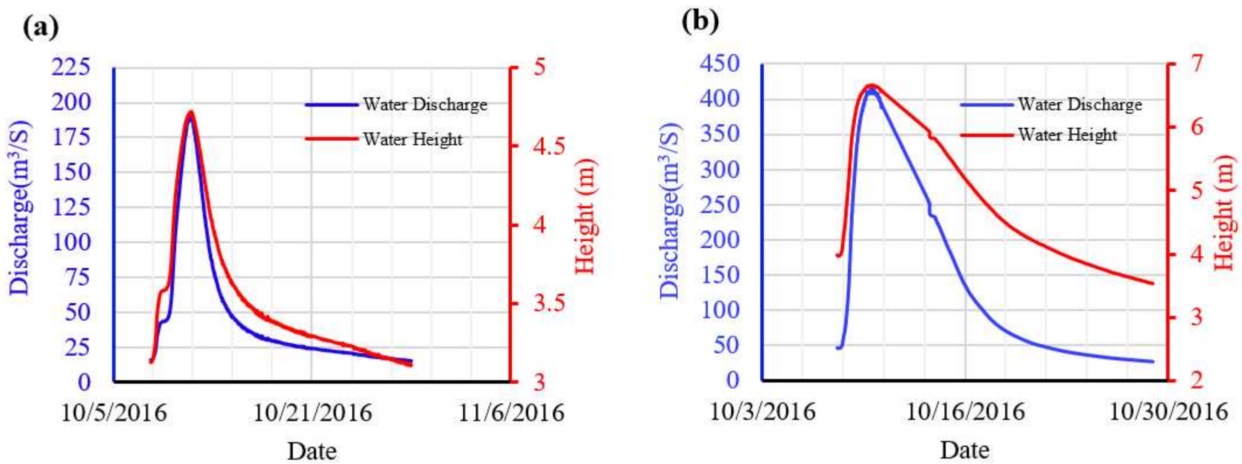

Figure 5-8. *The observed discharge and water height at the USGS stream gauges: (a) Observed discharge and river height at Lumber River near Maxton; (b) Observed discharge and river height at Lumber River near Lumberton*

A hydrologic analysis was conducted on the area around the Lumber River basin with the goal of predicting discharge in the ungauged streams within the Lumberton area. The geomorphological data in terms of DEM, land use, and soil data were used to determine the Soil Conservation Service (SCS) Curve Number (CN) in the form of a raster map to be used in the surface runoff calculation. Then, HEC-HMS (US Hydrologic Engineering Center, 2001) was used to perform hydrologic analysis using SCS Type 2 storm with the observed 200 mm (8 inches) storm rainfall on October 9th, 2016 (NOAA, 2018). Finally, the model parameters (CN and lag time) were properly adjusted to validate the calculated hydrograph with the observed one. The main results of the hydrologic analysis were hydrographs in the gaged streams to verify the model parameters and hydrographs in the ungauged streams to initiate a hydrodynamic analysis for the study area. Figure 5-9 presents the observed and calculated hydrographs on the same plot for the two gaged streams on the Lumber River and the other ungauged stream at the city of Red Springs, with the catchments locations in and around Lumberton. These hydrographs provide the input for the hydrodynamic analysis flood inundation map which allows the flood depth at each building to be determined. The hydrodynamic analysis process was conducted using HEC-RAS (Brunner, 2010) which provided the inundation depth in terms of a raster map as shown in Figure 5-10(a). The resulting flood inundation depth was compared with the FEMA flood insurance rate map (FIRM) which showed an excellent match between them as shown in Figure 5-10. The evolution of flooding from the hydrodynamic analysis at different times is shown in Figure 5-11. Water velocity was low enough to neglect its effect on the building damage and is not shown herein for brevity. A water surface elevation map (WSE) can also be generated and is again not shown for brevity since flood elevation above FFE is calculated and used to predict damage from the general fragility curves.

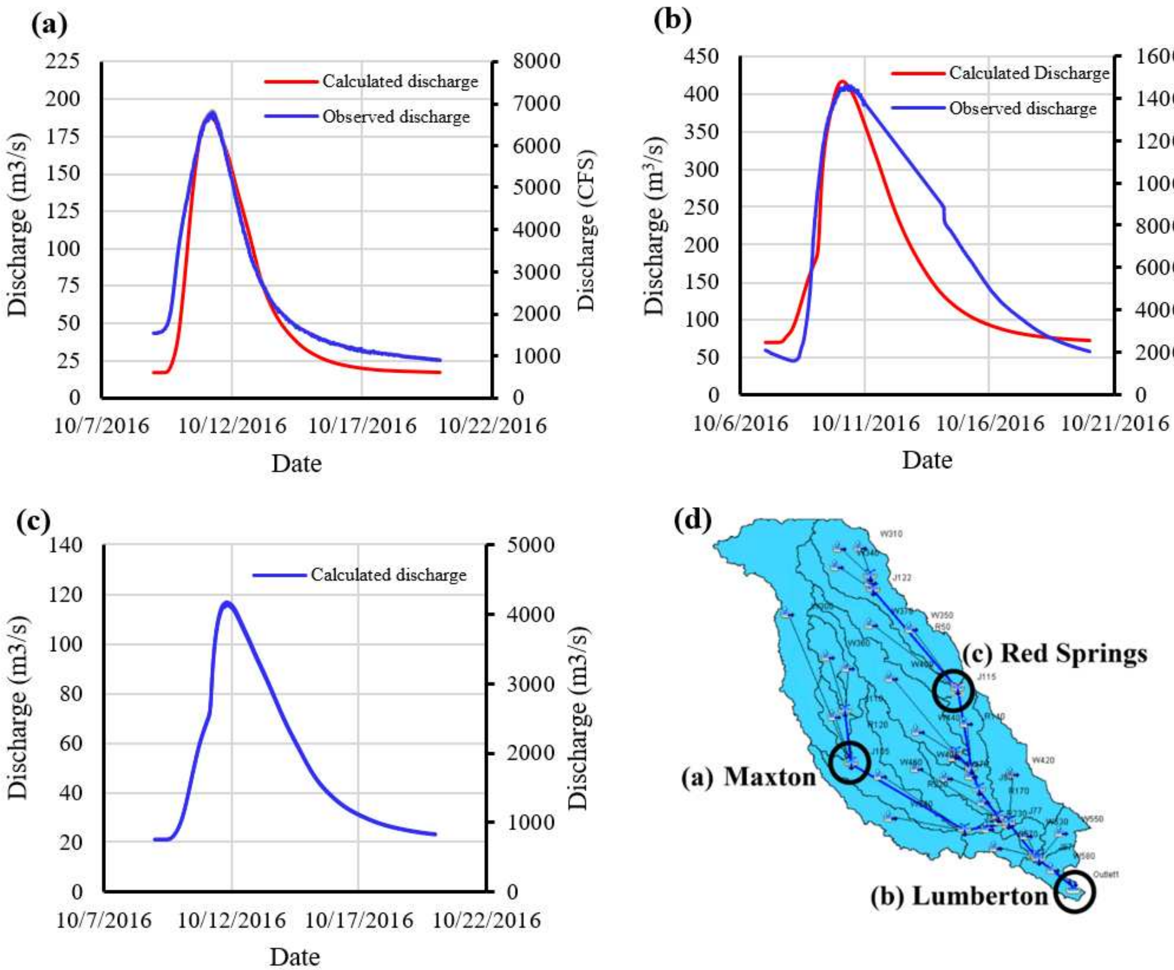

Figure 5-9. *Hydrologic study results at the major streams within the Lumberton area: (a) Observed vs calculated discharge for Lumber River near Maxton; (b) Observed vs calculated discharge for Lumber River near Lumberton; (c) Calculated discharge in the Red Springs stream; (d) Catchments location in and around Lumberton*

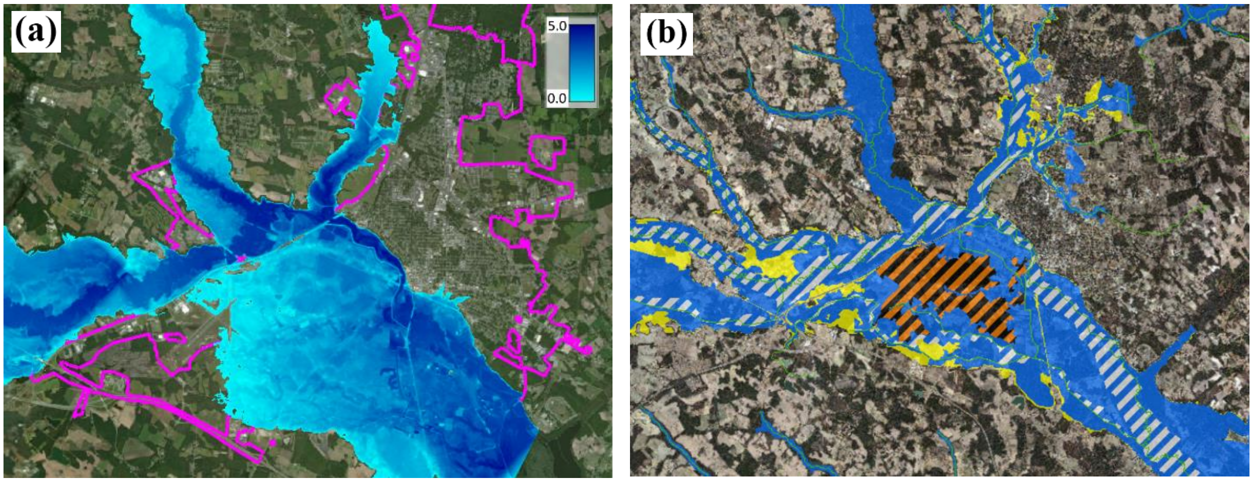

Figure 5-11. *Flood inundation depth (m) from Hurricane Matthew vs. FEMA flood insurance rate map (FIRM): (a) Flood inundation depth (m) from Hurricane Matthew; (b) FEMA flood rate map*

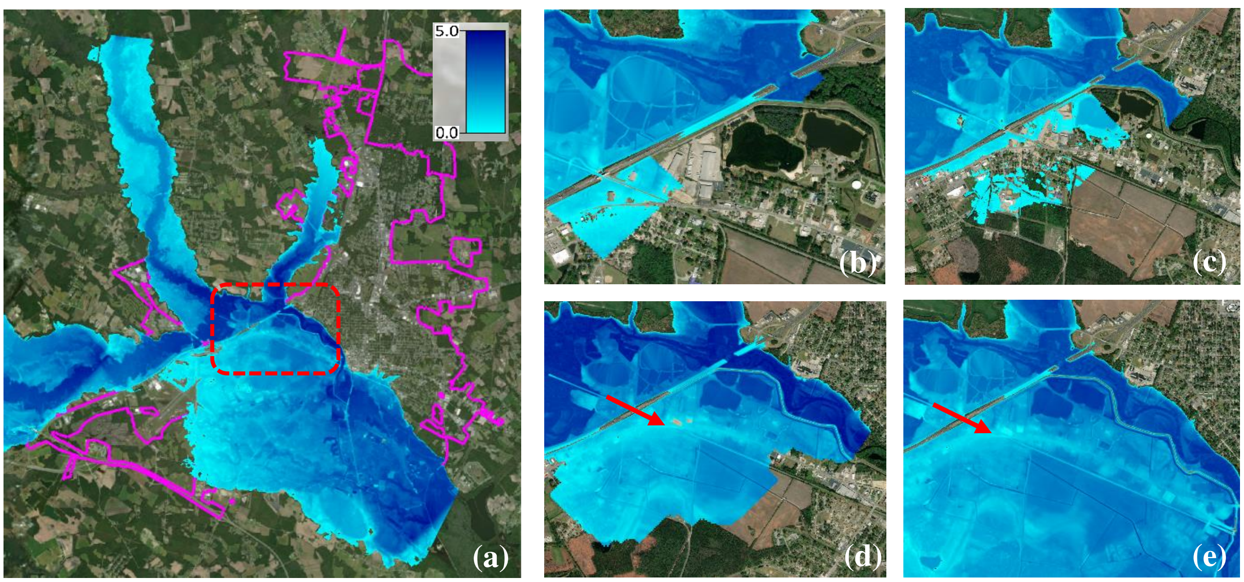

Figure 5-10. *Evolution of flooding after Hurricane Matthew in 2016 in Lumberton, NC: (a) Flood hazard map showing the state of flooding for all community; (b) Flood water flowing from the underpass; (c) The state of flooding at underpass and levee; (d) Flood water before approaching the residential area; (e) Maximum Flooding*

5.2.3 Exposure and Vulnerability Modeling

Most of the building inventory data needed for Lumberton, NC was extracted from the online spatial data platform of the State of North Carolina (State of NC, 2018). This includes buildings location, area, the value in US dollars, flood zone, occupancy (HAZUS-Based), year built, and each buildings first-floor elevation (FFE). However, this data is not enough to start the flood risk assessment process and more details about the buildings' characteristics and occupancy are needed to capture damage at a community level. Therefore, more than 20,000 buildings in and around Lumberton were navigated using Google Street Map View to collect the needed information about the buildings. This information includes building archetype, occupancy, number of stories, foundation type (slab on grade, and crawlspace), and qualitative assessment of the building maintenance (fair, good, well maintained). Afterwards, the developed 15 building archetypes portfolio in Chapter 2 was assigned to the building stock within the community based on each building occupancy along with the other collected physical information. Then, the fragility function associated with each building archetype was automatically assigned to each building to account for their flood vulnerability. Figure 5-12 shows a color-coded map for the flooded buildings only along with the number corresponding to each building archetype in the suite of 15 building archetypes.

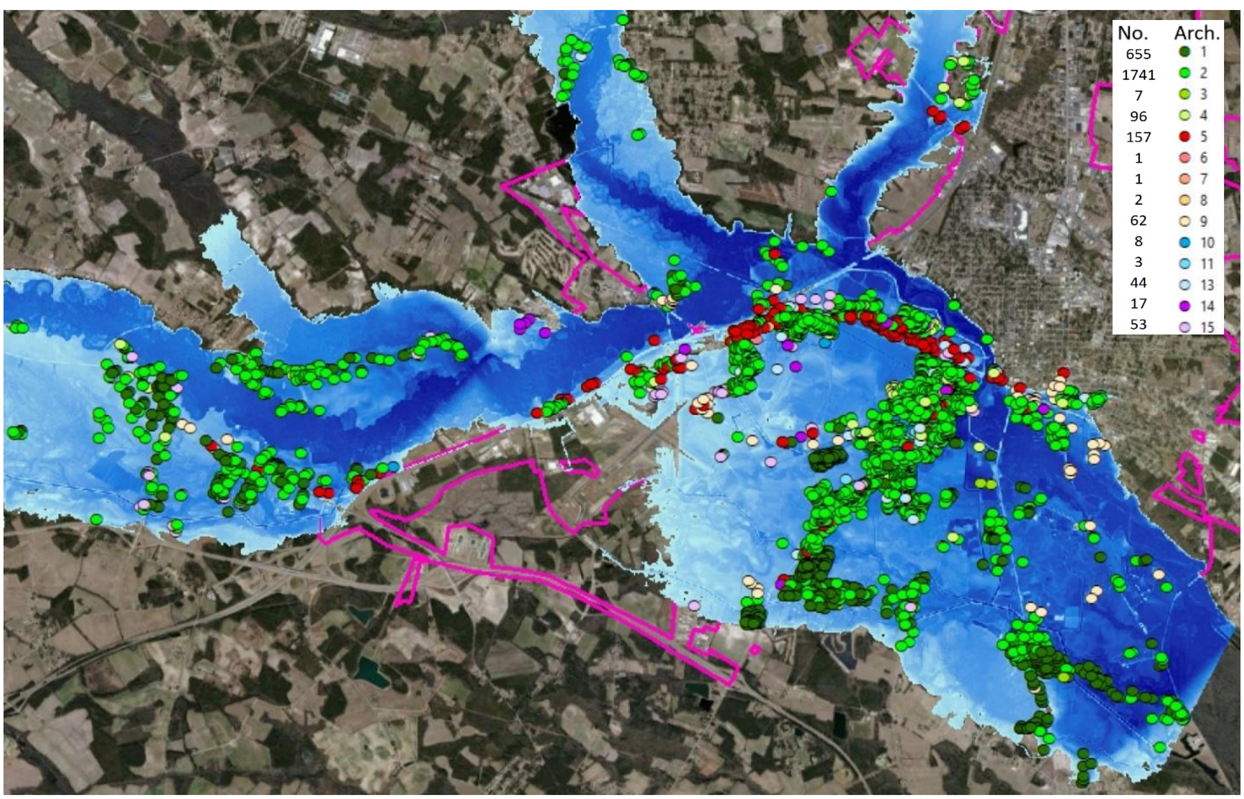

Figure 5-12. *The spatial location of the exposed buildings color-coded based on their archetype*

5.2.4 Flood Risk Analysis

The analysis results from the hydrodynamic analysis were overlaid with the community model of Lumberton to identify the exposed buildings. For buildings with slab-on-grade foundations, flood depth was calculated from FFE by subtracting FFE from water surface elevation (WSE). For buildings with crawlspace foundations, flood depth was calculated from ground elevation by subtracting the ground elevation from the WSE. The flood damage for all flooded buildings in the flood plain (some buildings in the floodplain were not flooded because of their higher elevation) was then calculated based on building archetype and flood depth only (flood duration was not included at this stage). Fragility functions were used to calculate the exceedance probability of each DS. Table 5-1 shows the number of the impacted buildings in five ranges of exceedance probability for each DS (P_DS). The summation of each column in this table should be equal to the total number of damaged buildings (2857). This table provides insight into how the fragilities can provide probabilistic damage prediction at the community level. For example, in the last row which includes the probability range of 80% < P_DS < 100%, there are 2209 buildings expected to exceed DS1, and 1741 buildings to exceed DS2 with a probability of more than 80%. It should be noted that the high number of buildings in DS0 with exceedance probability ranging from 0% to 20% is because DS0 only exists for buildings with a crawlspace foundation which are two archetypes (F1, and F3) out of the 15 building archetypes. However, this method will not enable comparisons between different mitigation measures at the community-level. Therefore, the probability of each building being in each DS was calculated using the framework illustrated previously in the flow chart presented in Figure 3-4 in Chapter 3. Each building was then assigned a DS based on the maximum probability of the five calculated probabilities of being in each DS as shown in Figure 5-13(a). Finally, total building flood losses as a percentage of the building market value were calculated based on the probability of being in each DS derived from the fragility function using Eq. (5-1). This was done by multiplying the probability of being in each DS by the replacement cost of each DS based on the concept developed in Chapter 3 of this dissertation. Figure 5-13(b) shows a color-coded map based on the calculated flood losses for all the impacted buildings within Lumberton.

$$L_f(IM = x) = \sum_{i=0}^{4} \left[P\left(DS_i \middle| IM = x\right) - P\left(DS_{i+1} \middle| IM = x\right) \right] \times Lr_{ci} \times V_t \qquad (5\text{-}1)$$

where $L_f(IM=x)$ = total building fragility-based losses in monetary terms at $IM=x$ (replacement or repair cost), $P(DS_i \mid IM=x)$ = exceedance probability of DS_i at $IM=x$, $P(DS_{i+1})$ = exceedance probability of DS_{i+1} at $IM=x$, Lr_{ci} = cumulative replacement cost ratio corresponding to DSi, and V_t = total building cost (replacement cost).

Table 5-1. *Damage states exceedance probability for the flooded buildings*

Exceedance Probability of a DS (Fragility)	Number of buildings (total=2857)				
	DS0	DS1	DS2	DS3	DS4
0% < P_DS < 20%	2201	396	567	2071	2822
20% < P_DS < 40%	5	72	115	355	25
40% < P_DS < 60%	7	72	144	293	7
60% < P_DS < 80%	30	108	290	121	3
80% < P_DS < 100%	614	2209	1741	17	0

The final analysis showed that there were 2857 buildings in the flood plain with 2400 buildings in an area where flood depth was above FFE, ranging from 0.0m up to 2.5m. Figure 5-13 shows a color-coded map for the exposed buildings based on their DSs and loss ratio. The total market value of the buildings in the floodplain was $554 million USD. The damage analysis, based on the calculated probability of being in each DS, showed that 18% (out of 2857 buildings) of the buildings are characterized as DS0, 5% of the flooded buildings are characterized as a DS1, 67% of the buildings are characterized as DS2, 9% of the buildings are characterized as DS3 with few buildings that are characterized as DS4. Virtually, all of the flooded buildings had flood losses ranging from 16% to 70% of their market value. The mean total building losses calculated for all flooded buildings in the floodplain using the fragility-based flood loss approach was $133 million which is 24% of the whole building stock market value for those located in the floodplain. These losses are calculated based on flood depth only without considering the impact of flood duration such that components will fail as soon as they get touched with water. It should be mentioned that the HAZUS-based flood losses calculated for residential buildings only were $93 million and using fragility functions based on empirical data from field studies were $116 million which was discussed in (Omar M Nofal and van de Lindt, 2020). These differences in the calculated losses are due to the resolution of the models including hazard, exposure, and vulnerability. Additionally, the flood losses calculated herein include all building archetypes in the flood plain and not only residential buildings. Finally, these results will serve as a base result to be compared with results from the mitigation analysis scenarios below.

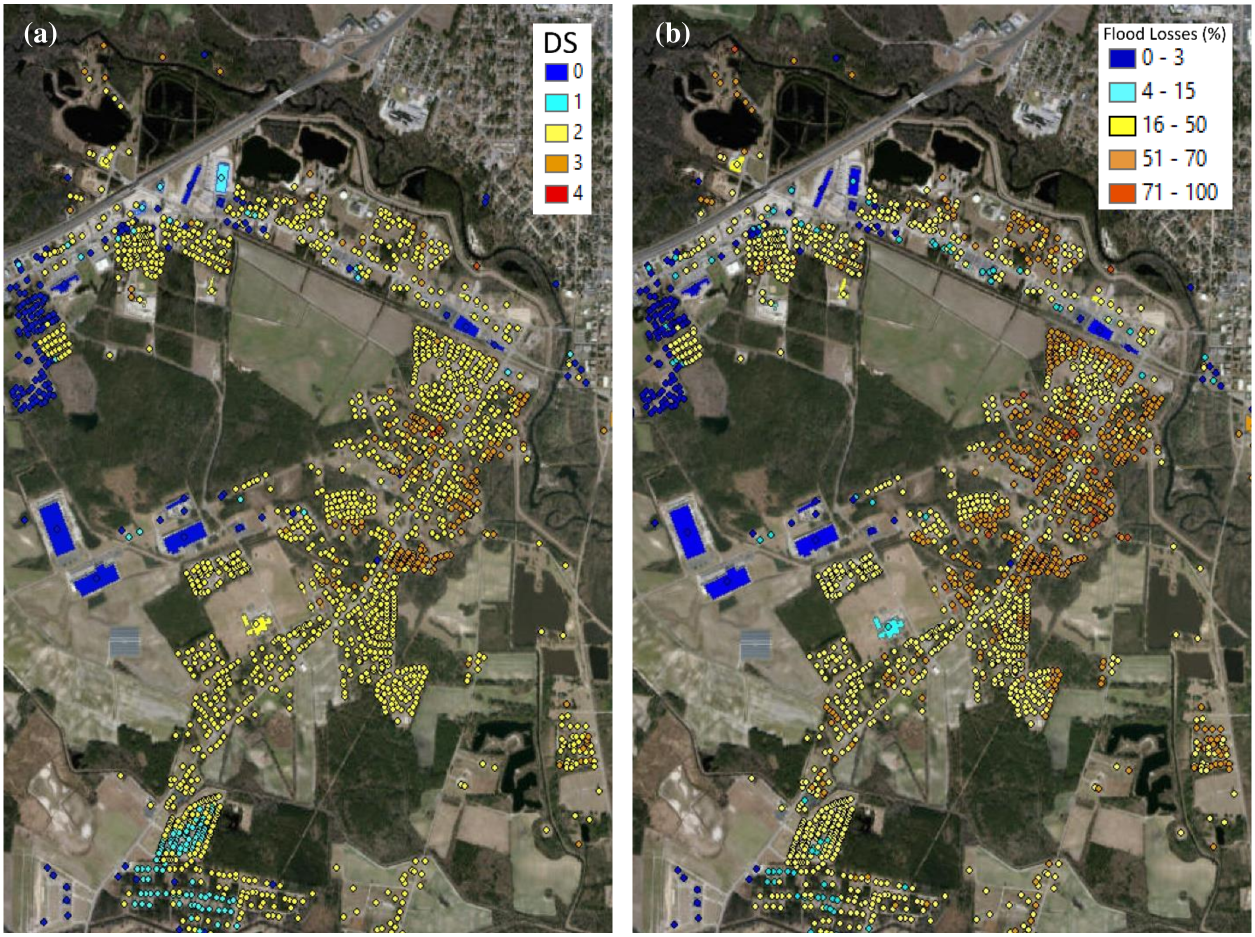

Figure 5-13. *Damage and losses to the exposed buildings: (a) Color-coded buildings based on fragility-based DS; (b) Color-coded buildings based on buildings loss percentage*

5.2.5 Flood Mitigation Analysis Using Building-Level Mitigation Measures

The building-level flood mitigation measures described earlier in Section 4.2 (e.g. flood barriers, pumps, elevating water-sensitive components) were applied on a selected percentage (e.g. 10%, 20%, 30%, … 100%) of flooded buildings. These mitigation techniques were solely investigated along with their combinations. The building percentages reflect the number of buildings that could apply flood mitigation. Some of these percentages are realistic (e.g., 30%) and others are theoretical for analysis purposes (e.g., 100%). Each building percentage was selected randomly for the total number of exposed buildings (2857 buildings) within the Lumberton community. An algorithm that calculates the monetary flood losses for each building associated with each mitigation scenario was then developed using the updated flood damage/loss curves for the portfolio of 15 building archetypes. Finally, the total community-level flood losses were calculated by summing the flood losses for all buildings.

Five mitigation scenarios for each mitigation technique and their combinations (six techniques) were investigated in terms of their overall community-level flood loss reduction. These mitigation measures were applied to a designated percent of buildings randomly scattered to represent certain households applying these mitigation measures. Different possibilities were considered to investigate the different protections that buildings can adapt to decrease their flood vulnerability. Therefore, 330 flood mitigation scenarios were investigated which account for the flood losses of 11 groups of buildings (randomly selected 10%, 20%, …. , 100% of the total building stock in the flood plain) after using five flood mitigation scenarios for six flood mitigation technique as shown in Figure 5-14. For example, five different flood barrier heights were investigated (0.2m, 0.4m, 0.6m, 0.8m, and 1.0m). These barriers could be used locally at each building or could be around a neighborhood to protect a group of buildings. Each flood barrier height was assigned to each percent of buildings across the community. This was repeated for all the combinations of barrier height and the percent of randomly selected buildings resulting in 55 different analyses. Additionally, a number of flood duration scenarios were investigated for all flooded buildings (10 days, 8 days, 6 days, 2 days, and 1 day). Another five mitigation scenarios that include elevating the select water-sensitive components listed in Table 4-1 in the residential buildings only along with the five duration scenarios from the previous analysis were also investigated.

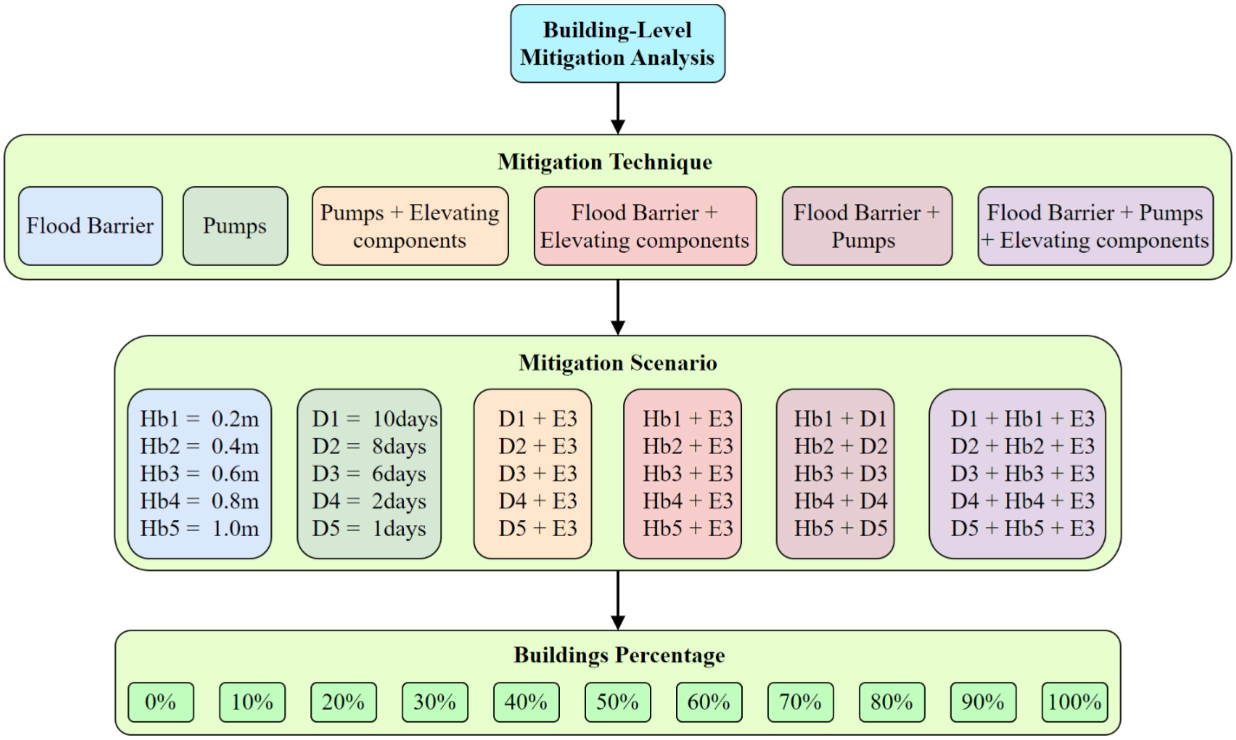

Figure 5-14. *A flow diagram showing the hierarchy of the 330 building-level mitigation scenarios including six mitigation techniques and five mitigation scenarios for each technique which are applied to 11 buildings groups based on randomly selected buildings percentages (E3 is the mitigation scenario that includes elevating select water-sensitive components listed in Table 4-1 for residential buildings only*

Other combinations of the three investigated mitigation techniques along with their associated scenarios were investigated to emphasize the role of building-level mitigation measures in reducing flood losses at the community-level. Therefore, flood mitigation scenarios that use flood barriers along with elevating components only, using pumps only, and elevating components and using pumps at the same time were investigated as shown in Figure 5-14. It should be mentioned that combining two mitigation scenarios is not the direct summation of the flood loss reduction from every single scenario. Rather, coupling two different mitigation techniques requires a new definition of the loss functions for each building archetype. This would require changing the input data (e.g., elevated building components vs non-elevated building components) or enforcing flood losses to be zero if flood depth is less than the barrier height or using a different flood loss function associated with a certain flood duration (e.g., using pumps). For example, the input data for the mitigation scenario that uses a 0.6m flood barrier along with elevating the select water-sensitive components is completely different from the mitigation scenario that uses a 0.6m flood barrier without elevating the select components. This leads to different loss curves at the same flood duration which explains the variation in the calculated flood losses. Similarly, combining mitigation scenarios using different flood barrier heights and flood durations has a similar effect.

Table 5-2 lists the number of buildings within the five ranges of exceedance probability for each DS for two select mitigation scenarios that have been applied for 100% of the damaged buildings (using a flood barrier with Hb=1.0m or using pumps to reduce the flood duration to 1 day). It shows that the number of buildings in the exceedance probability range 80% < P_DS < 100% are decreased for all DSs for both scenarios with an increase in the number of buildings within the other lower damage ranges in comparison with the baseline building damage analysis in Table 5-1. It also shows that applying a flood barrier with Hb=1.0m for all the buildings highly impacts the number of buildings within each range of the exceedance probability for DS0, DS1, and DS2 without any impacts on the number of buildings in DS3 and DS4. Additionally, using a flood barrier resulted in almost all of the buildings being in either the first range (0% < P_DS < 20%) or the last range (80% < P_DS < 100%). This can be explained such that applying a flood barrier for buildings with flood depths less than the barrier height results in the exceedance probability for all DSs being essentially zero. Table 5-2 also shows that using pumps to decrease flood duration to one day significantly impacted the number of buildings in DS3 and DS4. It also impacts the distribution of the buildings in the five exceedance probability ranges by increasing the number of buildings in the lower probability ranges with respect to baseline damage analysis in Table3. This could be explained by the previously illustrated relationship between flood duration and damage in Chapter 4 and how it impacts the exceedance probability for each DS, specifically for DS3 and DS4 as shown in Figure 4-7.

Table 5-2. *Damage states exceedance probability for the flooded buildings corresponding to two select mitigation scenarios*

Mitigation Scenario	Exceedance Probability of a DS (Fragility)	Number of buildings (total=2857)				
		DS0	DS1	DS2	DS3	DS4
Using a flood barrier H_b =1.0m	0% < P_DS < 20%	2344	1286	1323	2071	2822
	20% < P_DS < 40%	0	0	66	355	25
	40% < P_DS < 60%	0	0	77	293	7
	60% < P_DS < 80%	0	77	89	121	3
	80% < P_DS < 100%	513	1494	1302	17	0
Using pumps Dur =1 day	0% < P_DS < 20%	2201	329	362	1558	2857
	20% < P_DS < 40%	5	93	354	1253	0
	40% < P_DS < 60%	11	378	1201	46	0
	60% < P_DS < 80%	57	2001	938	0	0
	80% < P_DS < 100%	583	56	2	0	0

To compare the results from the 330 mitigation scenarios, the mean total building loss for each building within each mitigation scenario was calculated based on the probability of being in each DS using Eq. (6-1). Then, the flood losses for each building within each mitigation scenario were summed up to give one number that represents the mean total flood losses corresponding to each specific mitigation scenario. The analysis results for all the investigated flood mitigation scenarios are summarized in Figure 5-15 to provide better insight into the efficiency of each flood mitigation technique along with its associated mitigation scenarios. The analysis results revealed that using flood barriers of any height for any of the buildings groups can significantly decrease community-level flood losses as shown in Figure 5-15(a). Additionally, the results showed that using pumps to decrease flood duration will only be efficient if the flood duration is reduced to be in a range of one to two days as shown in Figure 5-15(b). Otherwise, relying on pumps to decrease the amount of flood losses will not be a reasonable approach. Elevating water-sensitive components can slightly reduce the amount of flood losses and works effectively if the flood duration is reduced to one or two days as shown in Figure 5-15(c), or if applied in combination with flood barriers as shown in Figure 5-15(d). Using a temporary flood barrier system shows better efficiency than decreasing flood duration in terms of decreasing flood losses. However, using both flood barriers and decreasing flood duration could significantly decrease the amount of flood losses as shown in Figure 5-15(e). Finally, using the three flood mitigation techniques at the same time, of course, showed the best performance as shown in Figure 5-15(f). The flood losses were reduced from $133 million to $50 million for the mitigation scenario that included flood barrier height of 1m at one-day flood duration along with elevating the select water-sensitive components which represents %62 of a flood loss reduction.

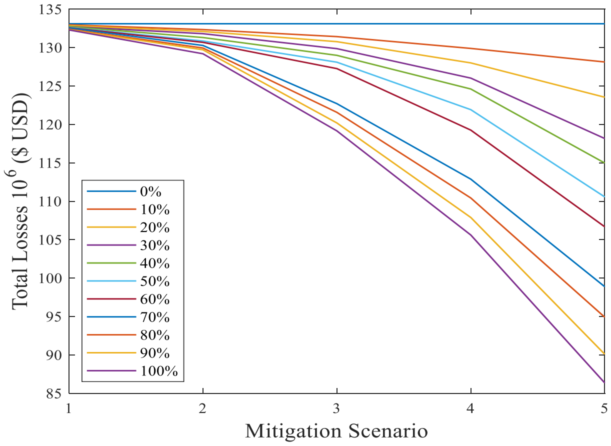

(a) Flood barriers

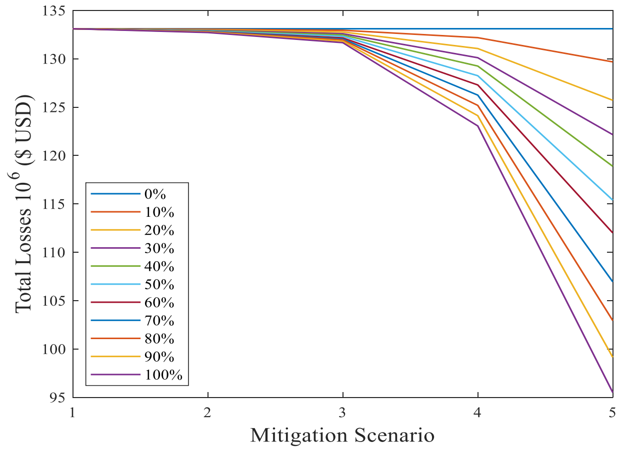

(b) Pumps

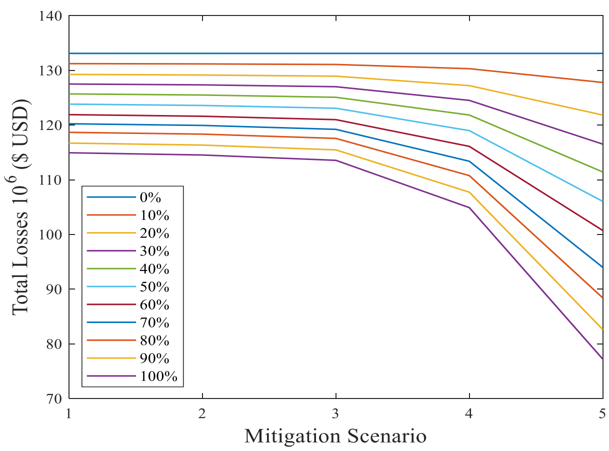

(c) Pumps+Elevating

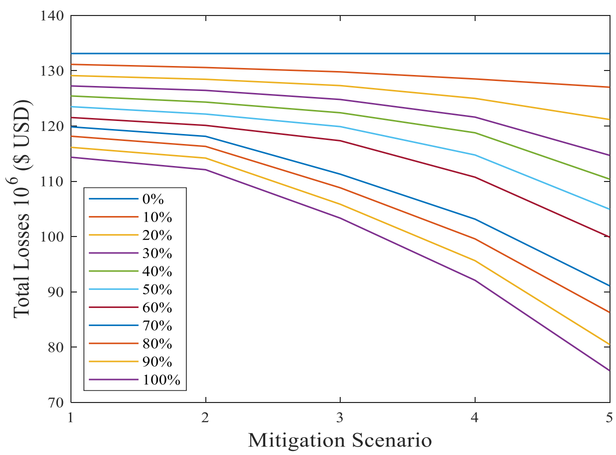

(d) Flood barriers+Elevating

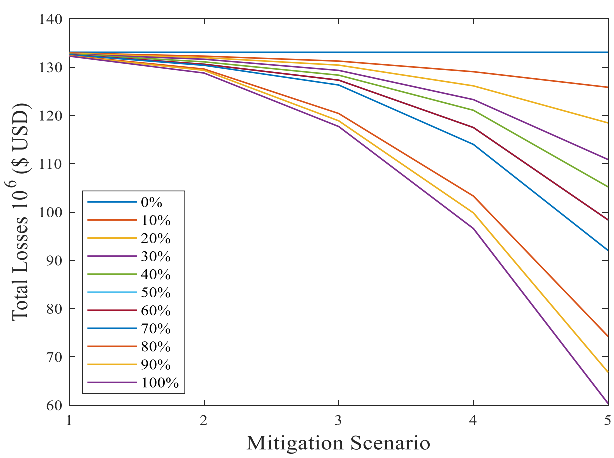

(e) Flood barriers+Pumps

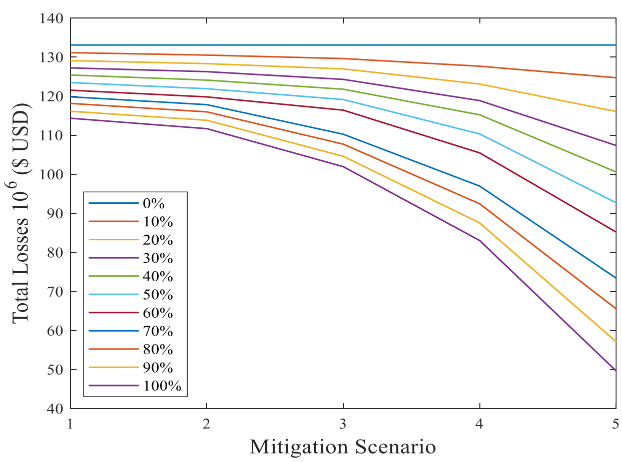

(f) Flood barriers+Pumps+ elevating

Figure 5-15. *Comparison between the state of community-level flood losses for different groups of buildings using a number of mitigation scenarios for different mitigation scenarios*

The spatial distribution of the calculated flood losses for four different scenarios (out of the 330 scenarios) across the community is presented in Figure 5-16 with a color-coded map for the baseline monetary flood losses for the west part of the Lumberton example. A closeup view for one of the impacted neighborhoods with color-coded buildings based on their monetary flood losses without using any flood mitigation measures (baseline flood losses) is shown in Figure 5-16(b). The state of flood losses for each building in the same neighborhood for the case using 1.0m height flood barriers, pumps to reduce to a one-day flood duration, and elevating the select building components are shown in Figure 5-16(c-e), respectively. These figures distinguish between the spatial effects of some of the investigated mitigation measures with respect to the baseline flood losses and how building-level mitigation measures could significantly reduce the community-level flood losses.

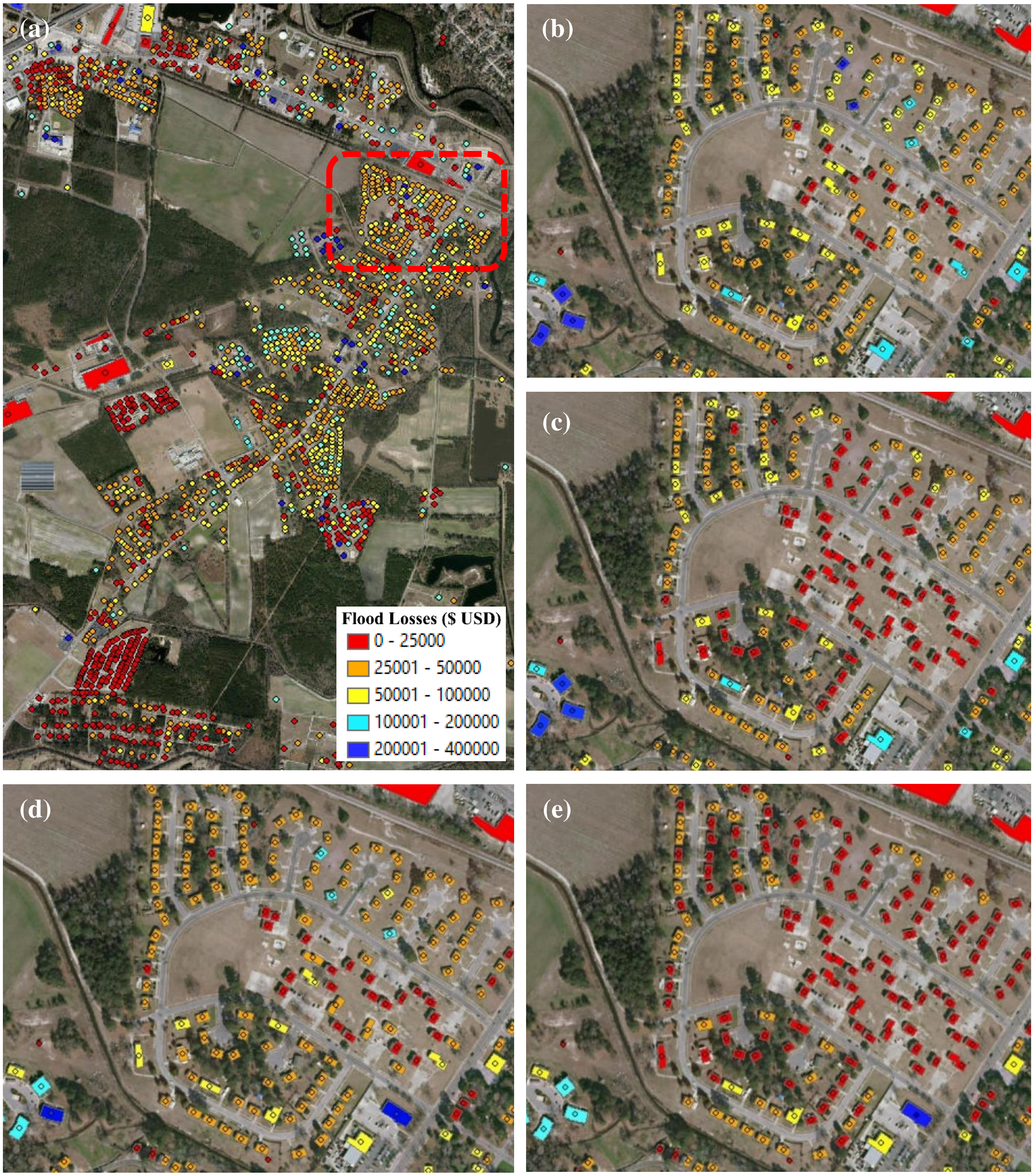

Figure 5-16. *The spatial distribution of flood losses across the community after using a number of mitigation measures: (a) Color-coded map for the baseline flood losses for buildings in the flood plain; (b) Color-coded buildings based on baseline flood losses for a select neighborhood; (c) The state of flood losses for same neighborhood after using a 1.0m height flood barrier system; (d) The state of flood losses for same neighborhood after using Pumps with 1 day flood duration; (e) The state of flood losses for same neighborhood after using 1.0m flood barrier, pumps with 1.0 day flood duration, and elevating the select water-sensitive components*

5.2.6 Flood Mitigation Analysis Using Community-Level Mitigation Measures

Figure 5-17(a) presents a map for the city of Lumberton that shows the location of the city and its physical boundaries along with the main levee (in red) that protects the west side of the city. The main two streams that deliver the water to the study area get connected at the mid-west of the city and are managed by an existing 3200 m long levee intended to protect the west side of the city as shown in the close-up view in Figure 5-17(b). Additionally, the embankments of the interstate highway (I-95) protect the northwest side of the city. However, the underpass at the intersection of the I-95 with the CSX railroad is considered a gap in the levee system as shown in 5-16(c) and recognized to be the main source of water entry to the west side of the city in previous floods.

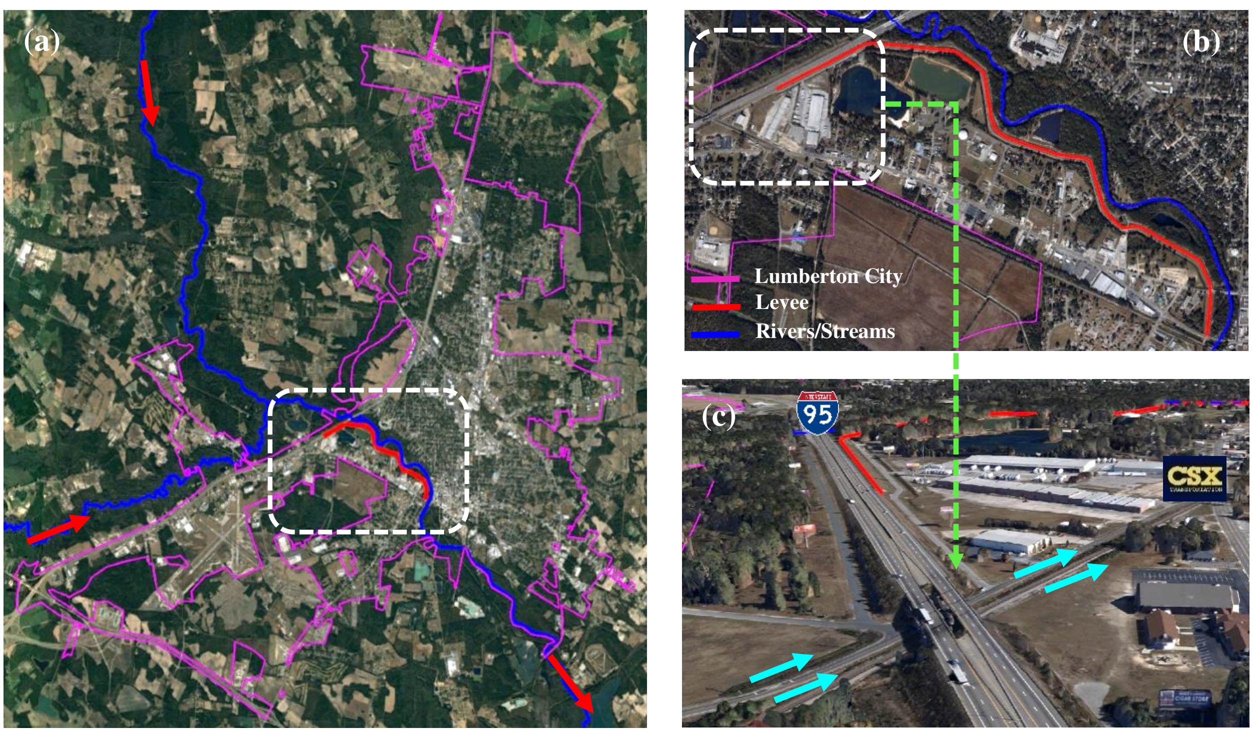

Figure 5-17. *Lumberton topography with rivers and hydraulic structures: (a) Rivers/streams and hydraulic structures spatial location with respect to Lumberton; (b) Close-up view on the levee location; (c) Close up view at underpass location (at the intersection of I-95 with CSX railroad)*

Levee overtopping was not observed in Lumberton for either Hurricane Matthew (2016) or Hurricane Florence (2018), but the water was able to breach into the west side of the city from the underpass location as shown in Figure 5-18(a) and Figure 5-18(b) which combined with the overtopping of Interstate highway (I-95) in several areas. The city/county emergency management anticipated the underpass location as a weak link two years later when a strong rainfall occurred in the wake of Hurricane Florence 2018, and constructed a temporary gravel/sand berm 1.5m in height as shown in Figure 5-18(c). This temporary berm was built to protect the west side of the city along with another sandbag line at the back and one pump as shown in Figure 5-18(b) and Figure 5-18(c). However, this system was not strong enough to withstand the event and was flushed away from the west side as shown in Figure 5-18(d-f). Currently, the city is investigating the feasibility of building flood gates at this location to block water entry from this area in the event of a storm. Another approach is to build a retention pond, but it is a relatively expensive solution with a number of restrictions for the construction locations and would require building acquisitions to proceed. Therefore, enhancing the current levee system is thought to be a more logical and acceptable solution. In terms of applying buyouts (i.e. acquisitions) as well as increasing building elevations, some buildings have already been approved for buyout through FEMA’s Hazard Mitigation Grant Program and some other buildings are beginning the process.

Figure 5-18. *A comparison between the flooding at the underpass during recent rainfall storms after Hurricane Matthew 2016 and Hurricane Florence 2018: (a) Flooding at the underpass due to Hurricane Matthew 2016; (b) Flooding at the underpass due to Hurricane Florence 2018; (c) The city efforts to build a temporary berm before Hurricane Florence 2018; (d) The temporary berm in the wake of Hurricane Florence 2018; (e) A close-up view of the first line of the berm along with the pump; (f) A close-up view on the second line of the berm*

The high-resolution framework proposed herein was used to investigate a suite of possible policy-based hazard, exposure, and vulnerability mitigation measures that were already implemented by the city of Lumberton along with investigating alternative mitigation policies. Figure 5-19(a) shows the locations of several of the proposed hazard mitigation measures. These mitigation measures are modeled in the study area as shown in Figure 5-19(b-d). For example, the flood gate and levee system enhancements were modeled as a weir/dike with specific assumed dimensions, side slopes, and elevations based on each mitigation scenario. Small mesh size was used at the levee/berm location to capture a detailed water flow at these locations. The retention pond was created in the DEM itself by editing the pixel values through a transformation of the DEM from raster to feature points and then changing the elevations of the points to the target elevations of the retention pond and transforming it back to a raster map.

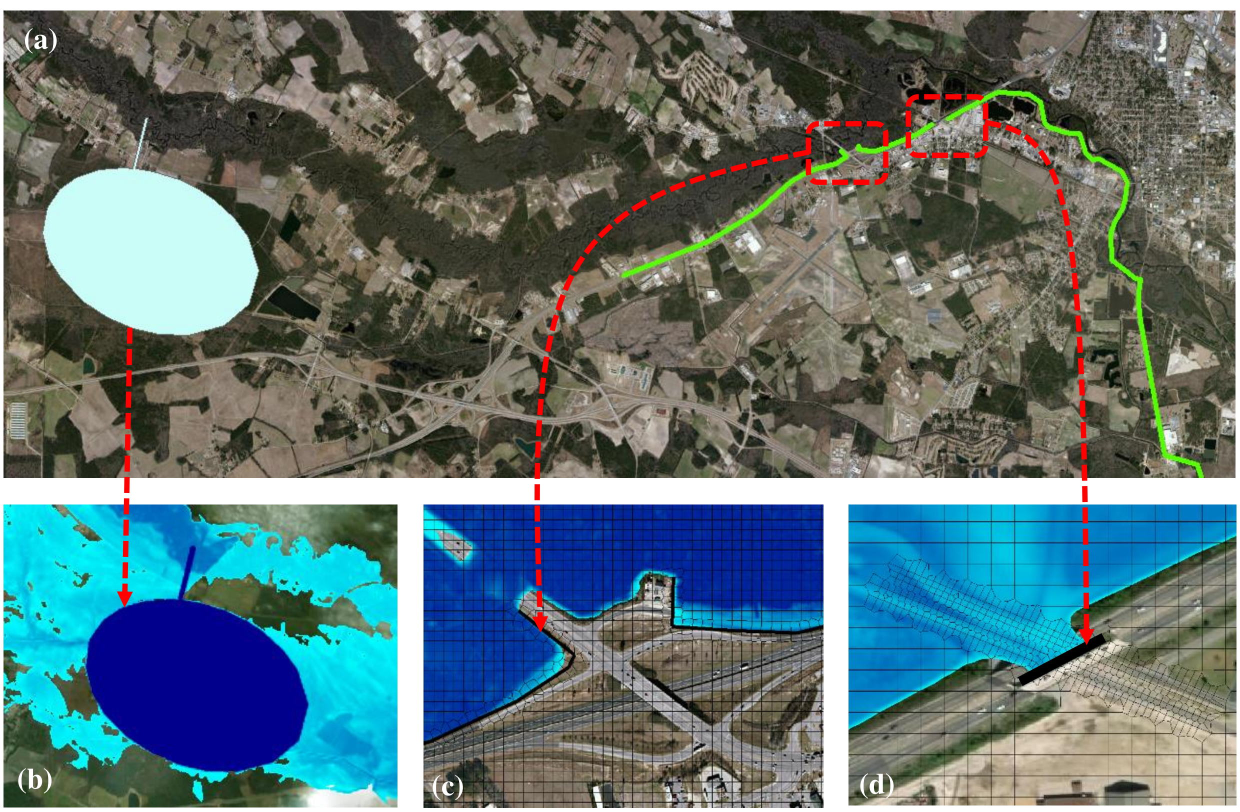

Figure 5-19. *A map shows the proposed locations of some of the hazard mitigation measures: (a) General view; (b) Retention pond; (c) Enhancing of the road embankments; (d) Flood gate*

There are several types of results ranging from hazard maps for each hazard mitigation scenario to their corresponding damage/loss estimates based on probabilistic vulnerability analysis. Therefore, the mitigation analysis is organized, such that scenario (0) does not include any mitigation measures (baseline flood losses) and scenario (1) includes only flood gates or temporary berms at critical locations. Five additional mitigation scenarios (2-6) include flood gate/temporary berms along with levee/embankment enhancement to increase its elevation. The next seven mitigation scenarios (7-13) include using retention/detention ponds with and without flood gates and levee enhancement are investigated. The retention pond flood mitigation scenarios include size, location, and base elevation as the three variables. A combination of mitigation scenarios (14-20) that includes building buyouts and elevation increases based on the proposed framework in Chapter 4 were also investigated. Then, a combination of hazard and exposure mitigation measures was investigated in scenarios (21-28). Table 5-3 describes the details of each mitigation scenario which include retention bond volume in m^3, the bottom elevation of the pond, and the top elevation of each segment of the levee enhancement. Retention ponds are special mitigation measures that typically require building acquisitions depending on their size and location. In this illustrative example, enhancing the levee system is divided into four segments as shown in Figure 5-20. The first two segments are part of the road embankments and the other two segments are part of the existing levee system. The earth profile of each one of these segments along with the investigated enhancement are shown in Figure 5-20(b-d).

Table 5-3. *Policy-based flood mitigation scenarios details*

Mitigation Scenario	Flood Gate	Retention Pond		No. of Building Acquisition	No. of Elevated Buildings	Levee Enhancement (Top Elev.)			
		Volume (m^3x10^6)	Elevation (m)			Part 1 (m)	Part 2 (m)	Part 3 (m)	Part 4 (m)
0	✗	✗	✗	✗	✗	✗	✗	✗	✗
1	✓	✗	✗	✗	✗	✗	✗	✗	✗
2	✓	✗	✗	✗	✗	✗	✗	✗	39.0
3	✓	✗	✗	✗	✗	✗	✗	39.0	39.0
4	✓	✗	✗	✗	✗	✗	39.0	39.0	39.0
5	✓	✗	✗	✗	✗	39.0	39.0	39.0	39.0
6	✓	✗	✗	✗	✗	39.6	39.6	39.6	39.6
7	✗	152.26	33.5	333	✗	✗	✗	✗	✗
8	✗	70.39	33.5	181	✗	✗	✗	✗	✗
9	✗	40.12	33.5	75	✗	✗	✗	✗	✗
10	✗	40.12	33.5	75	✗	✗	✗	38.7	38.7
11	✓	55.81	30.5	5	✗	✗	✗	38.7	38.7
12	✓	48.13	32.0	5	✗	✗	✗	38.7	38.7
13	✓	32.76	35.0	5	✗	✗	✗	38.7	38.7
14	✗	✗	✗	46	✗	✗	✗	✗	✗
15	✗	✗	✗	80	✗	✗	✗	✗	✗
16	✗	✗	✗	128	✗	✗	✗	✗	✗
17	✗	✗	✗	263	✗	✗	✗	✗	✗
18	✗	✗	✗	283	125	✗	✗	✗	✗
19	✗	✗	✗	297	309	✗	✗	✗	✗
20	✗	✗	✗	322	567	✗	✗	✗	✗
21	✓	✗	✗	93	✗	39.0	39.0	39.0	39.0
22	✓	✗	✗	124	✗	39.0	39.0	39.0	39.0
23	✓	✗	✗	165	✗	39.0	39.0	39.0	39.0
24	✓	✗	✗	206	120	39.0	39.0	39.0	39.0
25	✓	32.76	35.0	40	✗	✗	✗	38.7	38.7
26	✓	32.76	35.0	80	60	✗	✗	38.7	38.7
27	✓	32.76	35.0	114	126	✗	✗	38.7	38.7
28	✓	32.76	35.0	118	149	✗	✗	38.7	38.7

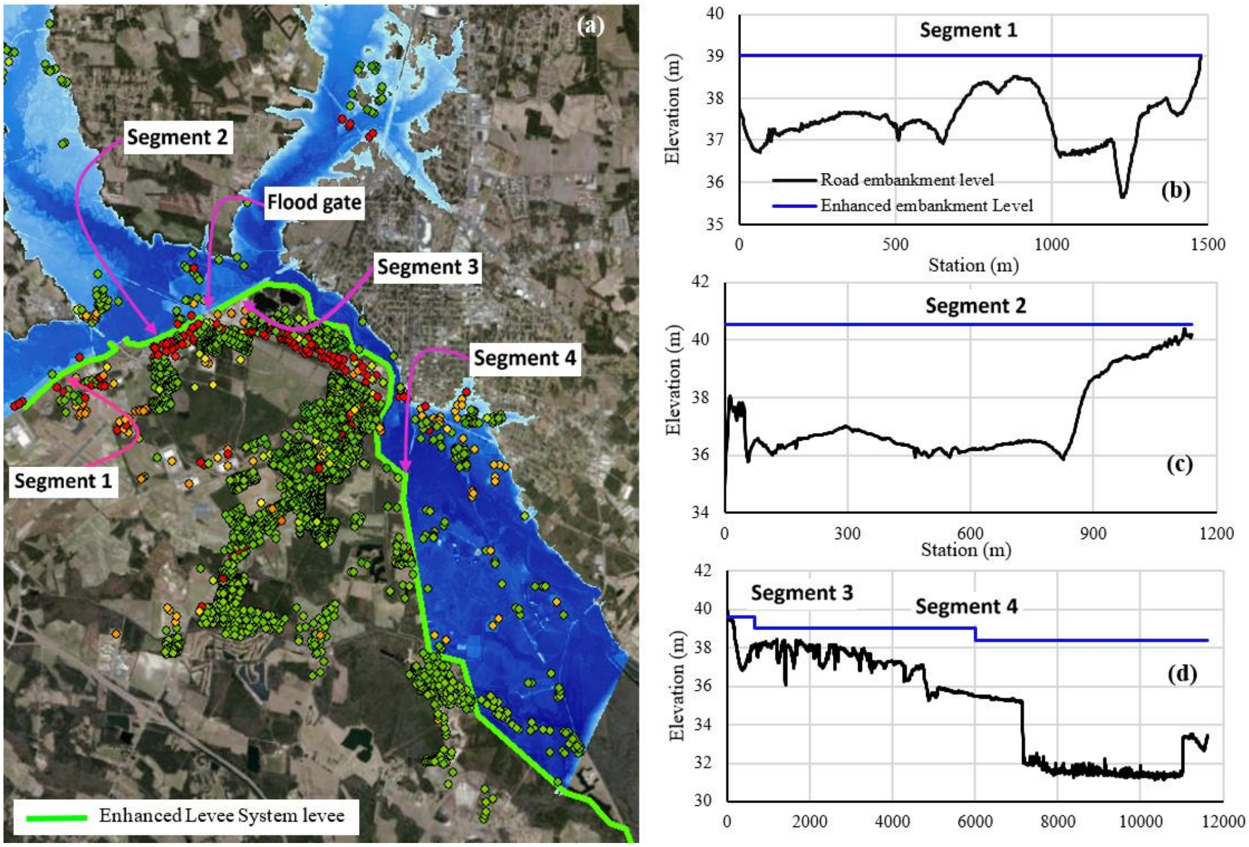

Figure 5-20. *Flood hazard map after using the proposed levee enhancement along with the location of the protected buildings: (a) Flood hazard map with enhanced levee system (b) Embankment profile for segment (1) before and after enhancement; (c) Embankment profile for segment (2) before and after enhancement; (d) Embankment profile for segment (3) before and after enhancement*

5.2.6.1 Flood gates/ temporary berm

Building a flood gate or a temporary berm that blocks water discharge from the underpass area is investigated as shown in Figure 5-21. The analysis showed that the water accumulated behind the gate (like a reservoir) with an increasing water elevation behind the gate and the highway (I-95) embankment as shown in Figure 5-21(b). Finally, the water overtopped the highway embankments from the left and right side of the underpass as the water surface elevation exceeded the embankments elevation as shown in Figure 5-21 (c). The final analysis showed that building a flood gate at the underpass location may not fully protect the floodplain from high-intensity flood hazards (e.g., Hurricane Matthew 2016) which was evident from Hurricane Florence as shown previously in Figure 5-18. However, these flood gates appear to perform very well with lower intensity hazards that might otherwise cause flooding. Therefore, some level of levee enhancement is considered herein along with the flood gate.

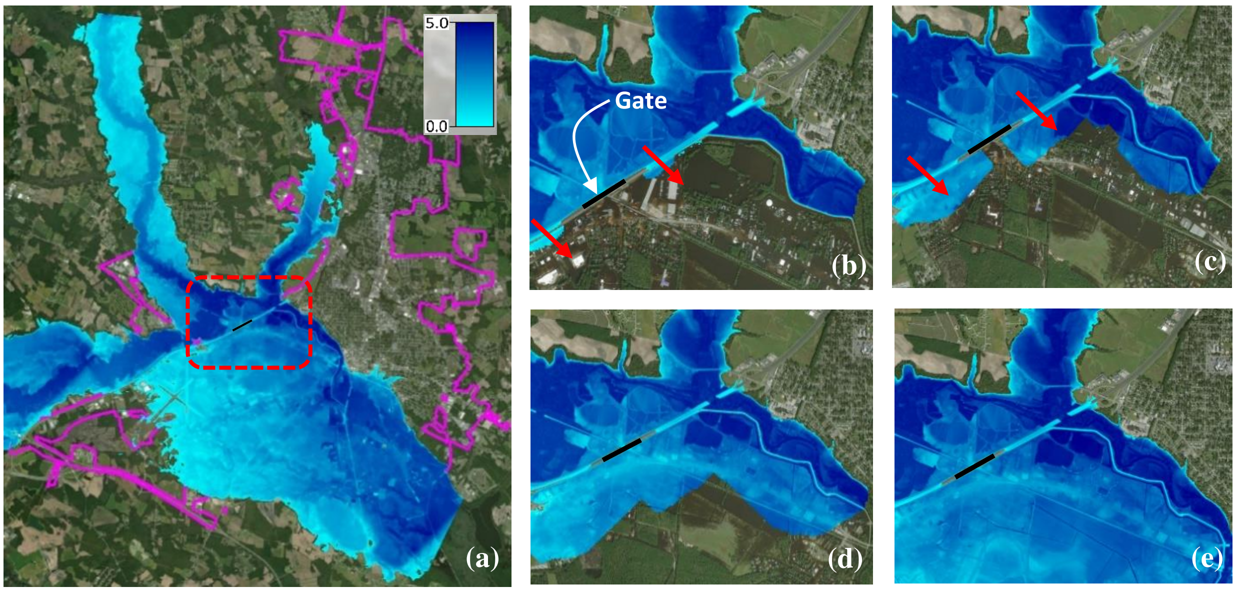

Figure 5-21. *Evolution of Hurricane Matthew 2016 flooding in Lumberton, NC along with using flood gates at the underpass location: (a) Flood hazard map showing the state of flood depth (m) with flood gates; (b) and (c) Water accumulation behind levees; (c) Flood water before approaching the residential area; (d) Maximum Flooding*

5.2.6.2 Permanent levees/floodwalls

Enhancement to the current levee system by increasing its elevation which includes the main levee and the embankments of highway I-95 combined with flood gates at the underpass location was investigated. After conducting several flood simulations, enhancements to levees and embankments are proposed as shown in Figure 5-22. The levee enhancement is divided into four segments with different elevations to restrict the overtopping of floodwater with the minimal amount of embankment work. Segment (1) requires filling 1.5km of the highway embankments as shown in the profile in Figure 5-22 (b), segment (2) requires filling of 1.2km of the highway embankment as shown in the provided profile in Figure 5-22 (c), and segment (3) requires enhancement to the old levee system with an elevation increase from 1.0m at certain locations up to 4.0m at other locations as shown in the profile in Figure 5-22 (d). The proposed enhancements are designed to protect more than 1900 buildings that were severely flooded from rainfall from Hurricane Matthew and provide further protection for more than 3800 buildings on the west side of the city at risk from an even more intense flooding event. However, this mitigation option would require elevating and/or applying a buyout policy for a number of buildings outside the protection zone. Figure 5-22 shows the flood hazard map corresponding to each embankment/levee enhancement scenario. It should be noted that the extent of flood protection was changed significantly beginning with scenario (5) resulting in full protection of the west side of the city because of the enhancements to the four segments of the embankments/levee. However, some locations such as the northeast side of the city became increasingly vulnerable to flooding under these scenarios because of the enhancements as shown in the shaded areas in Figure 5-22(d-f).

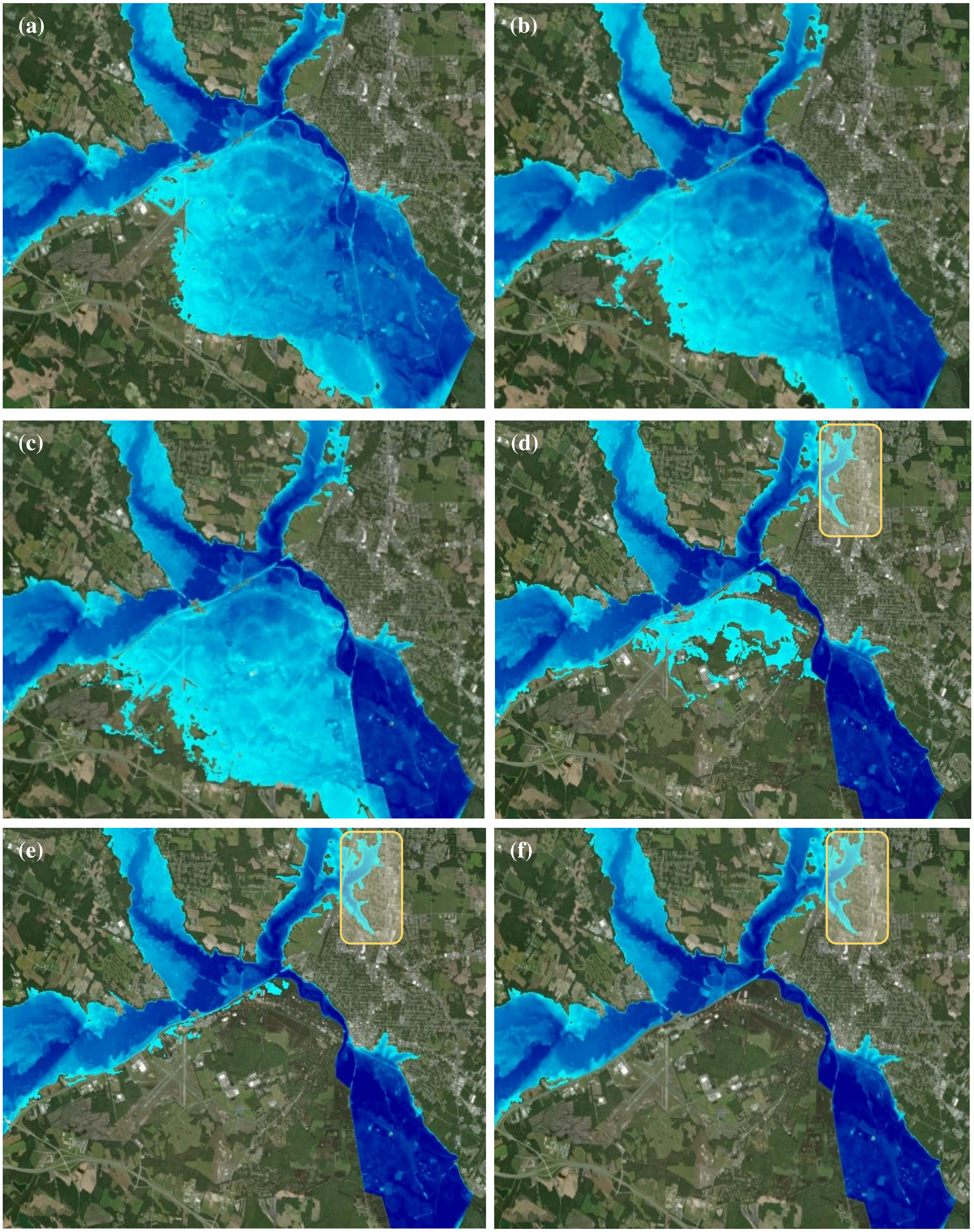

Figure 5-22. *Flood hazard map with the flood extent for different scenarios of levee enhancement: (a) Scenario 0; (b) Scenario 2; (c) Scenario 3; (d) Scenario 4; (e) Scenario 5; (f) Scenario 6*

5.2.6.3 Retention/Detention System

Constructing a large retention/detention pond was also investigated with size, location, and base elevation. Ponds require main channels/pipelines that collect water from upstream of the drainage area to the pond location. Analysis trials are conducted with only one large retention/detention pond without any other mitigation measures (scenario (7-8)) as shown in Figure 5-23(a, and b). Another analysis trial was conducted using a combination of a retention pond and levee enhancement (scenario (10)) as shown in Figure 5-23(c). Then, a different location for the pond was investigated using three different base elevations (scenario (11-13)) as shown in Figure 5-23(d-f). Although mitigation scenario (7) includes only one large retention pond that provides significant protection to the floodplain, it requires an excessive amount of excavation work (resulting in a very high cost) along with a large number of required building acquisitions (333 buildings). On the other hand, mitigation scenario (11) may provide better protection with a pond one-third the size of the retention pond used in scenario (7) combined with levee enhancement to some segments of the current levee system and buyout of only five buildings. This emphasizes the importance of choosing the best location and size of the retention system, but also the importance of information in the decision-making process.

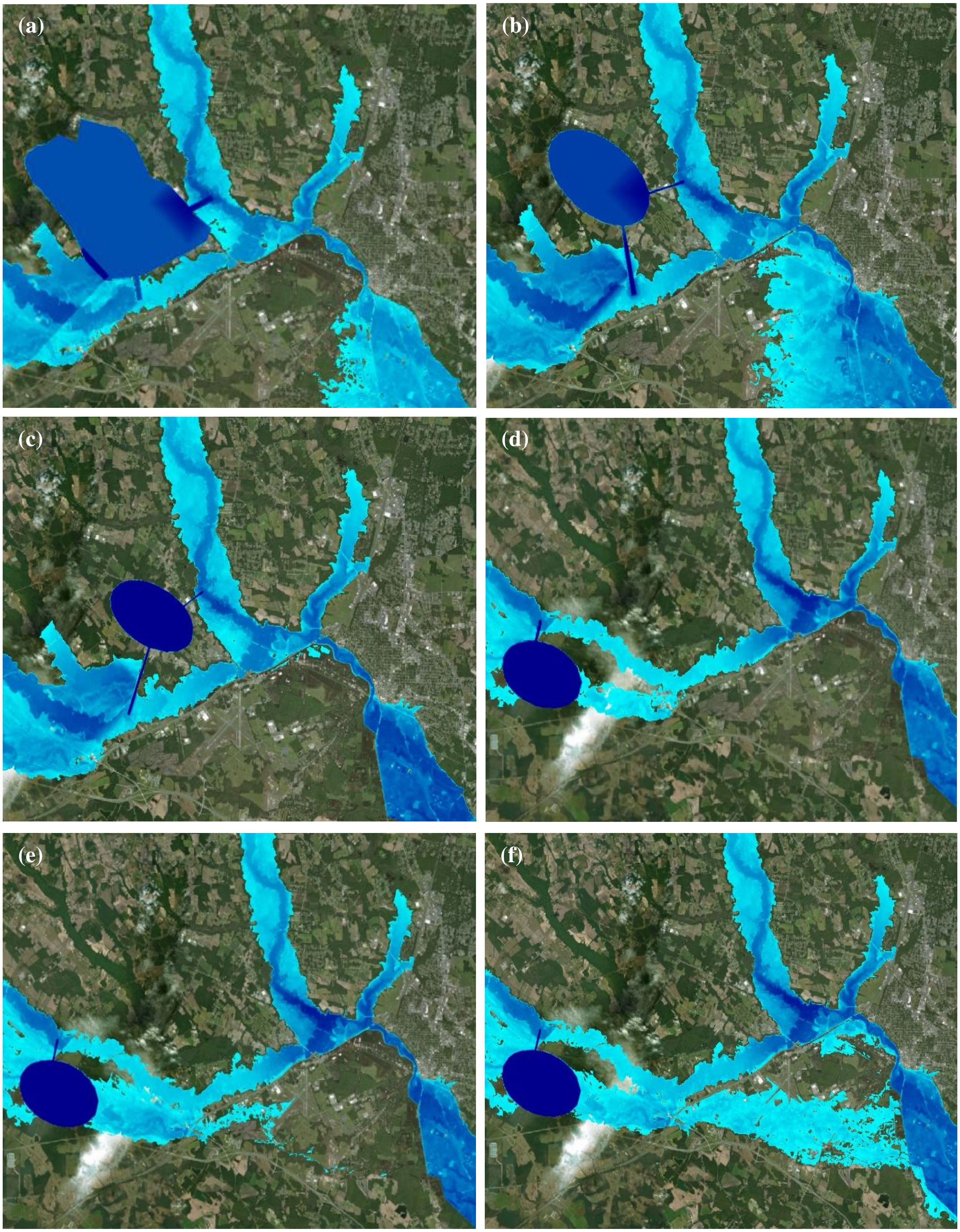

Figure 5-23. *Flood inundation map after applying different sizes and locations of retention ponds: (a) Scenario 7; (b) Scenario 8; (c) Scenario 10; (d) Scenario 11; (f) Scenario 12; (f) Scenario 13*

5.2.6.4 Buyout policy and elevating building first-floor elevation (FFE)

The community size and the number of vulnerable buildings (2000 buildings) make it difficult to consider a single approach such as buyouts for all buildings or elevate all buildings. However, each of these mitigation policies was applied alone for buildings in the flood plain as baseline cases in mitigation scenarios (14-20). Buildings that would be in DS4 and DS3 without any mitigation in place were prioritized to apply the buyout policy. However, for buildings with DS2, increasing the building FFE was proposed first and then the cost of increasing the building FFE was calculated. If the cost was more than half of the building's market value, a building buyout was applied for that building as illustrated in the flow chart in Chapter 4 in Figure 4-12. This approach was applied for mitigation scenarios (18-20). The analysis assumed that the building buyout value was equal to the published market value of the building on the North Carolina spatial data download. Then, home buyouts and building elevations are investigated as a part of scenario (5) which includes enhancements to four segments of the embankment/levee system using mitigation scenarios (21-24). Additionally, the buyouts and elevations are further investigated in scenarios (25-28) as a part of scenario (13) which includes using a retention pond on the west side of the city.

5.2.6.5 Discussion

The results for the 28 mitigation scenarios are summarized in Table 5-4 in terms of the number of impacted buildings and their designated DSs, the total flood loss and the amount of flood loss reduction, and the price and the number of either the buyout, elevation, or both. Additionally, stacked bar charts were created for all mitigation scenarios as shown in Figure 5-24. The spatial distribution of the building DS across the community (only flooded buildings are shown) for some select hazard mitigation scenarios is shown in Figure 5-25. The analyses revealed which mitigation measures may be successful for small return period events (e.g., 30-year or 50-year flood events) and which would not be effective for long return period events (e.g., 100-year or 500-year flood events). This is the case for mitigation scenario (1) which includes building a flood gate or temporary berms at the underpass location without using any other mitigation measures. This would retain the water behind the gate like a reservoir but, eventually, for severe flooding events, the water elevation may exceed the road embankment elevation and lead to water overtopping. Therefore, mitigation scenario (1) resulted in larger losses than the baseline scenario (0) for long return period events as shown in Figure 5-24(a). This helps to explain the negative value of the flood loss reduction for both mitigation scenarios (1) and (2) in Table 5-4 which means that there is no loss reduction for the (intense) baseline scenario. This can be explained such that the failure of the levee system would result in higher flood depths thereby increasing the amount of flood losses and the number of buildings designated as DS3. The analyses in this study also showed that the effect of more enhancements to the current embankment\levee system, namely, lower flood losses with substantially less buildings designated as DS3 and DS2 as shown in Figure 5-24(a). However, the number of buildings designated as DS4 slightly increased because of the increased flood depth behind the gate, and the levee system resulted in higher damage states for some buildings outside the protected area.

Table 5-4. *Analysis results for the 28 flood mitigation scenarios in this study*

Mitigation Policy	Mitigation Scenario	No. of Building Acquisition	Acquisition Price × $10^6	No. of Elevated Buildings	Elevation Price × $10^6	Flood Loss Reduction × $10^6	No. of Buildings in Floodplain	DS0	DS1	DS2	DS3	DS4	Losses × $10^6
Baseline	0	✗	✗	✗	✗	0.00	2857	525	162	1907	254	9	133.14
Flood gate	1	✗	✗	✗	✗	-16.36	2925	521	235	1707	452	10	149.50
Enhancing the current levee system	2	✗	✗	✗	✗	-1.81	2949	693	216	1750	260	30	134.95
	3	✗	✗	✗	✗	31.13	2970	1283	174	1289	163	61	102.01
	4	✗	✗	✗	✗	86.1	1426	841	57	366	70	92	47.04
	5	✗	✗	✗	✗	86.71	979	426	44	344	72	93	46.43
	6	✗	✗	✗	✗	86.74	970	416	44	345	71	94	46.40
Retention system	7	333	138.36	✗	✗	114.03	808	463	61	284	0	0	19.11
	8	181	47.43	✗	✗	77.33	2235	1179	107	926	23	0	55.81
	9	73	12.23	✗	✗	70.16	2177	985	87	1070	32	3	62.98
	10	75	12.23	✗	✗	102.87	630	221	33	330	40	6	30.27
	11	5	0.38	✗	✗	112.91	361	140	13	175	31	2	20.23
	12	5	0.38	✗	✗	111.11	477	187	28	228	32	2	22.03
	13	5	0.38	✗	✗	109.84	1141	824	55	227	33	2	23.30
Buyout and elevation	14	46	6.43	✗	✗	3.93	2811	525	162	1907	217	0	129.21
	15	80	15.66	✗	✗	8.71	2777	525	162	1907	183	0	124.43
	16	128	20.00	✗	✗	11.5	2729	525	162	1907	135	0	121.64
	17	263	32.3	✗	✗	19.2	2594	525	162	1907	0	0	113.94
	18	283	33.57	125	6.47	26.67	2449	525	162	1762	0	0	106.47
	19	297	34.15	309	15.87	37.2	2251	525	162	1564	0	0	95.94
	20	322	35.3	567	24.77	49.56	1968	525	162	1281	0	0	83.58
Buyout, elevation, and enhancing levees	21	93	8.97	✗	✗	94.33	886	426	44	344	72	0	38.31
	22	124	20.14	✗	✗	100.76	855	426	44	344	41	0	32.38
	23	165	40.85	✗	✗	111.09	814	426	44	344	0	0	22.05
	24	206	43.15	120	8.43	122.85	653	426	44	183	0	0	10.29
Buyout, elevation, and retention system	25	40	4.56	✗	✗	112.50	1106	824	55	227	0	0	20.64
	26	80	8.41	60	11.13	125.28	1006	824	55	127	0	0	7.86
	27	114	12.56	126	15.51	130.24	906	824	55	27	0	0	2.74
	28	118	13.11	149	16.59	131.33	879	824	55	0	0	0	1.81

There are mitigation measures that can provide full protection for the floodplain but they can be even more expensive than the price of all the infrastructure within the floodplain of the impacted community, which is the case with mitigation scenario (7). Although scenario (7) exhibits very low flood losses, it requires a large size retention system along with the acquisition of a large number of buildings (333 buildings). On the other hand, scenario (11) exhibits almost the same amount of flood loss reduction with a retention system size that less than one-third of the size of the retention system used in scenario (7) and requires the buyout of only five buildings as shown in Figure 5-24(b). Mitigation scenarios (11-13) exhibited almost the same amount of flood losses but the number of the impacted buildings was different. This can be explained by the fact that the size of the retention pond used in scenario (13) is smaller than in scenario (11) which allowed some water to overflow into the community as shown in Figure 5-23. However, the flood depth induced by this overflow was minor which resulted in the same number of buildings designated as DS1, DS2, and DS3 but increased the number of buildings designated as DS0 which is considered to be insignificant damage. This underscores the importance of choosing the best location and size of the mitigation measures for the floodplain.

Although applying the home buyout policy and/or elevating buildings requires substantial funding, it provides significant protection for the assets in the flood plain by removing\elevating the vulnerable buildings. However, these mitigation measures are conditioned on the household's decision of whether to apply for and accept a buyout and relocate, stay and mitigate, or take no action. The cost of these building-level options applied to a large number of buildings must be weighed against other hazard mitigation measures. For example, mitigation scenario (17) shows that almost $33 million USD is required to buyout all the buildings designated as DS3 and DS4 (263 buildings) which would result in a direct flood loss reduction of $20 million USD. Mitigation scenario (20) requires $35 million USD for the buyout and $24 million for building elevations and this would protect all the buildings designated as DS3 and DS4 (263 buildings) along with the protection of 626 buildings designated as DS2. However, with all these funds applied, there are still almost 2000 buildings that would be vulnerable to flooding with expected damage ranging from DS0 to DS2 and total flood losses of $83.6 million as shown in Figure 5-24(c). Indirect losses from household dislocation and the inability of businesses to operate on the local economy are important but are beyond the scope of the current analysis. They will be considered in future analyses using economic projection models.

This analysis conducted herein assumes that the household accepts the buyout based on the framework illustrated in Chapter 4. Therefore, a combination between the use of exposure and vulnerability mitigation measures (buyout and building elevation) and other hazard mitigation measures were investigated in mitigation scenarios (21-28). For mitigation scenarios (21-24), the impact of applying the home buyout and/or building elevations was investigated along with using the hazard mitigation measures applied in scenario (5), which includes building a flood gate and enhancing the current levee system. The results revealed that flood losses could be decreased from $46 million (for scenario 5) to $10 million (for scenario 24) if $43 million of funds are secured for home buyout and $8 million for increasing building elevation as shown on the left side of Figure 5-24(d). Finally, mitigation scenarios (25-28) investigated the impact of using the home buyout and/or building elevations along with building the retention system investigated in scenario (13). The analysis shows that the flood losses could be decreased from $23 million (for scenario 13) to $1.8 million (for scenario 28) if a fund of $13 million is secured for the home buyout along with $16 million for increasing buildings elevation as shown on the right side of Figure 5-24(d).

The stacked bar chart presented in Figure 5-24 summarizes the analysis results for the 28 mitigation scenarios along with their corresponding flood losses. Although enhancing the levee system using mitigation scenarios (1-3) results in almost the same number of damaged buildings, the amount of flood losses was significantly decreased because the damage severity was, on average, lowered. Enhancing the levee system using mitigation scenarios (4-6) resulted in flood losses of \$47.04, \$46.43, \$46.4 million USD, respectively. However, the number of impacted buildings for these mitigation scenarios was 1426, 979, 970 buildings, respectively, as shown in Table 5-4 and Figure 5-24. Although enhancing the levee system using mitigation scenarios (4-6) produces almost the same amount of flood losses, scenario (4) resulted in a larger number of impacted buildings than scenarios (5-6) by almost 450 buildings. This can be explained in that most of these 450 buildings were predicted to be in DS0 (insignificant damage) as shown in Fig. 12a which means that floodwater is below FFE with average losses per building being lower than \$2000. This difference is shown in the color-coded maps presented in Figure 5-25(b, and c) which clearly shows more red-colored buildings in the middle due to minor water overflow from the highway embankments using mitigation scenario (4). For a retention pond mitigation measure, Figure 5-24 shows the impact of pond size and location on the amount of flood losses and the number of the impacted buildings along with the required funds needed for building acquisition. Figure 5-24(b) shows that the retention system used for mitigation scenario (11) provides optimal flood loss reduction with the lowest number of impacted buildings and the required funds for building acquisition. Figure 5-25(d and e) show a color-coded map for the impacted buildings resulting from the retention systems used in mitigation scenarios (10) and (13). The results also reveal that using buyouts and building elevations alone is not sufficient to provide major flood protection even with \$60 million available which is shown in mitigation scenario (20) in Figure 5-

24(c). However, using all of these mitigation techniques in concert can work effectively for major flood protection as shown in Figure 5-24(d).

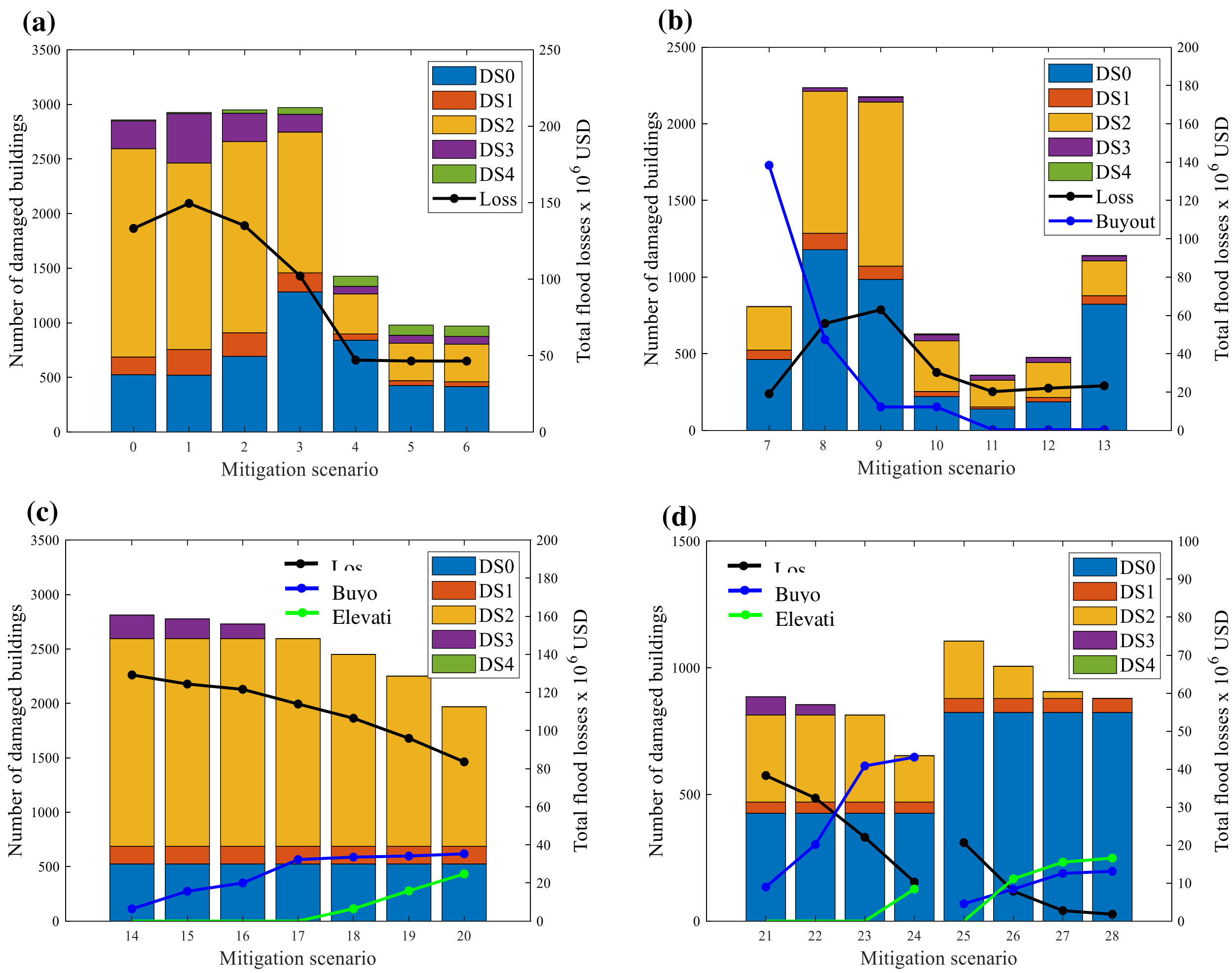

Figure 5-24. *Mitigation analysis results in terms of damage and losses corresponding to each one of the 28 mitigation scenarios: (a) Mitigation scenarios (0-6); (b) Mitigation scenarios (7-13); (c) Mitigation scenarios (14-20); (d) Mitigation scenarios (21-28)*

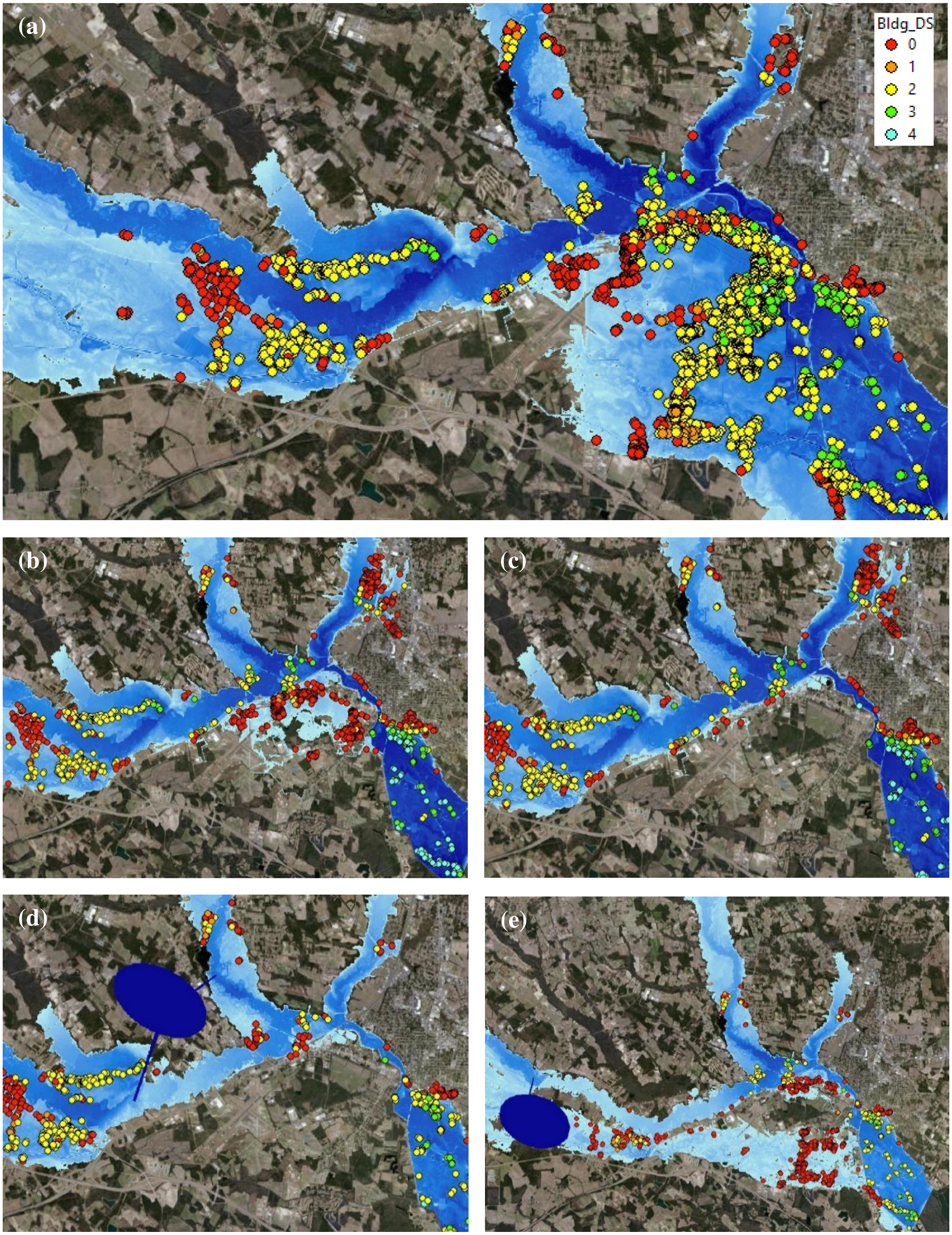

Figure 5-25. *The spatial distribution of buildings damage states corresponding to some select hazard mitigation scenarios: (a) Mitigation scenario (0); (b) Mitigation scenario (4); (c) Mitigation scenario (5); (d) Mitigation scenario (10); (e) Mitigation scenario (13).*

5.2.7 *Lumberton Testbed for IN-CORE Application*

The **I**nterdependent **N**etworked **Co**mmunity **R**esilience **M**odeling **E**nvironment (IN-CORE) is a computational resilience analysis environment that enables modeling of the natural hazards impact and resilience of communities. This environment incorporates risk analysis with the decision-making process to quantitatively compare alternative resilience strategies(IN-CORE, 2021). Figure 5-26 shows the main components for IN-CORE which include pyincore and IN-CORE web services and tools along with IN-CORE lab. Pyincore is a python package that allows users to apply hazards to infrastructure and includes the impact of the physical infrastructural damage on the socio-economic systems. IN-CORE web services are a suite of services that allows users to access hazard and fragility data to be used in pyincore. IN-CORE web tools are a group of viewers that allow users to visualize hazards, fragility curves, and recovery trajectories and download some of them to be used in either pyincore or other analysis platforms. IN-CORE lab is a customized Jupyter lab within pyincore that allows users to develop/run/test their models. Therefore, the community-level decision models within this dissertation will be done in IN-CORE and thus include incorporation of models into IN-CORE web services (hazard, exposure, and vulnerability models) along with their implementation into detailed examples.

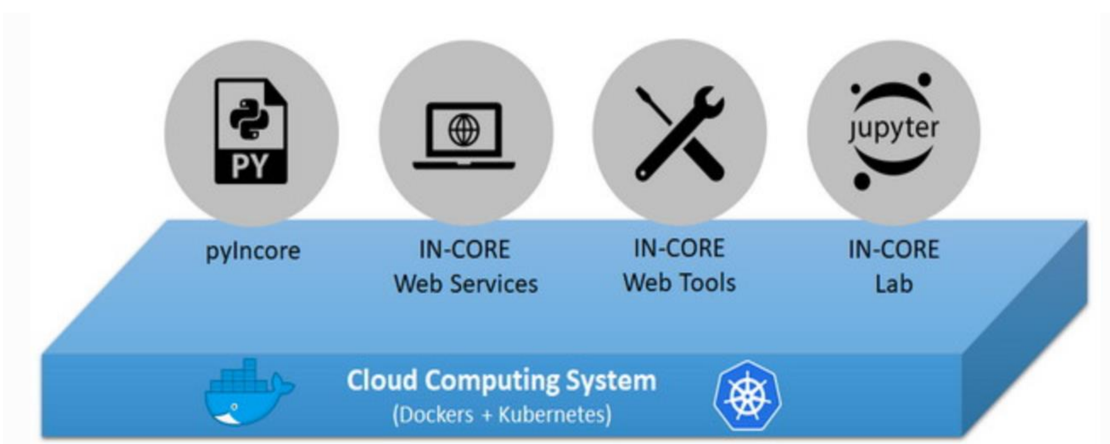

Figure 5-26. *IN-CORE components*

The developed portfolio of flood fragility functions developed in Chapter 2 was included in IN-CORE web tools as a part of the DFR3 viewer which could be accessed from the link shown in Figure 5-27. Also, a mapping algorithm was developed into IN-CORE to enable mapping these fragilities to any community which was also included in the DFR3 viewer. Figure 5-27 shows an example fragility curves for archetype F2 along with the lognormal parameters used to draw these curves. The hazard data developed for the flooding event after Hurricane Matthew was also included in IN-CORE Hazard Viewer as shown in Figure 6-28(a). The building inventory data for Lumberton was also uploaded into IN-CORE Data Viewer as shown in Figure 6-28(b). Also, a building damage analysis algorithm using Python (Jupyter Notebook) that uses these developed IN-CORE web tools was developed to account for building damage as a part of the IN-CORE testbed examples. Although this application is specific to Lumberton, the developed web tools could be applied to any community of interest and could be accessed by anyone.

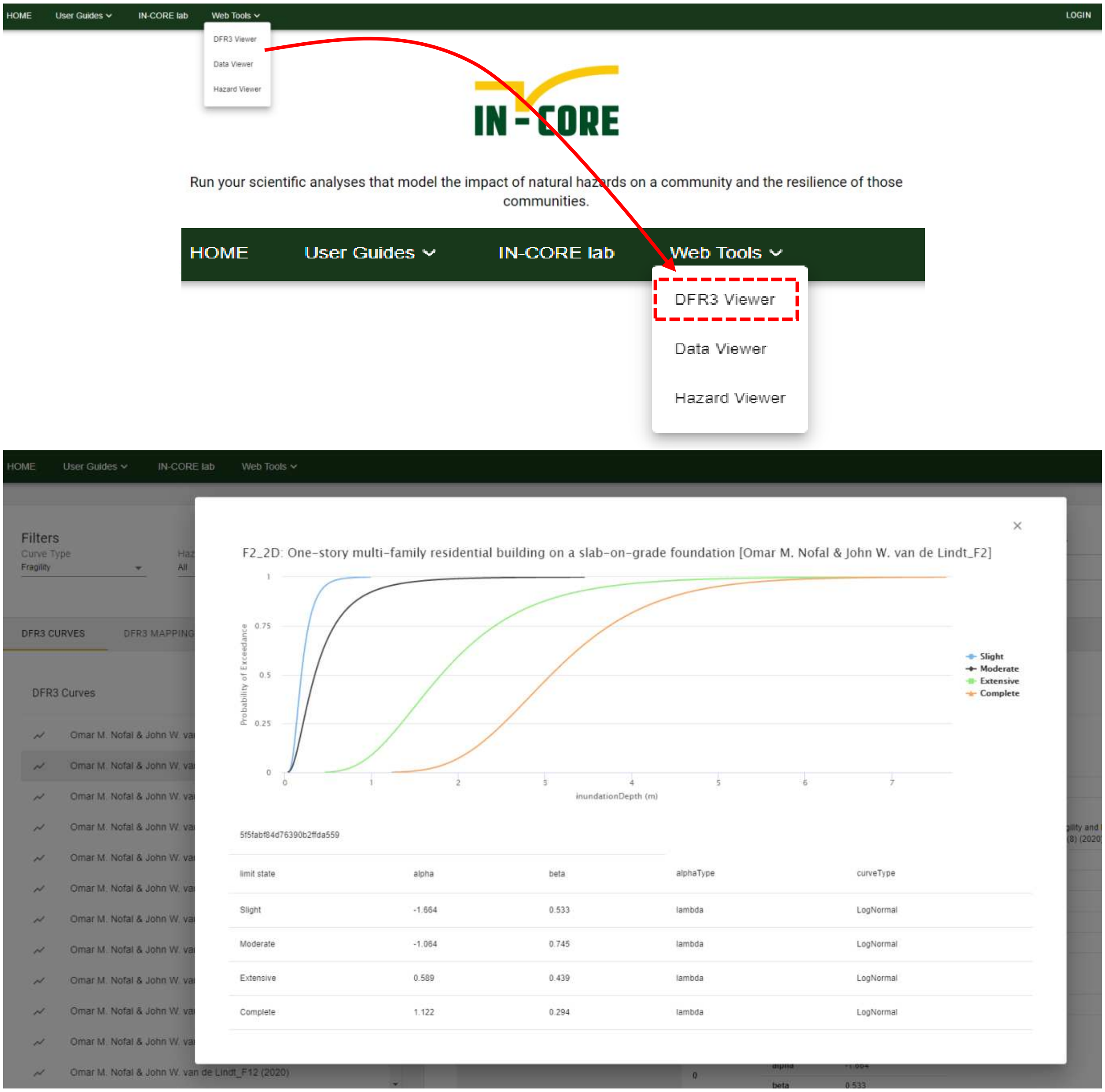

Figure 5-27. *IN-CORE website* [https://incore.ncsa.illinois.edu/DFR3Viewer]

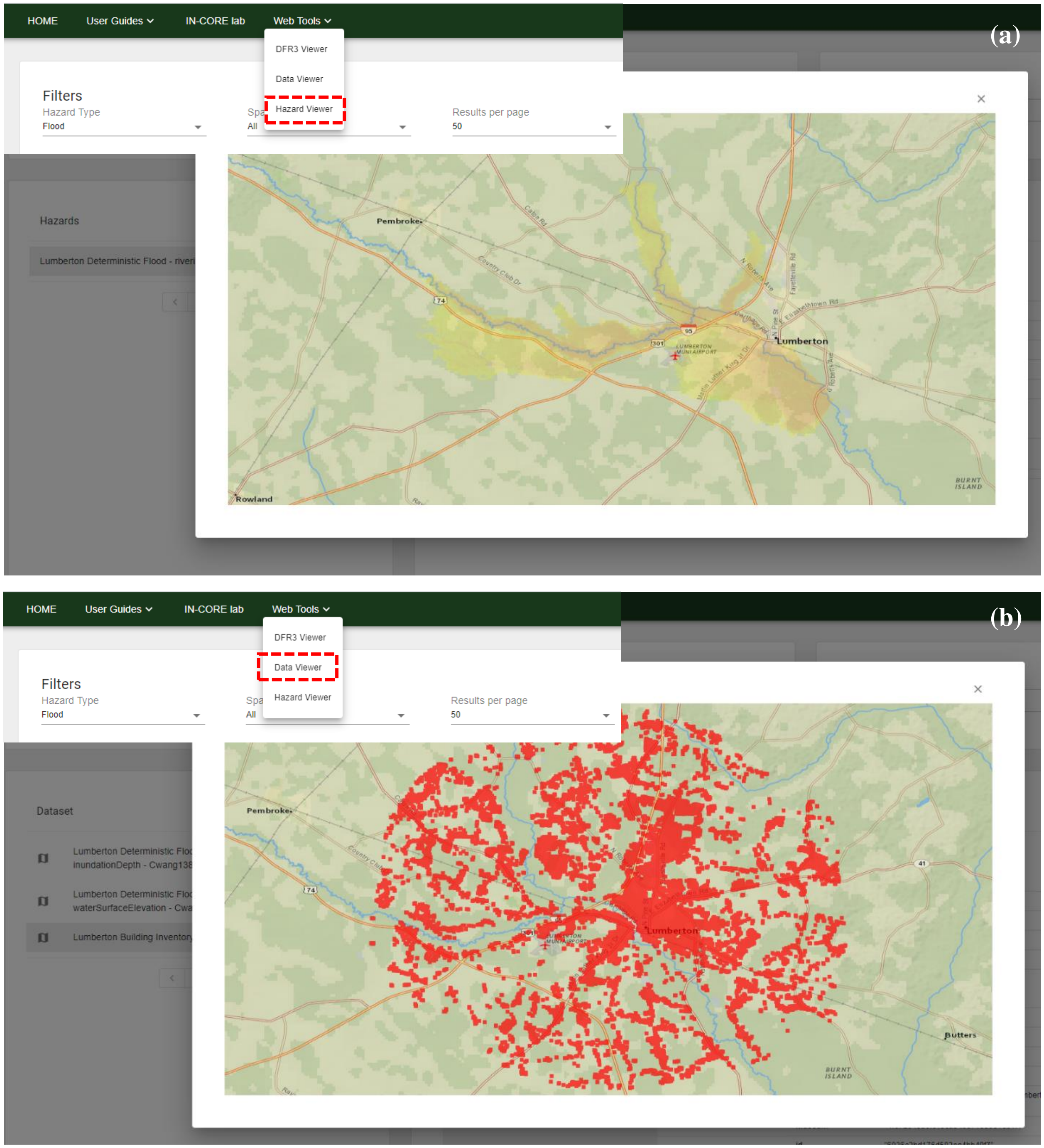

Figure 5-28. *IN-CORE website* [https://incore.ncsa.illinois.edu/DataViewer]

5.3 Example 2: The State of North Carolina

The state of North Carolina, located on the east coast of the United States, as shown in Figure 5-29, is a large coastal state in terms of area and population (29th and 9th, respectively out of 50 US states). The population of North Carolina according to the 2019 state census data was 10.49 million (US Census Bureau 2019), with more than five million buildings ranging from residential to commercial and industrial buildings as well as social institutions, such as schools and hospitals. North Carolina has a long history of damage and loss from coastal hazards, including hurricanes over the last several decades (e.g., Hurricane Floyd in 1999; Hurricane Matthew in 2016, Hurricane Florence in 2018). Hence, Hurricane Florence was selected as the illustrative example for the proposed multi-hazard hurricane risk analysis approach presented in Chapter 3. Full buildings data for North Carolina are published on the state's spatial data download website (State of North Carolina, 2019). These data include each building location, HAZUS-based occupancy, year built, FFE, number of stories, foundation type, roof shape, and market value. The spatial location of each building within North Carolina is indicated in gray in Figure 5-29(a). Close-up views on one of the coastal areas in North Carolina are shown in Figure 5-29(b and c) along with color-coded buildings based on the flood and wind archetype portfolio, respectively.

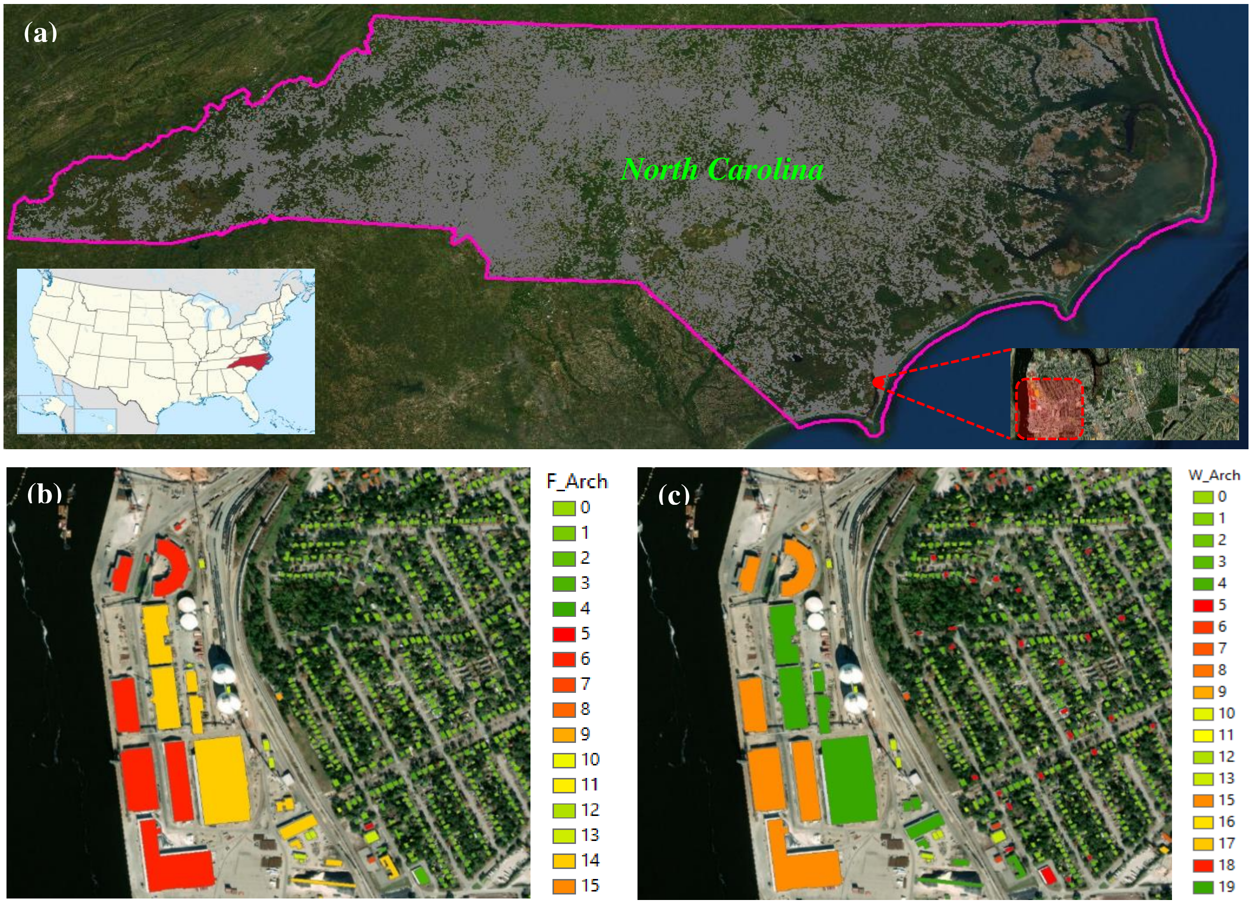

Figure 5-29. *(a) A schematic representation of the geographical location of the State of North Carolina with respect to USA along with the spatial location of the buildings within NC; A close-up view on a neighborhood on the bank of the Cape Fear River with color-coded buildings based on (b) The 15 flood archetypes; (c) The 19 wind archetypes*

5.3.1 Hazard Scenario

Hurricane Florence in 2018 was a devastating event for the state of North Carolina. Figure 5-30 shows the spatial evolution of hurricane Florence across the Atlantic until it made landfall in the southeast of North Carolina. A hazard map for each of the hurricane-induced hazards from 2018 Hurricane Florence was used for the multi-hazard hurricane risk analysis for the State of North Carolina, including surge, wave, and wind as shown in Figure 5-31. The wind hazard map based on the maximum wind speeds for North Carolina in terms of the 3-second guest wind speed is shown in Figure 5-31(a) with ranges from 4.0 m/s (9.0 mph) to 41.0 m/s (91.0 mph). However, only buildings experiencing wind speeds exceeding 31.0 m/s (61.0 mph) were considered in this study, because it is the lowest wind speed that would typically cause damage, i.e. based on a 50% exceedance probability of DS1 for the residential wind fragilities. Therefore, the zone with wind speeds exceeding 31.0 m/s (70.0 mph) is distinguished by the blue boundary line, as shown in Figure 5-31(a). The peak surge height for the flooded areas throughout North Carolina in this example is shown in Figure 5-31(b), not including additional flooding resulting from the rainfall-runoff. Figure 5-31(c) shows the wave hazard map based on the significant wave height.

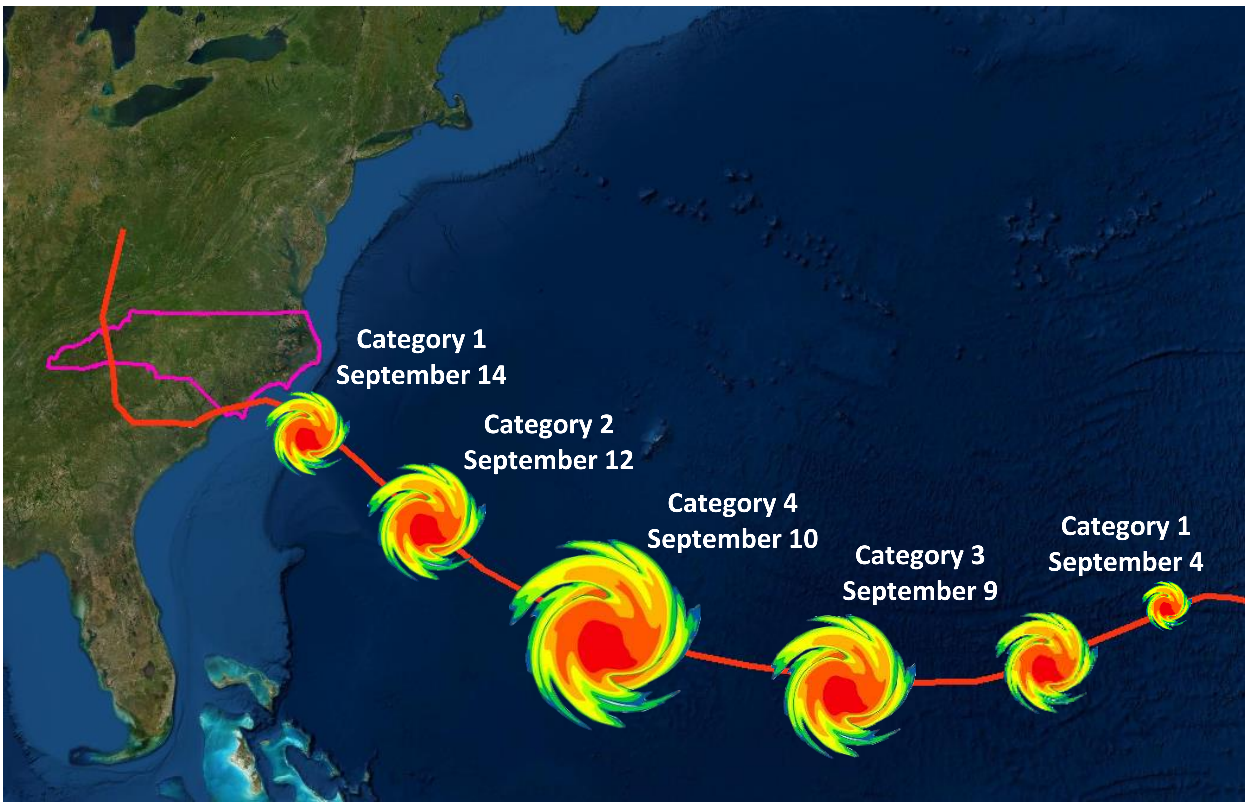

Figure 5-30. *Hurricane Florence in 2018 path and the category evolving over the time*

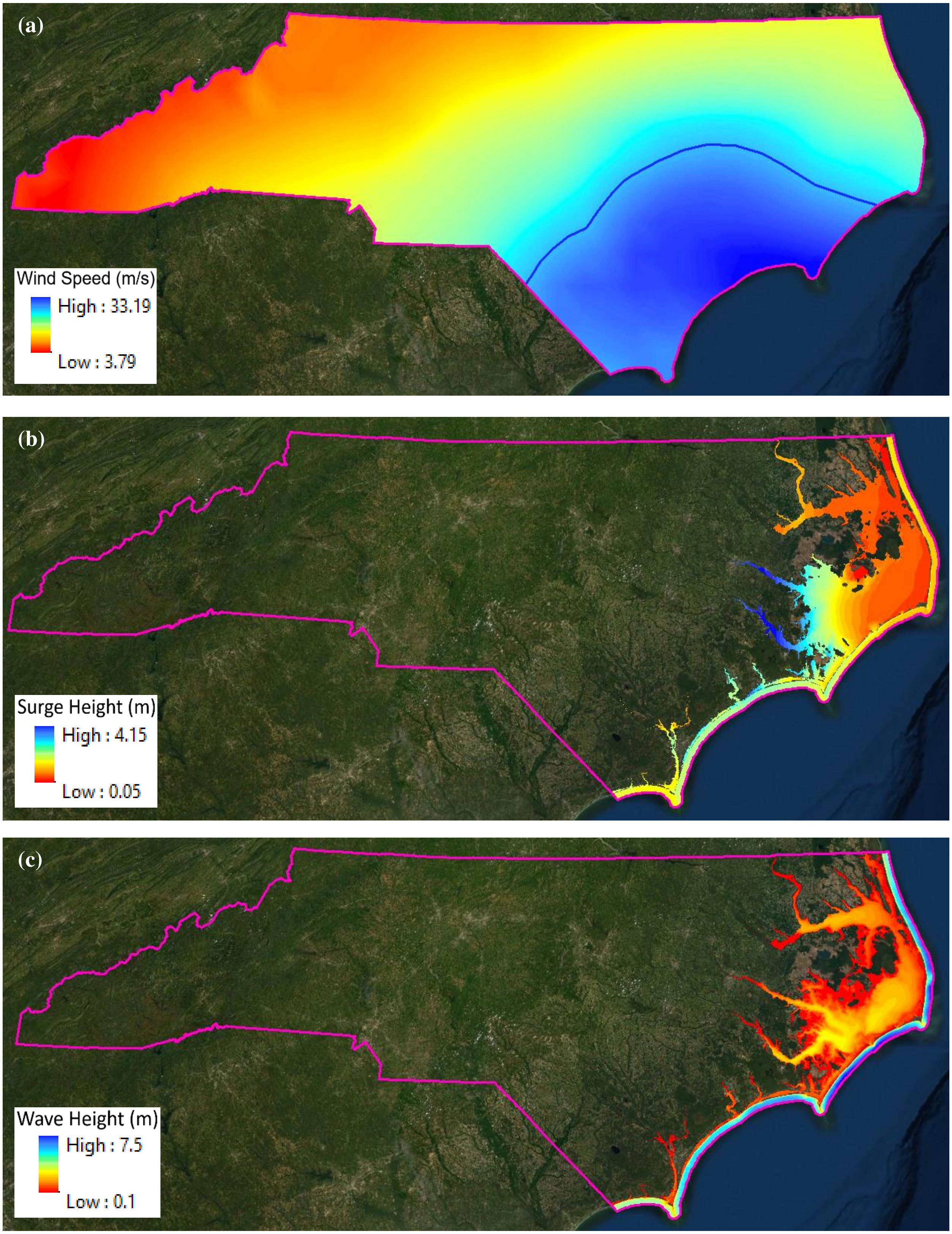

Figure 5-31. *Hazard maps for the hazards induced by the 2018 Hurricane Florence: (a) Wind hazard map (m/s); (b) Surge hazard map (m); (c) Wave hazard map (m)*

5.3.2 *Exposure and Vulnerability Modeling*

The building spatial data was overlaid with the hazard maps to identify the exposed buildings and their corresponding hazard intensities. The entire state of North Carolina was exposed to wind hazards from Hurricane Florence in 2018, but with different intensities. Therefore, as mentioned earlier to reduce the number of buildings to be analyzed, a wind speed threshold of 31.0 m/s (70.0 mph) was set to exclude any building experiencing wind speeds less than this threshold. For the surge and wave hazard, all buildings that are exposed to either surge or combined surge and wave are included in the analysis. Figure 5-32 shows the different exposure zones within the State of North Carolina, which are color-based on the type of hazards within each zone. Creating this wind threshold increased the number of exposed zone types to include the wind zone (blue), flood zone (yellow), surge-wave zone (orange), surge-wind zone (green), and surge-wave-wind zone (purple). However, the two new zones, surge zone, and surge-wave zone include wind hazard but the wind speed is less than the 31.0 m/s (70.0 mph) threshold, which is assumed to be not sufficient to cause any wind-related damage.

The exposure analysis results show that there are 845,067 buildings exposed to a wind speed of more than 31.0 m/s as shown in Figure 5-32. These include 834,595 buildings exposed to wind hazards only (based on the used wind speed threshold), 6,741 buildings exposed to combined surge and wind, and 3,465 buildings exposed to combined surge, wave, and wind. The exposure analysis results show that there are another 3,336 buildings exposed to surge only and 2,050 buildings exposed to combined surge and wave (with minor wind speeds that are less than the wind speed threshold of 31.0 m/s). Table 5-5 summarizes the number of exposed buildings corresponding to the number of hazard intensity ranges. For wind exposure, more than 208,000 buildings were exposed to a wind speed in the range of 37.0 m/s (83.0 mph) to 40.0 m/s (90.0 mph). For the storm surge hazard, more than 8,000 buildings were exposed to surge heights from 2.0m (6.6 ft) to 3.0m. (9.8 ft). For the wave hazard, more than 5,000 buildings were exposed to significant wave heights from 0.5m (1.6 ft) to 1.0m (3.3 ft).

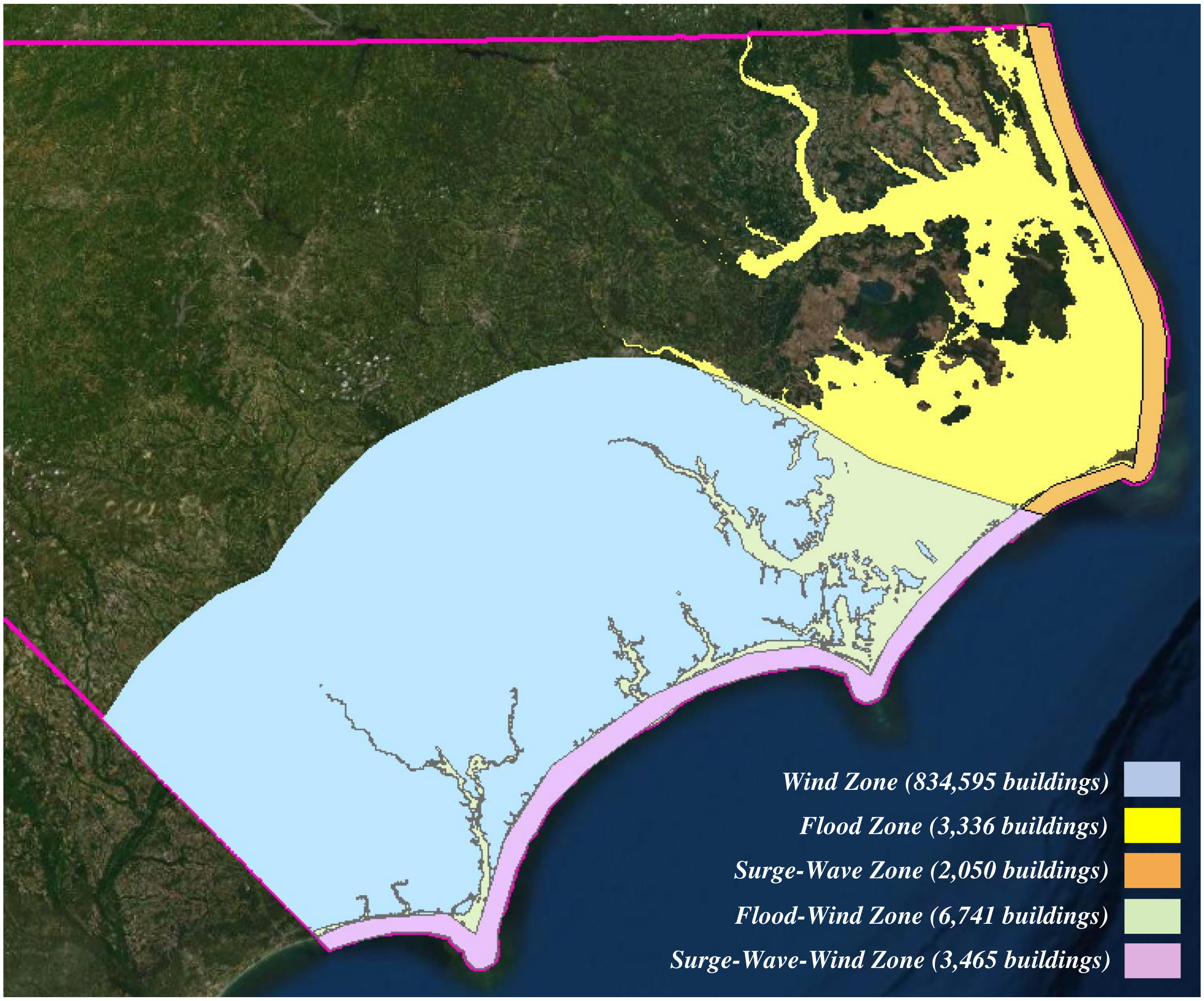

Figure 5-32. *The different exposed zones to hurricane-induced hazards for the state of North Carolina corresponding to the 2018 Hurricane Florence*

Table 5-5. *The number of buildings exposed to the hazards induced by Hurricane Florence (2018)*

Hazard type	Hazard intensity	Number of buildings
Wind (m/s)	$31.0 <= V_w < 34.0$	315706
	$34.0 <= V_w < 37.0$	320552
	$37.0 <= V_w < 40.0$	208543
	$40.0 <= V_w$	0
Surge (m)	$0.0 <= d_s < 1.0$	2434
	$1.0 <= d_s < 2.0$	8391
	$2.0 <= d_s < 3.0$	4763
	$3.0 <= d_s$	4
Wave (m)	$0.0 <= H_s < 0.5$	9648
	$0.5 <= H_s < 1.0$	5080
	$1.0 <= H_s < 2.0$	152
	$2.0 <= H_s$	0

There are more than five million buildings in North Carolina, but the vulnerability analysis only included the 857,046 identified as being exposed to hurricane-induced hazards. The building archetypes corresponding to each hazard were assigned to the exposed buildings only and the other buildings were removed from the analysis. Then, a fragility function corresponding to each building archetype associated with each hazard type was assigned to each exposed building using the mapping algorithm. Figure 5-33 shows color-coded maps for Carolina Beach (coastal community in North Carolina) based on the building archetypes associated with each hazard type. The digital elevation map (DEM) of the study area was used to extract the ground elevation (GE) of each building within the exposed area. Afterwards, the developed hazard maps based on Hurricane Florence were overlaid with the community model to account for the exposed buildings and the hazard intensity at each one of these buildings as shown in Figure 5-34. For example, the surge height was calculated by subtracting the FFE from the water surface elevation to account for the flood depth. Then, the GE was subtracted from the FFE to account for the absolute elevation from the ground for each building to be used in the surge-wave and flood fragility functions.

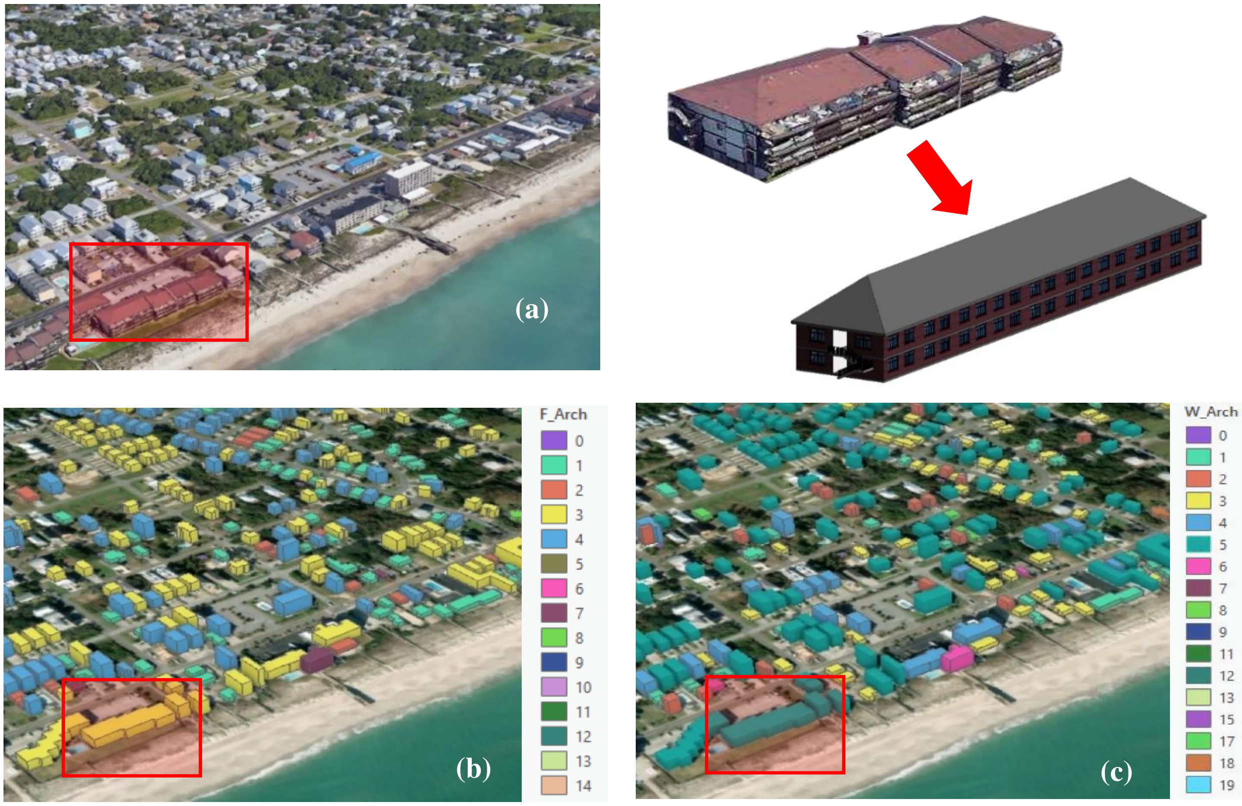

Figure 5-33. *Example of the archetypes assignment to each building within the community based on each mapped building archetype: (a) A Google earth close-up view on Carolina Beach, NC; (b) Color-coded buildings based on the 15 flood archetypes; (c) Color-coded buildings based on the 19 wind archetypes*

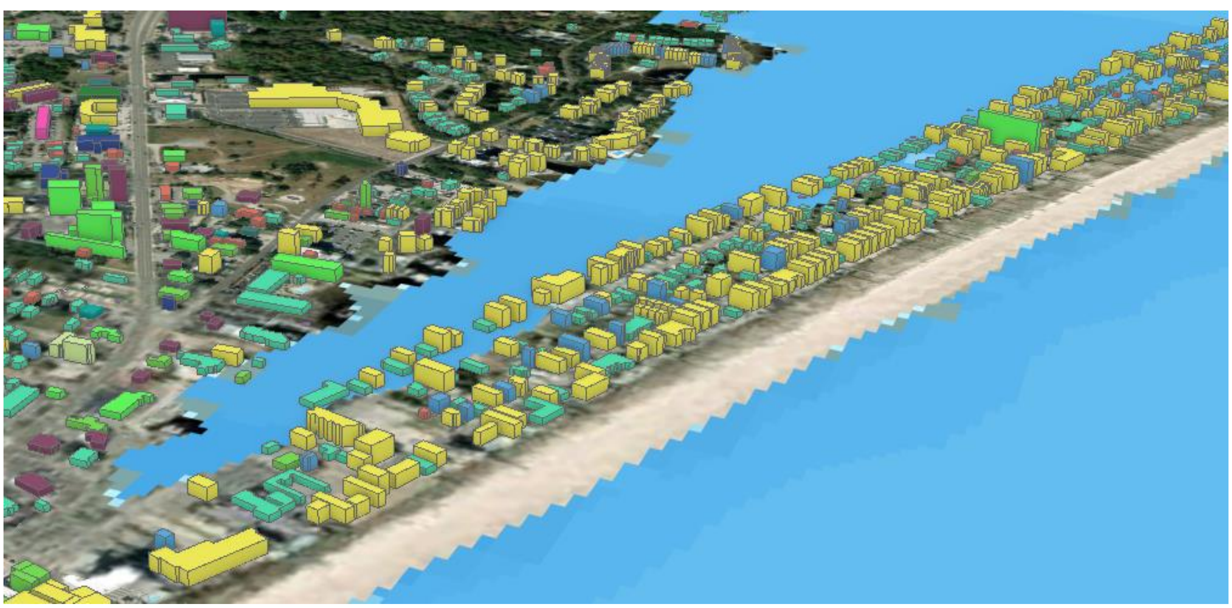

Figure 5-34. *The surge map overlaid with the community model for Carolina Beach (Coastal Community in North Carolina)*

5.3.3 Hurricane Risk Analysis

A damage and loss analysis algorithm based on the flowchart shown in Figure 3-11 in Chapter 3 was developed to read the hazard, exposure, and vulnerability of each building within the illustrative example. Then, the amount of damage and loss for the structural system and interior contents for each building was calculated in terms of the exceedance probability of each DS corresponding to each hazard (surge, wave, and wind). An extreme flood duration of 10 days was assumed in this analysis, but the model can incorporate any flood duration if desired. This duration simply damages any components within the building models that would otherwise be able to be dried or salvaged, so provides an upper bound on damage from a duration perspective. Table 5-6 provides a summary of the community-level risk analysis by dividing the probability of exceeding each DS corresponding to each hazard into six ranges and providing the number of buildings within each range. For example, there are 246 buildings with more than an 80% exceedance probability of DS3 corresponding to flood hazard (inundation), which is used to account for the content damage. However, there are 417 buildings with more than an 80% exceedance probability of DS3 corresponding to surge-wave hazard, which is used to account for structural damage. There are 34 buildings with more than an 80% exceedance probability of DS2 corresponding to wind hazard which is also used to account for structural damage. Finally, each building was assigned a DS based on the maximum probability of being in that DS corresponding to each hazard. Table 5-7 summarizes the number of buildings within each DS associated with each hazard along with their final DS assignment based on the maximum DS from surge-wave, wind, and flood.

Table 5-6. *Damage states exceedance probability corresponding to each hurricane-induced hazard for the exposed buildings on the coastal line of the State of North Carolina*

Hazard Type	Exceedance Probability of a DS (Fragility)	Number of buildings (total=857,046)				
		DS0	DS1	DS2	DS3	DS4
Surge-Wave	P_DS = 0%	-	849,396	850,150	852,389	853,930
	0% < P_DS < 20%	-	4,342	3,781	2,459	1,575
	20% < P_DS < 40%	-	568	596	956	899
	40% < P_DS < 60%	-	666	584	622	151
	60% < P_DS < 80%	-	912	941	203	126
	80% < P_DS < 100%	-	1,162	994	417	365
Flood	P_DS = 0%	850,377	846,895	847,913	851,860	-
	0% < P_DS < 20%	179	546	856	2,801	-
	20% < P_DS < 40%	108	426	491	1,239	-
	40% < P_DS < 60%	149	501	680	541	-
	60% < P_DS < 80%	421	555	1,039	359	-
	80% < P_DS < 100%	5,812	8,123	6,067	246	-
Wind	P_DS = 0%	-	512,983	365,893	669,698	770,389
	0% < P_DS < 20%	-	115,495	438,251	187,348	86,657
	20% < P_DS < 40%	-	51,475	35,184	0	0
	40% < P_DS < 60%	-	28,325	14,768	0	0
	60% < P_DS < 80%	-	81,910	2,916	0	0
	80% < P_DS < 100%	-	66,858	34	0	0

The final hurricane risk analysis showed that there were 857, 046 buildings exposed to the multiple hazards induced by Hurricane Florence in 2018 including surge, wave, and wind. Of those, simulation results showed that there were 686,990 buildings designated as DS0, which means they did not encounter any damage from surge, wave, or wind. However, 170,056 buildings received some level of damage ranging from DS1 up to DS4, as shown in the last row of Table 5-7. The content and structural damage for each building were calculated to account for the total building losses. Table 5-8 provides six loss ranges and the number of buildings within each range. The presented content losses in Table 8 were calculated as a percentage of the total value of the content, not the total building value. Similarly, the structural losses were calculated as a percentage of the total value of the building structural system. It should be noted that there are 686,990 buildings designated as DS0, but the number of buildings with zero losses is 685,514, which means there are 1,476 buildings designated DS0 but with losses greater than zero. These 1,476 buildings had crawlspace foundations (Archetypes F1 and F3) and experienced flood damage to components below FFE and insignificant content losses (0-4%).

Table 5-7. *Assigned damage states corresponding to each hurricane-induced hazard for the exposed buildings on the coastal line of North Carolina based on Hurricane Florence (2018)*

Hazard Type	Number of buildings (total=857,046)				
	DS0	DS1	DS2	DS3	DS4
Surge-Wave	855,382	0	941	3	720
Flood	848,150	1,167	6,758	971	-
Wind	695,237	150,333	11,476	0	0
Multi-Hazard	686,990	150,835	17,616	885	720

Table 5-8. *Calculated losses for the impacted buildings in North Carolina in terms of structural, content, and total losses based on Hurricane Florence (2018)*

Loss (%)	Number of buildings (total=857,046)		
	L_Content	L_Structure	L_total
L = 0	846,442	693,580	685,514
0% < L < 20%	2,314	134,957	163,695
20% < L < 40%	1,644	27,242	3,360
40% < L < 60%	3,693	752	3,385
60% < L < 80%	2,198	357	983
80% < L < 100%	755	158	109

Although some of the buildings that were exposed to surge-wave hazard were also exposed to wind hazard, the wind speed was not high enough to cause damage to many of these buildings. Therefore, only a few buildings had structural damage resulting from both wind and surge-wave at the same time. Further, the DSs of the buildings that were damaged by the wind did not exceed DS2, because the maximum wind speed during Hurricane Florence at landfall was only 41.0 m/s. Figure 5-35(a) shows the spatial location of the investigated 857,046 buildings investigated in this example. Figure 5-35(c) shows a close-up view of the locations where buildings were damaged by wind color-coded based on the wind DSs. Figure 5-35(b) shows a close-up view of the area around the Pamlico River that was severely impacted by surge-wave hazard. The surge height simulation in this area ranged from 2.25m to 2.65m, and the simulated significant wave height ranged from 0.5m to 0.75 m. The United States Geological Survey (USGS) sensor in this area recorded a high watermark of 2.3m (7.5ft) (Stacy R. Stewart and Robbie Berg, 2019), which suggests that the simulated surge height has a reasonable agreement with the field-measured data. Figure 5-35(d-f) shows a closer view of Washington, NC, located on the east bank of the Pamlico River with the impacted buildings color-coded based on their content, structural, and total damage, respectively, in terms of the DS assigned to each building. The risk analysis of the buildings vulnerable to the combined storm surge and waves revealed that although many buildings were not damaged structurally (DS0) as shown in Figure 5-35(e), some had slight to complete content damage (DS1-DS3) as shown in Figure 5-35(d) due to the flood inundation from hurricane storm surge. This affects the final DSs assigned to each one of these buildings, as shown in Figure 5-35(f) which are based on the maximum DS from content and structural damage.

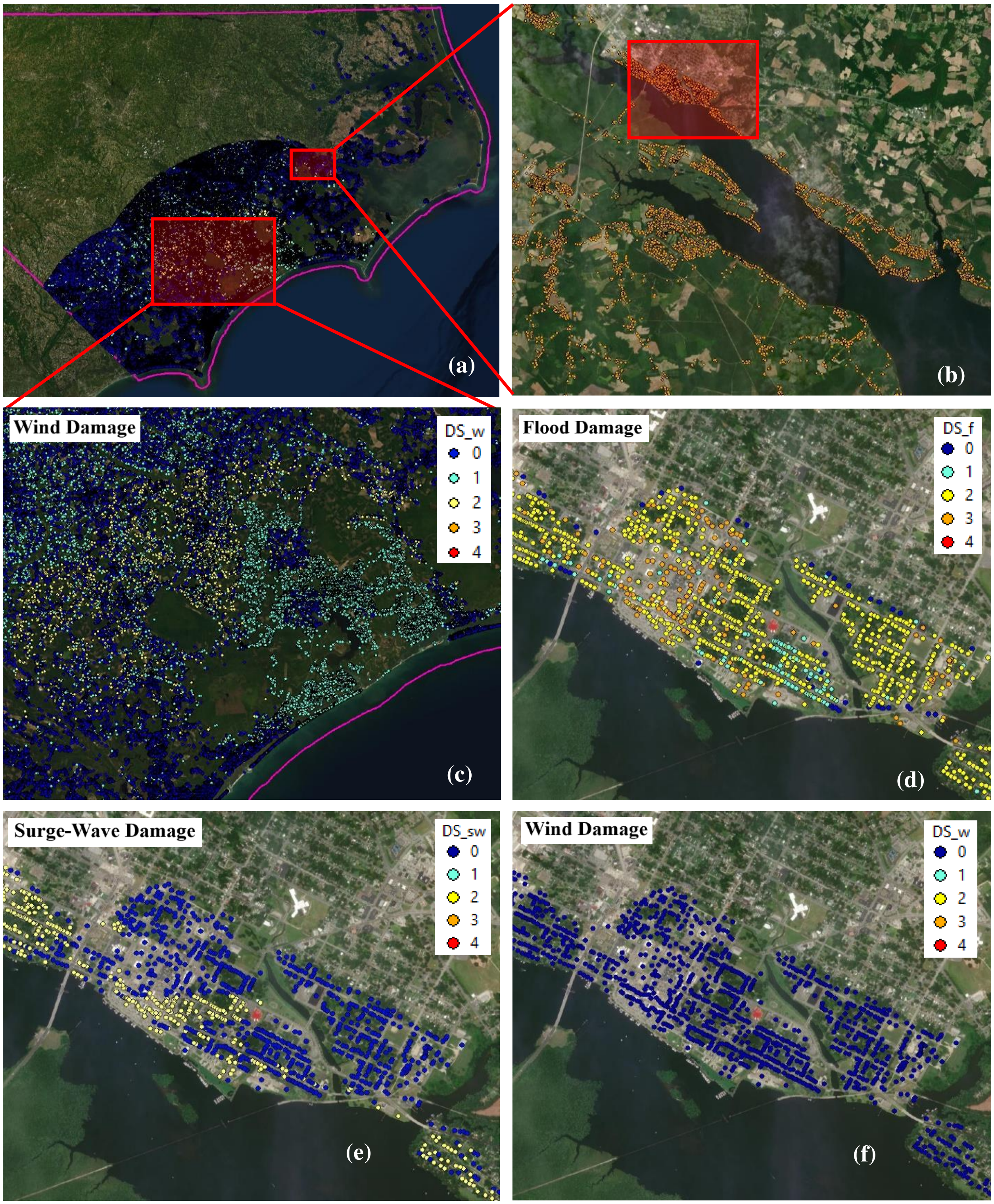

Figure 5-35. *The damage state for the exposed buildings on some selected locations on the coastal line of the State of North Carolina due to the 2018 Hurricane Florence: (a) The exposed buildings location; (b) A close-up view on the east bank of the Pamlico River; (c) A close-up view on the wind impacted locations; (d) Color-coded buildings based on content damage; (d) Color-coded buildings based on content damage; (d) Color-coded buildings based on structural damage; (d) Color-coded buildings based on total damage*

The structural and content losses corresponding to each building were calculated using Eq. (3-2) from Chapter 3. Figure 5-36 shows a close-up view of Washington, NC with color-coded buildings based on their losses as a percentage of the replacement cost corresponding to each building. Figure 5-36(a) shows the content loss as a percentage of the market value of the content and Figure 5-36(b) shows the structural losses as a percentage of the market value of the structural system. The loss analysis also showed that there were a large number of buildings with zero structural losses (blue dots) but had content losses up to 80% (red dots). This can be seen reflected in the final total building losses, as shown in Figure 5-36(c). The loss analysis results are consistent with the damage analysis results, as shown in Figure 5-36(d).

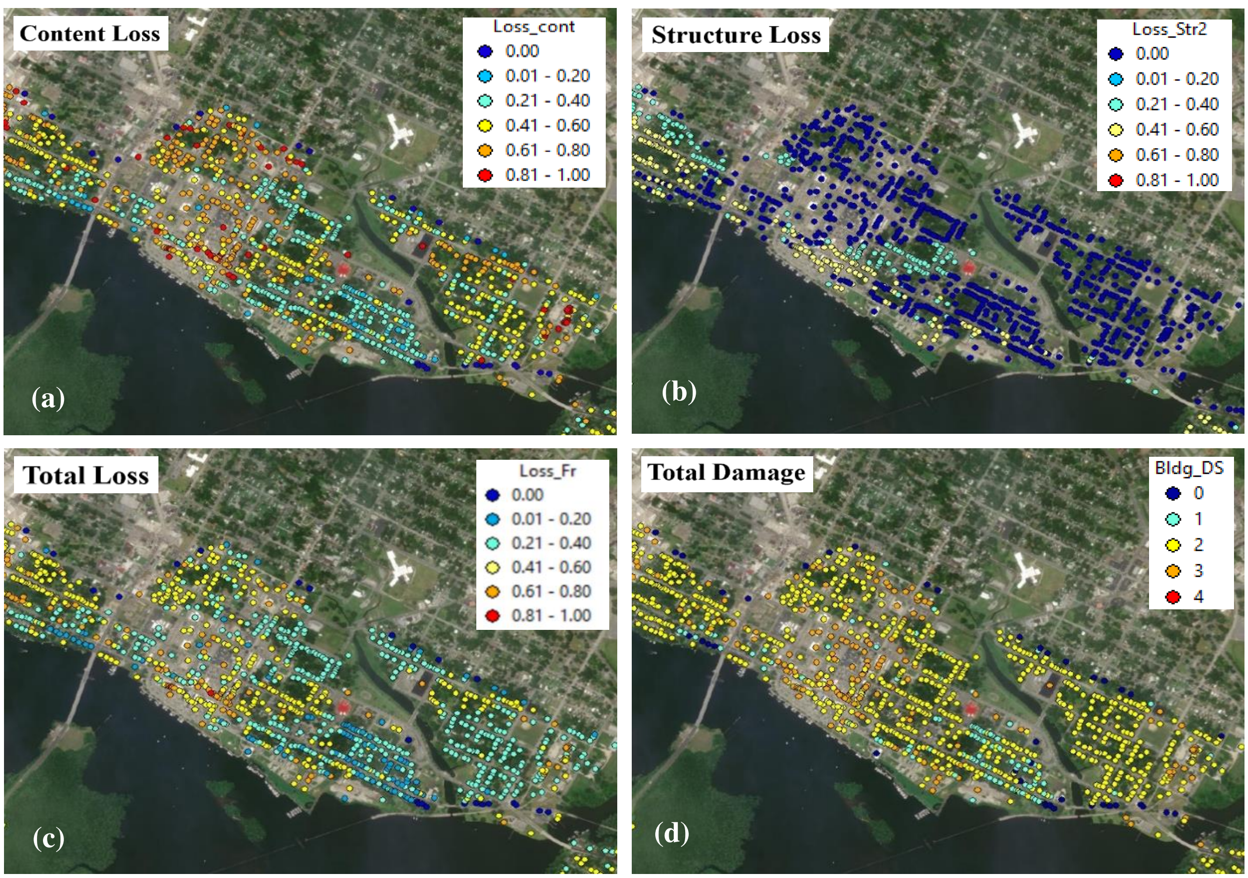

Figure 5-36. *The loss analysis results for the exposed buildings in Washington, NC due to the Hurricane Florence (2018): (a) Color-coded buildings based on content losses; (b) Color-coded buildings based on structural losses; (c) Color-coded buildings based on total losses; (d) Color-coded buildings based on building damage*

5.4 Example 3: Waveland, Mississippi

The coastal community of Waveland, Mississippi, was used to illustrate the framework developed in Chapter 3 in this dissertation. Waveland is a small coastal community located in Hancock County, Mississippi with a population of only 6300 people and 2700 buildings. Figure 5-37 shows the spatial location of Waveland within the state of Mississippi in the southern part of the U.S. with a close-up view of the city's location. Most of the buildings in Waveland are single-family dwellings with some multi-family and commercial buildings in the northern part of the community. Waveland was selected as an example community herein because of the repeated impacts of hurricane hazards including Hurricane Camille in August 1969 and Hurricane Katrina in August 2005. Waveland, Mississippi was ground zero for Hurricane Katrina's landfall in August 2005. Hurricane Katrina left massive devastation to the community built environment. After 14 years of Hurricane Katrina, Waveland, MS is still recovering and rebuilding.

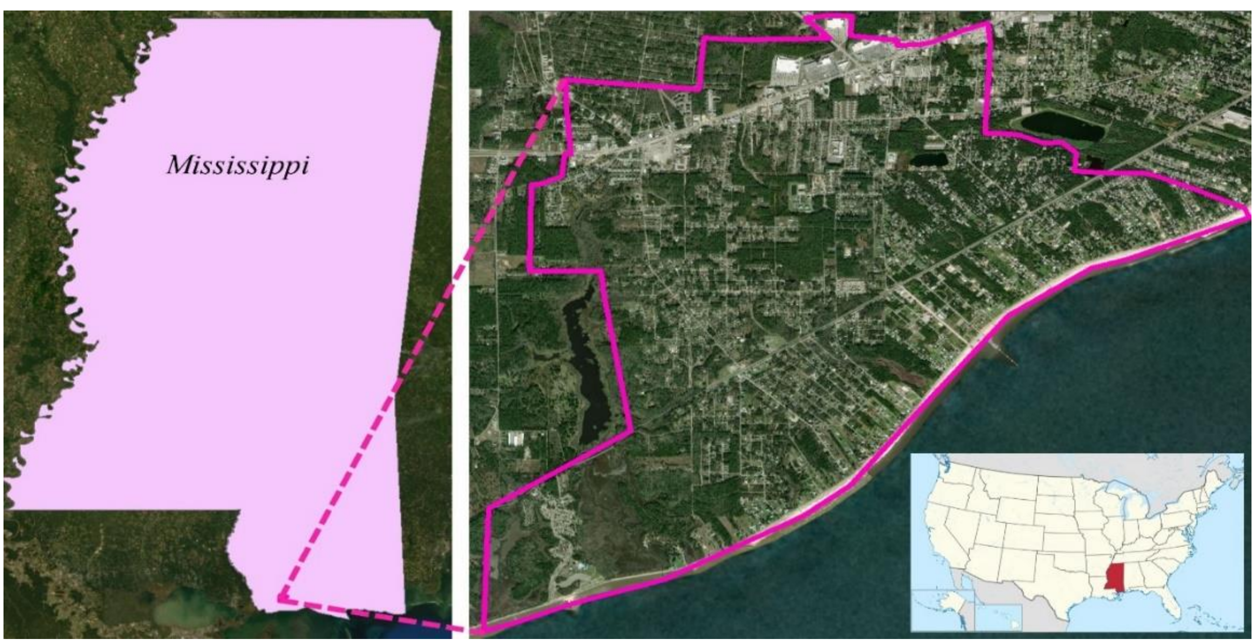

Figure 5-37. *The spatial location of Waveland city within Mississippi State*

5.4.1 Hazard Scenario

Hurricane Katrina started as a tropical depression in the Bahamas on August 23, 2005. The storm strengthened into a tropical storm on August 24 to make landfall as a category 1 storm in Florida on August 25. The storm weakened over land and gained strength again after entering the Gulf of Mexico and reach category 3 by the end of August 26. The storm kept gaining strength in the Gulf of Mexico to reach category 5 to be the fifth most intense Atlantic hurricane on record at the time. Hurricane Katrina was recognized as the strongest hurricane ever recorded in the Gulf of Mexico at the time before Hurricane Rita broke this record in the same year. Hurricane Katrina made its second landfall as a category 3 storm near the Louisiana-Mississippi border on August 29. Figure 5-38 shows the spatial evolution of Hurricane Katrina over time across the Gulf of Mexico.

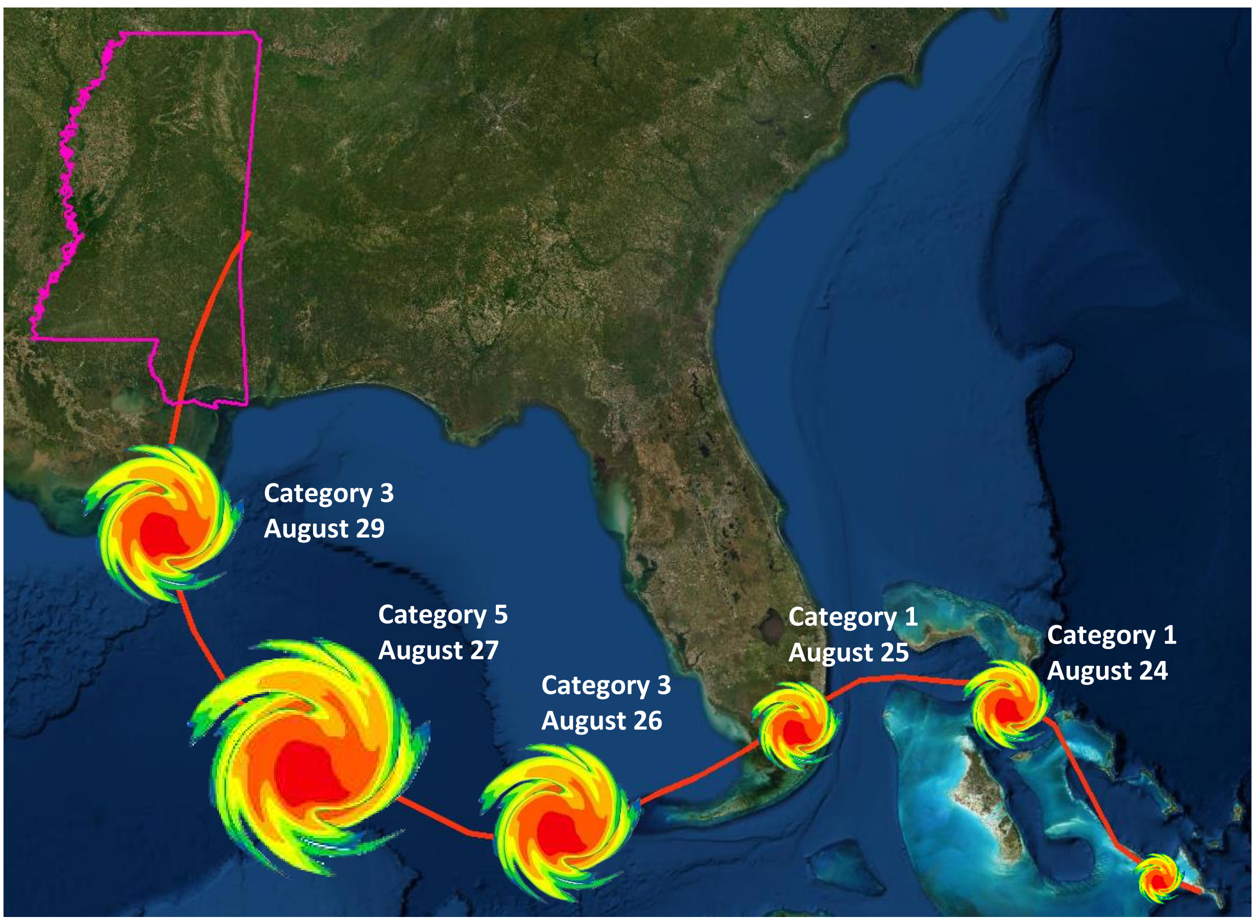

Figure 5-38. *Hurricane Katrina in 2005 path and the category evolving over the time*

The surge, wave, and wind hazard maps are based on the concept introduced in subsection 3.3.1 and similar to the previous application on the state of North Carolina. The wind hazard is modeled using a combination of the NOAA hurricane research division wind analysis system and an interactive objective kinematic wind analysis model. The surge and wave hazards are modeled using a tightly coupled ADCIRC and SWAN model. Figure 5-39 shows the resulted hazard maps for Waveland. Mississippi.

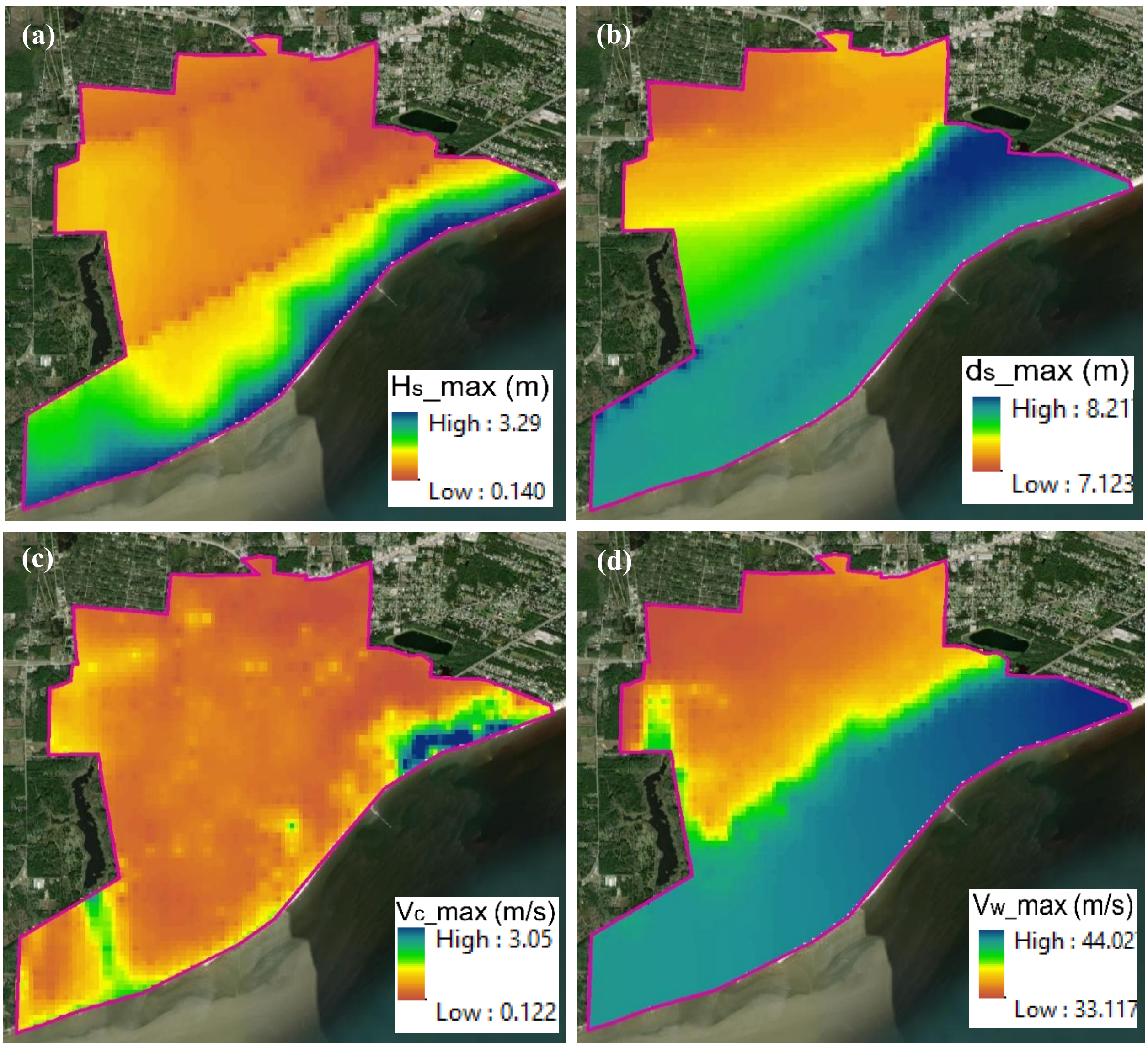

Figure 5-39. *Hazard maps for the multiple hazards driven by Hurricane Katrina 2005: (a) Maximum significant wave height (H_s_max (m)); (b) Maximum water level (surge) height (d_s_max (m)); (c) Maximum current speed (V_c_max (m/s)); (d) Maximum wind speed (V_w_max (m/s))*

5.4.2 Exposure and Vulnerability Modeling

The building spatial data for Waveland, Mississippi are not available online, but detailed building information was needed to build the community-level flood risk model. Therefore, detailed navigation of the 2700 buildings was conducted using Google Street Map View. Detailed building information was collected including building occupancy, foundation type, FFE, roof shape, number of stories along with many other data that could be visualized from the street view. Figure 5-40 shows a color-coded map based on the flood archetypes developed in Chapter 2.

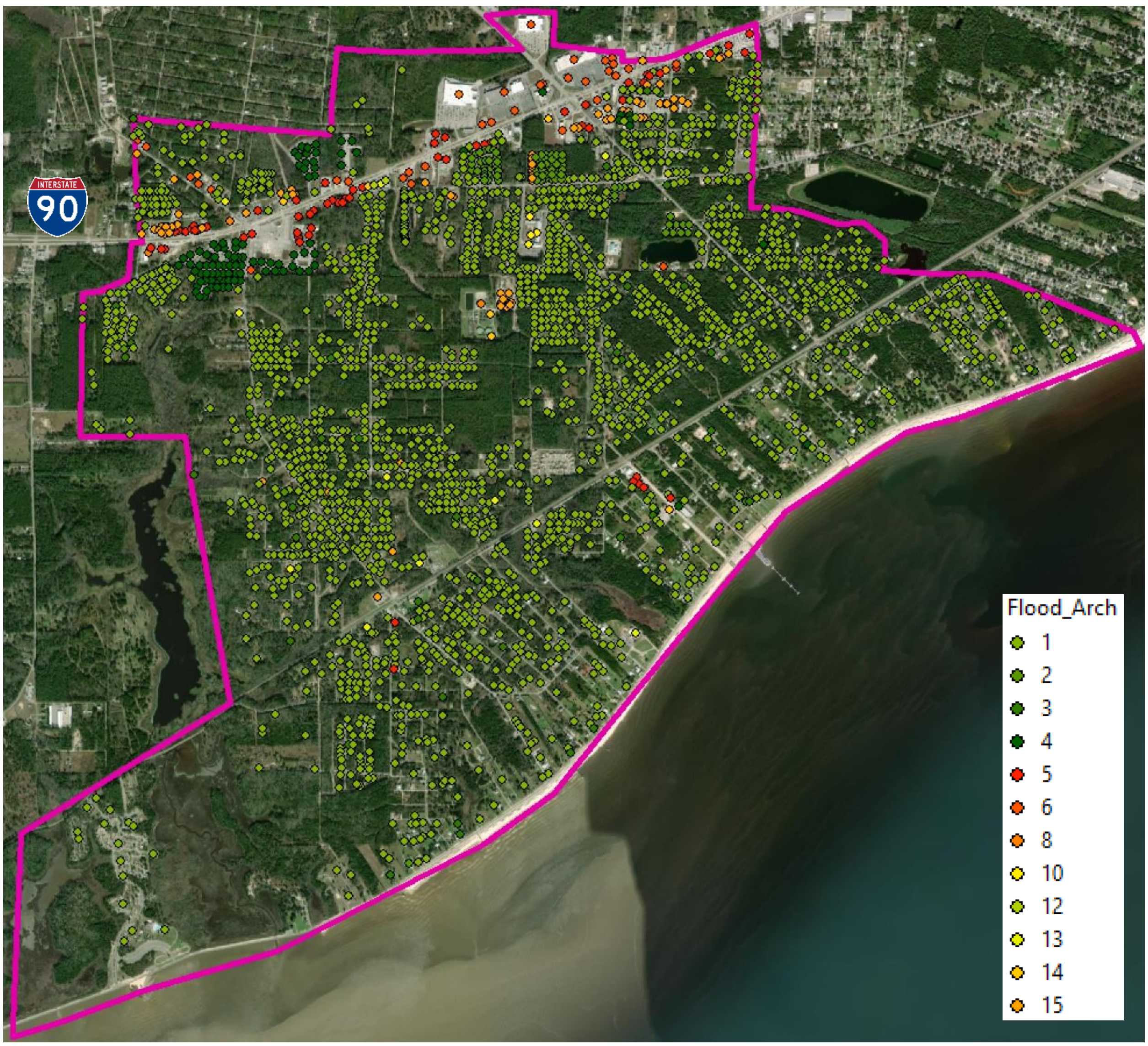

Figure 5-40. *Color-coded map based on the building flood archetypes*

Most of the buildings on the coast are residential buildings as shown in Figure 5-40 with residential buildings in green. Other building occupancies including commercial and social buildings show up as we move north inland. The developed flood archetypes developed in Chapter 2 along with the wind archetypes portfolio illustrated in Chapter 3 were assigned to each building based on their occupancy and their physical characteristics. Afterwards, the flood fragility corresponding to each hazard associated with each building archetype was assigned to the buildings using the concept developed in Chapter 3.

5.4.3 Hurricane Risk Analysis

The concept summarized in Chapter 3 was applied herein to Waveland, Mississippi to account for the damage state for each building and its corresponding amount of losses. Therefore, the hazard maps developed for hurricane Katrina in terms of surge, wave, and wind hazard layers were overlaid onto the community model. Figure 5-41 shows a schematic representation of the hurricane risk components for Waveland, MS including hazard, exposure, and vulnerability models. The intensity of each hazard (surge, wave, and wind) was extracted for each building within the example community. Then, the algorithm developed in subsection 3.3.4 was used to compute the exceedance probability of each DS corresponding to each hazard intensity. A single DS is assigned to each building based on the maximum probability of being in each DS calculated from each fragility function corresponding to each hazard using Eq. (3-1). Then, fragility-based losses were calculated by multiplying the probability of being in each DS by the replacement cost associated with each DS using Eq. (3-2). Buildings damage was calculated in terms of content damage, structure, and non-structural damage. The structural damage was further divided into damage caused by wind loads and damage caused by surge-wave loads. Finally, damage and loss results are mapped to the buildings to account for the spatial damage distribution across the community.

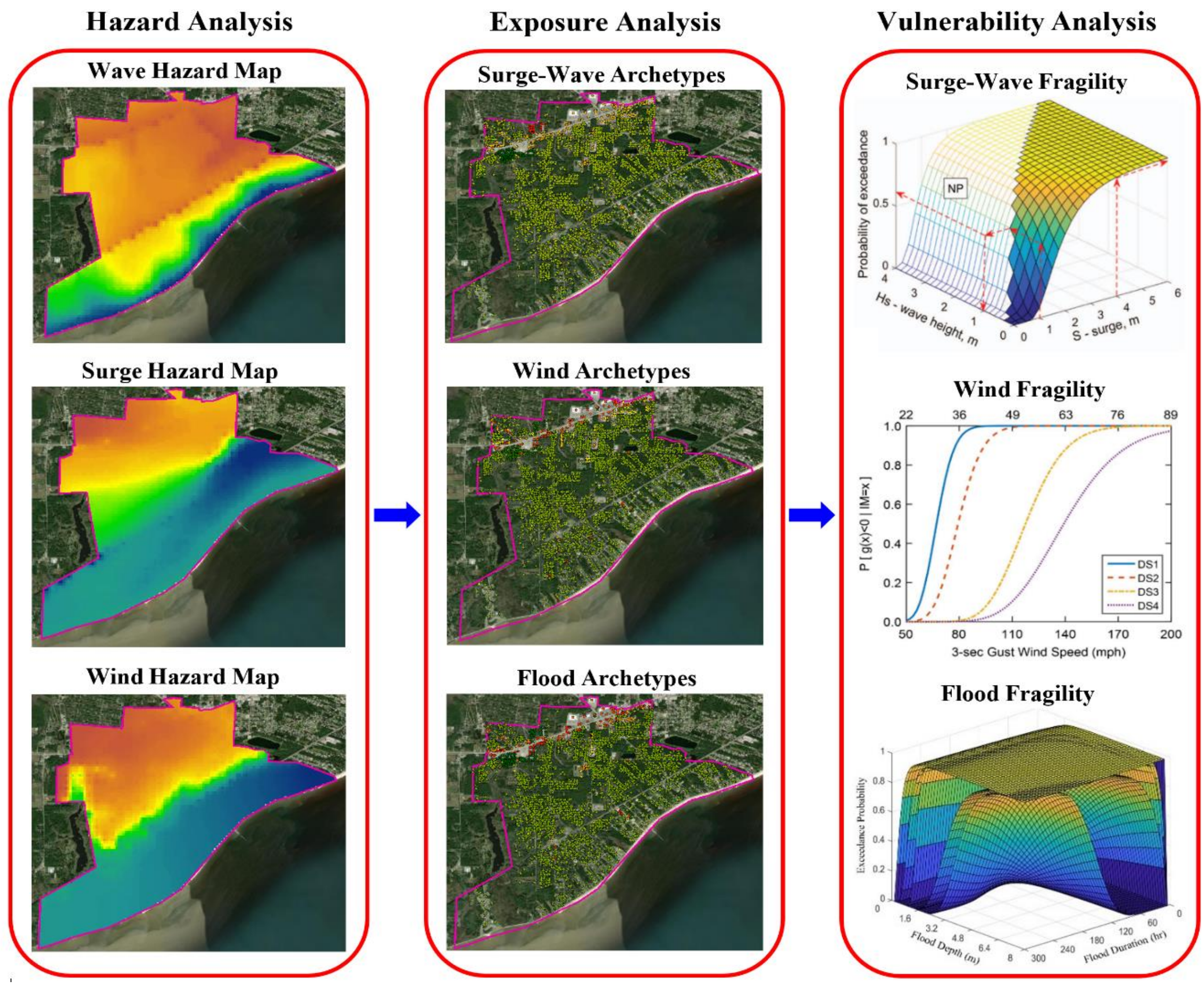

Figure 5- 41. *A schematic representation of the community-level hurricane multi-hazard risk analysis framework*

The damage analysis showed that most of the buildings experienced a DS4 level for surge-wave loads, with a few buildings designated as DS3. This is because of the high surge and waves driven by the Hurricane Katrina simulation, with surge heights exceeding 7.0 m and wave heights of more than 3.0 m, which when combined are easily enough to cause DS4 even for elevated buildings. For wind loads, most of the buildings were characterized as DS1 since the maximum wind speed was 44 m/s (wind speeds are not the full marine strength, but rather have been reduced due to canopy and overland roughness), which typically only causes damage to the building envelope. Thus, as was observed in Katrina, the surge-wave hazard was the dominant cause of building damage. In terms of content damage, most of the buildings were characterized as DS3, or complete damage to the building contents. Finally, assigning the maximum DS from surge-wave, wind, and static flooding results in characterizing most of the buildings as DS4 with losses ranging from 75-100% of the buildings' market value, as shown in Figure 5-42.

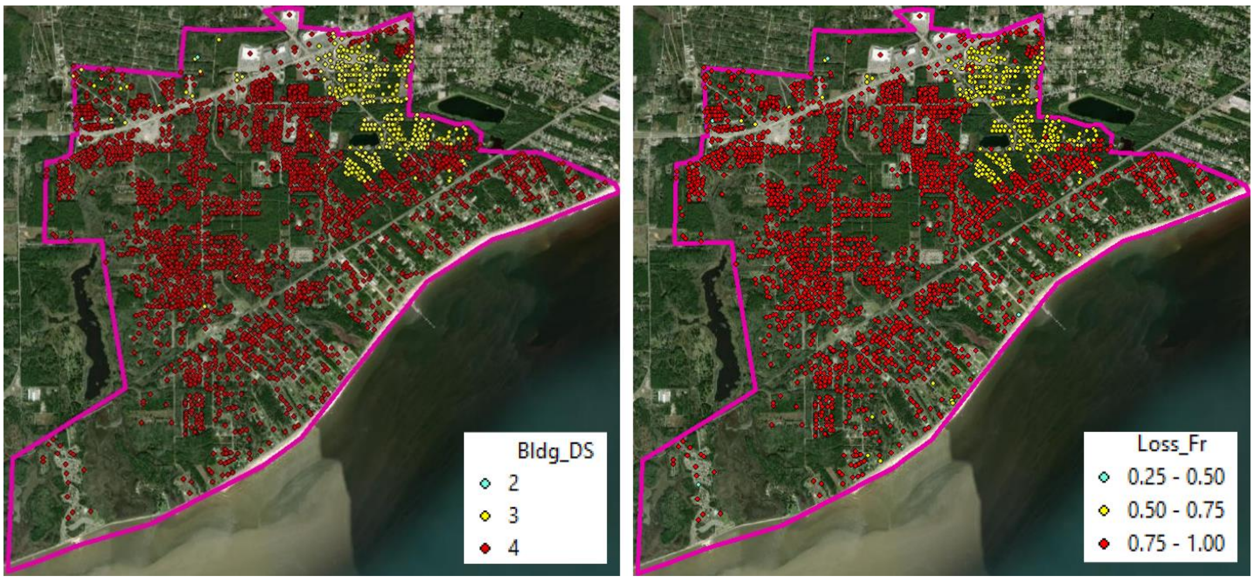

Figure 5-42. *Color-coded map for the spatial distribution of damage/loss across the example community: (a) Building DS; (b) Building loss ratio*

CHAPTER 6: SUMMARY AND CONCLUSIONS, CONTRIBUTIONS, AND RECOMMENDATIONS

6.1 Summary and Conclusions

In this dissertation, a high-resolution multi-hazard hurricane risk analysis approach for inland and coastal communities was developed to account for the broad hurricane-induced impacts at the community level. This was accomplished by developing component-based multi-variate probabilistic flood vulnerability functions which were applied to develop a portfolio of 15 building archetypes to model flood vulnerability at the community-level. These functions enabled the calculation of flood risk at a high-resolution for inland communities and provided a systematic approach for mitigation analysis at the component-, building-, and community-level. These fragility functions are adjustable such that they included the impact of using flood mitigation measures at the component- and building-level. Once the flood fragility functions were completed, they were combined with existing surge-wave and wind fragility functions to develop a convolutional vulnerability model for near-coast buildings. This model accounts for the impact of the hurricane-induced hazards (surge, waves, and wind) on the different building components including structural, non-structural, and interior contents. This was done by developing high-resolution models for the hazard, exposure, and vulnerability models. The methodology is extensible to include the impact of other hazards in the vulnerability model and scalable to be applied for small communities, large communities, or even at the regional level. A number of case studies were used to illustrate the applicability of the models. The methodology has been included in IN-CORE to provide proper access to the models along with an IN-CORE example Jupyter notebook.

Chapter 2 provides the basis for developing flood fragility functions for buildings and shows the new methodology to develop 2-D and 3-D flood damage fragilities and their associated loss estimates. The approach explained in this dissertation distinguished between a single-variable and multi-variate fragility and loss function by, initially, considering flood depth to develop 2D fragilities and loss curves and, then, considering both flood depth and flood duration to develop 3-D fragilities and loss surfaces. The proposed flood fragility and loss approaches do not require field study data to generate flood fragilities and probabilistic loss functions for buildings. This allows one to, in theory, create a damage fragility and loss prediction model for any building of interest. The 2D flood fragility and loss functions developed herein for the whole building and its components after propagating uncertainties in the flood depth and repair/replacement costs of each component compared favorably to the empirical losses in HAZUS-MH. Additionally, multi-variate 3D flood fragility and probabilistic loss surfaces for an entire building and its components were generated by propagating uncertainties in the flood depth, flood duration, and replacement cost of each component with existing data sources.

Based on the work presented in chapter 2, it can be concluded that:

1- Flood depth alone may not be enough to accurately predict the amount of damage, and subsequently, flood risk for buildings and the inclusion of flood duration would give a better estimate of the probability of building flood losses.
2- The proposed flood vulnerability approach could be extended to develop fragility functions for any building of interest and assemble a different building archetype portfolio for community-level analysis in order to capture performance and functionality following flood events.

Chapter 3 provided an approach to account for the vulnerability of coastal and inland communities to hurricane-induced hazards. This approach uses the developed flood fragility functions in Chapter 2 along with well-established fragility functions from the literature for surge-wave and wind hazards. For in-land communities, a detailed flood risk assessment procedure was illustrated to capture the spatial distribution of flood damage/losses, while propagating uncertainty through the analysis. The risk models were developed using high-resolution models of the hazard, exposure, vulnerability. For coastal communities, a high-fidelity (individual buildings used in the calculations) multi-hazard hurricane risk analysis method was developed to account for large-scale impacts of multiple loadings induced by hurricanes. The concept of combining building portfolios from different hazards was introduced to model hurricane vulnerability at large spatial scales. The combined impacts of surge, wave, and wind on the structural system and interior contents were the novel focus of this study. For the first time, five input variables were used as input for these fragility functions, namely the significant wave height, the surge still water depth, building elevation from the ground, maximum wind speed, and flood duration.

Based on the work presented in chapter 3, it can be concluded that:

3- The fragility-based multi-hazard vulnerability analysis approach developed herein can provide a mechanism to propagate uncertainty in damage and loss estimates for buildings and thereby allowing risk analysis at the community-level.

4- Combining the structural and content damage can provide a better estimate of the final damage/loss, as well as a better opportunity to investigate the impact of the different mitigation measures at the building-level.

5- The scalability of the methodology enables large-scale hurricane damage assessment with detailed quantification of the loadings and their associated impacts on both the structural system and the interior contents.

Chapter 4 provides a high-resolution approach to quantify the impact of a number of flood mitigation measures. The investigated flood mitigation measures have been qualitatively described in flood mitigation standards with less quantitative modeling approaches provided. A methodology that allows quantifying the impact of using component-level and building-level flood mitigation measures has been developed. Using flood barriers for buildings was investigated in terms of their damage/loss reduction at the building- and community-level. Additionally, the analysis provided a methodology to model the impact of decreasing flood duration using water pumps on flood losses by considering a number of flood duration scenarios associated with pumping scenarios. The impact of home mitigation such as rerouting ductwork or elevating water-sensitive components was also investigated using the component-based flood vulnerability method. The impact of using these building-level mitigation measures was applied to the developed portfolio of 15 building archetypes to model the community-level flood vulnerability. Additionally, a number of community-level flood control measures was investigated such as floodgates, levees, and retention systems. Afterwards, a suite of component-, building-, and community-level mitigation scenarios was then applied to one of the case studies in Chapter 5, namely Lumberton, NC. The community-level flood losses associated with each mitigation scenario were then calculated and compared with the baseline case (without any mitigation).

Based on the work presented in chapter 4, it can be concluded that:

6- Temporary flood barriers are the most efficient flood mitigation system in terms of significantly decreasing both building-level and community-level flood losses. However, this efficiency suddenly drops to zero if the flood depth exceeds the barrier height and it should be noted that the ability to deploy them rapidly enough is an unknown.

7- Using water pumps to decrease flood duration is only efficient if the water duration is reduced to be less than two days. This shorter flood duration range can save some non-structural components along with a complete savings of the structural system.

8- Elevating some select water-sensitive components with the proposed elevations can reduce flood losses by up to 13% of the total building replacement cost (for archetype F2, but may vary by archetype).

9- Although, some mitigation measures can provide protection for certain buildings in the flood plain, they may increase the flood vulnerability of other buildings which was the case when enhancing the embankment\levee system for Lumberton, NC. Therefore, considering this mitigation measure should be accompanied by either home buyouts or increased buildings elevations.

Chapter 5 provides several applications for the developed models and approaches in this dissertation using real case studies and historical hurricane hazards. For each case study, detailed hazard, exposure, vulnerability, and risk analysis was conducted along with the analysis results in terms of detailed buildings damage/loss.

6.2 Contributions

The research developed in this dissertation provides multiple contributions to the profession which are summarized such as follow:

Development of probabilistic multivariate flood fragility and loss functions: The proposed flood fragility and loss approaches propagate uncertainties in flood depth, flood duration, and the components' replacement costs. These functions do not require field study data to generate a flood fragility and probabilistic loss function for a building. They also allow the analyst to, in theory, create a damage fragility and loss prediction model for any building of interest. The generality and the scalability of the developed approach allow them to be used for different building types and facilities.

Development of the flood fragility archetype portfolio: A minimal building flood fragility and loss function portfolio was developed for 15 building archetypes. These archetypes were selected such that they could represent an array of building occupancies within a community and thereby model flood vulnerability at the community-level. The fragility functions for this building portfolio are available in IN-CORE to be used in community resilience analysis.

Development of high-resolution community-level flood risk analysis methodology: A high-resolution flood risk analysis approach was developed. This approach uses building-level information and a high-fidelity flood hazard model along with the fragility portfolio to map the flood risk to each building across the community. The approach allows the analyst to propagate uncertainties in the flood risk analysis at the community level and predict the damage to each building within the community in terms of the exceedance probability of a set of prescribed damage states.

Development of a quantitative high-resolution flood mitigation analysis approach: A high-resolution quantitative mitigation analysis approach was developed to account for the impact of different types of flood mitigation measures at the component-, building-, and community-level on the community-level flood loss reduction. This approach modifies the developed fragility functions to account for the impact of elevating the water-sensitive components, building elevation, and the using of flood barriers and water pumps.

Development of multi-hazard hurricane risk model: A multi-hazard high-resolution hurricane risk model was developed to account for the combined impacts of the hurricane-induced hazards including surge, wave, and wind on coastal communities in terms of the damage to the structural and non-structural components and the interior content. The resolution used in this model allows the analyst to calculate the vulnerability of each component within the building to account for the total building vulnerability.

Enabling community-level flood analysis using IN-CORE: The models developed within this dissertation research have been included in the **I**nterdependent **N**etworked **Co**mmunity **R**esilience Modeling **E**nvironment (IN-CORE) which allows users to use these models in different types of engineering, social, and economic analyses. The user will only have to upload the community of interest and the hazard model and then IN-CORE can use the damage analysis algorithm to predict the damage for each building within the community.

6.3 Recommendations

The research in this dissertation paved the way for other future research and thus a number of recommendations for future work are described below.

Population dislocation: The analysis results from the building damage analysis can be further used to account for the disruption to the different building sectors (e.g., residential sector, commercial sector, and the social institutions, etc.). The resulting disruption can be further used in social science models to account for the population dislocation.

Indirect economic losses: The damage to the different building sectors in the flood plain affects the economic activity inside and outside the floodplain due to population outmigration and business disruption. Therefore, further analyses should be pursued to account for the loss of customers and labor inside and outside the floodplain, and economic losses using a computable general equilibrium (CGE) economic model.

Post-hazard functionality: A comprehensive post-hazard functionality model should be developed using the output from the building damage analysis along with the output from other models that account for utilities disruption and population dislocation.

Building- and community-level recovery model: The building damage analysis results can be used as an initial recovery stage for a robust recovery model that accounts for the impact of both physical damage and the socio-economic information of the impacted household.

Wind-rainfall intrusion and wind-borne debris damage: The multi-hazard hurricane risk model accounts for the combined impact of surge, wave, and wind on structural and content damage. This model can further include other hazards such as rainfall intrusion and wind-borne debris damage.

Optimal mitigation strategies: Different types of mitigation measures were investigated in terms of their associated flood loss reduction. This analysis could be further used in multi-objective optimization to optimize the cost, post-hazard functionality, recovery, etc.

REFERENCES

Abdelhady, A. U., Lin, S.-Y., Xu, L., Sediek, O. A., Hlynka, A. W., El-Tawil, S., … Menassa, C. (2019). "A Distributed Computing Platform for Community Resilience Estimation." In *Conference: 13th International Conference on Applications of Statistics and Probability in Civil Engineering(ICASP13)*. Seoul, South Korea. https://doi.org/10.22725/ICASP13.203

Abdelhady, A. U., Spence, S. M. J., & McCormick, J. (2018). "Realizing hurricane resilient communities through distributed computing." In *Routledge Handbook of Sustainable and Resilient Infrastructure* (pp. 134–151). Routledge.

Abdelhady, A. U., Spence, S. M. J., & McCormick, J. (2020). "A framework for the probabilistic quantification of the resilience of communities to hurricane winds." *Journal of Wind Engineering and Industrial Aerodynamics*, *206*, 104376. https://doi.org/10.1016/j.jweia.2020.104376

ABI (2003). "Assessment of the Cost and Effect on Future Claims of Installing Flood Damage Resistant Measures." . Association of British Insurers London.

Adger, W. N. (2000). "Social and ecological resilience: are they related?" *Progress in Human Geography*, *24*(3), 347–364.

Adger, W. N. (2006). "Vulnerability." *Global Environmental Change*, *16*(3), 268–281. 10.1016/j.gloenvcha.2006.02.006

Adger, W. N., Hughes, T. P., Folke, C., Carpenter, S. R., & Rockström, J. (2005). "Social-ecological resilience to coastal disasters." *Science*, *309*(5737), 1036–1039.

Aerts, J. C. J. H., Botzen, W. J. W., Emanuel, K., Lin, N., de Moel, H., & Michel-Kerjan, E. O. (2014). "Evaluating flood resilience strategies for coastal megacities." *Science*, *344*(6183), 473–475.

Aerts, J. C. J. H., Botzen, W. J. W., Moel, H. de, & Bowman, M. (2013). "Cost estimates for flood resilience and protection strategies in New York City." .

Aglan, H. (2005). *Field testing of energy-efficient flood-damage-resistant residential envelope systems summary report*. Oak Ridge National Lab.(ORNL), Oak Ridge, TN (United States).

Alexander, D. E. (2002). *Principles of emergency planning and management*. Harpenden, England: Oxford University Press on Demand.

Amini, M., & Memari, A. M. (2020). "Review of literature on performance of coastal residential buildings under hurricane conditions and lessons learned." *Journal of Performance of Constructed Facilities*, *34*(6), 4020102. https://doi.org/10.1061/(ASCE)CF.1943-5509.0001509

Amini, M., & Memari, A. M. (2021a). "CFD-Based Evaluation of Elevated Coastal Residential Buildings under Hurricane Wind Loads." *Journal of Architectural Engineering*, *27*(3), 4021014. https://doi.org/10.1061/(ASCE)AE.1943-5568.0000472

Amini, M., & Memari, A. M. (2021b). "Comparative review and assessment of various flood retrofit methods for low-rise residential buildings in coastal areas." *Natural Hazards Review*, *22*(3), 4021009. https://doi.org/10.1061/(ASCE)NH.1527-6996.0000464

Amini, M. O., & van de Lindt, J. W. (2013). "Quantitative insight into rational tornado design wind speeds for residential wood-frame structures using fragility approach." *Journal of Structural Engineering*, *140*(7), 4014033.

Apel, H., Aronica, G. T., Kreibich, H., & Thieken, A. H. (2009). "Flood risk analyses - How detailed do we need to be?" *Natural Hazards*, *49*(1), 79–98. 10.1007/s11069-008-9277-8

Apel, H., Merz, B., Thieken, A. H., Apel, H., Merz, B., Thieken, A. H., … Engineering, S. (2010). "Quantification of uncertainties in flood risk assessments." *International Journal of River Basin Management*, *6*(2), 149–162. https://doi.org/10.1080/15715124.2008.9635344

ASCE (7-16) (2016). *Minimum Design Loads and Associated Criteria for Buildings and other Structures (7-16).*

Attary, N., Van De Lindt, J. W., Barbosa, A. R., Cox, D. T., & Unnikrishnan, V. U. (2019). "Performance-Based Tsunami Engineering for Risk Assessment of Structures Subjected to Multi-Hazards: Tsunami following Earthquake." *Journal of Earthquake Engineering*, *23*, 1–20.

Autodesk (2020). "Autodesk Revit Architecture." .

Ayyub, B. M. (2014). "Systems resilience for multihazard environments: Definition, metrics, and valuation for decision making." *Risk Analysis*, *34*(2), 340–355.

Baker, J., Shaw, W. D., Bell, D., Brody, S., Riddel, M., Woodward, R. T., & Neilson, W. (2009). "Explaining subjective risks of hurricanes and the role of risks in intended moving and location choice models." *Natural Hazards Review*, *10*(3), 102–112.

Balica, S. F., Douben, N., & Wright, N. G. (2009). "Flood vulnerability indices at varying spatial scales." *Water Science and Technology*, *60*(10), 2571–2580. 10.2166/wst.2009.183

Baradaranshoraka, M., Pinelli, J.-P., Gurley, K., Peng, X., & Zhao, M. (2017). "Hurricane wind versus storm surge damage in the context of a risk prediction model." *Journal of Structural Engineering*, *143*(9), 4017103. https://doi.org/10.1061/(ASCE)ST.1943-541X.0001824

Barbato, M., Petrini, F., Unnikrishnan, V. U., & Ciampoli, M. (2013). "Performance-based hurricane engineering (PBHE) framework." *Structural Safety*, *45*, 24–35. https://doi.org/10.1016/j.strusafe.2013.07.002

Barnett, J., Lambert, S., & Fry, I. (2008). "The Hazards of Indicators : Insights from the

Environmental Vulnerability Index." *Annals of the Association of American Geographers*, *98*(1), 102–119.

Bates, P. D., Horritt, M. S., Aronica, G., & Beven, K. (2004). "Bayesian updating of flood inundation likelihoods conditioned on flood extent data." *Hydrological Processes*, *18*(17), 3347–3370.

Beddoes, D. W., & Booth, C. (2015). "Reducing floodwater ingress rates through an exterior masonry wall of a domestic building: A pilot investigation." *Structural Survey*, *33*(3), 196–209.

Berkes, F., Folke, C., & Colding, J. (2000). *Linking social and ecological systems: management practices and social mechanisms for building resilience*. Cambridge, England: Cambridge University Press.

Bertinelli, L., Mohan, P., & Strobl, E. (2016). "Hurricane damage risk assessment in the Caribbean: An analysis using synthetic hurricane events and nightlight imagery." *Ecological Economics*, *124*, 135–144. https://doi.org/10.1016/j.ecolecon.2016.02.004

Bhamra, R., Dani, S., & Burnard, K. (2011). "Resilience: the concept, a literature review and future directions." *International Journal of Production Research*, *49*(18), 5375–5393. https://doi.org/10.1080/00207543.2011.563826

Black, R. D. (1975). *Flood proofing rural residences*. Ithaca, New York: Department of Agricultural Engineering, Cornell University.

Blanc, J., Hall, J. W., Roche, N., Dawson, R. J., Cesses, Y., Burton, A., & Kilsby, C. G. (2012). "Enhanced efficiency of pluvial flood risk estimation in urban areas using spatial–temporal rainfall simulations." *Journal of Flood Risk Management*, *5*(2), 143–152. https://doi.org/10.1111/j.1753-318X.2012.01135.x

Blazkova, S., & Beven, K. (2009). "A limits of acceptability approach to model evaluation and uncertainty estimation in flood frequency estimation by continuous simulation: Skalka catchment, Czech Republic." *Water Resources Research*, *45*(12). https://doi.org/10.1029/2007WR006726

Borden, K. A., Schmidtlein, M. C., Emrich, C. T., Walter W. Piegorsch, & Cutter, S. L. (2007). "Vulnerability of U . S . Cities to Environmental Hazards." *Journal of Homeland Security and Emergency Management*, *4*(2). http://doi.org/10.2202/1547-7355.1279

Bouwer, L. M., Bubeck, P., Wagtendonk, A. J., & Aerts, J. C. J. H. (2009). "Inundation scenarios for flood damage evaluation in polder areas." *Natural Hazards and Earth System Sciences*, *9*, 1995–2007. https://doi.org/10.5194/nhess-9-1995-2009

Bowker, P. (2007a). "Flood resistance and resilience solutions: an R&D scoping study." *DEFRA Report, London*.

Bowker, P. (2007b). *Improving the flood performance of new buildings: Flood resilient* *construction*. London: RIBA.

Briguglio, L., Cordina, G., Farrugia, N., & Vella, S. (2006). "Conceptualising and measuring economic resilience." In SATISH CHAND (Ed.), *Pacific Islands Regional Integration and Governance* (pp. 265–288). Canberra, Australia: ANU Press.

Brody, S. D., Zahran, S., Highfield, W. E., Bernhardt, S. P., & Vedlitz, A. (2009). "Policy learning for flood mitigation: a longitudinal assessment of the community rating system in Florida." *Risk Analysis: An International Journal*, *29*(6), 912–929.

Bruneau, M., Chang, S. E., Eguchi, R. T., Lee, G. C., O'Rourke, T. D., Reinhorn, A. M., … Von Winterfeldt, D. (2003). "A framework to quantitatively assess and enhance the seismic resilience of communities." *Earthquake Spectra*, *19*(4), 733–752.

Bruneau, M., & Reinhorn, A. (2006). "Overview of the resilience concept." In *Proceedings of the 8th US national conference on earthquake engineering* (Vol. 2040, pp. 18–22). San Francisco, California, USA.

Brunner, G. W. (1995). *HEC-RAS River Analysis System. Hydraulic Reference Manual. Version 1.0.* Hydrologic Engineering Center Davis CA.

Brunner, G. W. (2002). *HEC-RAS river analysis system: User's manual*. US Army Corps of Engineers, Institute for Water Resources, Hydrologic ….

Brunner, G. W. (2010). *HEC-RAS river analysis system: hydraulic reference manual*. US Army Corps of Engineers, Institute for Water Resources, Hydrologic ….

Bubeck, P., Botzen, W. J. W., Kreibich, H., & Aerts, J. C. J. H. (2013). "Detailed insights into the influence of flood-coping appraisals on mitigation behaviour." *Global Environmental Change*, *23*(5), 1327–1338.

Büchele, B., Kreibich, H., Kron, A., Thieken, A., Ihringer, J., Oberle, P., … Ihringer, J. (2006). "Flood-risk mapping : contributions towards an enhanced assessment of extreme events and associated risks." *Natural Hazards and Earth System Sciences*, *6*(4), 485–503.

Budiyono, Y., Aerts, J., Brinkman, J., Marfai, M. A., & Ward, P. (2015). "Flood risk assessment for delta mega-cities : a case study of Jakarta." *Natural Hazards*, *75*(1), 389–413. https://doi.org/10.1007/s11069-014-1327-9

Burton, C. G. (2015). "A validation of metrics for community resilience to natural hazards and disasters using the recovery from Hurricane Katrina as a case study." *Annals of the Association of American Geographers*, *105*(1), 67–86.

Bushra, N., Trepanier, J. C., & Rohli, R. V (2019). "Joint probability risk modelling of storm surge and cyclone wind along the coast of Bay of Bengal using a statistical copula." *International Journal of Climatology*, *39*(11), 4206–4217. https://doi.org/10.1002/joc.6068

Cai, H., Lam, N. S. N., Qiang, Y., Zou, L., Correll, R. M., & Mihunov, V. (2018). "A synthesis of disaster resilience measurement methods and indices." *International Journal of Disaster Risk Reduction*.

Candela, A., & Aronica, G. T. (2017). "Probabilistic flood hazard mapping using bivariate analysis based on copulas." *ASCE-ASME Journal of Risk and Uncertainty in Engineering Systems, Part A: Civil Engineering*, *3*(1), A4016002.

Cannon, T. (1994). "Vulnerability analysis and the explanation of 'natural'disasters." *Disasters, Development and Environment*, *1*, 13–30.

Chang, S. E., & Shinozuka, M. (2004). "Measuring improvements in the disaster resilience of communities." *Earthquake Spectra*, *20*(3), 739–755. https://doi.org/10.1193/1.1775796

Charvet, I., Macabuag, J., & Rossetto, T. (2017). "Estimating tsunami-induced building damage through fragility functions: critical review and research needs." *Frontiers in Built Environment*, *3*, 36. https://doi.org/10.3389/fbuil.2017.00036

Chung Yau, S., Lin, N., & Vanmarcke, E. (2011). "Hurricane damage and loss estimation using an integrated vulnerability model." *Natural Hazards Review*, *12*(4), 184–189. https://doi.org/10.1061/(ASCE)NH.1527-6996.0000035

Cimellaro, G. P., Reinhorn, A. M., & Bruneau, M. (2010). "Framework for analytical quantification of disaster resilience." *Engineering Structures*, *32*(11), 3639–3649.

Colten, C. E., Kates, R. W., & Laska, S. B. (2008). "Community resilience: Lessons from new orleans and hurricane katrina." *Community and Regional Resilience Initiative (CARRI) Research Report*, *3*.

Comes, T., & Van de Walle, B. (2014). "Measuring disaster resilience: The impact of hurricane sandy on critical infrastructure systems." *ISCRAM*, *11*, 195–204.

Contento, A., Xu, H., & Gardoni, P. (2020). "Probabilistic formulation for storm surge predictions." *Structure and Infrastructure Engineering*, 1–20. https://doi.org/10.1080/15732479.2020.1721543

Cost Finder (2020). "How Much Does it Cost to Build a Hospital." . Retrieved from http://cost-finder.com/how-much-does-it-cost-to-build-a-hospital/

Crawford, P., Mitrani-Reiser, J., Sutley, E., Do, T., Tomiczek, T., Nofal, O. M., … van de Lindt, J. Graettinger, A. (2021). "A measurement approach to develop flood-based damage fragilities for residential buildings following repeat inundation events." *Journal of Risk and Uncertainty in Engineering Systems, Part A: Civil Engineering*.

Cutter, S. L., Barnes, L., Berry, M., Burton, C., Evans, E., Tate, E., & Webb, J. (2008). "A place-based model for understanding community resilience to natural disasters." *Global Environmental Change*. 10.1016/j.gloenvcha.2008.07.013

Dale, K., M. Edwards, M. Middelmann, and C. Z. (2004). "Structural flood vulnerability and the

Australianisation of Black's curves." *Risk*.

Davies, A. L. K. H. N., & Jones, V. A. B. R. G. (2009). "Comparison of uncertainty sources for climate change impacts : flood frequency in England." *Climatic Change*, *92*(1–2), 41–63. https://doi.org/10.1007/s10584-008-9471-4

Dawson Foundation Repair (2020). "Foundation Repair." .

De Risi, R., Jalayer, F., De Paola, F., Iervolino, I., Giugni, M., Topa, M. E., … Gasparini, P. (2013). "Flood risk assessment for informal settlements." *Natural Hazards*, *69*(1), 1003–1032.

Deniz, Derya, Erin E. Arneson, Abbie B. Liel, Shideh Dashti, and A. N. J.-W. (2017). "Flood loss models for residential buildings , based on the 2013 Colorado floods." *Natural Hazards*, *85*(2), 977–1003. 10.1007/s11069-016-2615-3

Deniz, D., Sutley, E. J., van de Lindt, J. W., Peacock, W. G., Rosenheim, N., Gu, D., … Hamideh, S. (2019). "Flood Performance and Dislocation Assessment for Lumberton Homes after Hurricane Matthew." *13th International Conference on Applications of Statistics and Probability in Civil Engineering, ICASP13*. https://doi.org/10.22725/ICASP13.104

Dhonau, M., & Rose, C. B. (2016). *Homeowners guide to flood resilience*. Retrieved from http://www.knowyourfloodrisk.co.uk/sites/default/files/FloodGuide_ForHomeowners.pdf

Dierauer, J., Pinter, N., & Remo, J. W. F. (2012). "Evaluation of levee setbacks for flood-loss reduction, Middle Mississippi River, USA." *Journal of Hydrology*, *450*, 1–8.

Dietrich, J. C., Tanaka, S., Westerink, J. J., Dawson, C. N., Luettich, R. A., Zijlema, M., … Westerink, H. J. (2012). "Performance of the unstructured-mesh, SWAN+ ADCIRC model in computing hurricane waves and surge." *Journal of Scientific Computing*, *52*(2), 468–497. https://doi.org/10.1007/s10915-011-9555-6

Dietrich, J. C., Zijlema, M., Westerink, J. J., Holthuijsen, L. H., Dawson, C., Luettich Jr, R. A., … Stone, G. W. (2011). "Modeling hurricane waves and storm surge using integrally-coupled, scalable computations." *Coastal Engineering*, *58*(1), 45–65. https://doi.org/10.1016/j.coastaleng.2010.08.001

Dinan, T. (2017). "Projected increases in hurricane damage in the United States: the role of climate change and coastal development." *Ecological Economics*, *138*, 186–198. https://doi.org/10.1016/j.ecolecon.2017.03.034

Do, T. Q., van de Lindt, J. W., & Cox, D. T. (2020). "Hurricane Surge-Wave Building Fragility Methodology for Use in Damage, Loss, and Resilience Analysis." *Journal of Structural Engineering*, *146*(1), 4019177. https://doi.org/10.1061/(ASCE)ST.1943-541X.0002472

Doan, J. (2000). "Geospatial hydrologic modeling extension HEC-GeoHMS-user's manual-version 1.0." *US Army Corps of Engineers Hydrologic Engineering Center, Davis,* *California, USA*.

Domeneghetti, A., Vorogushyn, S., Castellarin, A., Merz, B., & Brath, A. (2013). "Probabilistic flood hazard mapping: effects of uncertain boundary conditions." *Hydrology and Earth System Sciences*, *17*(8), 3127–3140.

Dottori, F., Figueiredo, R., Martina, M. L. V, Molinari, D., & Scorzini, A. (2016). "INSYDE: a synthetic, probabilistic flood damage model based on explicit cost analysis." *Nat. Hazards Earth Syst. Sci*, *16*(12), 2577–2591. https://doi.org/10.5194/nhess-16-2577-2016

Dow, K., & Cutter, S. L. (2002). "Emerging hurricane evacuation issues: hurricane Floyd and South Carolina." *Natural Hazards Review*, *3*(1), 12–18.

Downton, M. W., Miller, J. Z. B., & Pielke Jr, R. A. (2005). "Reanalysis of US National Weather Service flood loss database." *Natural Hazards Review*, *6*(1), 13–22.

Dubois, D., & Guyonnet, D. (2011). "Risk-informed decision-making in the presence of epistemic uncertainty." *International Journal of General Systems*, *40*(02), 145–167.

Duncan, J. M., Brandon, T. L., Wright, S. G., & Vroman, N. (2008). "Stability of I-walls in New Orleans during hurricane Katrina." *Journal of Geotechnical and Geoenvironmental Engineering*, *134*(5), 681–691.

Dutta, D., Herath, S., & Musiake, K. (2003). "A mathematical model for flood loss estimation." *Journal of Hydrology*, *277*(1–2), 24–49. https://doi.org/10.1016/S0022-1694(03)00084-2

Egli, T. (2002). *Non structural flood plain management: measures and their effectiveness*. International Commission for the Protection of the Rhine (ICPR).

Egorova, R., Noortwijk, J. M. Van, & Holterman, S. R. (2010). "Uncertainty in flood damage estimation." *International Journal of River Basin Management*, *6*(2), 139–148. 10.1080/15715124.2008.9635343

Ellingwood, B. R., Rosowsky, D. V, Li, Y., & Kim, J. H. (2004). "Fragility assessment of light-frame wood construction subjected to wind and earthquake hazards." *Journal of Structural Engineering*, *130*(12), 1921–1930. https://doi.org/10.1061/(ASCE)0733-9445(2004)130:12(1921)

ESRI (2018). "Release 10.5.1." *Redlands, CA: Environmental Systems Research Institute*, *437*, 438.

Faisal, I. M., Kabir, M. R., & Nishat, A. (1999). "Non-structural flood mitigation measures for Dhaka City." *Urban Water*, *1*(2), 145–153.

Federal Emergency Management Agency (2019). "Disaster Public Files." . Retrieved from https://disasters.geoplatform.gov/publicdata/NationalDisasters/HurricaneMatthew/

FEMA (2003). *Multi-hazard Loss Estimation Methodology Hurricane Model (HAZUS-MH*

MR5): Technical Manual. Washington, D.C. Retrieved from https://www.fema.gov/sites/default/files/2020-09/fema_hazus_hurricane-model_user-manual_2.1.pdf

FEMA (2005). *Reducing Damage from Localized Flooding*.

FEMA (2009a). "Multi-hazard loss estimation methodology: Flood model." *HAZUS-MH MR4 Technical Manual*. Department of Homeland Security Federal Emergency Management Agency Washington, DC.

FEMA (2009b). "National disaster housing strategy." . Retrieved from https://www.fema.gov/media-library-data/20130726-1819-25045-9288/ndhs_core.pdf

FEMA (2009c). *Multi-hazard Loss Estimation Methodology: Earthquake Model (HAZUS-MH MR5) Technical Manual*. Washington, D.C.

FEMA (2009d). *Multi-hazard loss estimation methodology: Flood model (HAZUS-MH MR5) Technical Manual*. Washington, DC.

FEMA (2016a). "Hazard mitigation assistance cost share guide." . Retrieved from https://www.fema.gov/media-library-data/1463766664964-4e6dd22652cb7c8a6162904f3b1b2022/FinalHMACostShareGuide508.pdf

FEMA (2016b). *Guidance for flood risk analysis and mapping: Shallow Flooding Analyses and Mapping*.

FEMA (2020). "Building Resilient Infrastructure and Communities." .

FEMA P-1037 (2015). *Reducing Flood Risk to Residential Buildings That Cannot Be Elevated*. Retrieved from https://www.fema.gov/media-library-data/1443014398612-a4dfc0f86711bc72434b82c4b100a677/revFEMA_HMA_Grants_4pg_2015_508.pdf

Feyen, L., Dankers, R., Bódis, K., Salamon, P., & Barredo, J. I. (2012). "Fluvial flood risk in Europe in present and future climates." *Climatic Change*, *112*(1), 47–62.

Fidler, J., Wood, C., Ridout, B., & Heritage, E. (2004). "Flooding and historic buildings: technical advice note." .

Fixer (2020). "Construction Cost Analysis." .

Franchin, P., & Cavalieri, F. (2015). "Probabilistic assessment of civil infrastructure resilience to earthquakes." *Computer-Aided Civil and Infrastructure Engineering*, *30*(7), 583–600.

Freni, G., Loggia, G. La, & Notaro, V. (2010). "Uncertainty in urban flood damage assessment due to urban drainage modelling and depth-damage curve estimation." *Water Science and Technology*, *61*(12), 2979–2993. 10.2166/wst.2010.177

Frongia, S., Ruiu, A., & Sechi, G. M. (2017). "Water depth-damage functions for flood direct tangible damage evaluation in built-up areas in Sardinia (Italy)." In *10th World Congress of EWRA on Water Resources and Environment. Panta Rhei* (pp. 3–10). Tsakiris G., Tsihrintzis VA, Vangelis H., Tigkas D.

Fuchs, S., Heiss, K., & Hübl, J. (2007). "Towards an empirical vulnerability function for use in debris flow risk assessment." *Natural Hazards and Earth System Science*, *7*(5), 495–506.

Garrote, J., Bernal, N., Díez-Herrero, A., Martins, L. R., & Bodoque, J. M. (2019). "Civil engineering works versus self-protection measures for the mitigation of floods economic risk. A case study from a new classification criterion for cost-benefit analysis." *International Journal of Disaster Risk Reduction*, *37*, 101157. https://doi.org/10.1016/j.ijdrr.2019.101157

Glavovic, B. C. (2010). "The role of land-use planning in disaster risk reduction: An introduction to perspectives from Australasia." .

Grayson, J. M., Pang, W., & Schiff, S. (2013). "Building envelope failure assessment framework for residential communities subjected to hurricanes." *Engineering Structures*, *51*, 245–258. https://doi.org/10.1016/j.engstruct.2013.01.027

Grayson, M., Pang, W., & Schiff, S. (2012). "Three-dimensional probabilistic wind-borne debris trajectory model for building envelope impact risk assessment." *Journal of Wind Engineering and Industrial Aerodynamics*, *102*, 22–35.

Greer, A., & Brokopp Binder, S. (2017). "A historical assessment of home buyout policy: Are we learning or just failing?" *Housing Policy Debate*, *27*(3), 372–392.

Guo, Y., & van de Lindt, J. (2019). "Simulation of hurricane wind fields for community resilience applications: A data-driven approach using integrated asymmetric Holland models for inner and outer core regions." *Journal of Structural Engineering*, *145*(9), 4019089. https://doi.org/10.1061/(ASCE)ST.1943-541X.0002366

Haehnel, R. B., & Daly, S. F. (2004). "Maximum Impact Force of Woody Debris on Floodplain Structures." *Journal of Hydraulic Engineering*, *130*(2), 112–120. 10.1061/(ASCE)0733-9429(2004)130:2(112)

Haimes, Y. Y. (2009). "On the definition of resilience in systems." *Risk Analysis: An International Journal*, *29*(4), 498–501.

Hall, J., & Solomatine, D. (2008). "A framework for uncertainty analysis in flood risk management decisions." *International Journal of River Basin Management*, *6*(2), 85–98.

Handmer, J. (2002). "The chimera of precision: inherent uncertainties in disaster loss assessment." *International Journal of Mass Emergencies and Disasters*, *20*(3), 325–346.

Harris, D. J., Dunn, C. N., & Deering, M. K. (2010). "Flood risk assessment of complex riverine systems." In Richard N. Palmer (Ed.), *World Environmental and Water Resources Congress 2010: Challenges of Change* (pp. 4757–4768). Providence, Rhode Island, United States.

Hatzikyriakou, A., Lin, N., Gong, J., Xian, S., Hu, X., & Kennedy, A. (2016). "Component-based vulnerability analysis for residential structures subjected to storm surge impact from Hurricane Sandy." *Natural Hazards Review*, *17*(1), 5015005. https://doi.org/10.1061/(ASCE)NH.1527-6996.0000205

Hayes, B. D. (2004). "Interdisciplinary planning of nonstructural flood hazard mitigation." *Journal of Water Resources Planning and Management*, *130*(1), 15–25.

HAZUS-MH (2008). *Multi-hazard Loss Estimation Methodology*. Washington, D.C.: Department of Homeland Security Federal Emergency Management Agency, Mitigation Division.

He, J., Pan, F., & Cai, C. S. (2017). "A review of wood-frame low-rise building performance study under hurricane winds." *Engineering Structures*, *141*, 512–529. https://doi.org/10.1016/j.engstruct.2017.03.036

Hemmati, M., Ellingwood, B. R., & Mahmoud, H. N. (2020). "The Role of Urban Growth in Resilience of Communities under Flood Risk." *Earth's Future*, *8*(3), e2019EF001382. https://doi.org/10.1029/2019EF001382

Henderson, D. J., & Ginger, J. D. (2007). "Vulnerability model of an Australian high-set house subjected to cyclonic wind loading." *Wind and Structures*, *10*(3), 269–285. https://doi.org/10.12989/was.2007.10.3.269

Henry, D., & Ramirez-Marquez, J. E. (2012). "Generic metrics and quantitative approaches for system resilience as a function of time." *Reliability Engineering & System Safety*, *99*, 114–122. https://doi.org/10.1016/j.ress.2011.09.002

Hill, E., Wial, H., & Wolman, H. (2008). *Exploring regional economic resilience*. Working paper.

Hinkel, J. (2011). "Indicators of vulnerability and adaptive capacity" Towards a clarification of the science–policy interface.pdf." *Global Environmental Change*, *21*(1), 198–208.

Hirabayashi, Y., Mahendran, R., Koirala, S., Konoshima, L., Yamazaki, D., Watanabe, S., … Kanae, S. (2013). "Global flood risk under climate change." *Nature Climate Change*, *3*(9), 816–821. 10.1038/nclimate1911

Holub, M., & Fuchs, S. (2008). "Benefits of local structural protection to mitigate torrent-related hazards." *WIT Transactions on Information and Communication Technologies*, *39*, 401–411.

Home-Advisor (2019). "Home Advisor." . Retrieved from https://www.homeadvisor.com/?gclid=EAIaIQobChMI9OOambL05AIVExx9Ch3E3w6zEAAYASAAEgIrb_D_BwE

Home-Guides (2019). "Home Guides." . Retrieved from https://homeguides.sfgate.com/

Hori, M., & Schafer, M. J. (2010). "Social costs of displacement in Louisiana after Hurricanes Katrina and Rita." *Population and Environment*, *31*(1–3), 64–86.

Huang, P., Wang, F., Fu, A., & Gu, M. (2016). "Numerical simulation of 3-D probabilistic trajectory of plate-type wind-borne debris." *Wind and Structures*, *22*(1), 17–41.

HUD (2020). "CDBG-DR: Community Development Block Grant Disaster Recovery Program." . Retrieved from https://www.hudexchange.info/programs/cdbg-dr/

Hudson, P., Botzen, W. J. W., Kreibich, H., Bubeck, P., & Aerts, J. (2014). "Evaluating the effectiveness of flood damage mitigation measures by the application of propensity score matching." *Natural Hazards and Earth System Sciences*, *14*(7), 1731–1747.

Ii, B. L. T., Kasperson, R. E., Matson, P. A., Mccarthy, J. J., Corell, R. W., Christensen, L., … Schiller, A. (2003). "A framework for vulnerability analysis in sustainability science." *Proceedings of the National Academy of Sciences*, *100*(14), 8074–8079.

IN-CORE (2021). "IN-CORE Manual." . Retrieved from https://incore.ncsa.illinois.edu/doc/incore/index.html

IPCC (2012). *Intergovernmental Panel on Climate Change Report: Managing the risks of extreme events and disasters to advance climate change adaptation: special report of the intergovernmental panel on climate change*. New York, NY. Retrieved from https://www.ipcc.ch/site/assets/uploads/2018/03/SREX_Full_Report-1.pdf.

Irish, J. L., Resio, D. T., & Cialone, M. A. (2009). "A surge response function approach to coastal hazard assessment. Part 2: Quantification of spatial attributes of response functions." *Natural Hazards*, *51*(1), 183–205.

Irish, J. L., Resio, D. T., & Ratcliff, J. J. (2008). "The influence of storm size on hurricane surge." *Journal of Physical Oceanography*, *38*(9), 2003–2013.

Jakob, M., Holm, K., Weatherly, H., Liu, S., & Ripley, N. (2013a). "Debris flood risk assessment for Mosquito Creek, British Columbia, Canada." *Natural Hazards*, *65*(3), 1653–1681.

Jakob, M., Holm, K., Weatherly, H., Liu, S., & Ripley, N. (2013b). "Debris flood risk assessment for Mosquito Creek , British." *Natural Hazards*, *65*(3), 1653–1681. 10.1007/s11069-012-0436-6

Jakob, M., Stein, D., & Ulmi, M. (2012). "Vulnerability of buildings to debris flow impact." *Natural Hazards*, *60*(2), 241–261.

Jelesnianski, C. P. (1992). *SLOSH: Sea, lake, and overland surges from hurricanes* (Vol. 48). US Department of Commerce, National Oceanic and Atmospheric Administration ….

Johnson, D. R., Fischbach, J. R., & Ortiz, D. S. (2013). "Estimating surge-based flood risk with the coastal Louisiana risk assessment model." *Journal of Coastal Research*, (67), 109–126. https://doi.org/10.2112/SI_67_8

Jung, Y., & Merwade, V. (2011). "Uncertainty quantification in flood inundation mapping using generalized likelihood uncertainty estimate and sensitivity analysis." *Journal of Hydrologic Engineering*, *17*(4), 507–520.

Kakareko, G., Jung, S., Mishra, S., & Vanli, O. A. (2020). "Bayesian capacity model for hurricane vulnerability estimation." *Structure and Infrastructure Engineering*, 1–11. https://doi.org/10.1080/15732479.2020.1760318

Kelman, I., & Spence, R. (2004). "An overview of flood actions on buildings." *Engineering Geology*, *73*(3–4), 297–309. 10.1016/j.enggeo.2004.01.010

Khajwal, A. B., & Noshadravan, A. (2020). "Probabilistic Hurricane Wind-Induced Loss Model for Risk Assessment on a Regional Scale." *ASCE-ASME Journal of Risk and Uncertainty in Engineering Systems, Part A: Civil Engineering*, *6*(2), 4020020. https://doi.org/10.1061/AJRUA6.0001062

Kleinen, Thomas, & Petschel-held, G. (2007). "Integrated assessment of changes in flooding probabilities due to climate change." *Climatic Change*, *81*(3–4), 283–312. 10.1007/s10584-006-9159-6

Koliou, M., van de Lindt, J. W., McAllister, T. P., Ellingwood, B. R., Dillard, M., & Cutler, H. (2018). "State of the research in community resilience: progress and challenges." *Sustainable and Resilient Infrastructure*, 1–21. https://doi.org/10.1080/23789689.2017.1418547

Kourtis, I. M., Tsihrintzis, V. A., & Baltas, E. (2020). "A robust approach for comparing conventional and sustainable flood mitigation measures in urban basins." *Journal of Environmental Management*, *269*, 110822. https://doi.org/10.1016/j.jenvman.2020.110822

Kreibich, H., Christenberger, S., & Schwarze, R. (2011). "Economic motivation of households to undertake private precautionary measures against floods." *Natural Hazards and Earth System Sciences*, *11*(2), 309–321.

Kreibich, H., Piroth, K., Seifert, I., Maiwald, H., Kunert, U., Schwarz, J., … Thieken, A. H. (2009). "Is flow velocity a significant parameter in flood damage modelling?" *Natural Hazards and Earth System Science*, *9*(5), 1679–1692. 10.5194/nhess-9-1679-2009

Kreibich, H., Thieken, A. H., Petrow, T., Müller, M., & Merz, B. (2005). "Flood loss reduction of private households due to building precautionary measures--lessons learned from the Elbe flood in August 2002." *Natural Hazards and Earth System Sciences*.

Krzysztofowicz, R. (1999). "Bayesian theory of probabilistic forecasting via deterministic hydrologic model." *Water Resources Research*, *35*(9), 2739–2750.

Lamb, R., Keef, C., Tawn, J., Laeger, S., Meadowcroft, I., Surendran, S., … Batstone, C. (2010). "A new method to assess the risk of local and widespread flooding on rivers and coasts." *Journal of Flood Risk Management*, *3*(4), 323–336.

Lamond, J., Rose, C., Joseph, R., & Proverbs, D. (2016). *Supporting the uptake of low cost resilience: summary of technical findings (FD2682)*. London: Defra.

Leavitt, W. M., & Kiefer, J. J. (2006). "Infrastructure interdependency and the creation of a normal disaster: The case of Hurricane Katrina and the city of New Orleans." *Public Works Management & Policy*, *10*(4), 306–314.

Lee, K. H., & Rosowsky, D. V (2005). "Fragility assessment for roof sheathing failure in high wind regions." *Engineering Structures*, *27*(6), 857–868.

Leveson, N., Dulac, N., Zipkin, D., Cutcher-Gershenfeld, J., Carroll, J., & Barrett, B. (2006). "Engineering resilience into safety-critical systems." In E. Hollnagel, D. D. Woods, and N. Leveson (Eds.), *Resilience engineering: Concepts and precepts* (pp. 95–123). Abingdon, UK: Routledge.

Levin, S. A., Barrett, S., Aniyar, S., Baumol, W., Bliss, C., Bolin, B., … Gren, I.-M. (1998). "Resilience in natural and socioeconomic systems." *Environment and Development Economics*, *3*(2), 221–262.

Li, Q., Wang, C., & Zhang, H. (2016). "A probabilistic framework for hurricane damage assessment considering non-stationarity and correlation in hurricane actions." *Structural Safety*, *59*, 108–117.

Li, Y., & Ellingwood, B. R. (2006). "Hurricane damage to residential construction in the US: Importance of uncertainty modeling in risk assessment." *Engineering Structures*, *28*(7), 1009–1018. https://doi.org/10.1016/j.engstruct.2005.11.005

Li, Y., van de Lindt, J. W., Dao, T., Bjarnadottir, S., & Ahuja, A. (2012). "Loss analysis for combined wind and surge in hurricanes." *Natural Hazards Review*, *13*(1), 1–10. https://doi.org/10.1061/(ASCE)NH.1527-6996.0000058

Liebow, E. B. (1996). "At risk: natural hazards, people's vulnerability, and disasters." In P. Blaikie, T. Cannon, I. Davis, and B. Wisner (Eds.), *The challenge of disasters and our approach*. Abingdon, UK: Routledge.

Lin, C.-Y., & Cha, E. J. (2020). "Hurricane risk assessment for residential buildings in the southeastern US coastal region in changing climate conditions using artificial neural networks." *Natural Hazards Review*, *21*(3), 4020024. https://doi.org/10.1061/(ASCE)NH.1527-6996.0000390

Lin, N., Emanuel, K. A., Smith, J. A., & Vanmarcke, E. (2010). "Risk assessment of hurricane storm surge for New York City." *Journal of Geophysical Research: Atmospheres*, *115*(D18). Risk assessment of hurricane storm surge for New York City

Lin, N., & Shullman, E. (2017). "Dealing with hurricane surge flooding in a changing environment: part I. Risk assessment considering storm climatology change, sea level rise, and coastal development." *Stochastic Environmental Research and Risk Assessment*, *31*(9), 2379–2400. https://doi.org/10.1007/s00477-016-1377-5

Lin, P., & Wang, N. (2016). "Building portfolio fragility functions to support scalable community resilience assessment." *Sustainable and Resilient Infrastructure*, *1*(3–4), 108–122. https://doi.org/10.1080/23789689.2016.1254997

Lindell, M. K., Lu, J.-C., & Prater, C. S. (2005). "Household decision making and evacuation in response to Hurricane Lili." *Natural Hazards Review*, *6*(4), 171–179.

Liu, Y. B., Batelaan, O., De Smedt, F., Poórová, J., & Velcická, L. (2005). "Automated calibration applied to a GIS-based flood simulation model using PEST." In *Floods, from defence to management* (pp. 317–326). Nijmegen, Netherlands: CRC Press: Taylor&Francis Group.

López-Marrero, T., & Tschakert, P. (2011). "From theory to practice: building more resilient communities in flood-prone areas." *Environment and Urbanization*, *23*(1), 229–249.

Madni, A. M., & Jackson, S. (2009). "Towards a conceptual framework for resilience engineering." *IEEE Systems Journal*, *3*(2), 181–191.

Maguire, B., & Hagan, P. (2007). "Disasters and communities: understanding social resilience." *Australian Journal of Emergency Management, The*, *22*(2), 16.

Manyena, S. B. (2006). "The concept of resilience revisited." *Disasters*, *30*(4), 434–450. https://doi.org/10.1111/j.0361-3666.2006.00331.x

Martin-Breen, P., & Anderies, J. M. (2011). "Resilience: A literature review." *Brighton: Institute of Development Studies*.

Martínez-Gomariz, E., Forero-Ortiz, E., Guerrero-Hidalga, M., Castán, S., & Gómez, M. (2020). "Flood Depth–Damage Curves for Spanish Urban Areas." *Sustainability*, *12*(7), 2666. https://doi.org/10.3390/su12072666

Marvi, M. T. (2020). "A review of flood damage analysis for a building structure and contents." *Natural Hazards*, 1–29. https://doi.org/10.1007/s11069-020-03941-w

Masoomi, H., Ameri, M. R., & van de Lindt, J. W. (2018). "Wind performance enhancement strategies for residential wood-frame buildings." *Journal of Performance of Constructed Facilities*, *32*(3), 4018024. https://doi.org/10.1061/(ASCE)CF.1943-5509.0001172

Masoomi, H., & van de Lindt, J. W. (2016). "Tornado fragility and risk assessment of an archetype masonry school building." *Engineering Structures*, *128*, 26–43.

Masoomi, H., van de Lindt, J. W., Ameri, M. R., Do, T. Q., & Webb, B. M. (2019). "Combined wind-wave-surge hurricane-induced damage prediction for buildings." *Journal of Structural Engineering*, *145*(1), 4018227. https://doi.org/10.1061/(ASCE)ST.1943-541X.0002241

Massarra, C. C., Friedland, C. J., Marx, B. D., & Dietrich, J. C. (2019). "Predictive multi-hazard hurricane data-based fragility model for residential homes." *Coastal Engineering*, *151*, 10–21. https://doi.org/10.1016/j.coastaleng.2019.04.008

May, P. J. (1992). "Policy learning and failure." *Journal of Public Policy*, *12*(4), 331–354.

May, P. J. (1999). "Fostering policy learning: A challenge for public administration." *International Review of Public Administration*, *4*(1), 21–31.

McAllister, T. (2015). "Research needs for developing a risk-informed methodology for community resilience." *Journal of Structural Engineering*, *142*(8), C4015008.

McCullough, M. C., Kareem, A., Donahue, A. S., & Westerink, J. J. (2013). "Structural damage under multiple hazards in coastal environments." *Journal of Disaster Research*, *8*(6), 1042–1051. https://doi.org/10.20965/jdr.2013.p1042

McGrath, H., El Ezz, A. A., & Nastev, M. (2019). "Probabilistic depth–damage curves for assessment of flood-induced building losses." *Natural Hazards*, 1–14. https://doi.org/10.1007/s11069-019-03622-3

Memari, M., Attary, N., Masoomi, H., Mahmoud, H., van de Lindt, J. W., Pilkington, S. F., & Ameri, M. R. (2018). "Minimal building fragility portfolio for damage assessment of communities subjected to tornadoes." *Journal of Structural Engineering*, *144*(7), 4018072. https://doi.org/10.1061/(ASCE)ST.1943-541X.0002047

Merwade, V., Olivera, F., Arabi, M., & Edleman, S. (2008). "Uncertainty in flood inundation mapping: current issues and future directions." *Journal of Hydrologic Engineering*, *13*(7), 608–620.

Merz, B., Hall, J., Disse, M., & Schumann, A. (2010). "Fluvial flood risk management in a changing world." *Natural Hazards and Earth System Sciences*, *10*(3), 509–527.

Merz, B., Kreibich, H., & Lall, U. (2013). "Multi-variate flood damage assessment: a tree-based data-mining approach." *Natural Hazards and Earth System Sciences*, *13*(1), 53–64.

Merz, B., Kreibich, H., Thieken, A., & Schmidtke, R. (2004). "Estimation uncertainty of direct monetary flood damage to buildings." *Natural Hazards and Earth System Science*, *4*(1), 153–163. 10.5194/nhess-4-153-2004

Merz, B., & Thieken, A. H. (2005). "Separating natural and epistemic uncertainty in flood frequency analysis." *Journal of Hydrology*, *309*(1–4), 114–132. 10.1016/j.jhydrol.2004.11.015

Merz, B., & Thieken, A. H. (2009). "Flood risk curves and uncertainty bounds." *Natural Hazards*, *51*(3), 437–458. https://doi.org/10.1007/s11069-009-9452-6

Messner, F. (2007). *Evaluating flood damages: guidance and recommendations on principles and methodsT09-06-01*. HR Wallingford, UK: FLOODsite.

Middelmann-Fernandes, M. H. (2010). "Flood damage estimation beyond stage-damage functions: An Australian example." *Journal of Flood Risk Management*, *3*(1), 88–96. http://doi.org/10.1111/j.1753-318X.2009.01058.x

Mileti, D. (1999). *Disasters by design: A reassessment of natural hazards in the United States*. Washington, D.C.: Joseph Henry Press.

Milly, P. C. D., Wetherald, R. T., Dunne, K. A., & Delworth, T. L. (2002). "Increasing risk of great Floods in a changing climate." *Nature*, *415*(6871), 514.

Mishra, S., Vanli, O. A., Alduse, B. P., & Jung, S. (2017). "Hurricane loss estimation in wood-frame buildings using Bayesian model updating: Assessing uncertainty in fragility and reliability analyses." *Engineering Structures*, *135*, 81–94. https://doi.org/10.1016/j.engstruct.2016.12.063

Moel, H. De, & Aerts, J. C. J. H. (2011). "Effect of uncertainty in land use, damage models and inundation depth on flood damage estimates." *Natural Hazards*, *58*(1), 407–425. https://doi.org/10.1007/s11069-010-9675-6

Moel, H. De, & Aerts, J. C. J. H. (2015). "Integrated Direct and Indirect Flood Risk Modeling : Development and Sensitivity Analysis." *Risk Analysis*, *35*(5), 882–900. 10.1111/risa.12300

Moel, H. De, Aerts, J. C. J. H., & Koomen, E. (2011). "Development of flood exposure in the Netherlands during the 20th and 21st century." *Global Environmental Change*, *21*(2), 620–627. https://doi.org/10.1016/j.gloenvcha.2010.12.005

Moel, H. De, Asselman, N. E. M., & Aerts, J. C. J. H. (2012). "Uncertainty and sensitivity analysis of coastal flood damage estimates in the west of the Netherlands." *Natural Hazards and Earth System Sciences*, *12*, 1045–1058. 10.5194/nhess-12-1045-2012

Moel, H. De, Bouwer, L. M., & Aerts, J. C. J. H. (2014). "Uncertainty and sensitivity of flood risk calculations for a dike ring in the south of the Netherlands." *Science of the Total Environment*, *473*, 224–234. 10.1016/j.scitotenv.2013.12.015

Moel, H. De, Vliet, M. Van, & Aerts, J. C. J. H. (2014). "Evaluating the effect of flood damage-reducing measures : a case study of the unembanked area of Rotterdam , the Netherlands." *Regional Environmental Change*, *14*(3), 895–908. https://doi.org/10.1007/s10113-013-0420-z

Molinari, D., & Scorzini, A. R. (2017). "On the influence of input data quality to flood damage estimation: The performance of the INSYDE model." *Water*, *9*(9), 688.

Montz, B. E., & Gruntfest, E. (2002). "Flash flood mitigation: recommendations for research and applications." *Global Environmental Change Part B: Environmental Hazards*, *4*(1), 15–22.

Mukolwe, M. M. (2017). *Flood hazard mapping: uncertainty and its value in the decision-making process*. CRC Press.

Myers, C. A., Slack, T., & Singelmann, J. (2008). "Social vulnerability and migration in the wake of disaster: The case of Hurricanes Katrina and Rita." *Population and Environment*, *29*(6), 271–291. https://doi.org/10.1007/s11111-008-0072-y

Nadal, N. C., Zapata, R. E., Pagán, I., López, R., & Agudelo, J. (2009). "Building damage due to riverine and coastal floods." *Journal of Water Resources Planning and Management*, *136*(3), 327–336.

Næss, L. O., Norland, I. T., Lafferty, W. M., & Aall, C. (2006). "Data and processes linking vulnerability assessment to adaptation decision-making on climate change in Norway." *Global Environmental Change*, *16*(2), 221–233. https://doi.org/10.1016/j.gloenvcha.2006.01.007

Nascimento, N., Baptista, M., Silva, A., Machado, M. L., & Lima, J. C. De (2006). "Flood-damage curves : Methodological development for the Brazilian context." *Water Practice and Technology*, *1*(1). https://doi.org/10.2166/WPT.2006022

Nasiri, H., Yusof, M. J. M., & Ali, T. A. M. (2016). "An overview to flood vulnerability assessment methods." *Sustainable Water Resources Management*, *2*(3), 331–336. https://doi.org/10.1007/s40899-016-0051-x

National Academy of Engineering (2019). "A Fully Integrated Model of Interdependent Physical Infrastructure and Social Systems." *Summer Bridge Issue on Engineering for Disaster Resilience*, *49*(2), 43. Retrieved from https://www.nae.edu/File.aspx?id=212260

Naumann, Thomas, Johannes Nikolowski, and S. G. (2009). "Synthetic depth-damage functions – A detailed tool for analysing flood resilience of building types." In *Road Map towards a Flood Resilient Urban Environment, Proceedings of the Final Conference of the COST Action C*. Paris, France.

NC State (2018). *Hurricane Florence Recovery Recommendations: Building Communities Stronger and Smarter*. Retrieved from https://files.nc.gov/ncosbm/documents/files/Florence_Report_Full_rev20181016v10.pdf

Nicholas, J., Holt, G. D., & Proverbs, D. G. (2001). "Towards standardising the assessment of flood damaged properties in the UK." *Structural Survey*, *19*(4), 163–172.

Nigg, J. M., Barnshaw, J., & Torres, M. R. (2006). "Hurricane Katrina and the flooding of New Orleans: Emergent issues in sheltering and temporary housing." *The Annals of the American Academy of Political and Social Science*, *604*(1), 113–128.

NOAA (2018). "Advanced Hydrologic Prediction Service." . Retrieved from https://water.weather.gov/precip/

NOAA (2020). "NCFPM Lidar DEM: Statewide North Carolina (Phase 2)." . Retrieved from https://coast.noaa.gov/dataviewer/#/lidar/search/

Nofal, O. M. (2020). "Stochastic Modeling of Uncertainties in the Wind Load Pressure on Residential Buildings Using Different Stochastic Techniques." *Current Trends in Civil & Structural Engineering*, *6*(3). https://doi.org/10.33552/CTCSE.2020.06.000636

Nofal, O. M., Lindt, J. W. van de, Do, T. Q., Yan, G., Hamideh, S., Cox, D. T., & Dietrich, J. C.

(2021). "Methodology for Regional Multi-Hazard Hurricane Damage and Risk Assessment." *Journal of Structural Engineering*.

Nofal, O. M., Lindt, J. W. van de, Yan, G., Hamideh, S., & Dietrich, J. C. (2021). "Multi-Hazard Hurricane Vulnerability Model To Enable Resilence-Informed Decision." In S. El Baradei, A. Madian, A. Singh, and S. Yazdani (Eds.), *Proceedings of International Structural Engineering and Construction (ISEC-11).*

Nofal, O. M., & van de Lindt, J. W. (2020a). "High-Resolution Approach to Quantify the Impact of Building-Level Flood Mitigation and Adaptation Measures on Flood Losses at the Community-Level." *International Journal of Disaster Risk Reduction*, 101903. https://doi.org/10.1016/j.ijdrr.2020.101903

Nofal, O. M., & van de Lindt, J. W. (2020b). "Minimal Building Flood Fragility and Loss Function Portfolio for Resilience Analysis at the Community-Level." *Water*, *12*(8), 2277. https://doi.org/10.3390/w12082277

Nofal, O. M., & van de Lindt, J. W. (2020). "Probabilistic Flood Loss Assessment at the Community Scale: Case Study of 2016 Flooding in Lumberton, North Carolina." *ASCE-ASME Journal of Risk and Uncertainty in Engineering Systems, Part A: Civil Engineering*, *6*(2), 5020001. https://doi.org/10.1061/AJRUA6.0001060

Nofal, O. M., & van de Lindt, J. W. (2020). "Understanding flood risk in the context of community resilience modeling for the built environment: research needs and trends." *Sustainable and Resilient Infrastructure*. https://doi.org/10.1080/23789689.2020.1722546

Nofal, O. M., & van de Lindt, J. W. (2021). "High-Resolution Flood Risk Approach to Quantify the Impact of Policy Change on Flood Losses at Community-Level." *International Journal of Disaster Risk Reduction*.

Nofal, O. M., van de Lindt, J. W., & Do, T. Q. (2020). "Multi-variate and Single-variable Flood Fragility and Loss Approaches for Buildings." *Reliability Engineering & System Safety*, *202*, 106971. https://doi.org/10.1016/j.ress.2020.106971

NRC (2020). "Floodwater Detention and Retention Basins." *Natural Resilient Communities Solutions*.

NWS (2018). "Hurricane Florence 2018 Forcast." . Retrieved from https://www.nhc.noaa.gov/archive/2018/FLORENCE_graphics.php?product=5day_cone_no_line

O'Neill, H. K., McLean, A. J., Kalis, R., & Shultz, J. M. (2016). "Disaster averted: community resilience in the face of a catastrophic flood." *Disaster Health*, *3*(3), 67–77.

Olfert, A., & Schanze, J. (2009). "New approaches to ex-post evaluation of risk reduction measures: The example of flood proofing in Dresden, Germany." .

Osberghaus, D. (2015). "The determinants of private flood mitigation measures in Germany—

Evidence from a nationwide survey." *Ecological Economics*, *110*, 36–50.

Ouyang, M., & Duenas-Osorio, L. (2014). "Multi-dimensional hurricane resilience assessment of electric power systems." *Structural Safety*, *48*, 15–24.

Paille, M., Reams, M., Argote, J., Lam, N. S.-N., & Kirby, R. (2016). "Influences on adaptive planning to reduce flood risks among parishes in South Louisiana." *Water*, *8*(2), 57.

Paleo-Torres, A., Gurley, K., Pinelli, J.-P., Baradaranshoraka, M., Zhao, M., Suppasri, A., & Peng, X. (2020). "Vulnerability of Florida residential structures to hurricane induced coastal flood." *Engineering Structures*, *220*, 111004. https://doi.org/10.1016/j.engstruct.2020.111004

Park, S., John W. van de Lindt, & Yue Li (2014). "ABV Procedure Combined with Mechanistic Response Modeling for Roof- and Surge-Loss Estimation in Hurricanes." *Performance of Constructed Facilities*, *28*(2), 206–215. https://doi.org/10.1061/(ASCE)CF.1943-5509.0000397.

Park, S., van de Lindt, J. W., & Li, Y. (2013). "Application of the hybrid ABV procedure for assessing community risk to hurricanes spatially." *Natural Hazards*, *68*(2), 981–1000. https://doi.org/10.1007/s11069-013-0674-2

Pei, B., Pang, W., Testik, F., & Ravichandran, N. (2013). "Joint distributions of hurricane wind and storm surge for the city of Charleston in South Carolina." In *ATC & SEI Conference on Advances in Hurricane Engineering 2012* (pp. 703–714). https://doi.org/10.1061/9780784412626.062

Pei, B., Pang, W., Testik, F. Y., Ravichandran, N., & Liu, F. (2014). "Mapping joint hurricane wind and surge hazards for Charleston, South Carolina." *Natural Hazards*, *74*(2), 375–403. https://doi.org/10.1007/s11069-014-1185-5

Pinelli, J.-P., Simiu, E., Gurley, K., Subramanian, C., Zhang, L., Cope, A., … Hamid, S. (2004). "Hurricane damage prediction model for residential structures." *Journal of Structural Engineering*, *130*(11), 1685–1691. https://doi.org/10.1061/(ASCE)0733-9445(2004)130:11(1685)

Pistrika, A. (2010). "Flood damage estimation based on flood simulation scenarios and a GIS platform." *European Water*, *30*, 3–11.

Pistrika, A. K., & Jonkman, S. N. (2010). "Damage to residential buildings due to flooding of New Orleans after hurricane Katrina." *Natural Hazards*, *54*(2), 413–434. https://doi.org/10.1007/s11069-009-9476-y

Pistrika, A., Tsakiris, G., & Nalbantis, I. (2014). "Flood Depth-Damage Functions for Built Environment." *Environmental Processes*, *1*(4), 553–572. 10.1007/s40710-014-0038-2

Pita, G. L., Pinelli, J.-P., Gurley, K., Weekes, J., & Mitrani-Reiser, J. (2011). "Wind vulnerability curves for low-rise commercial-residential buildings in the Florida public hurricane loss model." In *Vulnerability, Uncertainty, and Risk: Analysis, Modeling, and Management: First International Symposium on Uncertainty Modeling and Analysis and Management (ICVRAM 2011); and Fifth International Symposium on Uncertainty Modeling and Anaylsis (ISUMA)* (pp. 618–625). Hyattsville, Maryland, United States. https://doi.org/10.1061/41170(400)75

Pita, G., Pinelli, J.-P., Gurley, K., & Mitrani-Reiser, J. (2015). "State of the art of hurricane vulnerability estimation methods: a review." *Natural Hazards Review*, *16*(2), 4014022. https://doi.org/10.1061/(ASCE)NH.1527-6996.0000153

Posner, A. J., & Georgakakos, K. P. (2017). "Quantifying the impact of community-scale flood mitigation." *International Journal of Disaster Risk Reduction*, *24*, 189–208. https://doi.org/10.1016/j.ijdrr.2017.06.001

Powell, M. D., Murillo, S., Dodge, P., Uhlhorn, E., Gamache, J., Cardone, V., … Annane, B. (2010). "Reconstruction of Hurricane Katrina's wind fields for storm surge and wave hindcasting." *Ocean Engineering*, *37*(1), 26–36. https://doi.org/10.1016/j.oceaneng.2009.08.014

PPD-21 (2013). "Presidential Policy Directive: Critical Infrastructure Security and Resilience." *US Department of Homeland Security*.

Proverbs, D., & Lamond, J. (2017). "Flood resilient construction and adaptation of buildings." In *Oxford Research Encyclopedia of Natural Hazard Science*.

Reese, S., Bradley, B. A., Bind, J., Smart, G., Power, W., & Sturman, J. (2011). "Empirical building fragilities from observed damage in the 2009 South Pacific tsunami." *Earth-Science Reviews*, *107*(1–2), 156–173. https://doi.org/10.1016/j.earscirev.2011.01.009

Rehman, K., & Cho, Y.-S. (2016). "Building damage assessment using scenario based tsunami numerical analysis and fragility curves." *Water*, *8*(3), 109.

Remo, J. W. F., Carlson, M., & Pinter, N. (2012). "Hydraulic and flood-loss modeling of levee, floodplain, and river management strategies, Middle Mississippi River, USA." *Natural Hazards*, *61*(2), 551–575.

Renschler, C. S., Frazier, A. E., Arendt, L. A., Cimellaro, G. P., Reinhorn, A. M., & Bruneau, M. (2010). *A framework for defining and measuring resilience at the community scale: The PEOPLES resilience framework*. Gaithersburg, MD: NIST.

Resio, D. T., Irish, J., & Cialone, M. (2009). "A surge response function approach to coastal hazard assessment–part 1: basic concepts." *Natural Hazards*, *51*(1), 163–182.

Resurreccion, J. Z., & Santos, J. R. (2013). "Uncertainty modeling of hurricane-based disruptions to interdependent economic and infrastructure systems." *Natural Hazards*, *69*(3), 1497–1518.

Rey, W., Mendoza, E. T., Salles, P., Zhang, K., Teng, Y.-C., Trejo-Rangel, M. A., & Franklin,

G. L. (2019). "Hurricane flood risk assessment for the Yucatan and Campeche State coastal area." *Natural Hazards*, *96*(3), 1041–1065. https://doi.org/10.1007/s11069-019-03587-3

Richards, P. J., Williams, N., Laing, B., McCarty, M., & Pond, M. (2008). "Numerical calculation of the three-dimensional motion of wind-borne debris." *Journal of Wind Engineering and Industrial Aerodynamics*, *96*(10–11), 2188–2202.

Romali, N. S., Yusop, Z., & Ismail, Z. (2015). "Flood damage assessment: A review of flood stage–damage function curve." In S. H. A. Bakar, M. A. Wahid, R. Hassan, W. Tahir, and S. R. M. Nasir (Eds.), *ISFRAM 2014* (pp. 147–159). Manhattan, New York City: Springer.

Rose, A. (2004). "Defining and measuring economic resilience to disasters." *Disaster Prevention and Management: An International Journal*, *13*(4), 307–314.

Rose, A. (2007). "Economic resilience to natural and man-made disasters: Multidisciplinary origins and contextual dimensions." *Environmental Hazards*, *7*(4), 383–398.

Rose, A., & Liao, S. (2005). "Modeling regional economic resilience to disasters: A computable general equilibrium analysis of water service disruptions." *Journal of Regional Science*, *45*(1), 75–112.

Rosenheim, N., Guidotti, R., Gardoni, P., and Peacock, W. (2019). "Integration of detailed household characteristic data with critical infrastructure and its implementation to post-hazard resilience modeling." *Sustainable and Resilient Infrastructure (under Review).*

Rosowsky, D. V, & Ellingwood, B. R. (2002). "Performance-based engineering of wood frame housing: Fragility analysis methodology." *Journal of Structural Engineering*, *128*(1), 32–38. https://doi.org/10.1061/(ASCE)0733-9445(2002)128:1(32)

Rözer, V., Kreibich, H., Schröter, K., Müller, M., Sairam, N., Doss-Gollin, J., … Merz, B. (2019). "Probabilistic models significantly reduce uncertainty in Hurricane Harvey pluvial flood loss estimates." *Earth's Future*, *7*(4), 384–394. https://doi.org/10.1029/2018EF001074

Rufat, S., Tate, E., Burton, C. G., & Maroof, A. S. (2015). "Social vulnerability to floods: Review of case studies and implications for measurement." *International Journal of Disaster Risk Reduction*, *14*, 470–486.

Rus, K., Kilar, V., & Koren, D. (2018). "Resilience assessment of complex urban systems to natural disasters: a new literature review." *International Journal of Disaster Risk Reduction*.

Saint-Geours, Nathalie, Frédéric Grelot, J-S. Bailly, and C. L. (2015). "Ranking sources of uncertainty in flood damage modelling a case study on the cost-benefit analysis of a flood mitigation project in the Orb Delta, France." *Journal of Flood Risk Management*, *8*(2), 161–172.

Sairam, N., Schröter, K., Carisi, F., Wagenaar, D., Domeneghetti, A., Molinari, D., … Merz, B. (2020). "Bayesian Data-Driven approach enhances synthetic flood loss models."

Environmental Modelling & Software, 104798. https://doi.org/10.1016/j.envsoft.2020.104798

Salman, A. M., Asce, A. M., Li, Y., & Asce, M. (2018). "Flood Risk Assessment , Future Trend Modeling , and Risk Communication : A Review of Ongoing Research." *Natural Hazards Review*, *19*(3), 04018011. https://doi.org/10.1061/(ASCE)NH.1527-6996.0000294.

Sasanakul, I., Vanadit-Ellis, W., Sharp, M., Abdoun, T., Ubilla, J., Steedman, S., & Stone, K. (2008). "New Orleans levee system performance during Hurricane Katrina: 17th Street Canal and Orleans Canal North." *Journal of Geotechnical and Geoenvironmental Engineering*, *134*(5), 657–667.

SBA (2020). "Disaster assistance." . Retrieved from https://www.sba.gov/funding-programs/disaster-assistance

Scawthorn, C., Asce, F., Flores, P., Blais, N., Seligson, H., Tate, E., … Lawrence, M. (2006). "HAZUS-MH Flood Loss Estimation Methodology . II . Damage and Loss Assessment." , *7*(2), 72–81.

Schanze, J., Zeman, E., & Marsalek, J. (2007). *Flood risk management: hazards, vulnerability and mitigation measures* (Vol. 67). Springer Science & Business Media.

Scheitlin, K. N., Elsner, J. B., Lewers, S. W., Malmstadt, J. C., & Jagger, T. H. (2011). "Risk assessment of hurricane winds for Eglin Air Force Base in northwestern Florida, USA." *Theoretical and Applied Climatology*, *105*(3), 287–296. https://doi.org/10.1007/s00704-010-0386-4

Schelfaut, K., Pannemans, B., Van der Craats, I., Krywkow, J., Mysiak, J., & Cools, J. (2011). "Bringing flood resilience into practice: the FREEMAN project." *Environmental Science & Policy*, *14*(7), 825–833.

Scira Menoni, & Pergalani, F. (1996). "An attempt to link risk assessment with land use planning: arecent experience in Italy." *Disaster Prevention and Management*, *5*(1), 6–21.

Scorzini, A. R., & Frank, E. (2017). "Flood damage curves: new insights from the 2010 flood in Veneto, Italy." *Journal of Flood Risk Management*, *10*(3), 381–392. https://doi.org/10.1111/jfr3.12163

Smith, D. I. (1994). "Flood Damage Estimation - A review of Urban Stage-Damage Curves and Loss Functions." *Water SA*. Retrieved from http://www.heraldlive.co.za/

Soetanto, R., & Proverbs, D. G. (2004). "Impact of flood characteristics on damage caused to UK domestic properties: the perceptions of building surveyors." *Structural Survey*. https://doi.org/10.1108/02630800410538622

Spekkers, M. H., Kok, M., Clemens, F., & Ten Veldhuis, J. A. E. (2014). "Decision-tree analysis of factors influencing rainfall-related building structure and content damage." *Natural Hazards and Earth System Sciences*, *14*(9), 2531–2547.

Stacy R. Stewart, & Robbie Berg (2019). *Hurricane Florence: National Hurricane Center Tropical Cyclone Report*.

State of NC (2018). "NORTH CAROLINA'S SPATIAL DATA DOWNLOAD." .

State of North Carolina (2019). "North Carolina Spatial Data." . Retrieved from https://sdd.nc.gov/

Statista (2020). "Most expensive hurricanes in the United States as of April 2020, by insured property losses." .

Strassberg, G., Jones, N. L., & Maidment, D. R. (2011). *ARC hydro groundwater: GIS for hydrogeology*. Esri Press.

Sydnor, S., Niehm, L., Lee, Y., Marshall, M., & Schrank, H. (2017). "Analysis of post-disaster damage and disruptive impacts on the operating status of small businesses after Hurricane Katrina." *Natural Hazards*, *85*(3), 1637–1663.

Ten Veldhuis, J. A. E., & Clemens, F. (2010). "Flood risk modelling based on tangible and intangible urban flood damage quantification." *Water Science and Technology*, *62*(1), 189–195.

Teng, J., Jakeman, A. J., Vaze, J., Croke, B. F. W., Dutta, D., & Kim, S. (2017). "Flood inundation modelling: A review of methods, recent advances and uncertainty analysis." *Environmental Modelling and Software*, *90*, 201–216. 10.1016/j.envsoft.2017.01.006

Tesliuc, E. D., & Lindert, K. (2002). *Vulnerability: A quantitative and qualitative assessmentGuatemala Poverty Assessment Program*. Citeseer.

Thieken, A.H., Ackermann, V., Elmer, F., Kreibich, H., Kuhlmann, B., Kunert, U., Maiwald, H., Merz, B., Müller, M., Piroth, K. and Schwarz, J. (2008). "Methods for the evaluation of direct and indirect flood losses." In *4th international symposium on flood defense: managing flood risk, reliability and vulnerability*. Toronto, Ontario, Canada.

Thieken, A. H., Mariani, S., Longfield, S., & Vanneuville, W. (2014). "Preface: Flood resilient communities–managing the consequences of flooding." *Nat. Hazards Earth Syst. Sci*, *14*, 33–39.

Thieken, A. H., Müller, M., Kreibich, H., & Merz, B. (2005). "Flood damage and influencing factors: New insights from the August 2002 flood in Germany." *Water Resources Research*, *41*(12).

Thieken, A. H., Olschewski, A., Kreibich, H., Kobsch, S., & Merz, B. (2008). "Development and evaluation of FLEMOps–a new Flood Loss Estimation MOdel for the private sector." *WIT Transactions on Ecology and the Environment*, *118*, 315–324.

Thurston, N., Finlinson, B., Breakspear, R., Williams, N., Shaw, J., & Chatterton, J. (2008). "Developing the evidence base for flood resistance and resilience." *R&D Summary Report,* *Joint Defra/EA Flood and Coastal Erosion, London*.

Tokgoz, B. E., & Gheorghe, A. V (2013). "Resilience quantification and its application to a residential building subject to hurricane winds." *International Journal of Disaster Risk Science*, *4*(3), 105–114.

Tomiczek, T., Kennedy, A., & Rogers, S. (2014). "Collapse limit state fragilities of wood-framed residences from storm surge and waves during Hurricane Ike." *Journal of Waterway, Port, Coastal, and Ocean Engineering*, *140*(1), 43–55. https://doi.org/10.1061/(ASCE)WW.1943-5460.0000212

Tomiczek, T., Kennedy, A., Zhang, Y., Owensby, M., Hope, M. E., Lin, N., & Flory, A. (2017). "Hurricane damage classification methodology and fragility functions derived from Hurricane Sandy's effects in Coastal New Jersey." *Journal of Waterway, Port, Coastal, and Ocean Engineering*, *143*(5), 4017027. https://doi.org/10.1061/(ASCE)WW.1943-5460.0000409

Török, I. (2018). "Qualitative assessment of social vulnerability to flood hazards in Romania." *Sustainability*, *10*(10), 3780. https://doi.org/10.3390/su10103780

Tran, H. T., Balchanos, M., Domerçant, J. C., & Mavris, D. N. (2017). "A framework for the quantitative assessment of performance-based system resilience." *Reliability Engineering & System Safety*, *158*, 73–84.

Triola, M. F. (2010). *Elementary statistics*. Pearson/Addison-Wesley Reading, MA.

Tsakiris, G. (2014). "Flood risk assessment : concepts , modelling , applications." *Natural Hazards and Earth System Sciences*, *14*(5), 1361–1369. https://doi.org/10.5194/nhess-14-1361-2014

Unnikrishnan, V. U., & Barbato, M. (2017). "Multihazard interaction effects on the performance of low-rise wood-frame housing in hurricane-prone regions." *Journal of Structural Engineering*, *143*(8), 4017076. https://doi.org/10.1061/(ASCE)ST.1943-541X.0001797

Up-Codes (2019). "Up Codes." . Retrieved from https://up.codes/

US Census Bureau (2019). "QuickFacts: North Carolina." . https://www.census.gov/quickfacts/NC

US Hydrologic Engineering Center (2001). *The Hydrologic Modeling System (HEC-HMS)*. US Army Corps of Engineers, Hydrologic Engineering Center.

USDA (2020). "Disaster Assistance Programs." . Retrieved from https://www.fsa.usda.gov/programs-and-services/disaster-assistance-program/

USGS (2018). "National Water Information System: Mapper." . Retrieved from https://maps.waterdata.usgs.gov/mapper/index.html van de Lindt, J. W., Peacock, W. G., Mitrani-Reiser, J., Rosenheim, N., Deniz, D., Dillard, M., … Crawford, P. S. (2020). "Community Resilience-Focused Technical Investigation of the 2016 Lumberton, North Carolina, Flood: An Interdisciplinary Approach." *Natural Hazards Review*, *21*(3), 4020029. https://doi.org/10.1061/(ASCE)NH.1527-6996.0000387

van de Lindt, J. W., Peacock, W. G., Mitrani-Reiser, J., Rosenheim, N., Deniz, D., Dillard, M. K., … Fung, J. F. (2018). *The Lumberton, North Carolina Flood of 2016: A Community Resilience Focused Technical Investigation (Special Publication (NIST SP)-1230)*. Gaithersburg, Maryland.

van de Lindt, J. W., & Taggart, M. (2009). "Fragility Analysis Methodology for Performance-Based Analysis of Wood-Frame Buildings for Flood." *Natural Hazards Review*, *10*(3), 113–123. https://doi.org/10.1061/(ASCE)1527-6988(2009)10:3(113)

van Manen, S. E., & Brinkhuis, M. (2005). "Quantitative flood risk assessment for Polders." *Reliability Engineering & System Safety*, *90*(2–3), 229–237.

Van Ootegem, L., Verhofstadt, E., Van Herck, K., & Creten, T. (2015). "Multivariate pluvial flood damage models." *Environmental Impact Assessment Review*, *54*, 91–100.

Van Verseveld, H. C. W., Van Dongeren, A. R., Plant, N. G., Jäger, W. S., & Den Heijer, C. (2015). "Modelling multi-hazard hurricane damages on an urbanized coast with a Bayesian Network approach." *Coastal Engineering*, *103*, 1–14. https://doi.org/10.1016/j.coastaleng.2015.05.006

Vickery, P. J., Masters, F. J., Powell, M. D., & Wadhera, D. (2009). "Hurricane hazard modeling: The past, present, and future." *Journal of Wind Engineering and Industrial Aerodynamics*, *97*(7–8), 392–405. https://doi.org/10.1016/j.jweia.2009.05.005

Vickery, P. J., Skerlj, P. F., Lin, J., Twisdale Jr, L. A., Young, M. A., & Lavelle, F. M. (2006). "HAZUS-MH hurricane model methodology. II: Damage and loss estimation." *Natural Hazards Review*, *7*(2), 94–103. https://doi.org/10.1061/(ASCE)1527-6988(2006)7:2(94)

Vorogushyn, S., Merz, B., Lindenschmidt, K. E., & Apel, H. (2010). "A new methodology for flood hazard assessment considering dike breaches." *Water Resources Research*, *46*(8). 10.1029/2009WR008475

Walker, B., Holling, C. S., Carpenter, S., & Kinzig, A. (2004). "Resilience, adaptability and transformability in social–ecological systems." *Ecology and Society*, *9*(2).

Wang, C., Zhang, H., Feng, K., & Li, Q. (2017). "Assessing hurricane damage costs in the presence of vulnerability model uncertainty." *Natural Hazards*, *85*(3), 1621–1635. https://doi.org/10.1007/s11069-016-2651-z

Wenger, C. (2015a). "Better use and management of levees: reducing flood risk in a changing climate." *Environmental Reviews*, *23*(2), 240–255.

Wenger, C. (2015b). "Building walls around flood problems: The place of levees in Australian flood management." *Australasian Journal of Water Resources*, *19*(1), 3–30.

Westerink, J. J., Luettich Jr, R. A., Blain, C. A., & Scheffner, N. W. (1994). *ADCIRC: an advanced three-dimensional circulation model for shelves, coasts, and estuaries. Report 2. User's manual for ADCIRC-2DDI*. Army Engineer Waterways Experiment Station Vicksburg Ms.

Wills, J. A. B., Lee, B. E., & Wyatt, T. A. (2002). "A model of wind-borne debris damage." *Journal of Wind Engineering and Industrial Aerodynamics*, *90*(4–5), 555–565.

Wobus, C., Lawson, M., Jones, R., Smith, J., & Martinich, J. (2014). "Estimating monetary damages from flooding in the U nited S tates under a changing climate." *Journal of Flood Risk Management*, *7*(3), 217–229.

Woolf, S., Twigg, J., Parikh, P., Karaoglou, A., & Cheaib, T. (2016). "Towards measurable resilience: A novel framework tool for the assessment of resilience levels in slums." *International Journal of Disaster Risk Reduction*, *19*, 280–302.

World Health Organization (2020). "Medical devices by facility provincial hospital." . Retrieved from https://www.who.int/medical_devices/survey_resources/medical_devices_by_facility_provincial_hospitals_kenya.pdf

Xu, Yueping, Martijn J. Booij, and A. E. M. (2007). "Propagation of discharge uncertainty in a flood damage model for the Meuse River." In S. Begum, M. J. F. Stive, and J. W. Hall (Eds.), *Flood Risk Management in Europe* (pp. 293–310). Springer, Dordrecht.

Yi, C. S., Lee, J. H., & Shim, M. P. (2010). "GIS-based distributed technique for assessing economic loss from flood damage: Pre-feasibility study for the Anyang Stream Basin in Korea." *Natural Hazards*, *55*(2), 251–272. https://doi.org/10.1007/s11069-010-9524-7

Zhang, W., Lin, P., Wang, N., Nicholson, C., & Xue, X. (2018). "Probabilistic prediction of postdisaster functionality loss of community building portfolios considering utility disruptions." *Journal of Structural Engineering*, *144*(4), 4018015. https://doi.org/10.1061/(ASCE)ST.1943-541X.0001984

Zoraster, R. M. (2010). "Vulnerable populations: Hurricane Katrina as a case study." *Prehospital and Disaster Medicine*, *25*(1), 74–78.

APPENDIX A

F1: One-Story Single-Family Residential Building

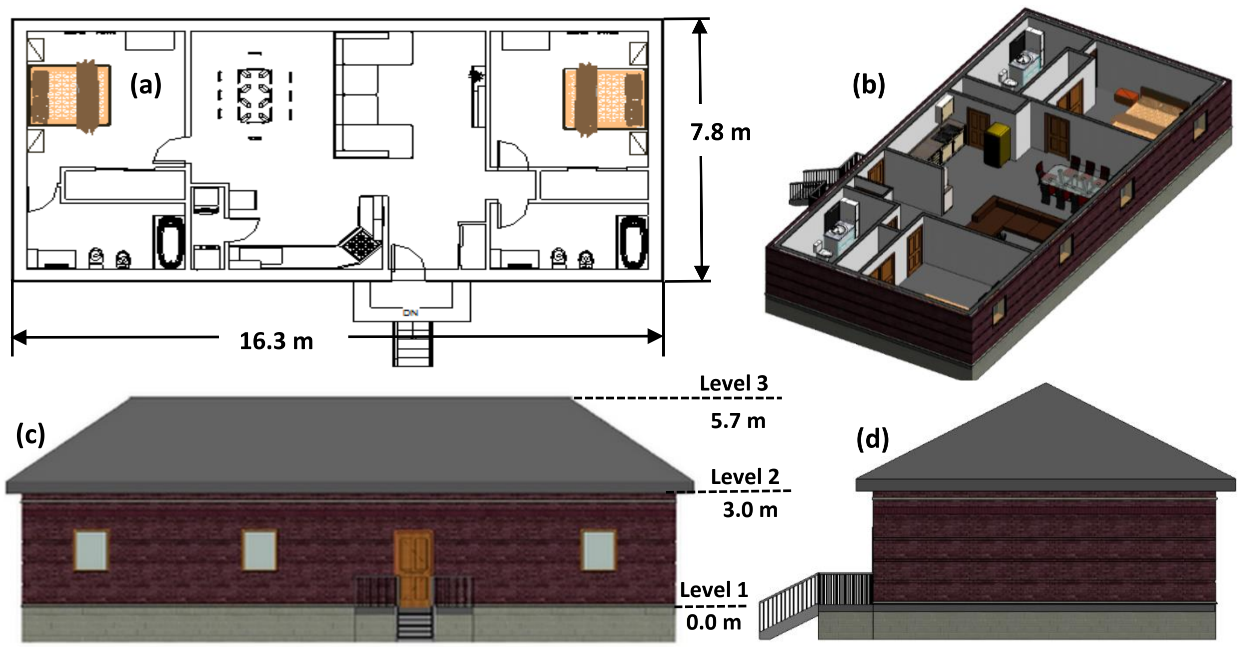

Figure A1. F1 archetype plans and sections: (a) Plan view; (b) 3-D view; (c) Front view; (d) Side view

F2: One-Story Multi-Family Residential Building

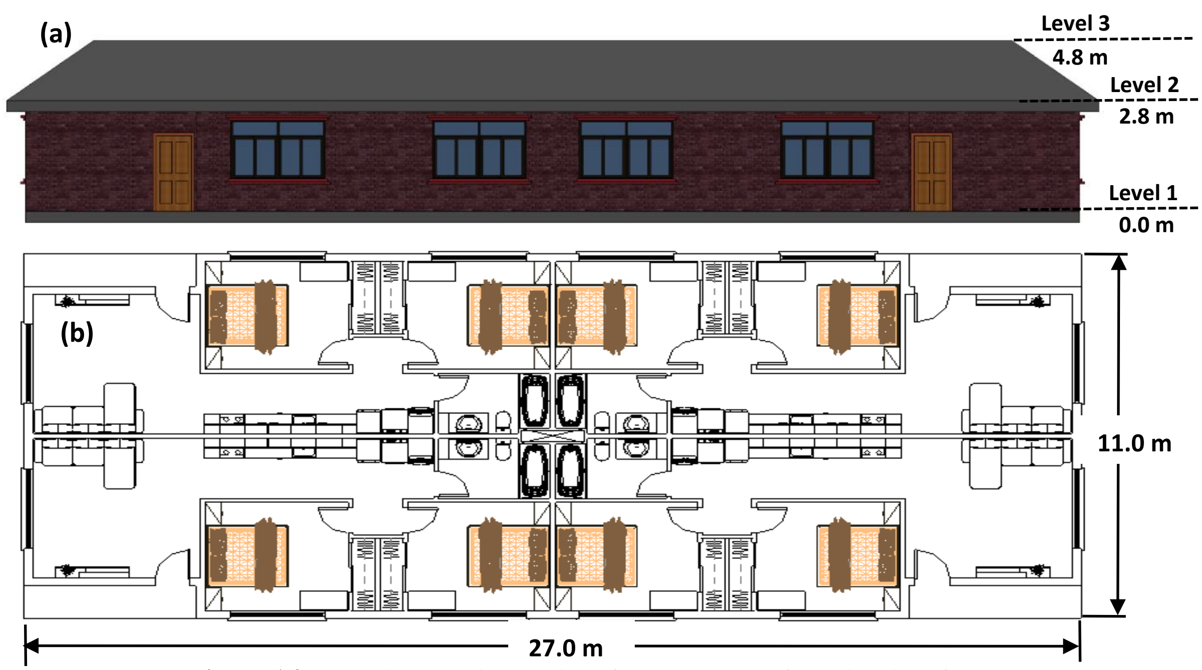

Figure A2. F2 archetype plans and sections: (a) Front view; (b) Plan view

F3: Two-Story Single-Family Residential Building

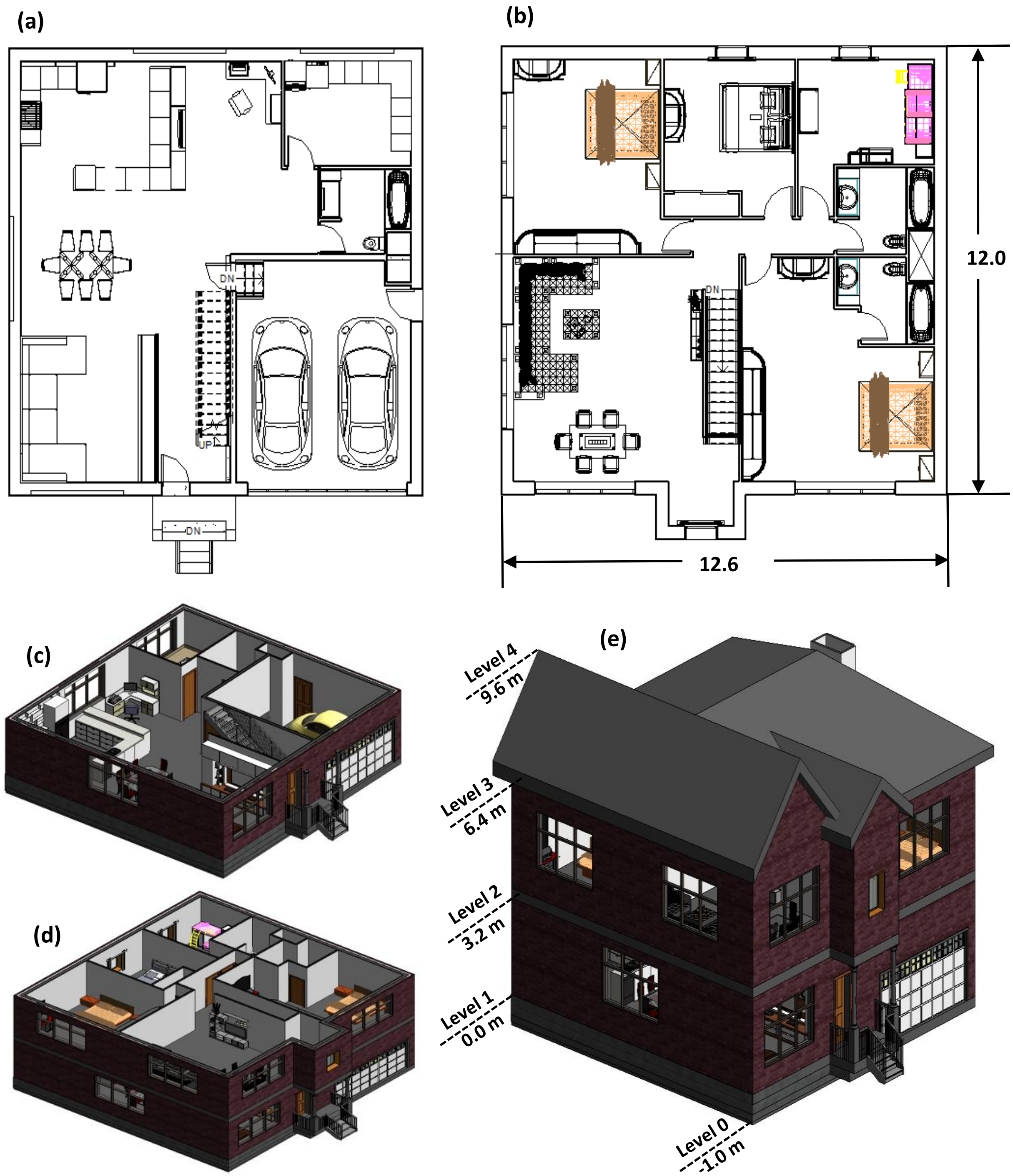

Figure A3. F3 archetype plans and sections: (a) First-story plan view; (b) Second-story plan view; (c) First-story 3-D view; (d) Second-story 3-D view; (e) Building 3-D view

F4: Two-Story Multi-Family Residential Building

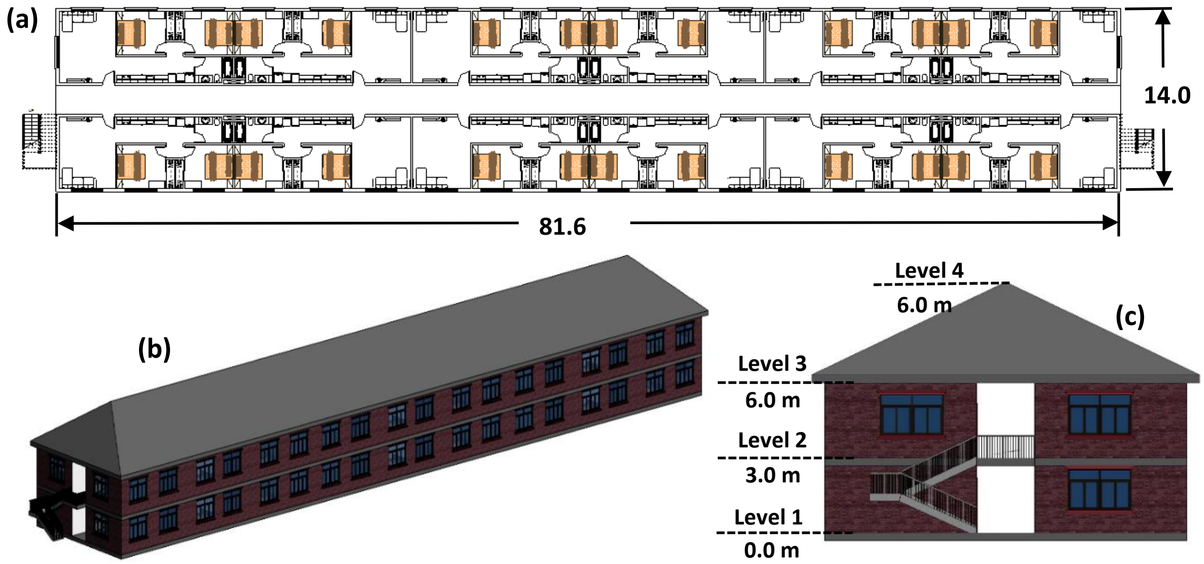

Figure A4. F4 archetype plans and sections: (a) Plan view; (b) 3-D view; (c) Side view

F5: Small Grocery Store/Gas Station with a Convenience Store

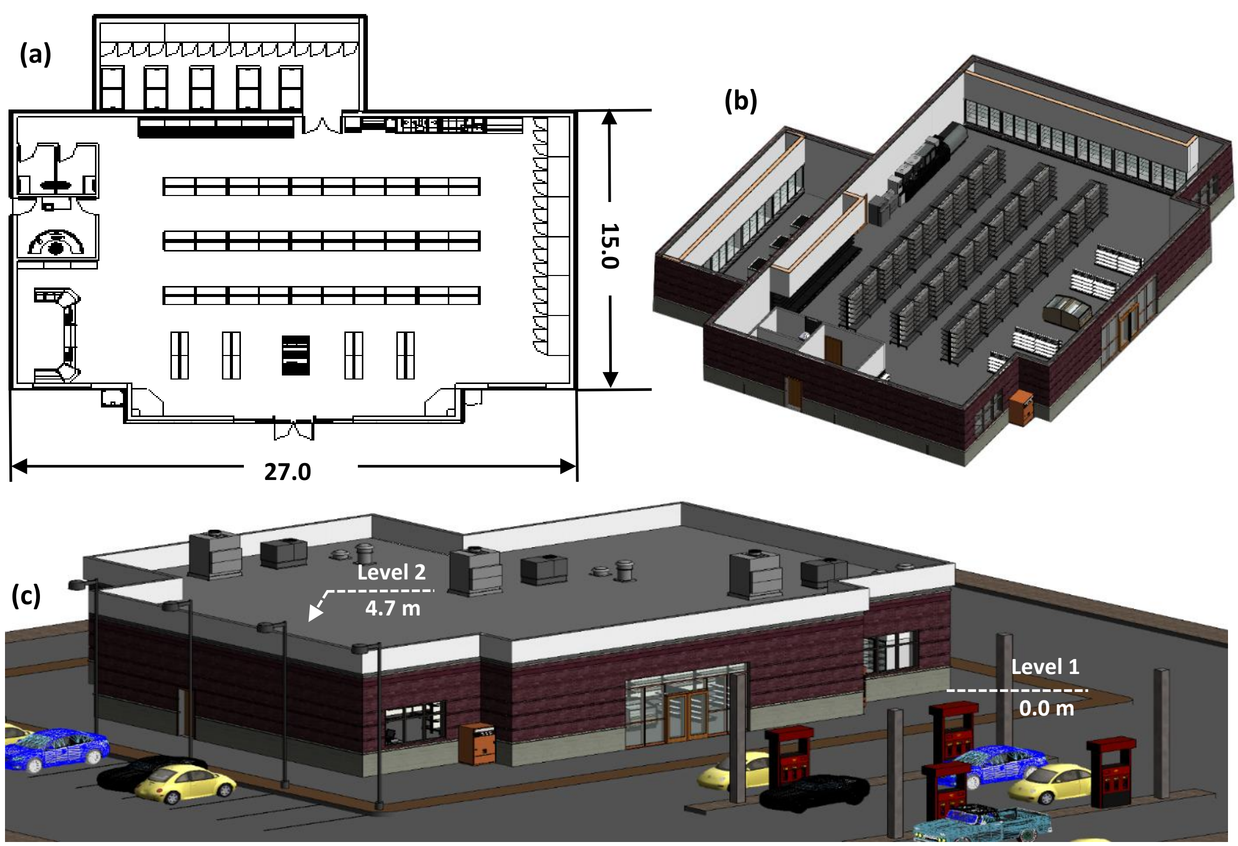

Figure A5. F5 archetype plans and sections: (a) Plan view; (b) 3-D view for the store; (c) 3-D view for the whole gas station

F6: Multi-unit retail building (strip mall)

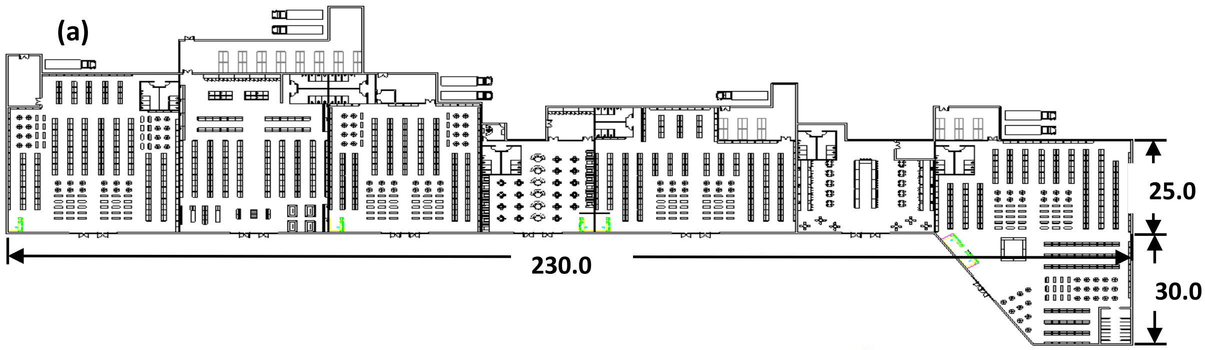

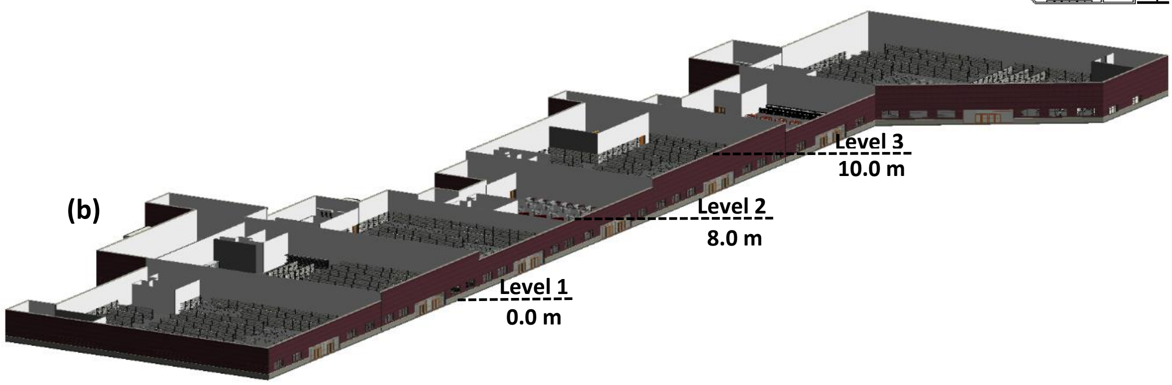

Figure A6. F6 archetype plans and views: (a) Plan view; (b) 3-D view

F7: Small multi-unit commercial building

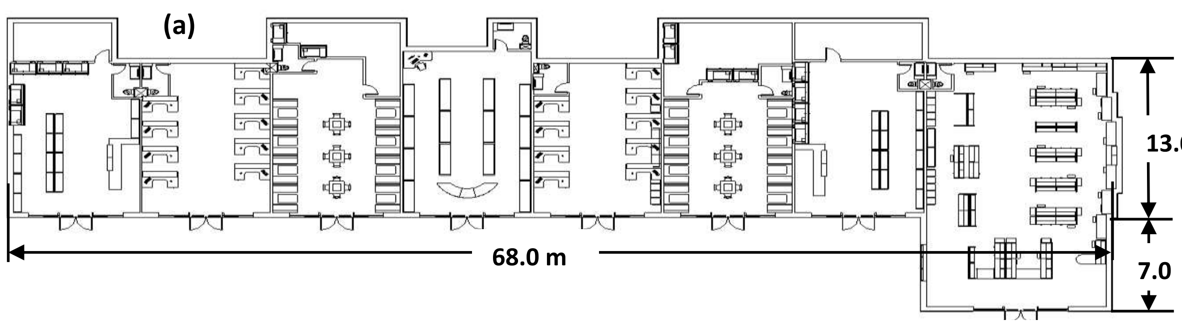

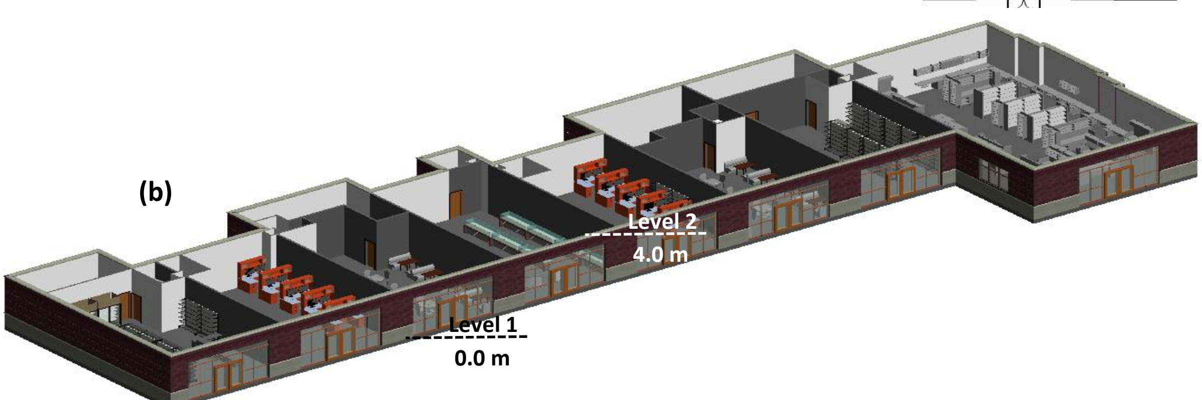

Figure A7. F7 archetype plans and views: (a) Plan view; (b) 3-D view

F8: Super retail center

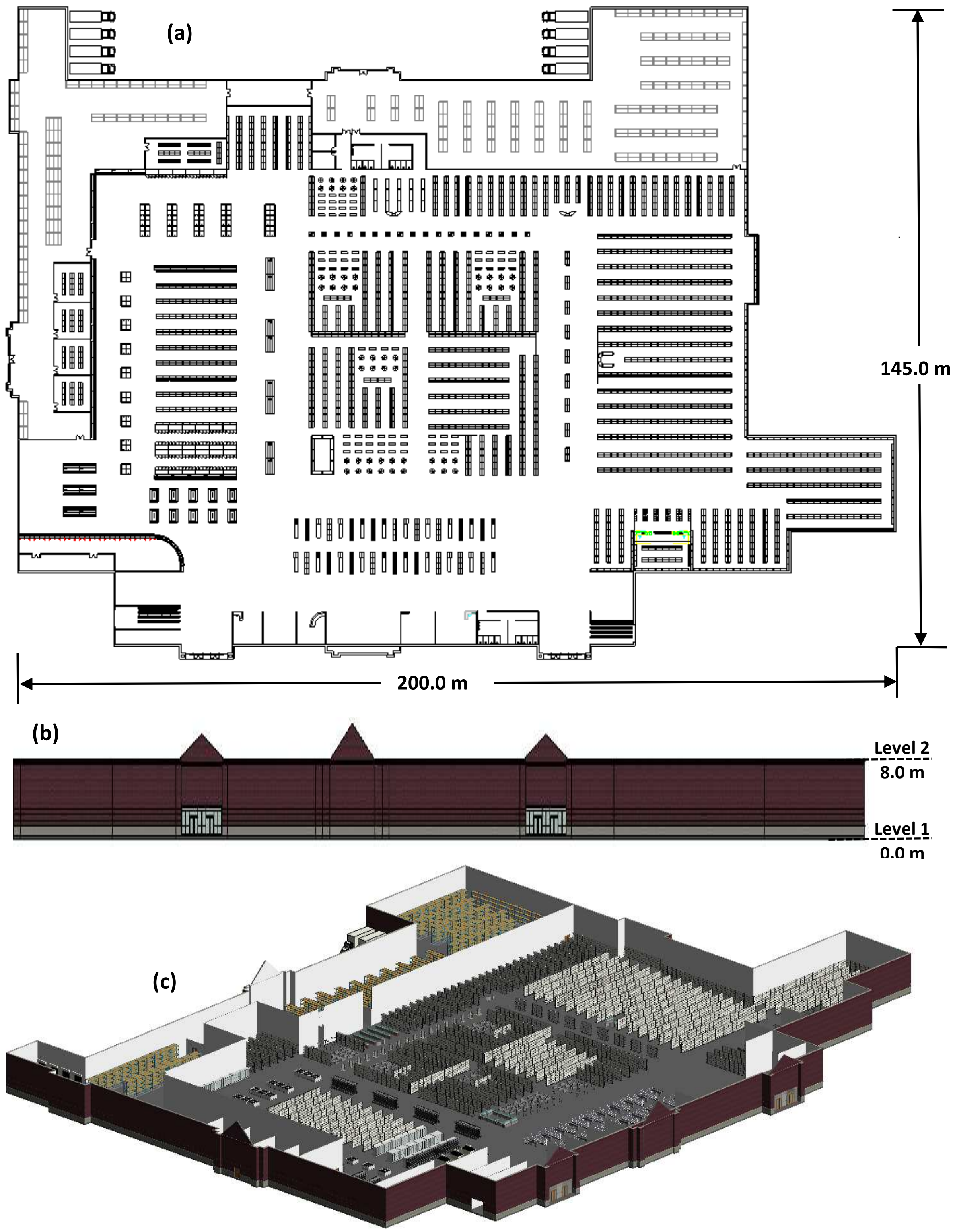

Figure A8. F8 archetype plans and sections: (a) Plan view; (b) Side view for the store; (c) 3-D view for the whole Market.

F9: Industrial building

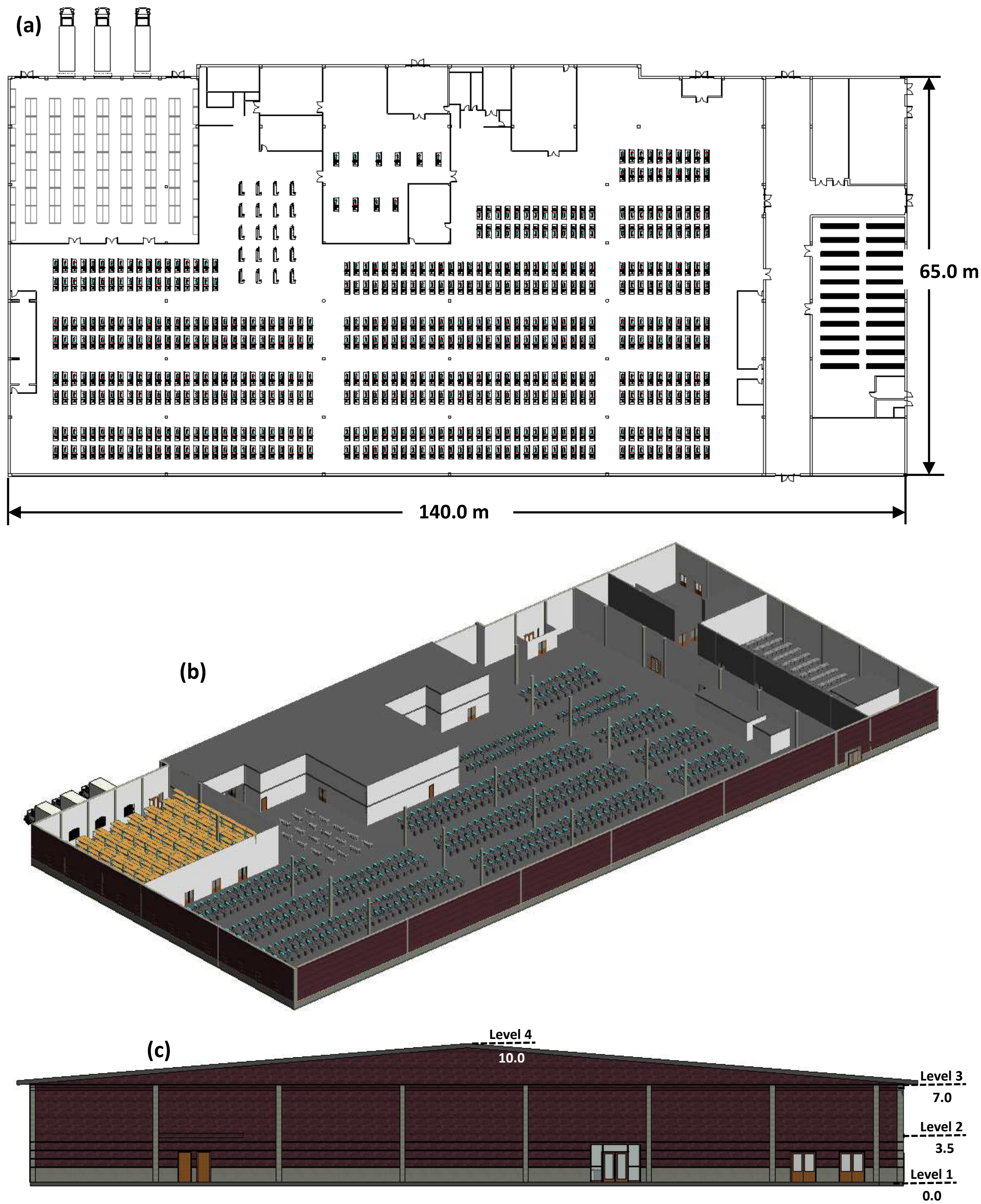

Figure A9. F9 archetype plans and sections: (a) Plan view; (b) 3-D view for the industrial building; (c) Side view.

F11: Two-story School

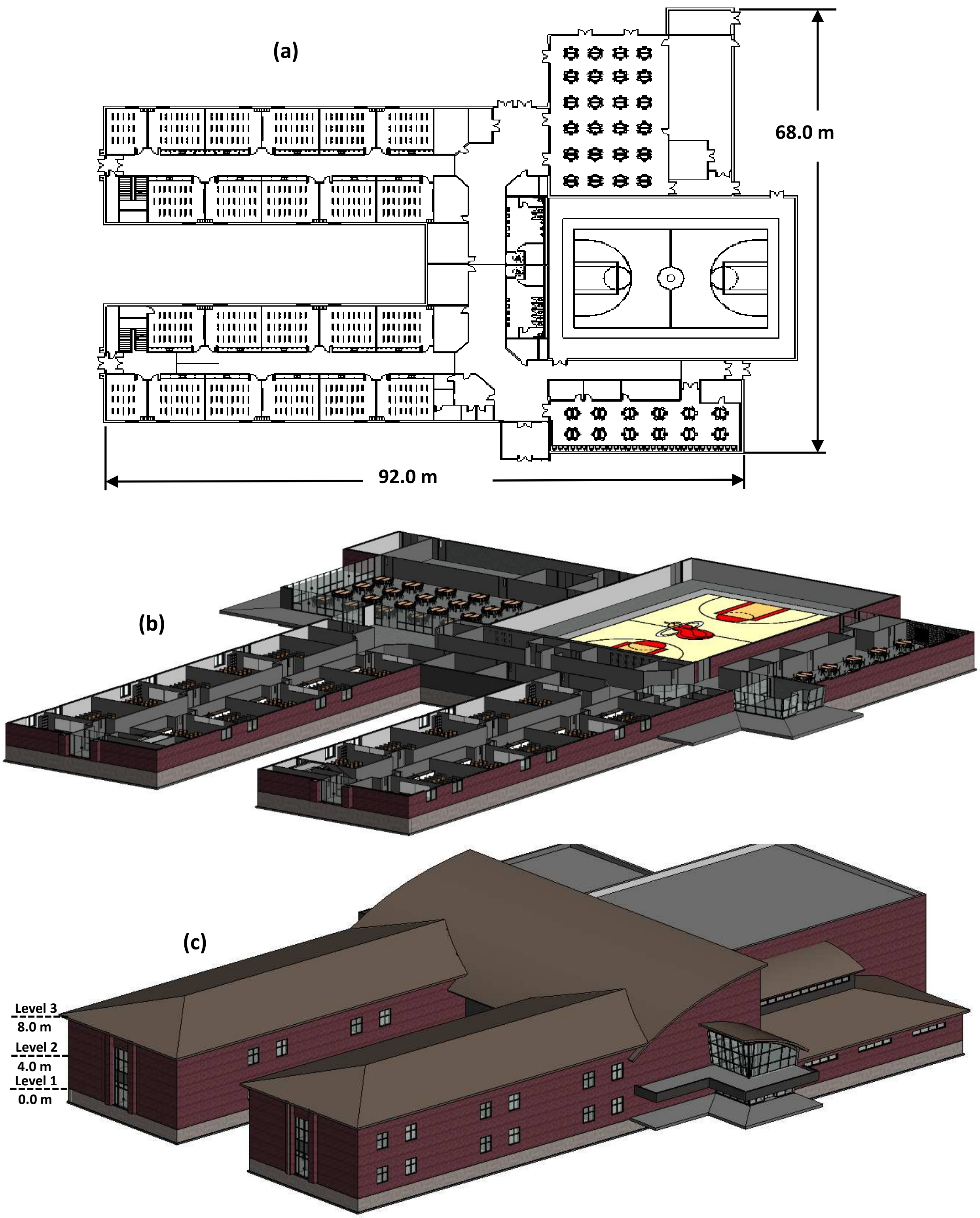

Figure A10. F10 archetype plans and sections: (a) Plan view; (b) 3-D view for the interior of the school; (c) 3-D view for the whole school.

F12: Hospital/Clinic

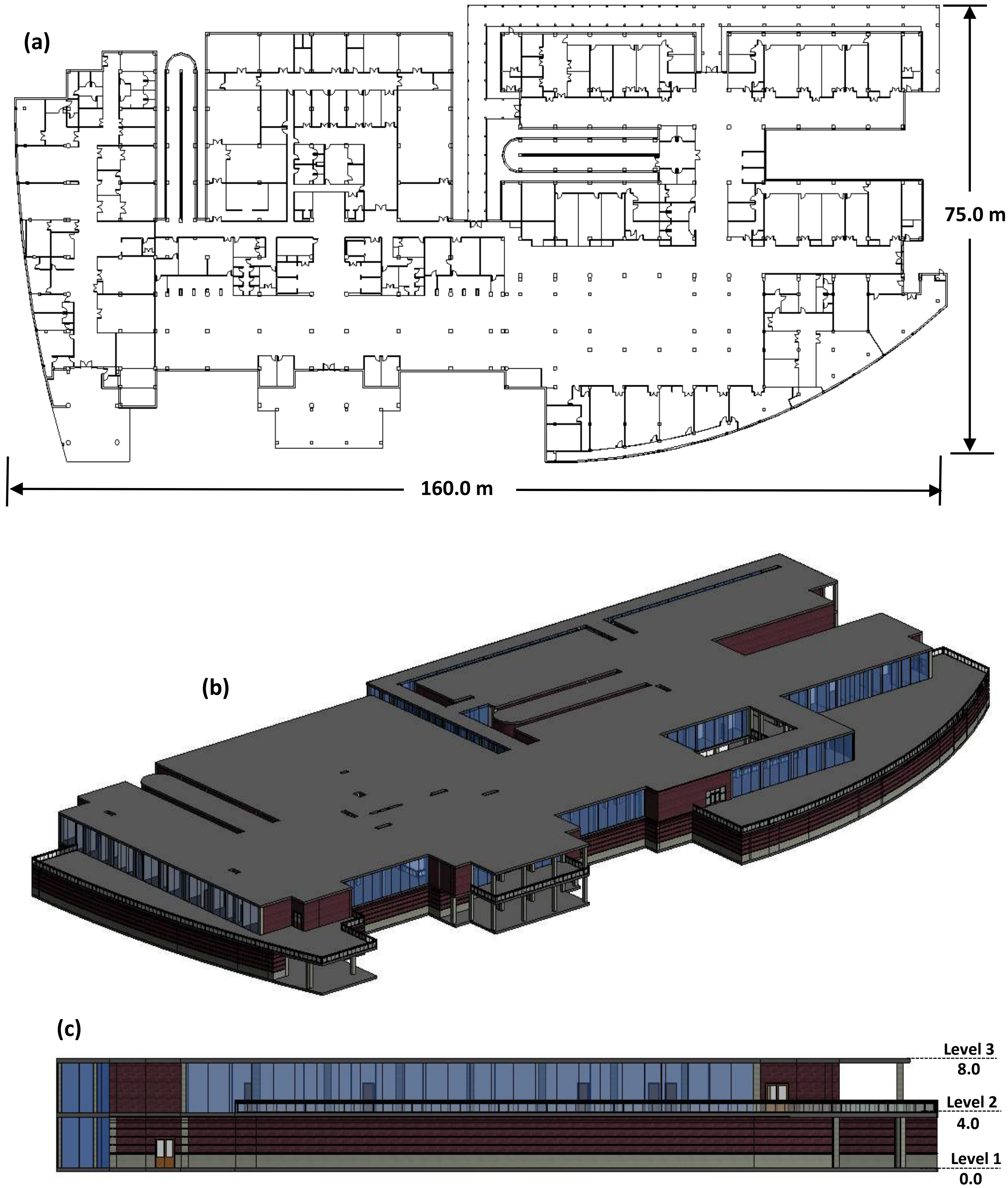

Figure A11. F12 archetype plans and sections: (a) Plan view; (b) 3-D view for the interior of the hospital; (c) 3-D view for the whole hospital.

F13: Community center (church)

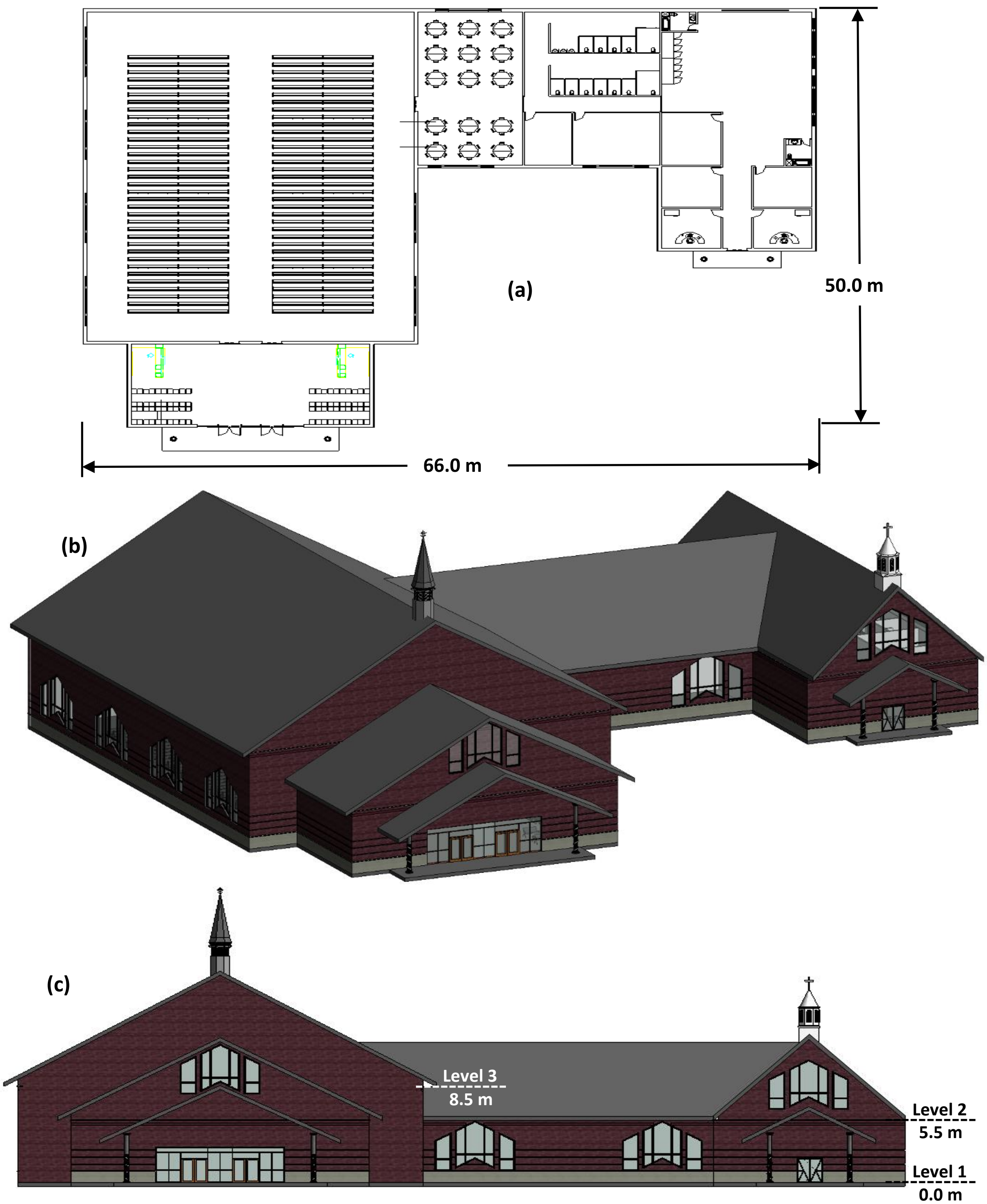

Figure A12. F12 archetype plans and sections: (a) Plan view; (b) 3-D view for the church; (c) Side view for the whole church.

F14: Office building

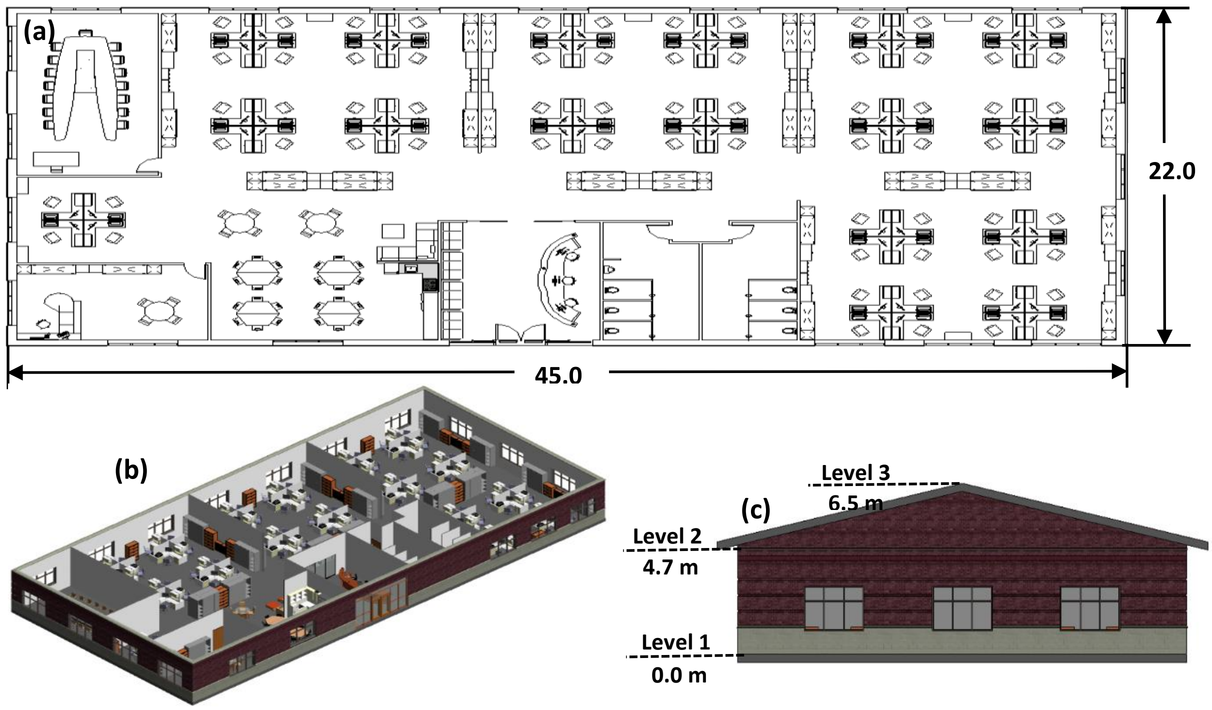

Figure A13. F14 archetype plans and sections: (a) Plan view; (b) 3-D views for the office building; (c) Side view.

15: Warehouse (small/large box)

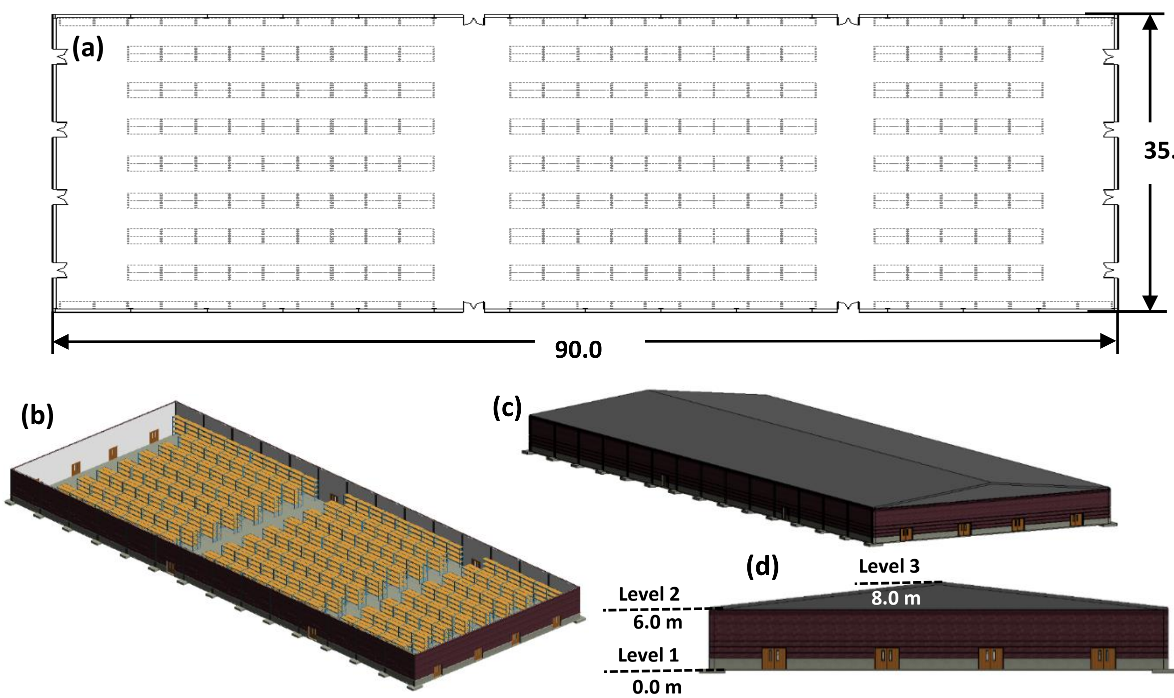

Figure A14. F15 archetype plans and sections: (a) Plan view; (b, and c) 3-D views for the warehouse; (d) Side view for the warehouse.

APPENDIX B

F1: One-Story Single-Family Residential Building

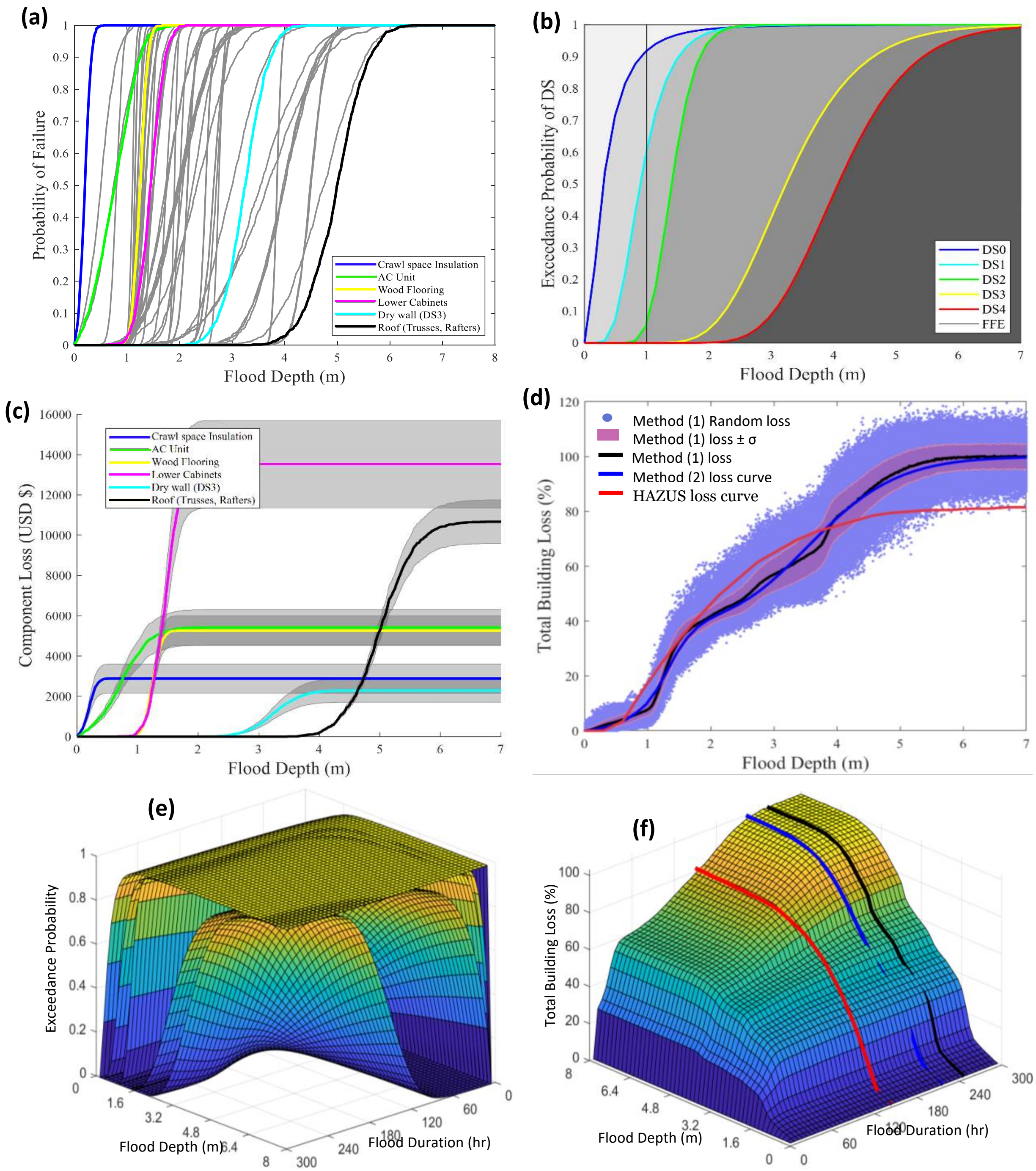

Figure B1. F1 archetype analysis results: (a) Component fragility curves; (b) Building fragility curves; (c) Selected components loss curves; (d) Building loss curves; (e) Building fragility surfaces; (f) Building loss surface.

F2: One-Story Multi-Family Residential Building

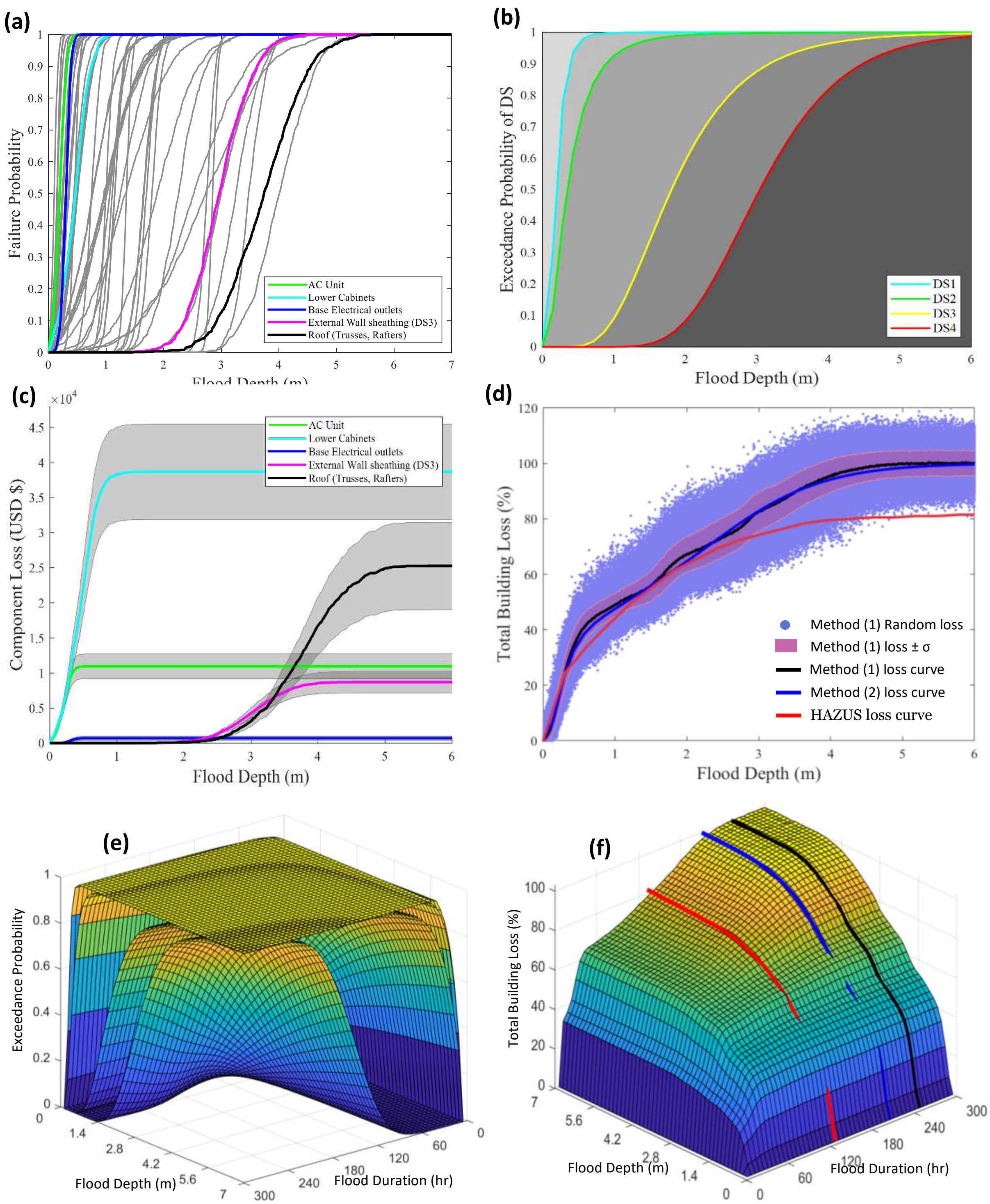

Figure B2. F2 archetype analysis results: (a) Component fragility curves; (b) Building fragility curves; (c) Selected components loss curves; (d) Building loss curves; (e) Building fragility surfaces; (f) Building loss surface.

F3: Two-Story Single-Family Residential Building

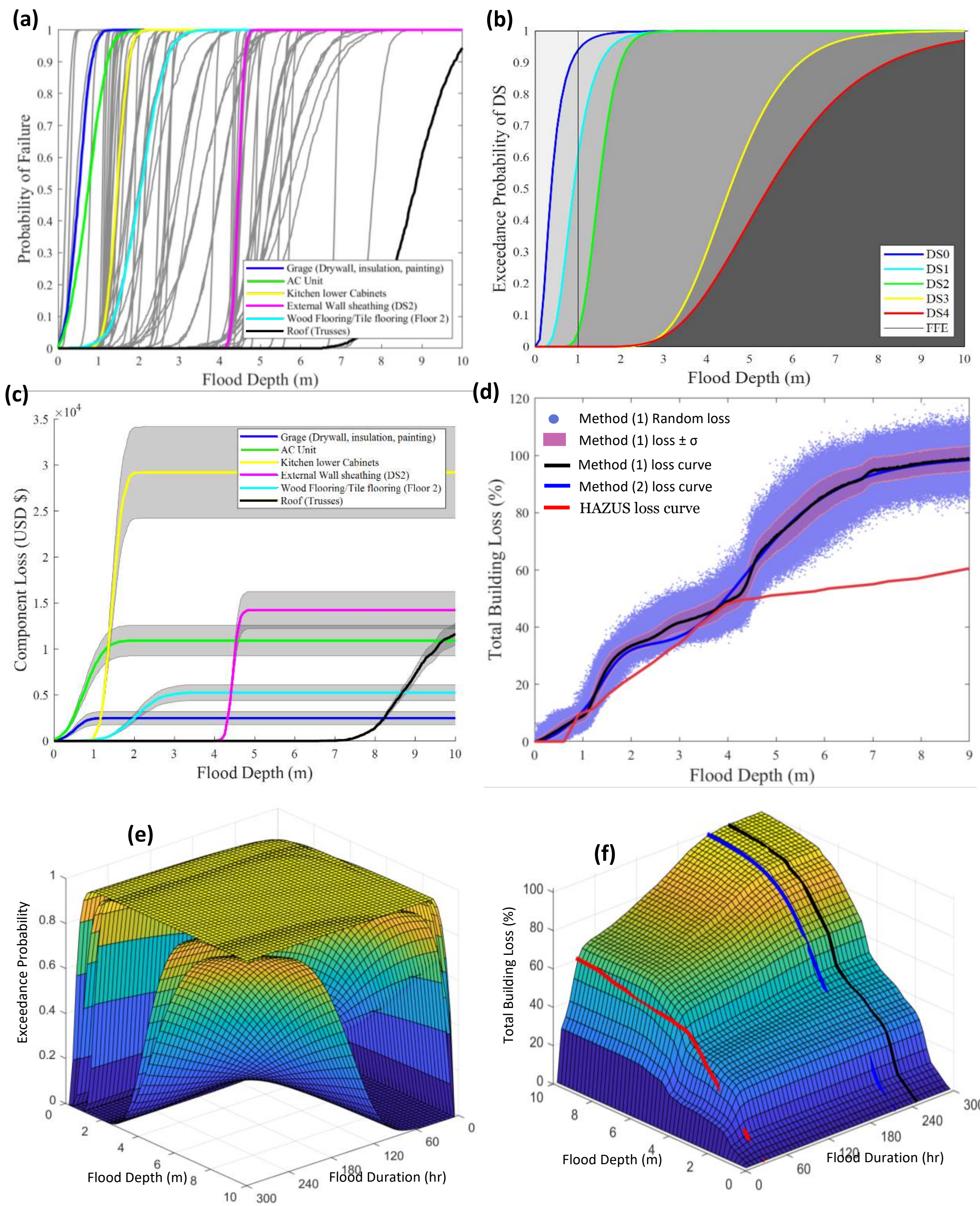

Figure B3. F3 archetype analysis results: (a) Component fragility curves; (b) Building fragility curves; (c) Selected components loss curves; (d) Building loss curves; (e) Building fragility surfaces; (f) Building loss surface.

F4: Two-Story Multi-Family Residential Building

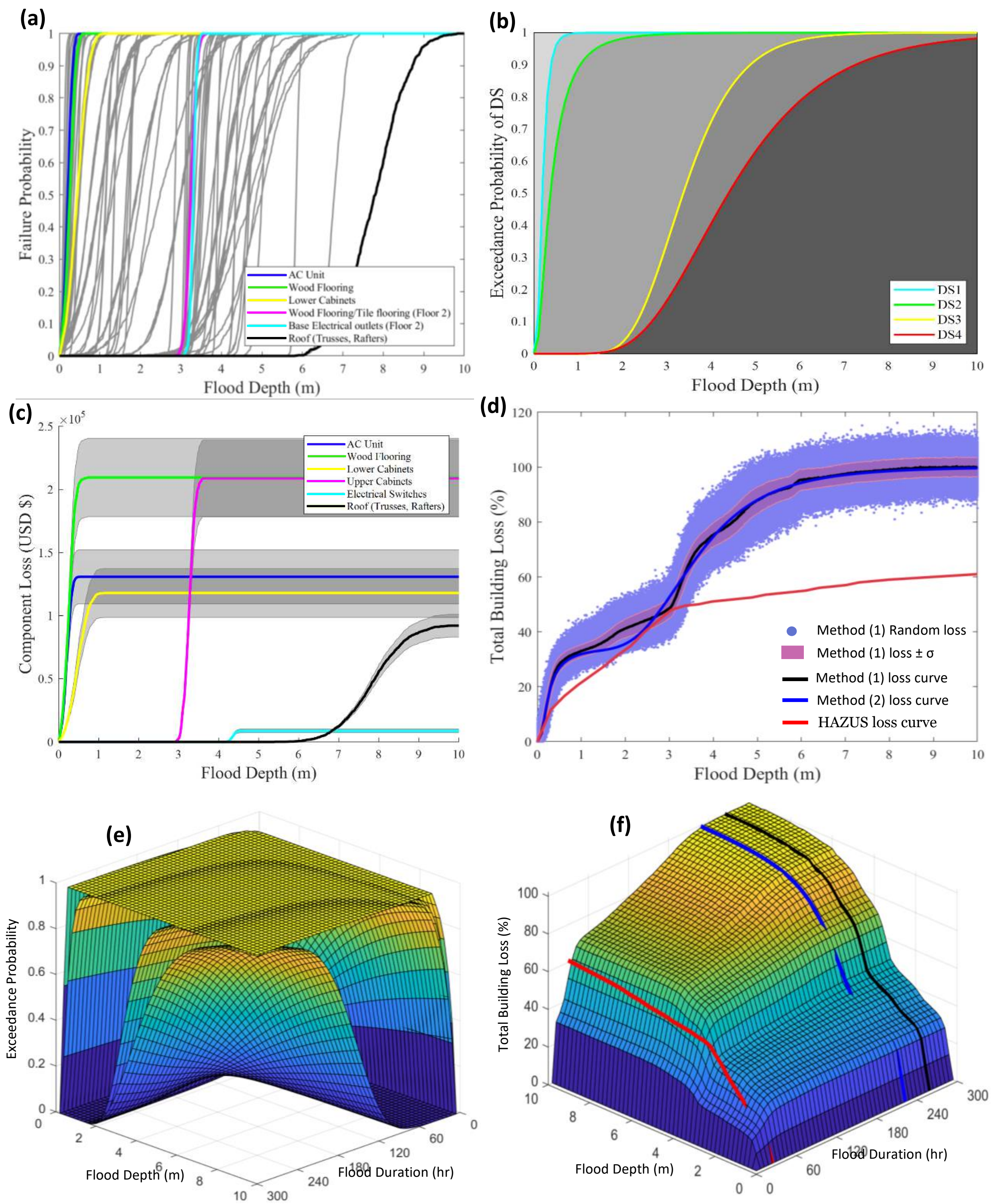

Figure B4. F4 archetype analysis results: (a) Component fragility curves; (b) Building fragility curves; (c) Selected components loss curves; (d) Building loss curves; (e) Building fragility surfaces; (f) Building loss surface.

F5: Small Grocery Store/Gas Station with a Convenience Store

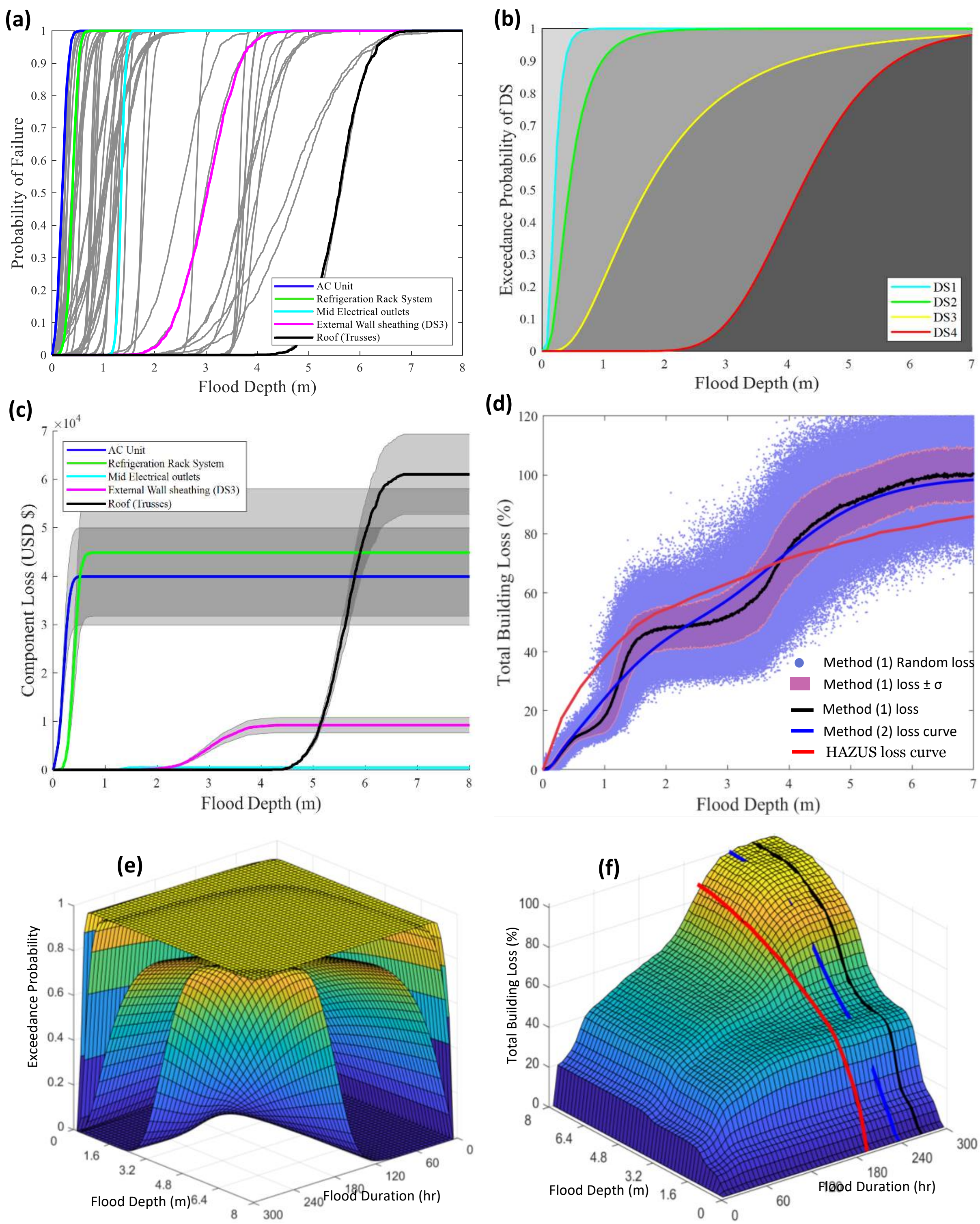

Figure B5. F5 archetype analysis results: (a) Component fragility curves; (b) Building fragility curves; (c) Selected components loss curves; (d) Building loss curves; (e) Building fragility surfaces; (f) Building loss surface.

F6: Multi-unit retail building (strip mall)

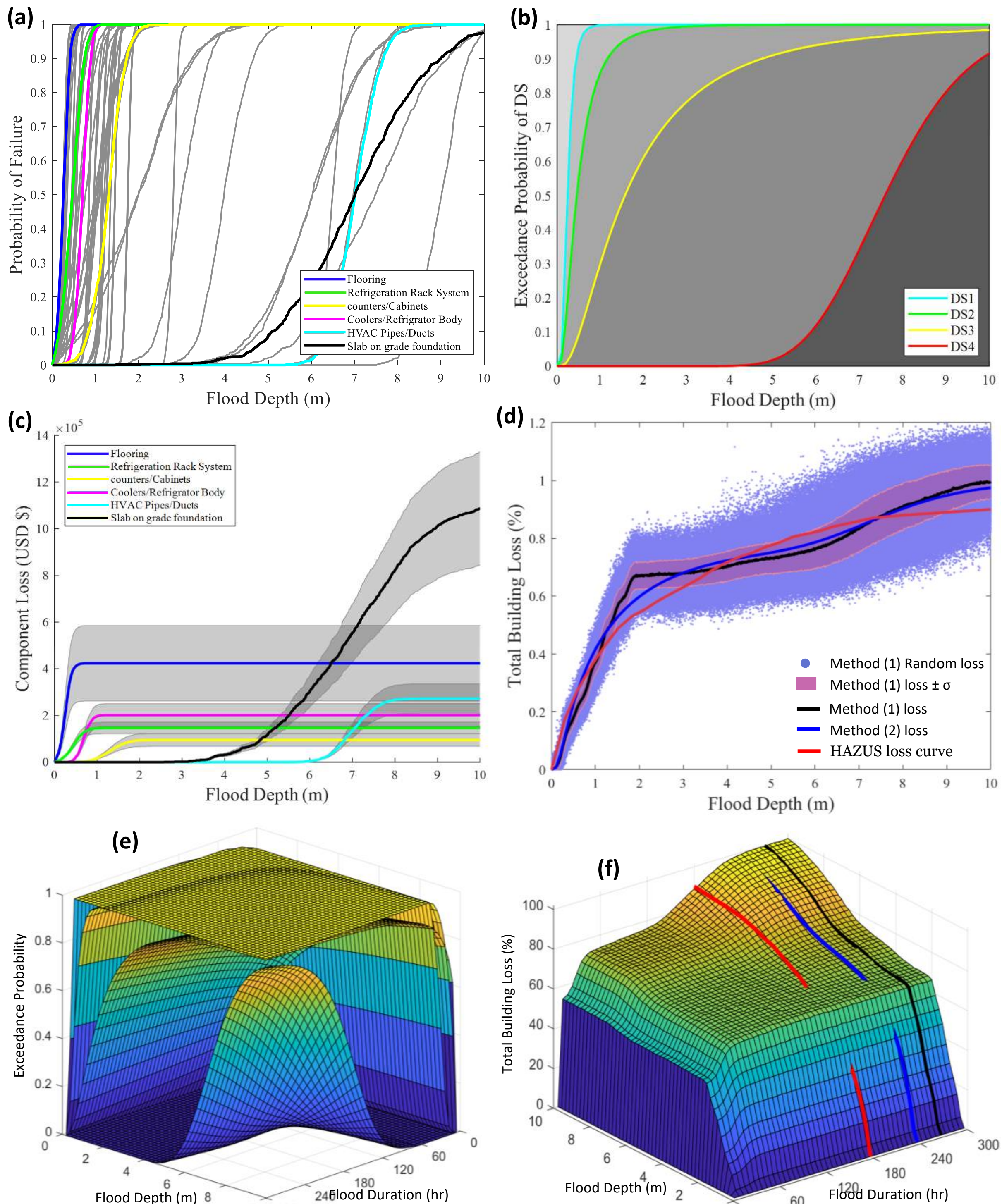

Figure B6. F6 archetype analysis results: (a) Component fragility curves; (b) Building fragility curves; (c) Selected components loss curves; (d) Building loss curves; (e) Building fragility surfaces; (f) Building loss surface.

F7: Small multi-unit commercial building

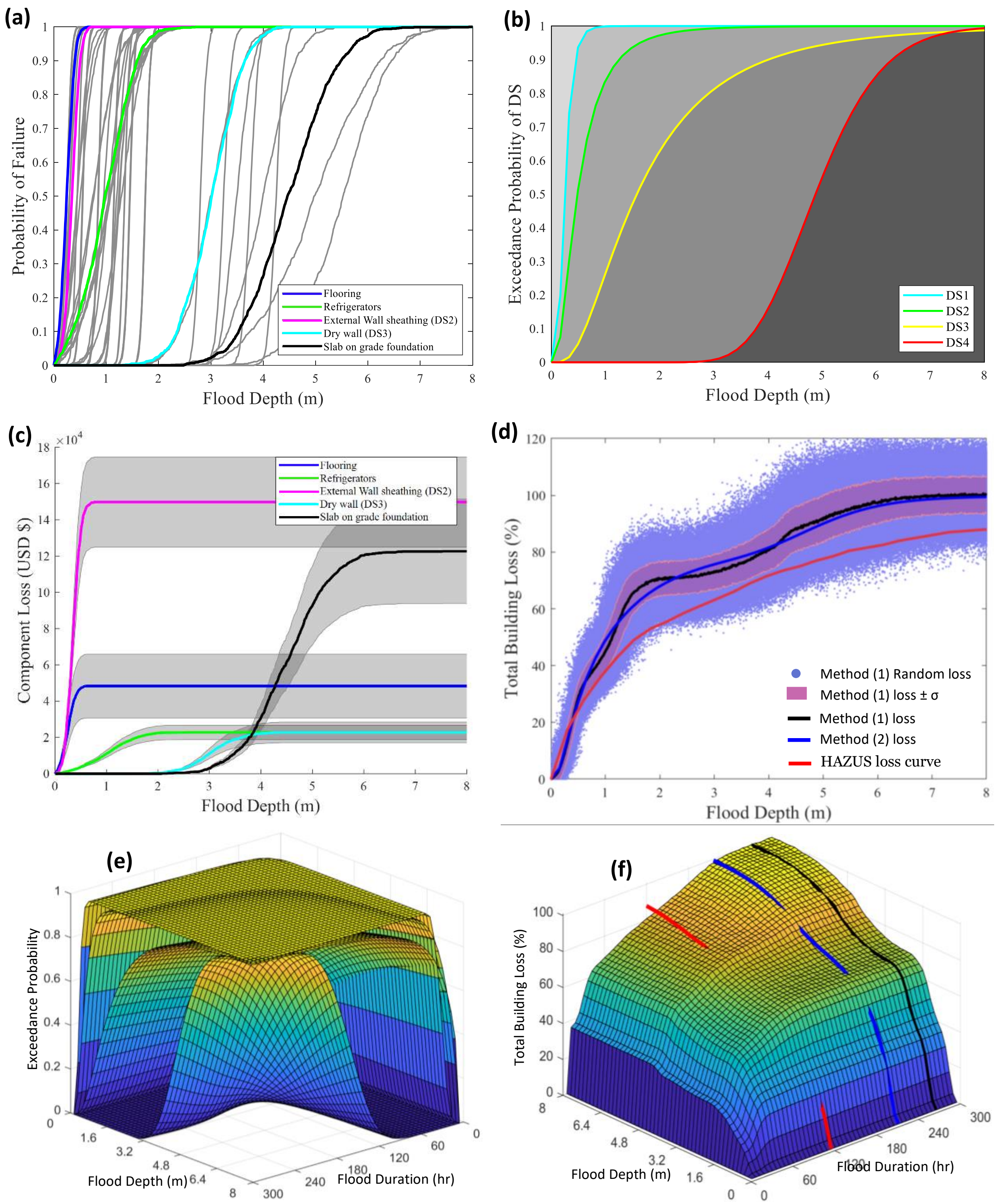

Figure B7. F7 archetype analysis results: (a) Component fragility curves; (b) Building fragility curves; (c) Selected components loss curves; (d) Building loss curves; (e) Building fragility surfaces; (f) Building loss surface.

F8: Super retail center

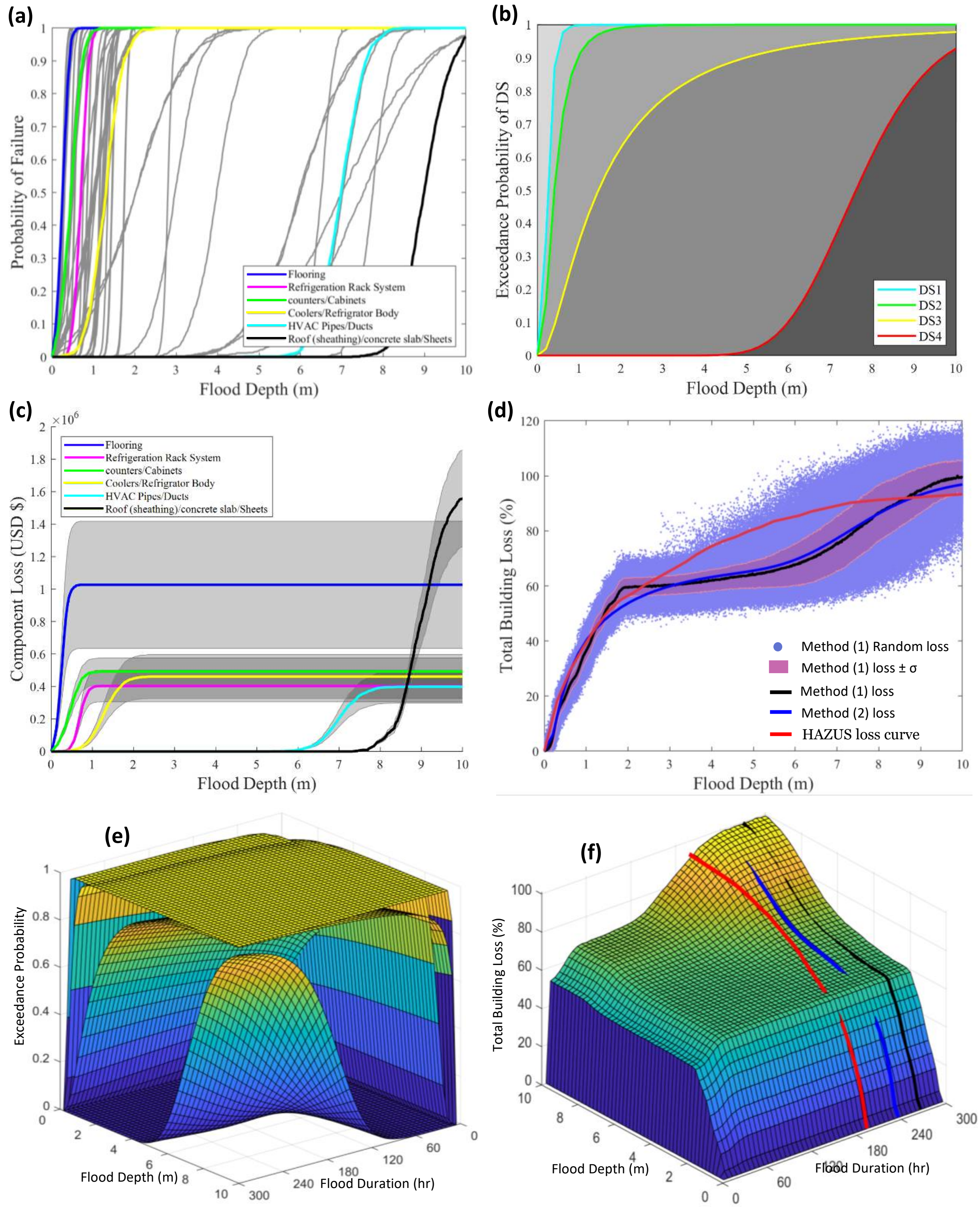

Figure B8. F8 archetype analysis results: (a) Component fragility curves; (b) Building fragility curves; (c) Selected components loss curves; (d) Building loss curves; (e) Building fragility surfaces; (f) Building loss surface.

F9: Industrial building

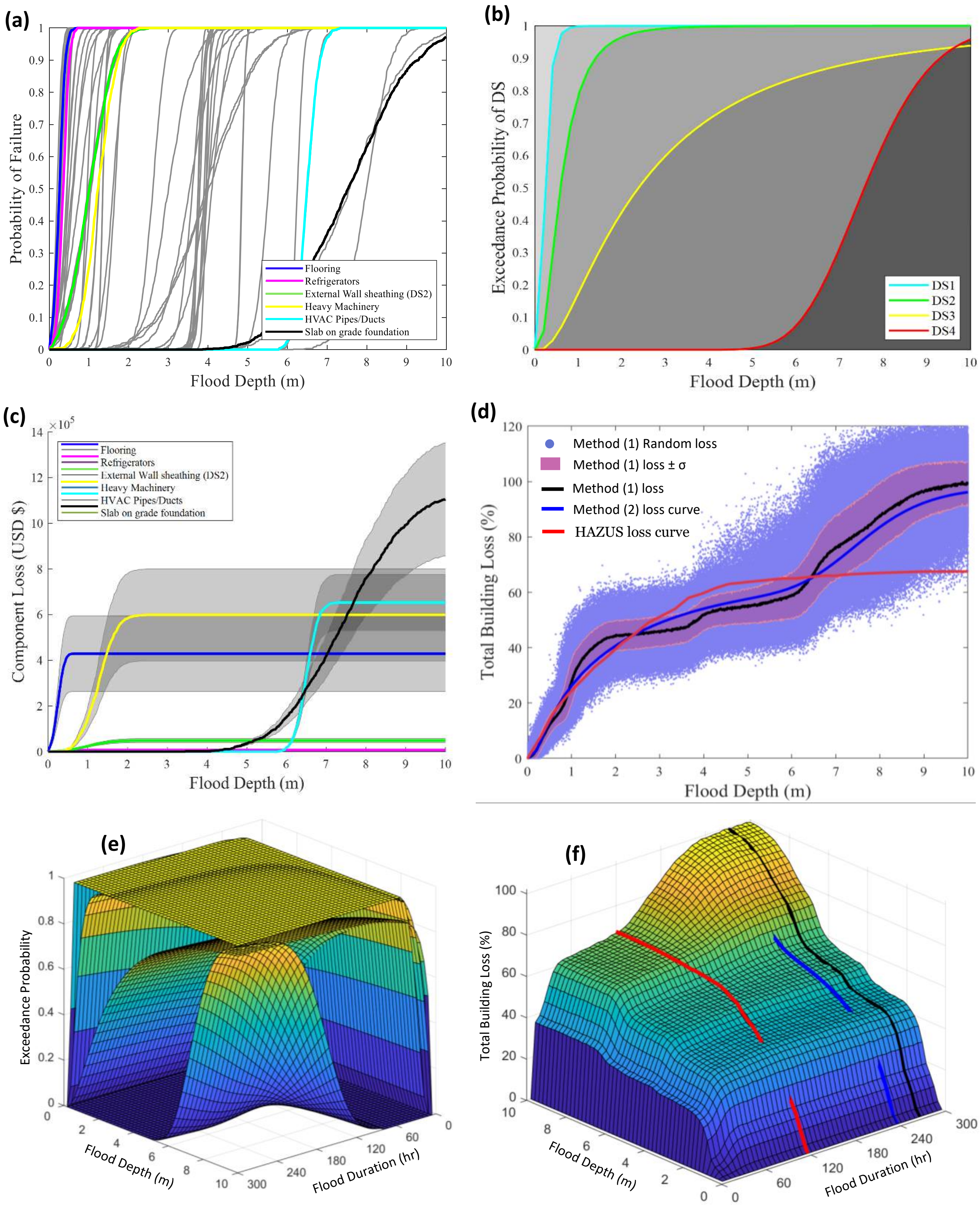

Figure B9. F9 archetype analysis results: (a) Component fragility curves; (b) Building fragility curves; (c) Selected components loss curves; (d) Building loss curves; (e) Building fragility surfaces; (f) Building loss surface.

F10: One-story School

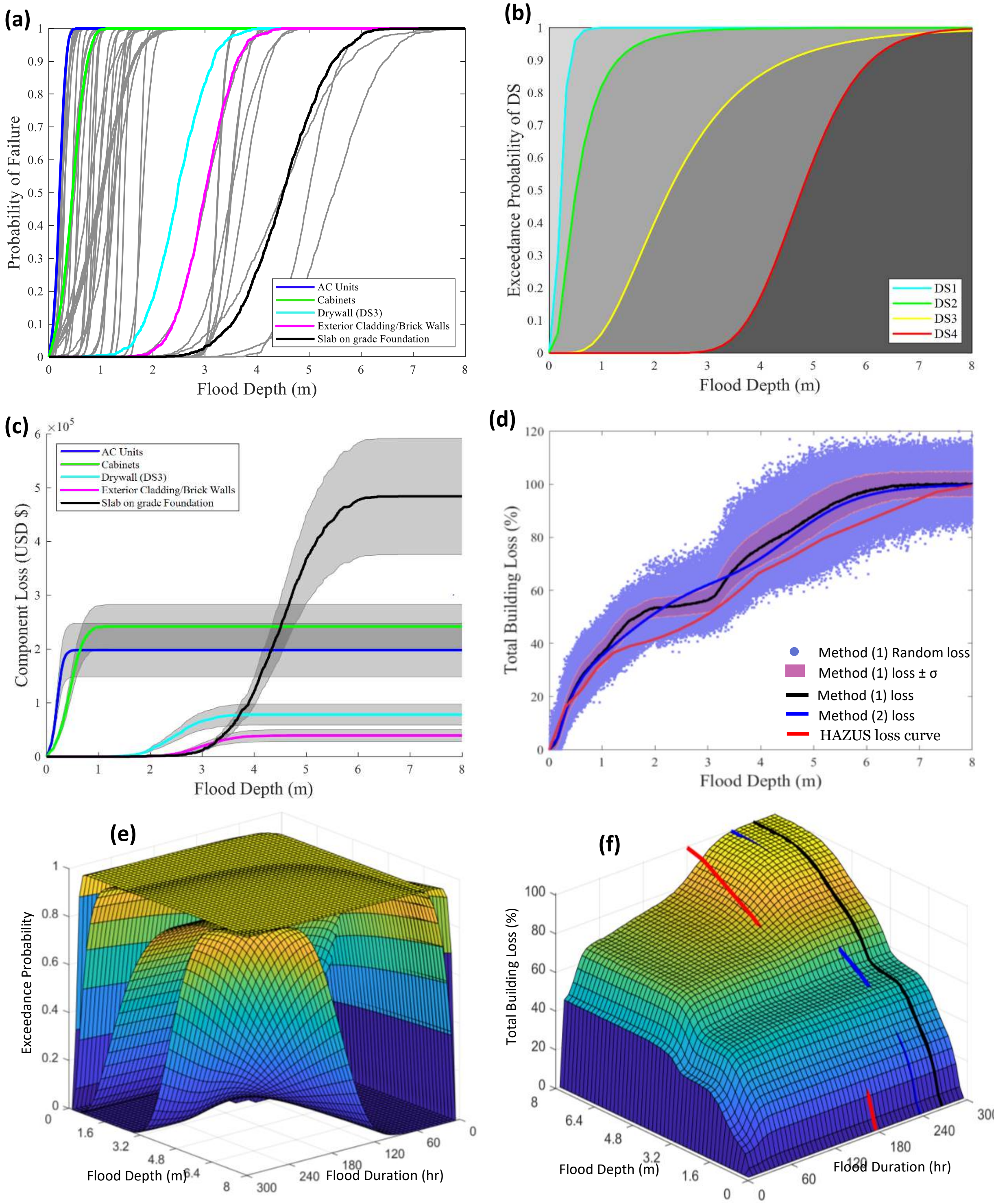

Figure B10. F10 archetype analysis results: (a) Component fragility curves; (b) Building fragility curves; (c) Selected components loss curves; (d) Building loss curves; (e) Building fragility surfaces; (f) Building loss surface.

F11: Two-story School

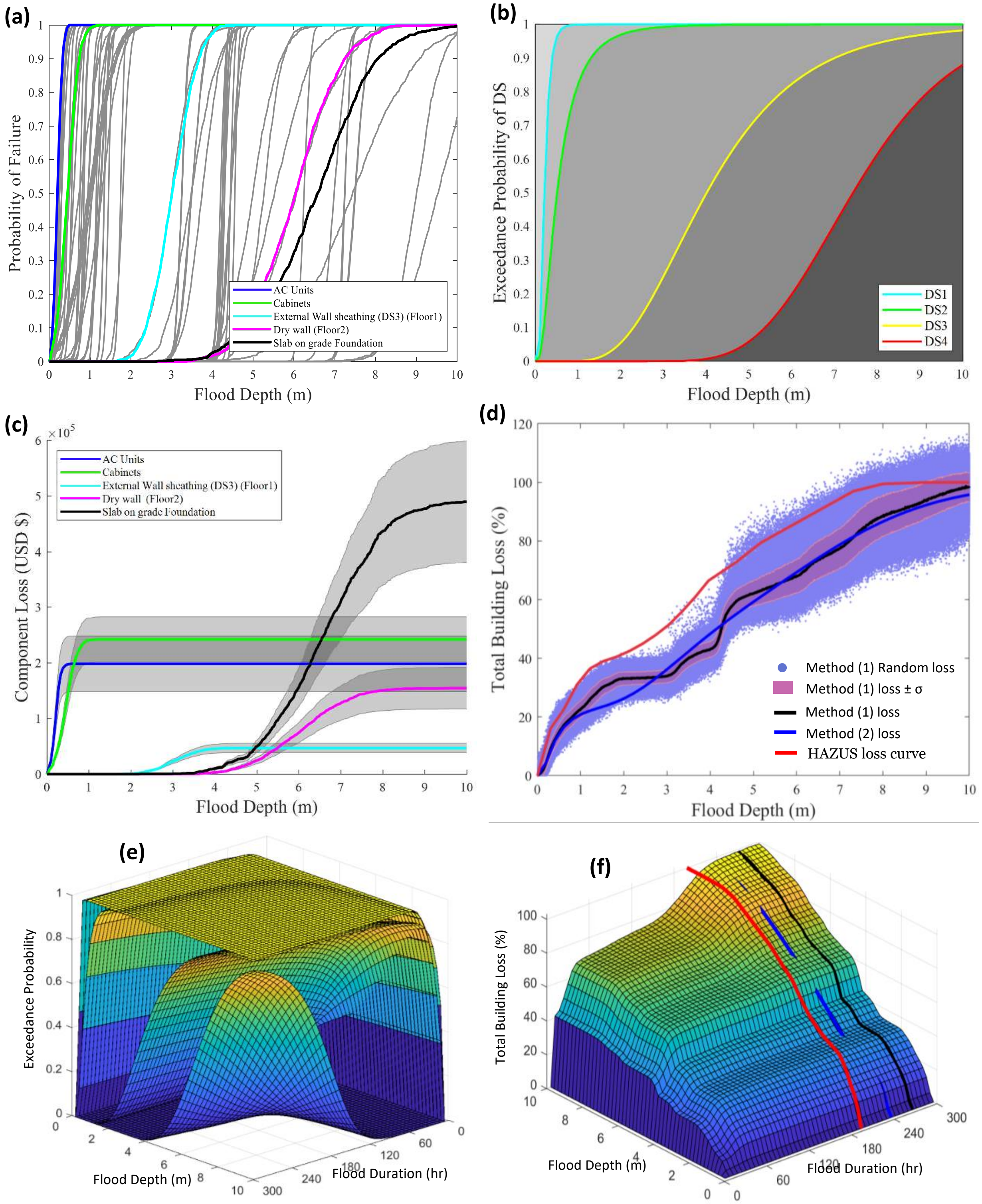

Figure B11. F11 archetype analysis results: (a) Component fragility curves; (b) Building fragility curves; (c) Selected components loss curves; (d) Building loss curves; (e) Building fragility surfaces; (f) Building loss surface.

F12: Hospital

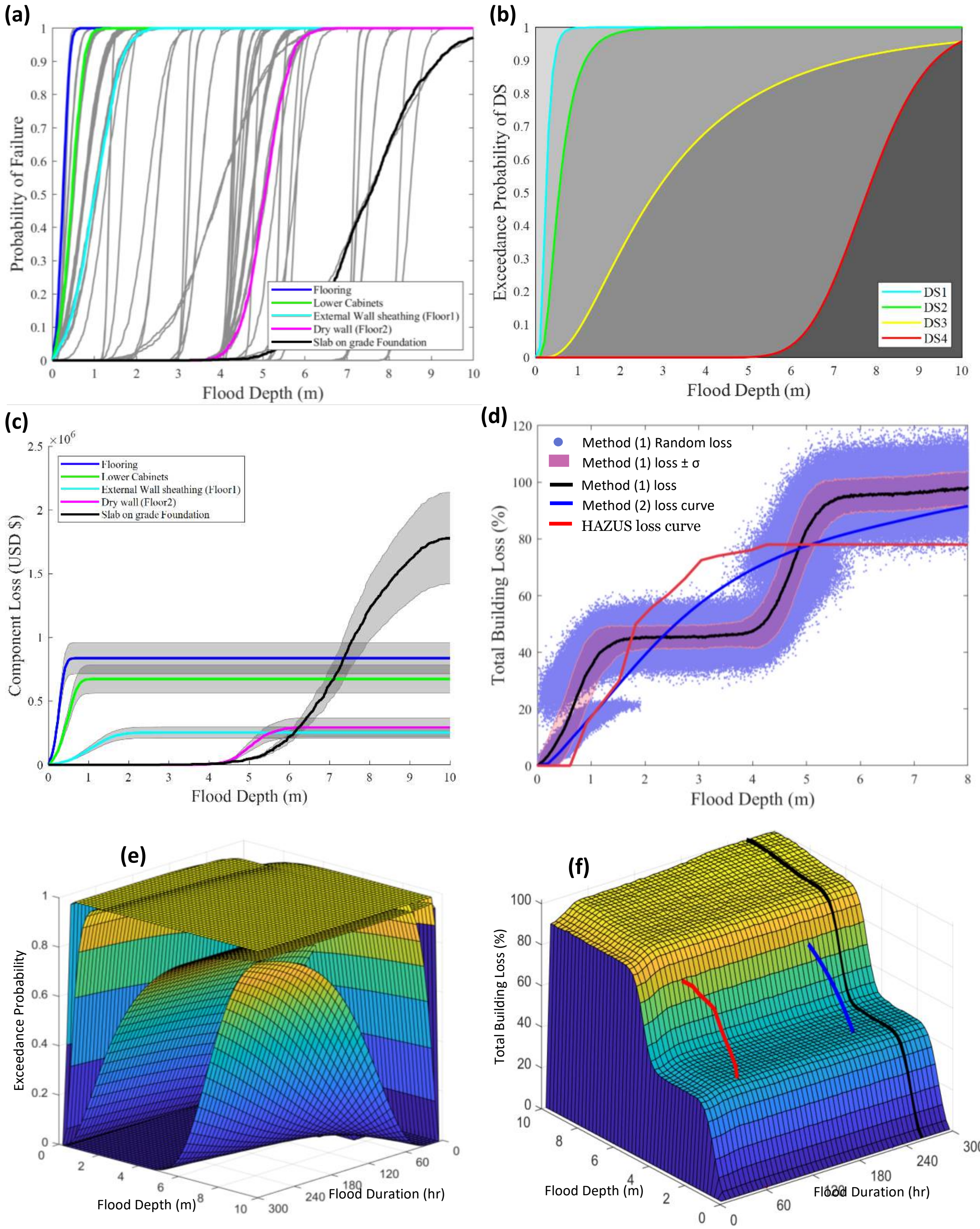

Figure B12. F12 archetype analysis results: (a) Component fragility curves; (b) Building fragility curves; (c) Selected components loss curves; (d) Building loss curves; (e) Building fragility surfaces; (f) Building loss surface.

F13: Community center (place of worship)

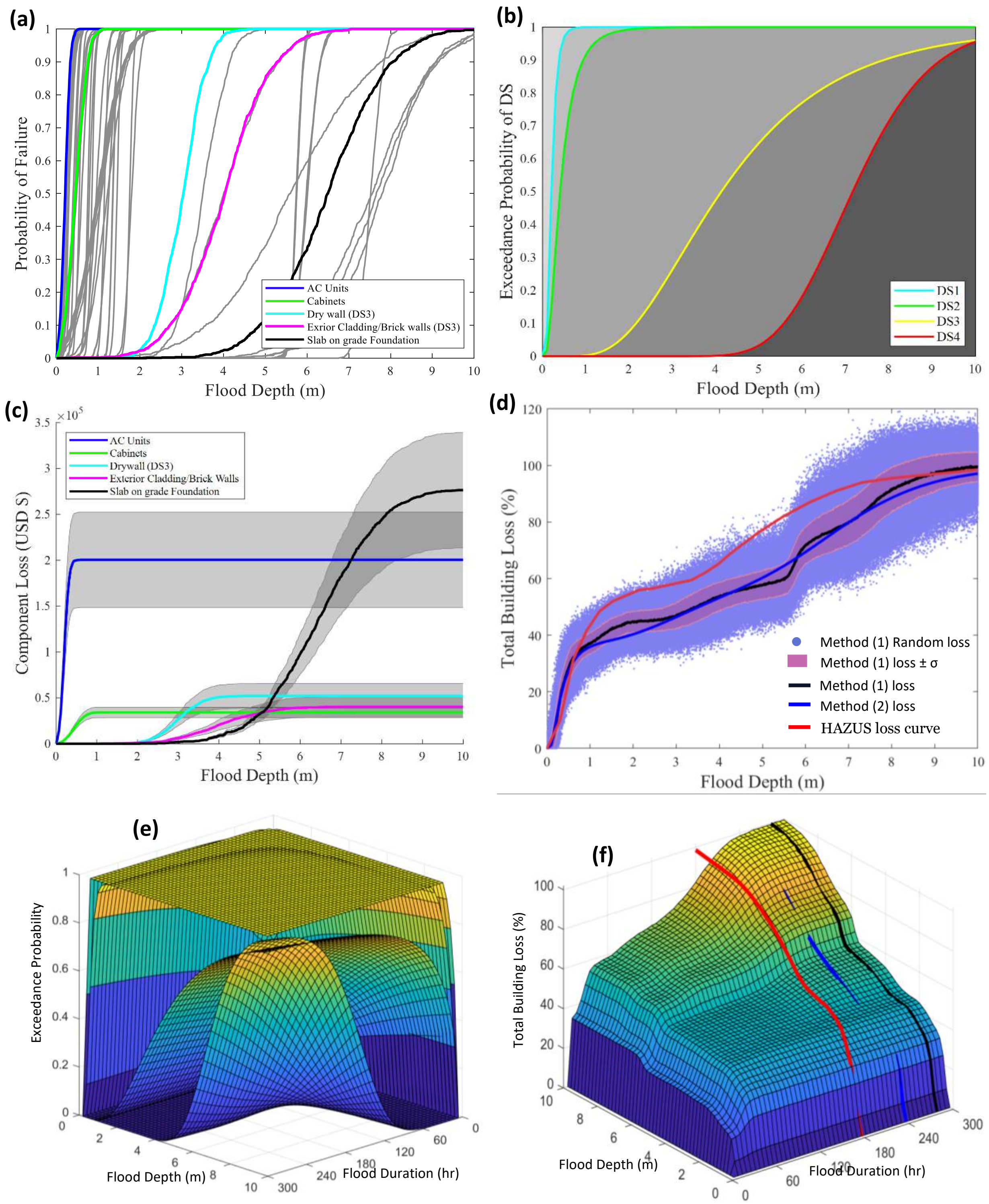

Figure B13. F13 archetype analysis results: (a) Component fragility curves; (b) Building fragility curves; (c) Selected components loss curves; (d) Building loss curves; (e) Building fragility surfaces; (f) Building loss surface.

F14: Office building

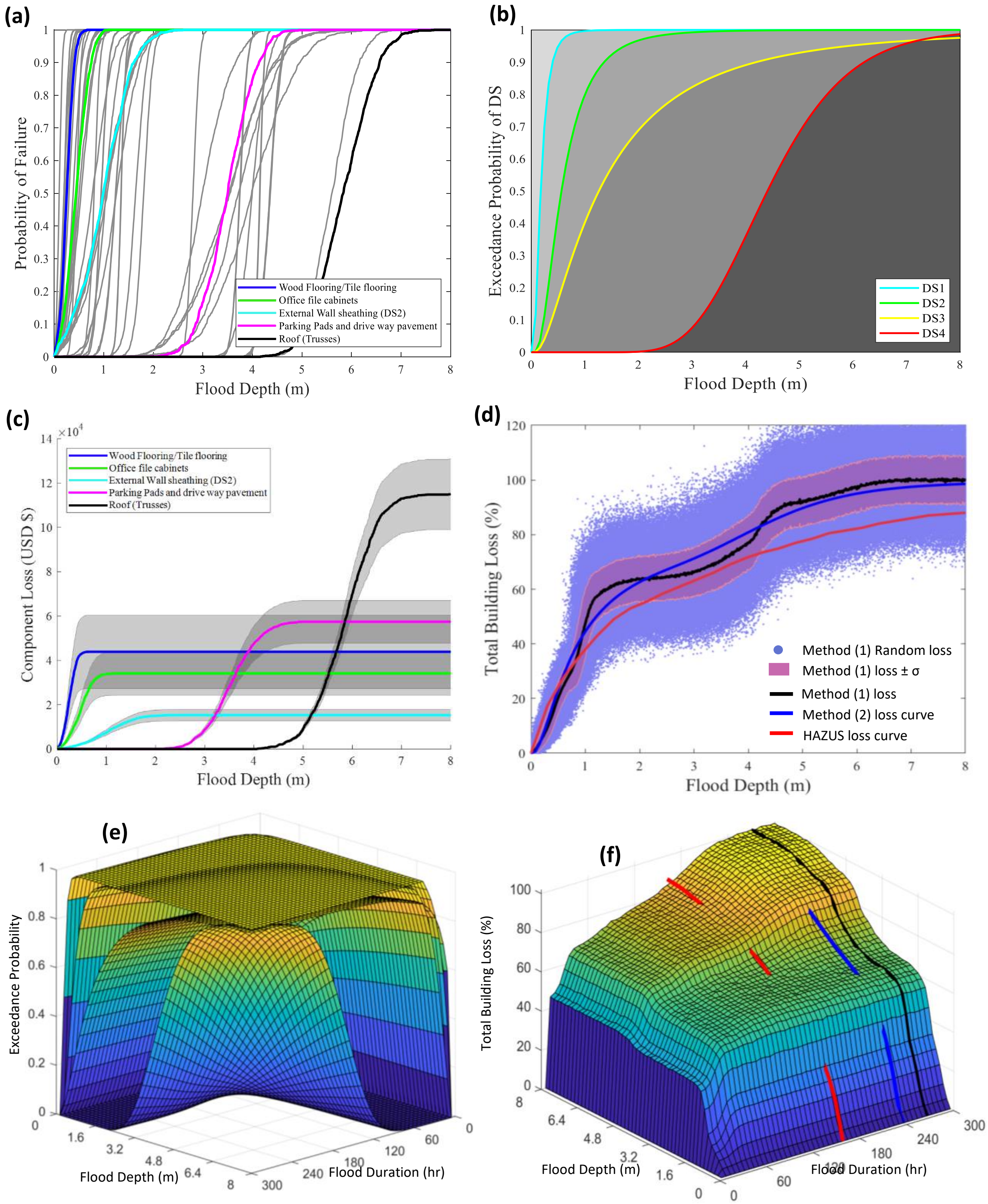

Figure B14. F14 archetype analysis results: (a) Component fragility curves; (b) Building fragility curves; (c) Selected components loss curves; (d) Building loss curves; (e) Building fragility surfaces; (f) Building loss surface.

F15: Warehouse (small/large box)

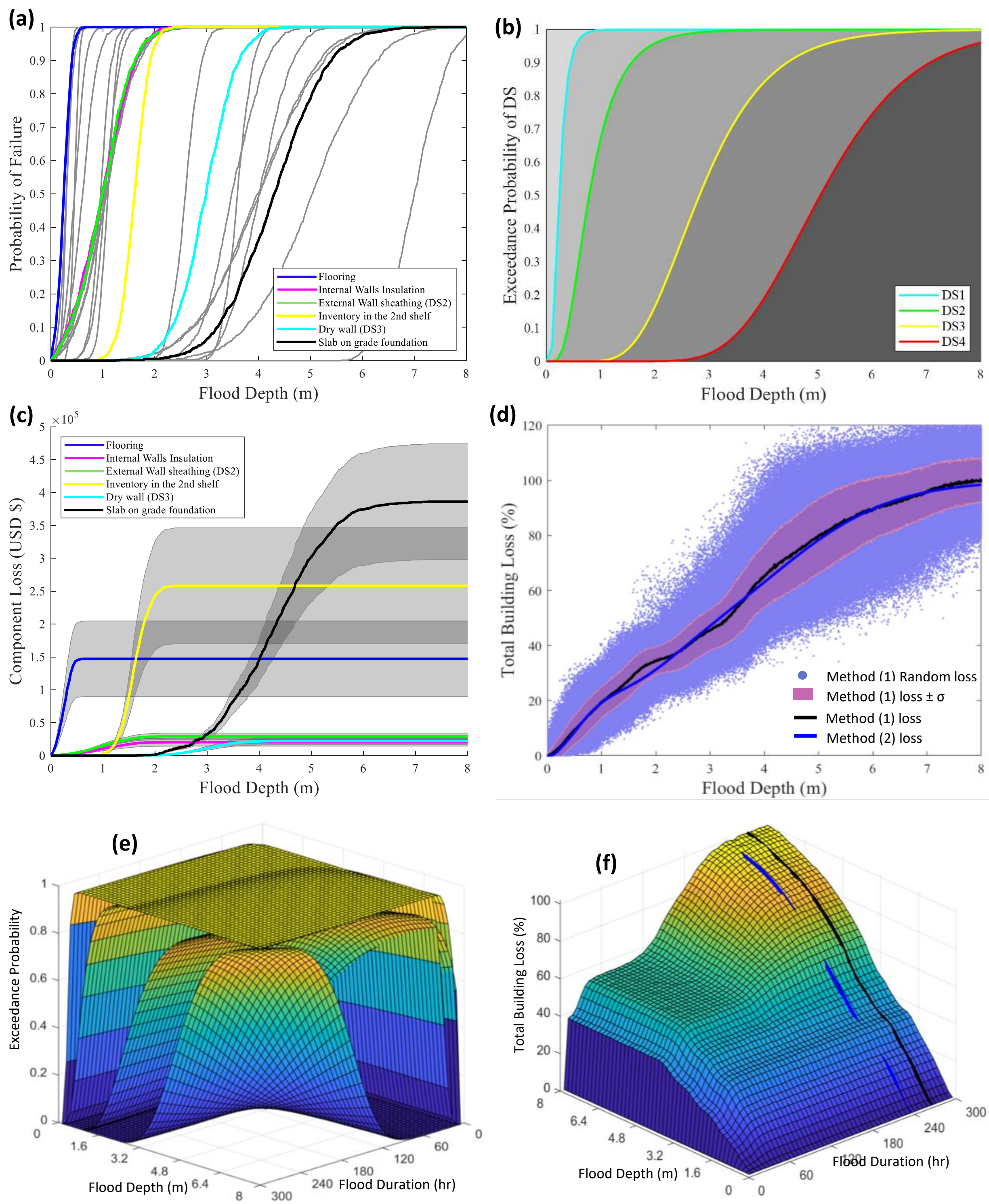

Figure B15. F15 archetype analysis results: (a) Component fragility curves; (b) Building fragility curves; (c) Selected components loss curves; (d) Building loss curves; (e) Building fragility surfaces; (f) Building loss surface.